UNIVERSITY OF STRATHCLYDE

Department of Mechanical Engineering

ON-ORBIT MANOEUVRING USING SUPERQUADRIC POTENTIAL FIELDS

Ahmed Badawy B.Sc., M.Sc.

A thesis presented in fulfilment to the requirements for the degree of

DOCTOR OF PHILOSOPHY

2007

ACKNOWLEDGEMENT

This research could not have been conducted without help and support of my parents who despite being away in Egypt, always encourage me to complete this thesis as best as I can. So whatever I express, my gratitude toward them, it is really less than what they deserve.

I also wish to express my appreciation to my wife who left her parents to be with me during these busy years. She was the one who suffered a lot to help me conduct this research. Although she is yet to know what is going around, my daughter plays a wonderful role in relieving stresses accompanying this hard time.

A special appreciation and thanks to Prof. McInnes who gave me a wonderful example of cooperation and guidance throughout the research. He devoted a lot of time and effort in discussion, revision, and stimulating suggestions that greatly enhanced my scientific knowledge.

A real help and support were offered by the Department of Mechanical Engineering at the University of Strathclyde. Everyone did their utmost to help and offer an ideal research environment for researchers.

A. Badawy

ABSTRACT

On-orbit manoeuvring represents an essential process in many space missions such as orbital assembly, servicing and reconfiguration. A new methodology, based on the potential field method along with superquadric repulsive potentials, is discussed in this thesis. The methodology allows motion in a cluttered environment by combining translation and rotation in order to avoid collisions. This combination reduces the manoeuvring cost and duration, while allowing collision avoidance through combinations of rotation and translation.

Different attractive potential fields are discussed: parabolic, conic, and a new hyperbolic potential. The superquadric model is used to represent the repulsive potential with several enhancements. These enhancements are: accuracy of separation distance estimation, modifying the model to be suitable for moving obstacles, and adding the effect of obstacle rotation through quaternions.

Adding dynamic parameters such as object translational velocity and angular velocity to the potential field can lead to unbounded actuator control force. This problem is overcome in this thesis through combining parabolic and conic functions to form an attractive potential or through using a hyperbolic function. The global stability and convergence of the solution is guaranteed through the appropriate choice of the control laws based on *Lyapunov*'s theorem.

Several on-orbit manoeuvring problems are then conducted such as on-orbit assembly using impulsive and continuous strategies, structure disassembly and reconfiguration and free-flyer manoeuvring near a space station. Such examples demonstrate the accuracy and robustness of the method for on-orbit motion planning.

CONTENTS

ACKNOWLEDGEMENT **III**

ABSTRACT **IV**

CONTENTS **V**

LIST OF FIGURES **IX**

LIST OF TABLES **XV**

NOMENCLATURE **XVI**

1. INTRODUCTION 1

1.1 Background **1**

1.2 Motion Planning Classification **3**

1.3 Configuration Space **5**

1.4 Motion Planning Methods **6**

1.4.1 Skeleton (Roadmap) 6

1.4.2 Cell decomposition 8

1.4.3 Other methods 9

1.5 Potential Field Methods **9**

1.5.1 Force involving artificial repulsion (FIRAS) 12

1.5.2 Gaussian function 13

1.5.3 Power law function 15

1.5.4 Superquadric functions 16

1.5.5 Harmonic potential functions 17

1.5.6 Navigation functions 17

1.5.7 Fuzzy potential 18

1.6 Thesis Objectives **18**

1.7 Thesis Organization **19**

1.8 List of Publications **21**

2. ATTRACTIVE POTENTIAL FUNCTIONS 22

2.1 Introduction 22

2.2 *Lyapunov*'s Stability Theorem 23

2.2.1 Definitions: 24

2.2.2 *Lyapunov*'s second theorem 24

2.3 Translational Attractive Potential 25

2.3.1 Parabolic-well 26

2.3.2 Conic-well 28

2.3.3 Parabolic-well attractive potential with velocity term 29

2.3.4 Conic-well attractive potential with velocity term 30

2.3.5 Hyperbolic attractive potential 30

2.3.6 Hyperbolic attractive potential with velocity term 32

2.4 Rotational Attractive Potential 32

2.4.1 Orientation definition 32

2.4.2 Rotational potential function 34

2.4.3 Rotational potential function with angular velocity term 35

2.5 Global Attractive Potential 38

2.5.1 Example I 38

2.5.2 Example II 44

2.6 Conclusions 49

3. SUPERQUADRIC OBSTACLE REPRESENTATION 50

3.1 Introduction 50

3.2 Inside-Outside Function 52

3.3 Superquadrics and Motion Planning 53

3.4 Separation Distance 54

3.4.1 Approximate Euclidian distance 54

3.4.2 Pseudo-distance 55

3.4.3 Radial Euclidian distance 56

3.4.4 Rigid Body Radial Euclidian distance 57

3.5 Attitude-Distance Effect 59

3.6 Superquadric Obstacle Representation 61

3.6.1 Parallelepiped shape (cuboid) 61

3.6.2 Cylindrical obstacle (beam) 67

3.7 Conclusions 71

4. SUPERQUADRIC OBSTACLE POTENTIAL 73

4.1 Introduction 73

4.2 Types of Obstacle Potential 73

4.2.1 Avoidance potential 74

4.2.2 Approach potential 74

4.3 Obstacle Potential of Parallelepiped Element 78

4.3.1 Cuboid obstacle potential using the modified pseudo distance 78

4.3.2 Cuboid obstacle potential using the rigid body radial Euclidian distance 81

4.4 Obstacle Potential of a Cylindrical Element 85

4.5 Conclusions 86

5. GLOBAL POTENTIAL FUNCTION 88

5.1 Introduction 88

5.2 Continuous Control 89

5.3 Impulsive Control 96

5.4 Conclusions 103

6. ORBITAL ASSEMBLY 105

6.1 Introduction 105

6.2 Proximity Motion 106

6.3 On-Orbit Assembly Strategies 111

6.4 On-Orbit Continuous Control **112**
6.4.1 Continuous assembly using conic and parabolic potentials 112
6.4.2 Continuous assembly using hyperbolic potential 122
6.5 On-Orbit Impulsive Control **127**
6.5.1 Example I 128
6.5.2 Example II 136
6.5.3 Complex structure assembly 139
6.6 Conclusions **147**

7. ORBITAL RECONFIGURATION **148**
7.1 Introduction **148**
7.2 Free Flyer Manoeuvring Near a Space Station **149**
7.3 Structure Reconfiguration **154**
7.4 Conclusions **173**

8. CONCLUSIONS **174**
8.1 Review **174**
8.2 Future Work **177**

References **179**

Appendix A: Quaternion Algebra **188**
A.1 Introduction **188**
A.2 Quaternion Parameters Determination **189**

LIST OF FIGURES

Fig. 1.1 Space exploration rovers 2
Fig. 1.2 Motion planning phases 2
Fig. 1.3 Motion planning levels of complexity 4
Fig. 1.4 Three link mechanism 5
Fig. 1.5 The visibility graph 7
Fig. 1.6 The Voronoi diagram 8
Fig. 1.7.a) Global potential with FIRAS rectangular obstacle representation 12
Fig. 1.7.b) Global potential with FIRAS circular obstacle representation 13
Fig. 1.8 Global potential with Gaussian obstacle representation 14
Fig. 1.9 Global potential with power law obstacle representation, N = 10 15
Fig. 1.10 Global potential with superquadric obstacle representation 16
Fig. 1.11 Thesis roadmap 20
Fig 2.1 Parabolic-well attractive potential 27
Fig 2.2 Conic-well attractive potential 28
Fig 2.3 Hyperbolic-well attractive potential 31
Fig. 2.4 Manoeuvring object motion in 3D 40
Fig. 2.5.a) Manoeuvring object total impulses 40
Fig. 2.5.b) Manoeuvring object impulses in the *x*-direction 41
Fig. 2.5.c) Manoeuvring object impulses in the *y*-direction 41
Fig. 2.5.d) Manoeuvring object impulses in the *z*-direction 42
Fig. 2.6.a) Manoeuvring object error quaternion 42
Fig. 2.6.b) Manoeuvring object angular velocities 43
Fig. 2.6.c) Manoeuvring object torques 43
Fig. 2.7 Manoeuvring object motion in 3D 45
Fig. 2.8.a) Manoeuvring object velocity 46
Fig. 2.8.b) Manoeuvring object acceleration 46
Fig. 2.9.a) Manoeuvring object error quaternions 47
Fig. 2.9.b) Manoeuvring object angular velocity 47
Fig. 2.9.c) Manoeuvring object angular acceleration 48
Fig. 2.9.d) Manoeuvring object control torque 48
Fig. 3.1 Superquadric surface vector 51

Fig. 3.2 Superquadric shapes 52
Fig. 3.3 Radial Euclidian distance 57
Fig. 3.4 Possible collision configuration 58
Fig. 3.5 Orientation effect on separation distance 59
Fig. 3.6 Two object configuration 60
Fig. 3.7 Separation distance vs. quaternion parameter about *z*-axis 61
Fig. 3.8 Cuboid element representation using a superquadric function 63
Fig 3.9.a) Cuboid iso-distance contours, modified pseudo distance method, Eq. (3.7), ($\alpha = 1$) 64
Fig. 3.9.b) Cuboid iso-distance contours, modified pseudo distance method ($\alpha = 100$) 64
Fig. 3.9.c) Cuboid iso-distance contours radial distance method, Eq. (3.12), ($\alpha = 1$) 65
Fig. 3.9.d) Cuboid iso-distance contours radial distance method ($\alpha = 100$) 65
Fig. 3.9.e) Cuboid iso-distance contours, rigid body radial distance method, Eq. (3.16), ($\alpha = 1$) 66
Fig. 3.9.f) Cuboid iso-distance contours, rigid body radial distance method ($\alpha=100$) 66
Fig. 3.10 Cylindrical element representation using a superquadric function 67
Fig. 3.11.a) Beam iso-potential contours, pseudo distance method, Eq. (3.7), (cross section) 68
Fig. 3.11.b) Beam iso-potential contours, pseudo distance method (longitudinal section) 69
Fig. 3.11.c) Beam iso-distance contours, radial distance method, Eq. (3.12), (cross section) 69
Fig. 3.11.d) Beam iso-distance contours, radial distance method (longitudinal section) 70
Fig. 3.11.e) Beam iso-distance contours, radial distance for rigid body method, Eq. (3.16), (cross section) 70
Fig. 3.11.f) Beam iso-distance contours, radial distance for rigid body method (longitudinal section) 71
Fig. 4.1.a) Avoidance potential function ($\alpha = 1$) 75

Fig. 4.1.b) Avoidance potential function (α = 10) 76
Fig. 4.1.c) Approach potential function (α = 1) 76
Fig. 4.1.d) Approach potential function (α = 10) 77
Fig. 4.2 Radial Euclidian distance 82
Fig. 5.1 Initial configuration 91
Fig. 5.2.a) Object configuration at t = 70 sec 91
Fig. 5.2.b) Object configuration at t = 93 sec 92
Fig. 5.2.c) Final object configuration at t = 130 sec 92
Fig. 5.3 Object trajectories 93
Fig 5.4.a) Object velocities in *x*-direction 93
Fig 5.4.b) Object velocities in *z*-direction 94
Fig 5.4.c) Object accelerations in *x*-direction 94
Fig 5.4.d) Object accelerations in *z*-direction 95
Fig 5.5.a) Object angular velocities about *y*-axis 95
Fig 5.5.b) Object angular accelerations about *y*-axis 96
Fig. 5.6 Initial object configuration 98
Fig. 5.7.a) Object configuration at t = 165 sec 98
Fig. 5.7.b) Object configuration at t = 220 sec 99
Fig. 5.7.c) Object configuration at t = 310 sec 99
Fig. 5.7.d) Final object configuration at t = 1000 sec 100
Fig. 5.8 Object trajectories 100
Fig. 5.9.a) Object impulses in *x*-direction 101
Fig. 5.9.b) Object impulses in *z*-direction 101
Fig. 5.10.a) Object error quaternion about *y*-axis 102
Fig. 5.10.b) Object angular velocities about *y*-axis 102
Fig. 5.10.c) Object torques about *y*-axis 103
Fig. 6.1 Inertial, local orbiting and body frames for the i^{th} manoeuvring object 107
Fig. 6.2 Initial object configuration 113
Fig. 6.3.a) Object configuration t = 124 sec 114
Fig. 6.3.b) Object configuration t= 838 sec 114
Fig. 6.3.c) Object configuration t = 3470 sec 115
Fig. 6.3.d) Assembled structure t = 5300 sec 115

Fig. 6.4.a) Object velocities in the *x*-direction 116
Fig. 6.4.b) Object accelerations in the *x*-direction 116
Fig. 6.4.c) Object velocities in the *y*-direction 117
Fig. 6.4.d) Object accelerations in the *y*-direction 117
Fig. 6.4.e) Object velocities in the *z*-direction 118
Fig. 6.4.f) Object accelerations in the *z*-direction 118
Fig. 6.5.a) Error quaternions of Objects 1, 3, 9, and 11 119
Fig. 6.5.b) Angular velocity about *x*-axis of objects 1, 3, 9, and 11 119
Fig. 6.5.c) Error quaternions of objects 5, 6, 7, and 8 120
Fig. 6.5.d) Angular velocity about *z*-axis of objects 5, 6, 7, and 8 120
Fig. 6.5.e) Torque about *x*-axis of objects 1, 3, 9, and 11 121
Fig. 6.5.f) Torque about z-axis of objects 5, 6, 7, and 8 121
Fig. 6.6 Initial object configuration 123
Fig. 6.7.a) Object configuration (t = 37 sec) 124
Fig. 6.7.b) Object configuration (t = 120 sec) 124
Fig. 6.7.c) Object configuration (t = 180 sec) 125
Fig. 6.7.d) Final object configuration (t = 300 sec) 125
Fig. 6.8.a) Object velocities in *x*-direction 126
Fig. 6.8.b) Object velocities in *z*-direction 126
Fig. 6.8.c) Object angular velocities about *y*-axis 127
Fig. 6.9.a) Initial object configuration 129
Fig. 6.9.b) Object configuration at t = 5800 sec 130
Fig. 6.9.c) Object configuration at t = 6370 sec 130
Fig. 6.9.d) Object configuration at t = 8300 sec 131
Fig. 6.9.e) Object configuration at t = 8900 sec 131
Fig. 6.9.f) Assembled structure at t = 9800 sec 132
Fig. 6.10.a) Object trajectories 132
Fig. 6.10.b) Object error quaternions 133
Fig. 6.10.c) Object angular velocities 133
Fig. 6.11.a) Impulse in the *x*-direction (object 7) 134
Fig. 6.11.b) Impulse in the *z*-direction (object 7) 134
Fig. 6.11.c) Overall potential (object 7) 135

Fig. 6.11.d) Rate of change of the overall potential (object 7) 135
Fig. 6.12.a) Object trajectories 136
Fig. 6.12.b) Impulses in the *x*-direction (object 7) 137
Fig. 6.12.c) Impulses in the *z*-direction (object 7) 137
Fig. 6.12.d) Overall potential (object 7) 138
Fig. 6.12.e) Rate of change of the overall potential (object 7) 138
Fig. 6.13.a) Initial object configuration 139
Fig. 6.13.b) Object configuration at t = 760 sec 140
Fig. 6.13.c) Object configuration at t = 1630 sec 140
Fig. 6.13.d) Object configuration at t = 2670 sec 141
Fig. 6.13.e) Object configuration at t = 3725 sec 141
Fig. 6.13.f) Assembled structure at t = 4000 sec 142
Fig. 6.14.a) Object trajectories (object 1 to 7) 142
Fig. 6.14.b) Plate element trajectories (object 15 and 16) 143
Fig. 6.14.c) Impulse in *x*-direction (object 1) 143
Fig. 6.14.d) Impulse in *y*-direction (object 1) 144
Fig. 6.14.e) Impulse in *z*-direction (object 1) 144
Fig. 6.15.a) Error quaternions about the *x*-axis 145
Fig. 6.15.b) Error quaternions about the *y*-axis 145
Fig. 6.15.c) Error quaternions about the *z*-axis 146
Fig. 6.15.d) Continuous control torque about the *y*-axis 146
Fig. 7.1 International space station using superquadric model 149
Fig. 7.2 Free-flyer trajectory 152
Fig. 7.3 Free-flyer rotation 152
Fig. 7.4.a) Free-flyer thrust impulses in *x*-direction 153
Fig. 7.4.b) Free-flyer thrust impulses in *z*-direction 153
Fig. 7.5 Required control torque about *y*-axis 154
Fig. 7.6.a) Initial object configuration 155
Fig. 7.6.b) Object configuration (t = 20 sec) 156
Fig. 7.6.c) Object configuration (t = 40 sec) 156
Fig. 7.6.d) Object configuration (t = 145 sec) 157
Fig. 7.6.e) Object configuration (t = 230 sec) 157

Fig. 7.6.f) Object configuration (t = 260 sec) 158
Fig. 7.6.g) Final configuration (t = 400 sec) 158
Fig. 7.7.a) Impulse in the *x*-direction 159
Fig. 7.7.b) Impulse in the *y*-direction 159
Fig. 7.7.c) Impulse in the *z*-direction 160
Fig. 7.8.a) Error quaternions about the *x*-axis 160
Fig. 7.8.b) Error quaternions about the *y*-axis 161
Fig. 7.8.c) Error quaternions about the *z*-axis 161
Fig. 7.8.d) Angular velocity about the *x*-axis 162
Fig. 7.8.e) Angular velocity about the *y*-axis 162
Fig. 7.8.f) Angular velocity about the *z*-axis 163
Fig. 7.9.a) Control torque about the *x*-axis 163
Fig. 7.9.b) Control torque about the *y*-axis 164
Fig. 7.9.c) Control torque about the *z*-axis 164
Fig. 7.10.a) Object configuration (t = 15 sec) 165
Fig. 7.10.b) Object configuration (t = 42 sec) 166
Fig. 7.10.c) Object configuration (t = 7 sec) 166
Fig. 7.10.d) Object configuration (t = 200 sec) 167
Fig. 7.11.a) Impulse in the *x*-direction 167
Fig. 7.11.b) Impulse in the *y*-direction 168
Fig. 7.11.c) Impulse in the *z*-direction 168
Fig. 7.12.a) Error quaternion about the *x*-axis 169
Fig. 7.12.b) Error quaternion about the *y*-axis 169
Fig. 7.12.c) Error quaternion about the *z*-axis 170
Fig. 7.12.d) Angular velocity about the *x*-axis 170
Fig. 7.12.e) Angular velocity about the *y*-axis 171
Fig. 7.12.f) Angular velocity about the *z*-axis 171
Fig. 7.13.a) Control torque about the *x*-axis 172
Fig. 7.13.b) Control torque about the *y*-axis 172
Fig. 7.13.c) Control torque about the *z*-axis 173

LIST OF TABLES

Table 5.1 Element translation cost 103
Table 6.1 Element translation cost 129
Table 6.2 Element translation cost 136
Table 6.3 Element translation cost 147
Table 7.1 First phase translation cost 155
Table 7.2 Second phase translation cost 165

1. INTRODUCTION

1.1 Background

Mobile robots and manipulators are widely used for terrestrial, subsea, and space applications. Terrestrial applications are vast, ranging from industrial to domestic usage (Palacín et al., 2004). In industrial applications, combinations of mobile robots and manipulators serve for mechanical assembly (Yuan, 2002), material handling (Neuhaus and Kazerooni, 2001), and spot welding (Pires and Loureiro, 2003). Medical robot applications are a further success (and challenge) assisting during microsurgeries and rehabilitation (Salcudean et al., 1999; Cepolina and Michelini, 2004). Mobile robots also play a role in subsea and ocean operations where they are able to reach extreme depth and perform assembly and maintenance tasks (Antonelli et al., 2001). Well known space applications serve for assembly, service, and repair (McQuade and McInnes, 1997; Roger, 2003). Other robotic applications are in rough terrain such as mining and rescue (Lagnemma and Dubowsky, 2004; Shimoda et al., 2005). Planetary exploration such as Lunar and Mars rovers, Fig. 1.1, are well known applications which require highly automated, unattended robotic motion planning (Hayati et al., 1996). Challenges for such applications have been discussed (Weisbin et al., 1999; Schenker et al., 2000).

As robots are used to perform certain tasks they always require motion; motion is an essential action without which a robot will lose its functionality. Since robots are not the sole object in their workspace, robot motion planning research is a key area of robot technology. Intelligent motion planning (MP) algorithms attempt to advance from repetitive pre-programmed tasks to fully autonomous operations. Research development has been undertaken in theory, computational capabilities and sensors. Determining a collision-free path between some start and goal configuration, in addition to the required dynamic parameters, forces and moments, is the ultimate goal of motion planning analysis.

(a) ESA EXOMARS Rover

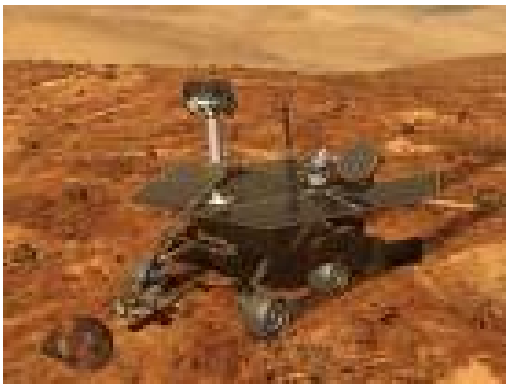

(b) NASA Mars Exploration Rover (MER)

Fig. 1.1 Space exploration rovers

Various aspects of MP problems have been investigated either through theoretical or experimental analysis. Generally, the MP problem aims to find if a region of space is reachable from another through a continuous path. It is therefore the process of selecting a path and the associated set of input forces and torques from the set of all possible motions and inputs, while ensuring that all constraints are satisfied.

Three closely linked problems constitute MP: path planning, trajectory planning, and motion control, Fig. 1.2. The first phase aims to define the kinematic parameters, position and orientation, of the manoeuvring object, whereas the second phase aims to generate the required translational velocity and angular velocity profile to generate motion to the goal. Path planning is therefore a subset of trajectory planning. Finally, the motion control phase aims to drive the manoeuvring object to follow the reference trajectory as closely as possible.

Fig. 1.2 Motion planning phases

1.2 Motion Planning Classification

MP algorithms depend on the availability of sensed data such as obstacle shapes and kinematics. MP methods based mainly on sensed data are normally termed local methods, used when there is not enough global data about the workspace. So-called global methods are used otherwise, when complete knowledge of the workspace is available. It is also possible to utilize local methods in the case of a well known environment with either stationary or moving obstacles, but with an optimized path. A combination of global and local methods can be used to generate a global optimal plan, with the local sensory based approach reaching to unforeseen obstacles. Ensuring global knowledge of the workspace is not simple due to limited sensing capabilities and sensor range limitations. On the other hand, local MP may lead to unfeasible trajectories as a complete world model is not available. Information exchange between different manoeuvring objects through decentralized control enhances the amount of world information available to each of them.

A second classification of MP depends on the obstacle kinematic properties, either static or dynamic. In the static case, all obstacles are known as in case of robotic assembly in a production process. On the other hand, in dynamic MP problems the manoeuvring objects sense data whilst in motion. Consequently, new data is continuously generated so on-line control is required. Generally, dynamic MP is the norm whereas static MP is an exception as every MP problem can be solved as dynamic one, while the inverse is not true.

Other issues in MP problems occur when dealing with articulated or linked bodies or deformable problems, where objects shapes will change during motion. These deformable MP problems are common as a wide range of robots are equipped with manipulators or links. The level of complexity of MP problems with respect to objects representations, object dynamic properties, the type of manoeuvring object under control, and constraint types is illustrated in Fig. 1.3.

Objects in the environment can be represented as spherical shapes for simplicity, although the real shape is required in cases where the spherical shape occupies significantly more space than its actual size, or in case of the final docking phase where objects engage.

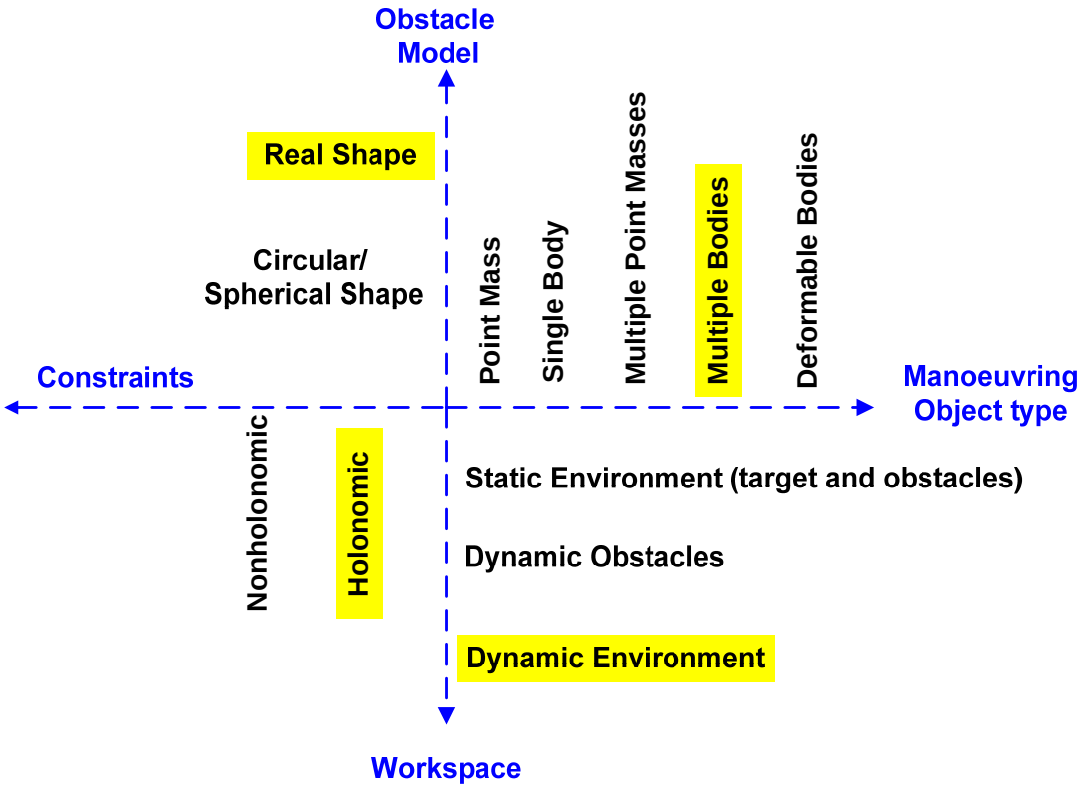

Fig. 1.3 Motion planning levels of complexity

Manoeuvring objects range from point mass robots to deformable or articulated ones. The more degrees of freedom (DOF) associated with manoeuvring objects, the greater the complexity of the MP problem. Object dynamic properties have a large influence on the degree of complexity of MP problem. Static objects are much easier to handle as their positions are known, whereas moving objects add more variables to the MP problem. Finally, the types of constraints, holonomic or nonholonomic, affect the number of DOF required to represent the system. Holonomic constraints reduce the number of DOF associates with the obstacles, whereas nonholonomic constraints that depend on velocity and position do not affect the number of DOF (Latombe, 1991). Lastly, bounded forces and torques are required and affect the choice of MP algorithm as real actuators can saturate.

A general review of MP algorithms is discussed in the following sections. Motion planning problem is solved within different spaces such as the Cartesian (physical or task) space or configuration space. Motion parameters in the Cartesian space are defined through position coordinates and orientation parameters such as Euler

angles, direction cosines, or quaternions. Since the rest of the thesis deals with Cartesian spaces, a brief discussion of the configuration space is introduced in the following section.

1.3 Configuration Space

Like real physical space, Configuration space (C-Space) is defined by a set of independent parameters or generalized coordinates, which describe the position of every point on the manoeuvring object at any time based on classical mechanics. For a point robot in three dimensions, the C-Space is identical to the physical space with the same number of DOF in $\Re^3$, while for N point robots the configuration space is $\Re^{3N}$. A rigid rod in 2D, for example, requires three parameters to represent the C-Space: two coordinates for the position of a reference point, which could be any point on the rod, and one angle representing the rod orientation about a perpendicular axis.

As an example of a three link mechanism, Figure 1.4 shows a possible set of generalized coordinates θ_1, θ_2 and θ_3. Each configuration in the workspace corresponds to a point in the C-space. Moreover, the motion of an articulated body appears as a curve in the C-Space. After generation of the C-Space, all MP problems are essentially identical.

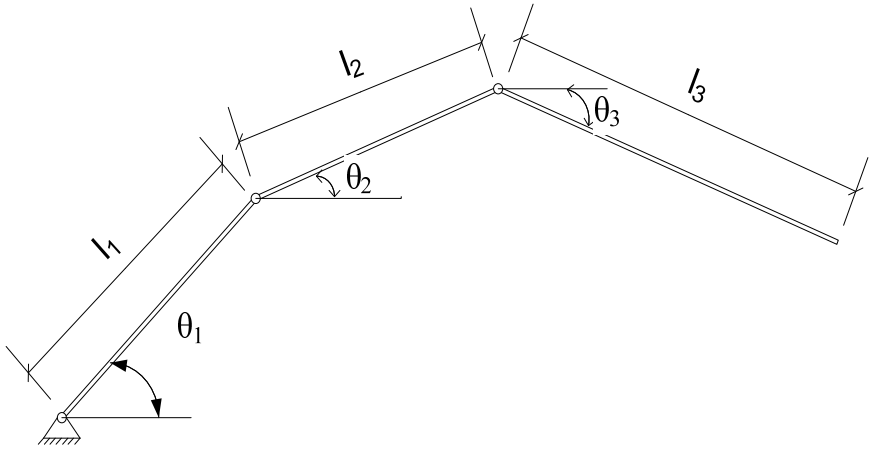

Fig. 1.4 Three link mechanism

Representing points of both manoeuvring objects and obstacles in C-Space determines whether collisions will occur. If any manoeuvring object point in C-Space lies inside any obstacle or any other manoeuvring object, then collision will occur. Furthermore, another case occurs when a point of any manoeuvring object lies on the boundary of any other object, so that smooth contact will occur. Many computational methods are able to search for C-Space collisions (Branicky and Newman, 1990; Hwang and Ahuja, 1992).

1.4 Motion Planning Methods

Large numbers of methods exist to solve the MP problem. However a few key methods are defined: skeleton, cell decomposition, potential field, mathematical programming, and boundary following methods. Designing a high performance motion planner usually requires the utilization of more than one MP approach such as combining the potential field method along with the cell decomposition method (Chiou et al., 1999). A brief discussion of key methods is provided before going on to discuss the potential field method. These approaches are either complete or incomplete. Completeness is defined as finding a path if it is exist, otherwise returning a failure. Incomplete approaches may terminate in a position other than the goal, such as a local minimum, but nevertheless the path exists. Complete algorithms may fail to find a solution if the resolution of the algorithm is not good enough to find a free path (Goldberg, 1994).

1.4.1 Skeleton (Roadmap)

All possible configurations are retracted into a network of one-dimensional lines, the roadmap, limiting the MP problem to graph-searching. Various methods are constructed which depend on this basic idea. For 2D problems, the visibility graph and the Voronoi diagram are commonly used.

The visibility graph, which is one of the earliest roadmap methods, was suggested by *Nilsson* (Nilsson, 1969) as a collection of lines connecting all polygonal obstacles vertices. They can be connected by lines without crossing another obstacle. The

shortest path will then be chosen as the optimum one between the start and goal point, as shown in Fig. 1.5.

The Voronoi diagram is used when it is required to maintain some distance between the manoeuvring object and obstacles. Constructing a Voronoi diagram is done through defining a set of points called nodes. These nodes are the intersecting points of equidistant contour lines surrounding the obstacles. The Voronoi diagram divides the space into regions with only one edge or polygon inside, as shown in Fig. 1.6.

More complexity arises when dealing with 3D MP problems using the visibility graph or the Voronoi diagram. A general method of constructing a skeleton in higher dimensions is constructed through a process called *Silhouette*. This process is based on projecting an object from a higher dimensional space to a lower one, and then tracing the boundaries. This operation could be repeated reaching a set of one-dimensional lines. A simpler Voronoi diagram for 3D objects has been discussed (Dattasharma and Keerthi, 1995). After generating enough free configurations, the roadmap is built by connecting them. This is a very efficient MP approach, especially when high number of DOF exist (Kavraki and Latombe, 1998).

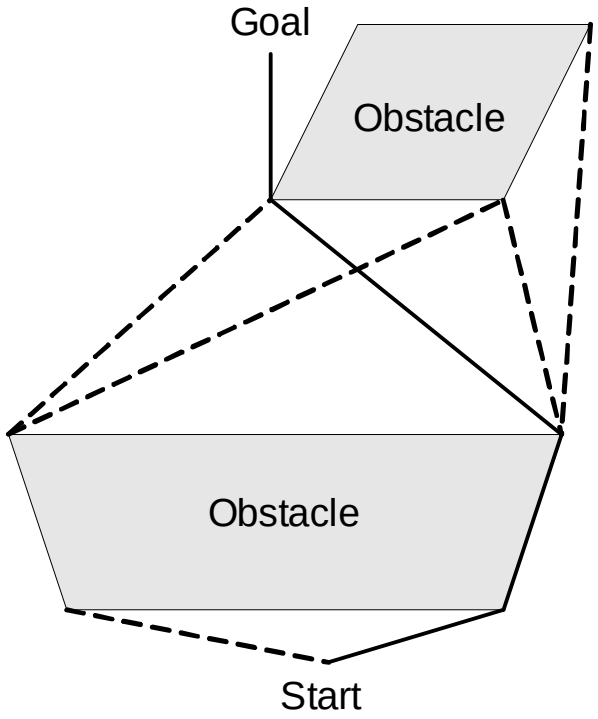

Fig. 1.5 The visibility graph

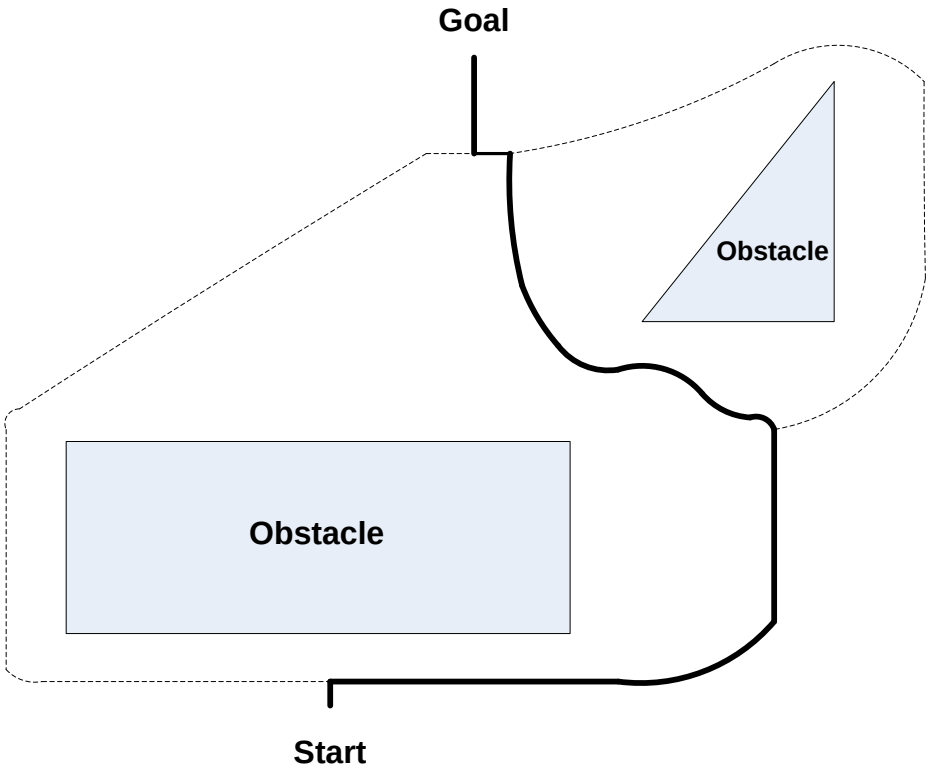

Fig. 1.6 The Voronoi diagram

The roadmap method has also been adapted to dynamic environments of both free-flying and articulated robots (Van den Berg and Overmars, 2005). A possible combination of the visibility graph and the Voronoi diagram is achieved through introducing the visibility graph into the Voronoi diagram (Wein et al., 2007).

1.4.2 Cell decomposition

In this method, the free C-Space is decomposed into simple adjacent regions, called *cells*. A free path connecting start and goal points is obtained through connecting the start and goal cells with continuous free cells, called a *connectivity graph.* Two ways are used to perform cell decomposition: exact and approximate cell decomposition.

Exact cell decomposition, *object dependent*, uses obstacles boundaries to form the cells whose union is the free space. This produces a smaller number of cells with higher computation complexity (Brock, 1999).

In approximate cell decomposition, *object independent*, methods a small, simple cell is chosen then tested whether it is a free cell or belongs to the configuration obstacles. The free space representation is strictly inclusive in the union of these small cells, however it does not represent the whole free space since the cells do not tightly enclose obstacles. Some cells may contain both free space and configuration obstacles; hence they could not be used to find a path (Brooks and Lozano-Pérez, 1982).

Cells lying entirely in the free space are used to construct the connectivity graph. If no connectivity graph is found, higher cell decomposition resolution might be a solution otherwise no free path exists between the initial and goal configurations (Latombe, 1991). Approximate methods are used initially to solve the MP problem, refining until a solution is found or no path is obtained. Cell decomposition is guaranteed to find a free path if exists, otherwise the algorithm returns failure.

1.4.3 Other methods

Other methods are defined such as: mathematical programming and boundary following methods. In mathematical programming, the free space is defined as a set of inequalities, then an optimum curve connecting the start and the goal position is found. Nonlinear programming is used to solve the motion planning problem by minimizing path length subject to constraints (Henrich, 1997).

The objective of the boundary following method is to command the manoeuvring object to move toward its goal in a straight line. In case of being obstructed by an obstacle, the manoeuvring object traces the obstacle edges. This approach is adapted to work with a scene filled with unknown obstacles of arbitrary shape and size. Data about the environment are collected on-line with sensors (Lumelsky and Stepanov, 1987).

1.5 Potential Field Methods

Many physical systems relax their configuration to attain the lowest possible energy state. This idea has been adopted and used in the motion planning algorithms for manipulators and robots as the artificial potential field method (Khatib, 1986).

Each location in the workspace has some scalar potential associated with it. The potential depends on the relative position between both goal and obstacles positions, and the manoeuvring object. A virtual attractive potential field representing a goal and virtual repulsive potential field representing obstacles are merged together to generate a global potential field, the gradient of which in principle provides a collision-free path to the goal. The method is widely used for autonomous mobile robot path planning in fixed workspaces where both target and obstacles are stationary. The method is also adapted to deal with moving obstacles (Tzafestas et al., 2002) and moving goal points through defining a potential function that is velocity dependent (Ge and Cui, 2002). The method is defined over both the Cartesian space and the configuration space (Barraquand et al., 1991). However, limitations of this simple and elegant approach arise when the superposition of the repulsive potential and attractive potential creates local minima. In addition motion oscillation in the presence of obstacles and in narrow passages, and the problem of trapping between two close obstacles also arise (Koren and Borenstein, 1991).

Another advantage of the potential field method appears in its unified approach to fulfil the MP problem, unlike other methods which divide it as seen in Fig. 1.1. The outputs of this method are geometrical, dynamical, and lead directly to a control law. A detailed description of this method is introduced in the subsequent sections as the rest of the thesis is implemented using the potential field method.

As the number of DOF increases, an exact solution of MP problem is ineffective (Sharir, 1997). When choosing potential field methods (PFM) to perform the MP process, an important question should be answered. Which PFM is most suitable for the current MP problem? The answer to this question is not a matter of choice, it mainly depends on the manoeuvring object, workspace, computational capabilities, convergence requirements and obstacle dynamic properties.

During the past three decades, many PFMs have been investigated. Some suggest how to represent obstacles; others define how to generate both attractive and repulsive potentials. The two main types of MP problems, global and local, both utilize potential field functions. The majority of the potential field methods use a local path planner such as: force involving artificial repulsion (FIRAS), Gaussian distribution, power law function, superquadric, and Newtonian potential (Chuang

and Ahuja, 1998), whereas harmonic potential functions and the navigation function are considered as global path planners. In local path planning, potential functions, both attractive and repulsive, are formed separately then added to form the global potential. This has on-line capability since no prior information about the workspace is required and the information is gathered whilst in motion. For global path planning potential functions all information about the workspace should be available from the start of the process, hence optimized paths can be obtained if these exist without local minima formation.

Other techniques such as the vector potential field and sliding mode theory are used. The vector potential field produces a smooth and bounded control. It can provide better performance compared to scalar field (Masoud and Bayoumi, 1993; Masoud and Masoud, 2000). Sliding mode theory is used with the potential field function to perform fast manoeuvres (Jan and Chiou, 2003).

The potential field method has also been developed for space applications in areas such as proximity manoeuvring (Roger and McInnes, 2000), large angle slew manoeuvres (McInnes, 1994; McInnes, 1995; McInnes, 1996; Radice and McInnes, 1999; Wisniewski and Kulczycki, 2005), formation-flying (McQuade et al., 2003; Avanzini et al., 2005a; Avanzini et al., 2005b), and autonomous and distributed motion planning for satellite swarms (Izzo and Pettazzi, 2005; Izzo and Pettazi, 2007). Other work has focused on the assembly of large, complex space structures using extensions of the potential field methodology (Badawy and McInnes, 2006c; Badawy and McInnes, 2006b; Badawy and McInnes, 2007c). Here the adjacency matrix of the graph of the final structure is used to form a global potential field (McQuade and McInnes, 1998). The structure can then be re-configured by modifying the adjacency matrix as required. A related approach has been used for the autonomous assembly of a group of homogeneous components by defining and summing vector fields which capture sets of behaviours. The final configuration of the system is defined by the equilibrium state of the dynamical system formed by the vector fields, in a similar manner to the global minimum of an artificial potential field (Izzo et al., 2005).

1.5.1 Force involving artificial repulsion (FIRAS)

A region of obstacle influence is chosen for symmetrical obstacles, d_{min}, beyond which no effect of the obstacle potential occurs. A continuous differentiable function for obstacle potential is defined as:

$$V_{obs} = \begin{cases} \frac{1}{2} A \left(\frac{1}{d} - \frac{1}{d_{min}} \right)^2 & \text{if } d \le d_{min} \\ 0 & \text{if } d > d_{min} \end{cases} \tag{1.1}$$

where d is the shortest distance between the manoeuvring object and obstacle. The obstacle potential gain A and the minimum distance d_{min} are chosen according to the MP characteristics (Khatib, 1986). The FIRAS obstacle representation, Fig. 1.7.a, is simple as no difficult distance calculations are made. Unfortunately the local minimum problem occurs when superimposed with a spherical symmetric attractive potential, even for the case of a single flat sided object.

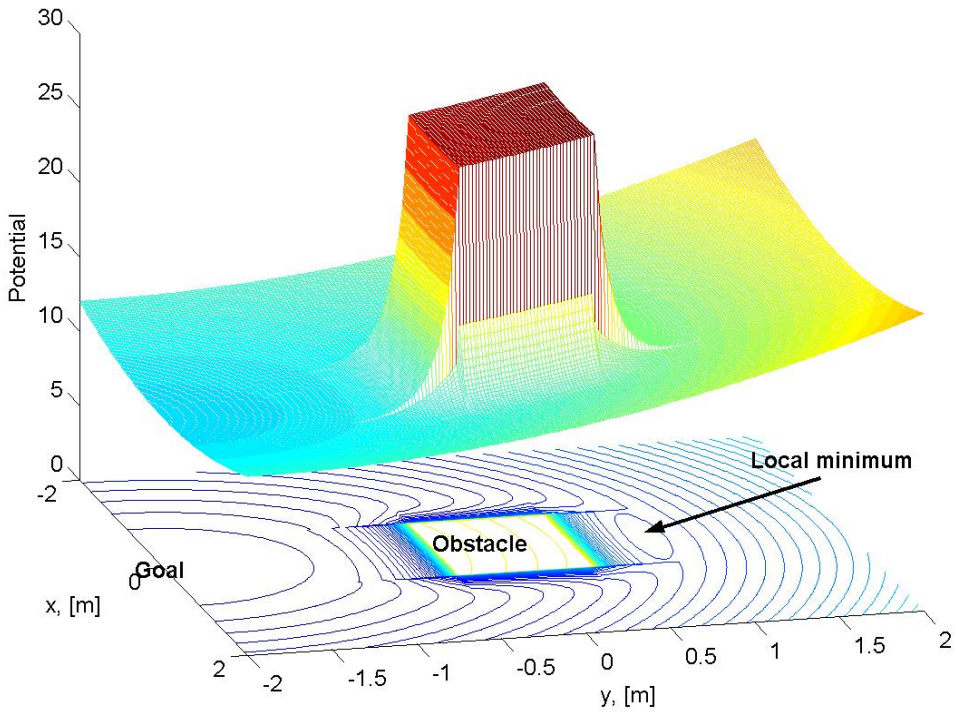

Fig. 1.7.a) Global potential with FIRAS rectangular obstacle representation

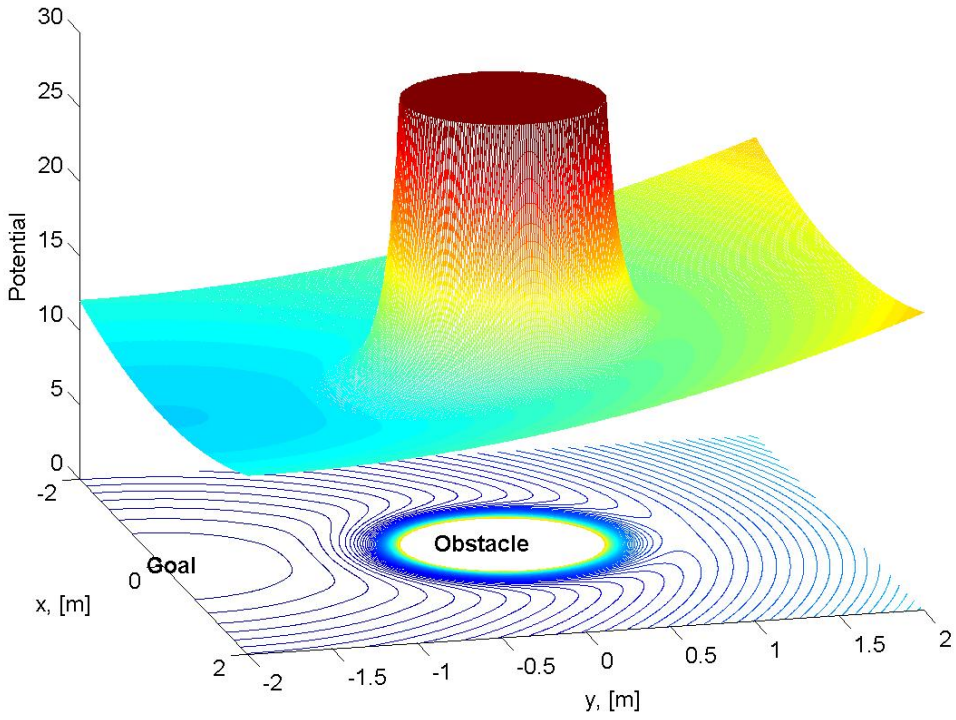

Fig. 1.7.b) Global potential with FIRAS circular obstacle representation

Another example of FIRAS obstacle representation, but with a circular edge obstacle, is shown in Fig. 1.7.b, with no local minimum formation. The spherical symmetry of both the attractive and the repulsive potential forms a field having no local minima in this case.

1.5.2 Gaussian function

Obstacle representation through a Gaussian potential function provides a region of high potential surrounding the obstacle. This region should be chosen to prevent any manoeuvring object from colliding with the obstacle. Due to the symmetry of the Gaussian function, this region will be spherical regardless of the real obstacle shape. This spherical symmetry property coincides with that of the attractive potential well and consequently no local minimum forms due to a single obstacle. The obstacle potential is defined as (McQuade, 1997):

$$V_{obs} = A\,exp\left\{-\frac{1}{\sigma}\left|\mathbf{r}-\mathbf{r}_{obs}\right|^2\right\} \tag{1.2}$$

where σ is the width of the Gaussian function, $\mathbf{r}$ is the position vector of the manoeuvring object, and $\mathbf{r}_{obs}$ is the obstacle position vector. The repulsive amplitude A to ensure collision avoidance is shown to be:

$$A = \frac{\lambda\sigma\left(D+\left|\mathbf{r}_{obs}\right|-\left|\mathbf{r}_{G}\right|\right)}{2D\,exp\left\{-\frac{D^2}{\sigma}\right\}} \tag{1.3}$$

where λ is a scaling factor, $\mathbf{r}_G$ is the goal position vector, and D is the effective dimension of the obstacle which should be chosen to be larger than the actual obstacle size. Figure 1.8 shows the total potential function using the Gaussian function to represent an obstacle of 3 [m] effective dimension using the function width can be calculated as:

$$\sigma = D/3 \tag{1.4}$$

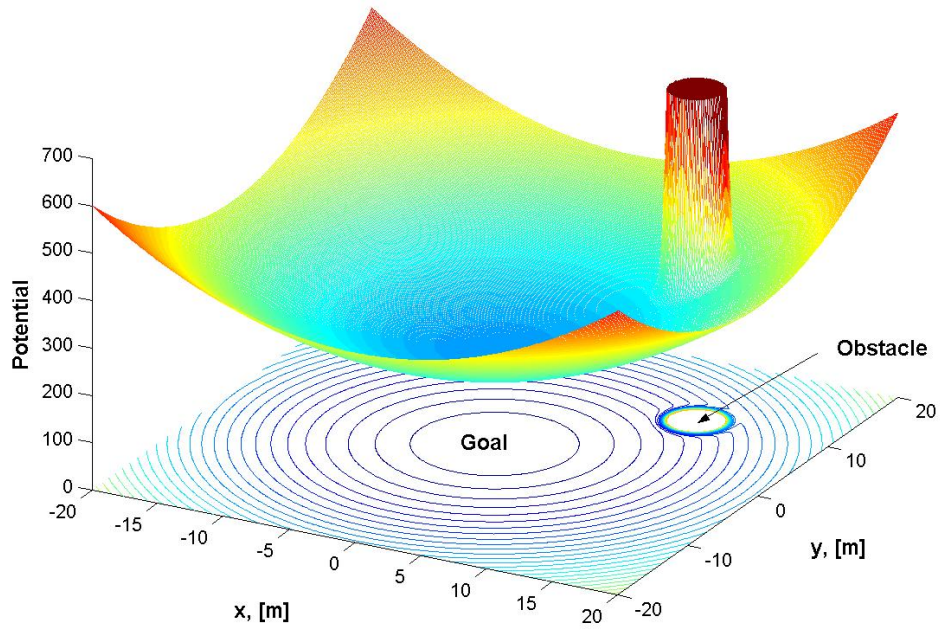

Fig. 1.8 Global potential with Gaussian obstacle representation

1.5.3 Power law function

This method defines another obstacle potential function similar to that of the Gaussian function without the exponential term. The obstacle is, again, enclosed by a spherical region. The obstacle potential is defined as (McQuade, 1997):

$$V_{obs} = \frac{A}{\left|\mathbf{r} - \mathbf{r}_{obs}\right|^{2N}} \tag{1.5}$$

The obstacle potential amplitude, A, is calculated the same manner as for the Gaussian function to set the saddle point on the obstacle surface. Then it can be shown that:

$$A = \frac{\lambda\left(D + \left|\mathbf{r}_{obs}\right| - \left|\mathbf{r}_{G}\right|\right)D^{2N+1}}{2N} \tag{1.6}$$

The obstacle effective dimension, D, depends on the exponent N. This controls the sharpness of the obstacle potential. The total potential function is shown in Fig. 1.9.

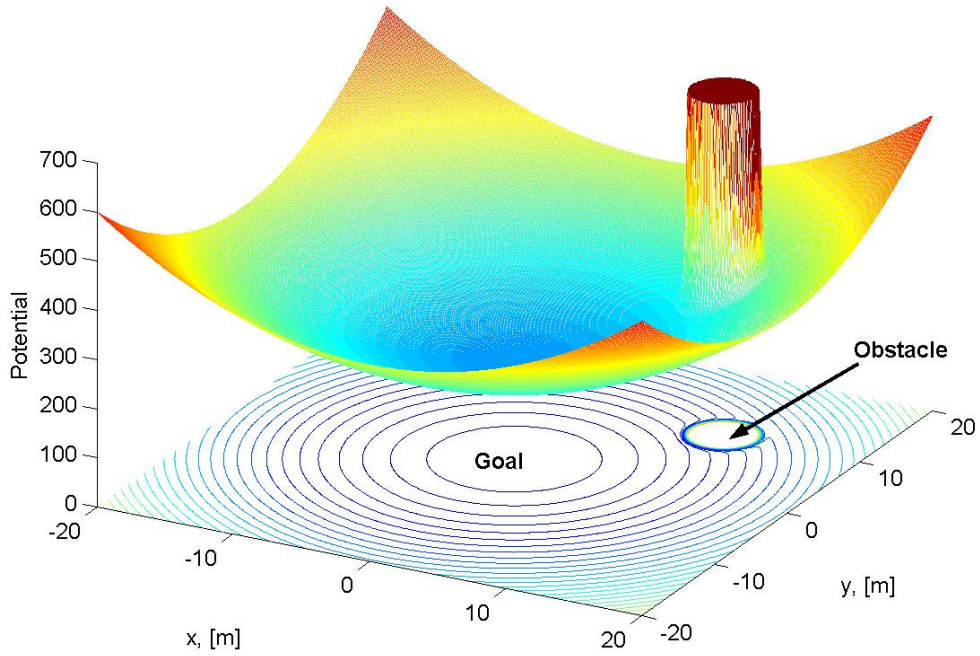

Fig. 1.9 Global potential with power law obstacle representation, N = 10

1.5.4 Superquadric functions

As explained for the FIRAS function, local minimum formation due to a single obstacle occurs due to the superposition of two different isopotential contour lines, due to the existence of straight edge objects. These objects, along with objects of general shapes, exist in many MP problems such as the autonomous assembly problem which is under investigation in this thesis.

Superquadric functions are able to represent almost all shapes in a relatively simple manner. They divide the space into three parts: inside, on-surface, and outside, and form a solid model of objects (Barr, 1981). These solid models can be added together to form more complicated objects (Krivic and Solina, 1993; Solina et al., 1994).

Limitations on superquadric usage in MP problems are mainly due to the possibility of local minimum occurrence in the presence of multiple obstacles, while the absence of local minimum is guaranteed in the presence of one obstacle only (Lee, 2004). A detailed explanation and enhancement of this method will be presented in the subsequent chapters as it is the main core of the thesis.

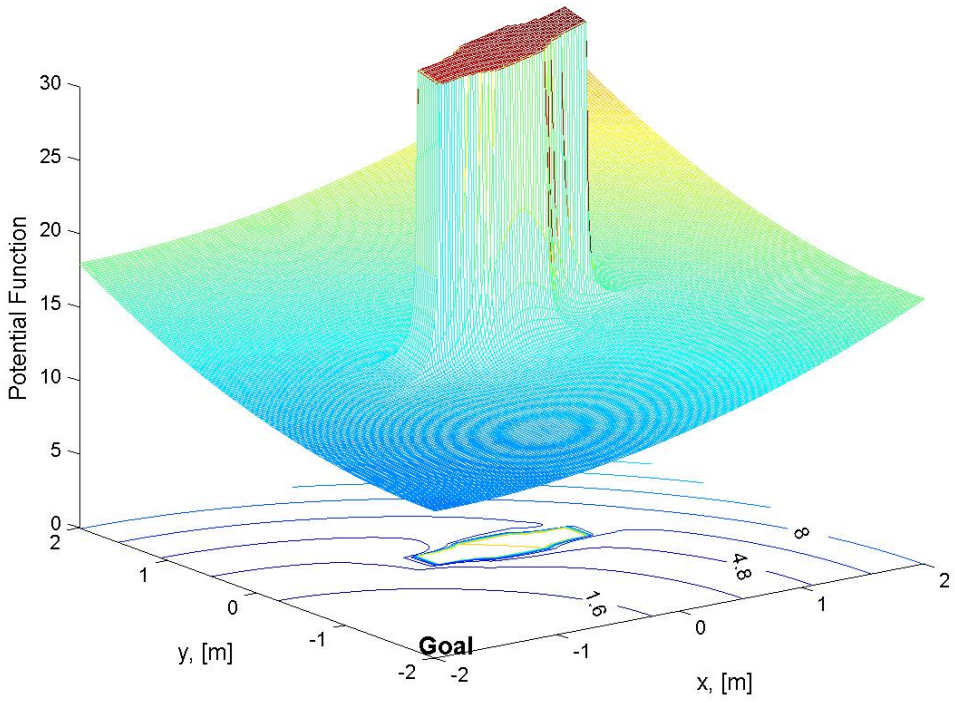

Fig. 1.10 Global potential with superquadric obstacle representation

1.5.5 Harmonic potential functions

The use of the harmonic potential functions will completely eliminate local minima formation even in a highly cluttered environment. Obstacle representation can be through a panel method, which was originally used to solve the potential fluid flow problem around an arbitrary object. The obstacle repulsion is represented as an outward normal flow, while the goal attraction appears as a uniform flow to simulate the potential field (Kim and Khosla, 1992).

The manoeuvring object velocity may reach zero at a point rather than the goal point, a stagnation point, but this point is not stable. The stagnation, saddle point may lie on the obstacle itself, hence increasing the panel strength will push the saddle point away. Although, the harmonic function does not have local minima, obstacle avoidance can not be guaranteed in a cluttered environment as the outward normal velocity may become negative on some points on the panel (Masoud and Masoud, 2002).

The Laplace artificial potential is also used to generate a local minima free field. The potential function has a maximum value of 1 and the desired goal configuration is assigned a value of 0. As the Laplace equation may not be solved in closed form, a discrete from is developed by a grid solver method (Connolly, 1990; Roger and McInnes, 2000).

1.5.6 Navigation functions

A navigation function is constructed in the C-Space and is considered as a global methodology, losing the simplicity of local MP but gaining the ability to form local minimum free paths. A deficiency of the navigation function is that convergence is not guaranteed from all initial configurations. Obstacles are usually modelled through disc-shape obstacle functions, but mapping from real world shapes to the circular disc-shape model is performed through a diffeomorphism operation (Rimon and Kodischek, 1992).

1.5.7 Fuzzy potential

Everywhere in the workspace, a manoeuvring object is affected by a scheme of repulsive and attractive potentials. Some of these potentials are not required for collision avoidance such as those from obstacles either away from the manoeuvring object or which do not intersect its path. In some case, even if a large obstacle is located near the manoeuvring object, but the manoeuvring object velocity vector is parallel to the obstacle edge, the potential is not required.

Fuzzy logic adds a variable to the potential function which is termed the *importance* variable. It is used to scale the effect of different obstacles according to a number of parameters: separation distance, separation angle, and robot speed (McFetridge and Ibrahim, 1998; Ta and Baltes, 2006).

1.6 Thesis Objectives

Building an MP algorithm that is able to control complex on-orbit assembly problems is the key goal of this thesis. Potential field methods are developed using superquadric repulsive potentials. The potential fields are developed for both impulsive and continuous motion control.

The complexity of the assembly problem considered in this thesis is highlighted in Fig. 1.3. Assembly of any structure involves the use of multiple objects with different shapes and sizes. As all objects under assembly are simultaneously in motion, and each is considered as an obstacle to others, the environment is considered dynamic. Manipulating objects of different shapes and sizes imposes a new demand on their modelling; hence the superquadric model is chosen for its ability to represent almost all solid models parametrically.

The key contribution of this thesis is the integration of translational and rotational motion through the use of quaternions to define the orientation of the superquadric potential fields. Analytic control laws are found which enable translation and/or rotation of multiple extended rigid bodies to a final goal configuration.

1.7 Thesis Organization

An introduction to various methods of motion planning has been discussed in *chapter one* emphasizing potential field methods and their components: attractive and repulsive potentials. Different forms of attractive potential are defined in *chapter two* using parabolic, conical, and a new hyperbolic function.

Defining the repulsive potential first requires an investigation of the mathematical formulation of the superquadric model which is described in *chapter three*. The original form of superquadric functions is not suitable for representing obstacles; hence some modification is needed through generating deformable superquadric surfaces from the geometric obstacle shape to a spherical shape.

The distance between two superquadric surfaces is then calculated in a new general form regardless the shape and size of the obstacle. Finally, obstacle representations of some common shapes are discussed such as, parallelepiped and beams.

Superquadric repulsive potentials are investigated in *chapter four* for parallelepiped and beam elements for both avoidance and approach potentials. The dependency of those potential on the separation distance is estimated for both types of objects whereas only the parallelepiped element is discussed in detail.

In *chapter five*, the global potential is formed for the first time in the thesis. Two different control schemes are introduced in this chapter: continuous control using low thrust propulsion and impulsive control using on/off thrusters. The stability analysis conducted depends on the chosen control strategy to find an appropriate control law. Examples of four manoeuvring objects; two plates and two disks which switch their positions simultaneously are presented at the end of each control strategy discussion.

The main objective of the thesis is presented in *chapter six*, where the on-orbit structural assembly idea is discussed. Impulsive and continuous control strategies are used with selected potential functions to assemble cube and truss structures. Natural orbital mechanics is added to the forced motion depending on the control strategy. Combinations of parabolic and conical attractive potentials are presented for continuous low thrust control followed by their substitution with a new hyperbolic attractive potential.

Large space structure assembly is also considered using the impulsive control strategy. This contains different object shapes with different sizes.

Orbital reconfiguration is discussed in *chapter seven* through two applications. Free-flyer manoeuvring near a larger space facility, the International Space Station (ISS), is considered first followed by reconfiguration of a space structure. This is conducted through disassembly of some objects and then reassembly of them in a different configuration to illustrate the power and flexibility of the method.

A final review and discussion of the work of the thesis is presented in *chapter eight*. The overall roadmap for the thesis is shown in Fig. 1.11.

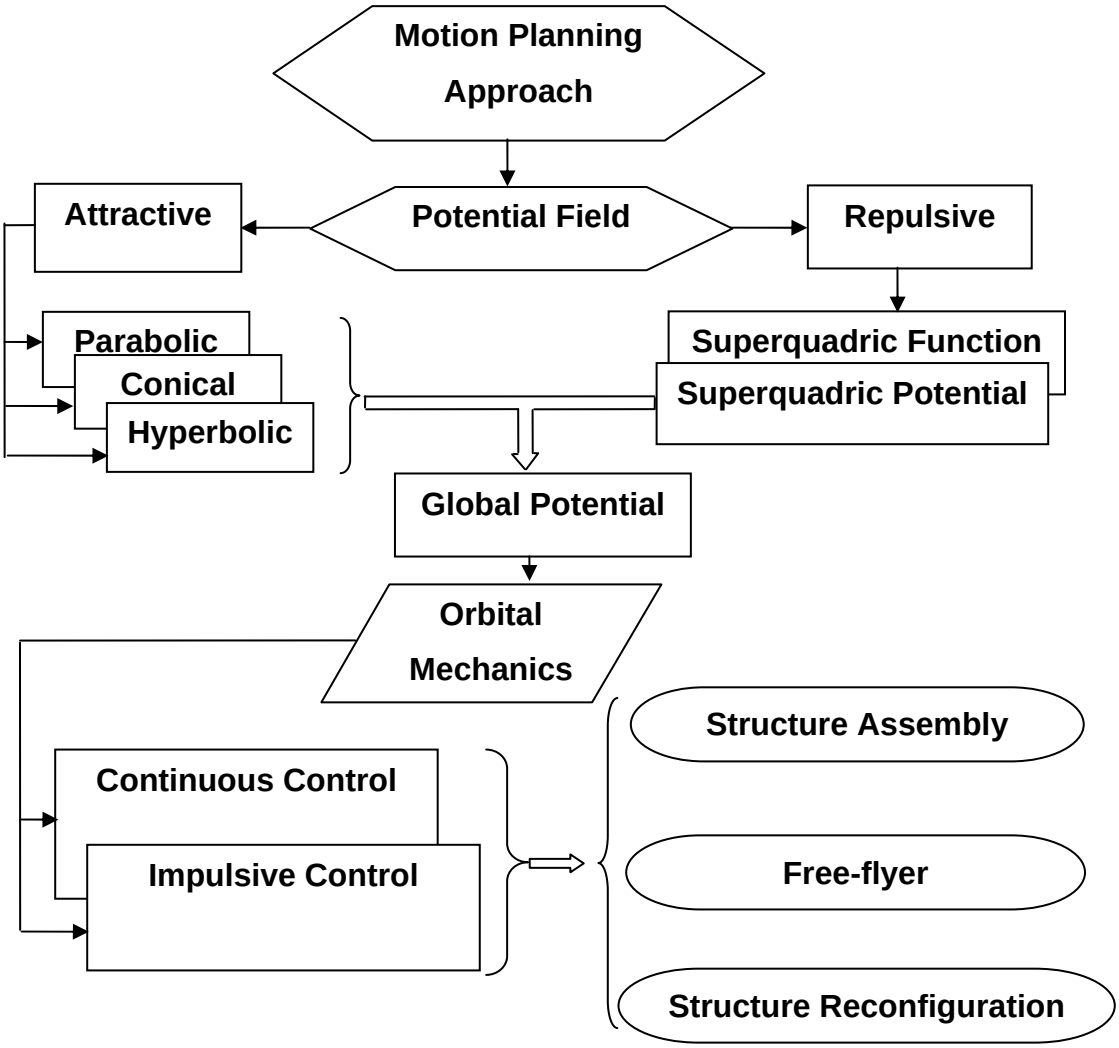

Fig. 1.11 Thesis roadmap

1.8 List of Publications

1. Badawy A. and McInnes C.R., "Separation Distance for Robot Motion Control using Superquadric Obstacle Potentials", International Control Conference, Glasgow, Scotland, 2006, paper no. 25.
2. Badawy A., and McInnes C.R., "Autonomous Structure Assembly Using Potential Field Functions", 57th International Astronautical Congress, Valencia, Spain, 2006, IAC-06-C1.P.3.04.
3. Badawy A., and McInnes C.R., "On-Orbit Assembly Using Potential Fields", accepted for publication in The Journal of Guidance, Control, and Dynamics, submitted Nov. 2006.
4. Badawy A. and McInnes C.R., "Free Flyer Manoeuvring Round a Space Station", The Twelfth International Conference on Aerospace Science and Aviation Technology, ASAT-12, Cairo, Egypt, 2007, paper no. 36.
5. Badawy A. and McInnes C.R., "Robot Motion Planning using Hyperboloid Potential Functions", World Congress on Engineering, London, 2-4 July 2007, paper ICME 15.
6. Badawy A. and McInnes C.R., "Generalized Potential Function Approach for On-Orbit Assembly", 58th International Astronautical Congress, Hyderabad, India, 2007, IAC-07-C1.2.07.

2. ATTRACTIVE POTENTIAL FUNCTIONS

2.1 Introduction

Many physical systems relax their configuration to attain the lowest possible energy state. This idea has been adopted and used in motion planning algorithms for manipulators and mobile robots as the artificial potential field method (Khatib, 1986). Scalar potential field theory constructs an electric field resulting from a point charge. It then models how charged particles move under the influence of electrostatic fields. Spatial derivatives of scalar potential fields form vector fields. These spatially continuous vector fields then define the motive force acting on charged particles (Chuang, 1998).

For robot path planning, the attractive potential field is a function defined with the goal position at its global minimum. A manoeuvring object will then move down the gradient of the potential field towards this global minimum, and with a suitable dissipation function will come to rest. The goal configuration will be defined by both a goal position and orientation. The Euclidean distance between a manoeuvring object and the goal position is used to define the translational attractive potential while error quaternions are used to define a rotational attractive potential. In order to reach the global minimum of the attractive potential field, both a final position and orientation must be achieved. In the subsequent analysis it will be assumed that continuous torques are available for attitude control and both continuous and discrete impulses are available for translational control. Potential fields that are a function of position generate required velocities, whereas those that are a function of position and velocity generate required accelerations. This is similar to the configuration of agile robot free-flyers which use control moment gyros and pulsed thrusters for actuation.

The overall attractive potential is the summation of both the translational and rotational attractive potentials. The translational attractive potential aims to null the Euclidian distance between a manoeuvring object and its goal position, while the rotational attractive potential aims to null the error quaternion relative to the required final orientation.

In principle attractive potential functions should be defined to ensure convergence to the goal. The most common means of investigating such convergence is through the use of *Lyapunov* methods which consider convergence to be equivalent to nonlinear stability.

2.2 *Lyapunov*'s Stability Theorem

Lyapunov's stability theorems were developed at the end of the 19th century in the doctoral thesis of Russian mathematician *Alexander M. Lyapunov* in 1892 (Csáki, 1972; Sastry, 1999). His work discussed the general problem of nonlinear stability of motion and remained little known in the West, but now forms a key part of nonlinear control. Stability analysis of nonlinear systems was classified by *Lyapunov* into two groups:

1. Methods based on finding the solution of the system (linearization). Once the solution is found it is possible to determine whether the system is stable or not (from the system eigenvalues).
2. Methods which do not require a solution. The stability condition is then decided through the existence of a scalar function which satisfies *Lyapunov*'s conditions.

Deciding whether a system is stable or not without finding its solution is a very attractive idea, especially in many cases where no general method exists to find the solution of system of differential equations (nonlinear systems).

The *Lyapunov* method hinges of defining a scalar function which is analogous to the effective energy of the system. If, under certain conditions, it can be shown that the scalar *Lyapunov* function is monotonically decreasing, the stability (and convergence) is proven.

2.2.1 Definitions:

1. Consider a multivariable continuous function $V(\mathbf{x})$ which maps $\Re^n \to \Re$. It is considered positive definite if its value has positive sign over the region $\Re^n$.

   $V(0) = 0$ and $V(\mathbf{x}) > 0 \qquad \forall \mathbf{x} \in \Re^n - \{0\}$

2. Consider a multivariable continuous function $V(\mathbf{x})$ which maps $\Re^n \to \Re$. It is considered negative definite if its value has negative sign over the region $\Re^n$.

   $V(0) = 0$ and $V(\mathbf{x}) < 0 \qquad \forall \mathbf{x} \in \Re^n - \{0\}$

3. Consider a multivariable continuous function $V(\mathbf{x})$ which maps $\Re^n \to \Re$. It is considered positive semi-definite if its value has positive sign over the region $\Re^n$ and equal zero for some points other than the origin.

   $V(0) = 0$ and $V(\mathbf{x}) \geq 0 \qquad \forall \mathbf{x} \in \Re^n - \{0\}$

4. Consider a multivariable continuous function $V(\mathbf{x})$ which maps $\Re^n \to \Re$. It is considered negative semi-definite if its value has negative sign over the region $\Re^n$ and equal zero for some points other than the origin.

   $V(0) = 0$ and $V(\mathbf{x}) \leq 0 \qquad \forall \mathbf{x} \in \Re^n - \{0\}$

2.2.2 *Lyapunov*'s second theorem

Let $\mathbf{x} = \mathbf{x}_G$ be an equilibrium point for a system described by a set of differential equations $\dot{\mathbf{x}} = f(\mathbf{x})$. Let $V(\mathbf{x})$ be a real, continuously differentiable, positive definite scalar function that maps $\Re^n \to \Re$. Then if its time derivative $W(\mathbf{x})$ is negative definite, then $V(\mathbf{x})$ is asymptotically *Lyapunov* stable.

If a suitable *Lyapunov* function can be found, then *Lyapunov*'s theorem can be used to prove the nonlinear stability of an equilibrium point of a set of differential equations. This will be seen as equivalent to demonstrating convergence of a manoeuvring robot to a goal.

2.3 Translational Attractive Potential

Steady motion toward a goal position should be guaranteed by the translational attractive potential. It considers the manoeuvring object as a point mass translating towards the goal. The translational attractive potential is constructed according to the available sensed data as:

1. Position attractive potential, where only position information is needed to define the attractive potential, consequently defined as:

$$V_{att,trans} = \frac{\lambda_p}{m}\left|\mathbf{r} - \mathbf{r}_G\right|^m \tag{2.1}$$

2. Position and velocity attractive potential, where both should be sensed. This function can also be used in tracking problems as (Ge and Cui, 2000):

$$V_{att,trans} = \frac{\lambda_p}{m}\left|\mathbf{r} - \mathbf{r}_G\right|^m + \frac{\lambda_v}{n}\left|\dot{\mathbf{r}} - \dot{\mathbf{r}}_G\right|^n \tag{2.2}$$

These attractive potential functions are not differentiable with respect to $\mathbf{r}$ at $\mathbf{r} = \mathbf{r}_G$ for $0 < m \le 1$, and with respect to $\dot{\mathbf{r}}$ at $\dot{\mathbf{r}} = \dot{\mathbf{r}}_G$ for $0 < n \le 1$. If the exponents m and n are chosen as unity, a conic-well potential function is generated which gives constant control force throughout the workspace. However, singularity problems at the goal position are produced. If the exponents are chosen to be greater than unity, a parabolic-well is formed which generates a control force that increases with distance and is unbounded as $\left|\mathbf{r} - \mathbf{r}_G\right| \to \infty$.

A combination of parabolic and conic well potentials could be constructed to have the advantages of both through defining the first within some range from the goal position. Consequently, the control force remains bounded and avoids the singularity problem encountered when using the conic well. Beyond this range, the conic well is the best choice as the control force will be constant wherever the manoeuvring object is located (Latombe, 1991).

Different types of translational attractive potentials and their stability analysis will be discussed in the subsequent subsections before utilizing them in the global potential.

2.3.1 Parabolic-well

The parabolic-well attractive potential is used in many applications where only position information is sensed. Two possible MP methods are derived using this function. The first solves for the control force, whereas the second solves for the required velocity considering an ideal controller for both of them. To be able to use the function proposed in Eq. (2.1) with the exponent $m = 2$ as a potential function, it should satisfy *Lyapunov*'s conditions, Fig. 2.1. A positive definite parabolic potential is then defined as:

$$V_{att,trans} = \frac{\lambda_p}{2}(\mathbf{r} - \mathbf{r}_G).(\mathbf{r} - \mathbf{r}_G) \tag{2.3}$$

The time derivative of the proposed function, $W_{att,trans}$ will be:

$$W_{trans} = \boldsymbol{\lambda}_p \dot{\mathbf{r}}.(\mathbf{r} - \mathbf{r}_G) \tag{2.4}$$

Let k be a positive function such that the manoeuvring object velocity is defined as (Casasco and Radice, 2003):

$$\dot{\mathbf{r}} = -k \frac{\nabla V_{att,trans}}{|\nabla V_{att,trans}|} \tag{2.5}$$

where

$$\nabla = \lceil \partial/\partial x \;\; \partial/\partial y \;\; \partial/\partial z \rceil^T \tag{2.6.a}$$

and

$$k = v_{max}\left(1 - e^{-\beta V_{att,trans}}\right) \tag{2.6.b}$$

Using the previous relations, it is concluded that W_{trans} is negative definite as:

$$W_{trans} = -\boldsymbol{\lambda}_p v_{max}\left(1 - e^{-\boldsymbol{\beta} V_{att,trans}}\right)(\mathbf{r} - \mathbf{r}_G).\frac{(\mathbf{r} - \mathbf{r}_G)}{|\mathbf{r} - \mathbf{r}_G|} \tag{2.7}$$

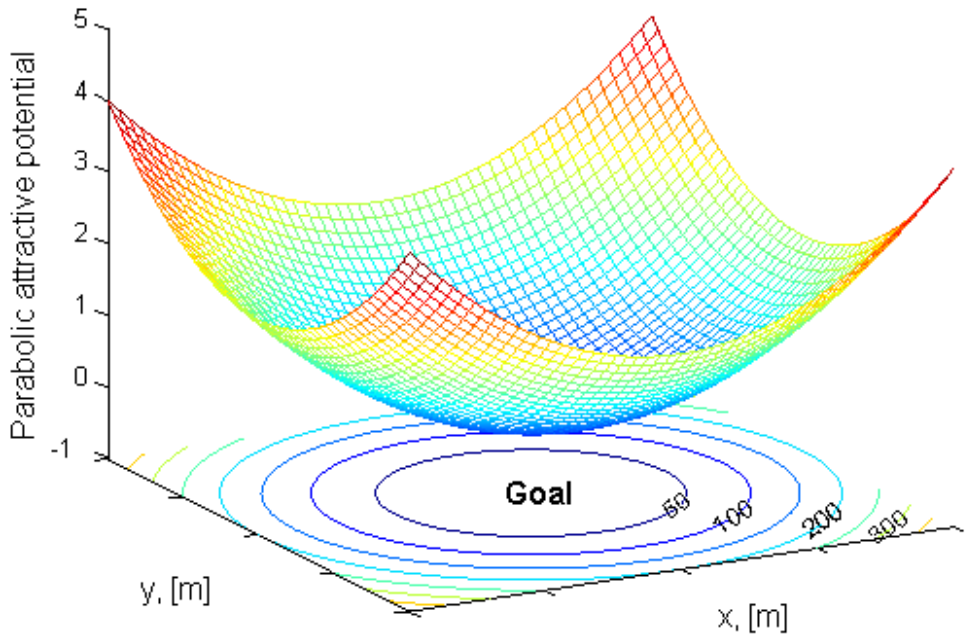

Fig. 2.1 Parabolic-well attractive potential

Using *Lyapunov*'s second theorem, the proposed function is a *Lyapunov* function, and consequently the solution of the given system is globally asymptotically stable with maximum controlled velocity v_{max}. The function k is used to shape the approach to the goal and to limit the velocity of the manoeuvring object. However, convergence to the goal is exponential.

Another definition for the function k which is adequate for close range that satisfies a bounded time approach to the goal point rather than exponential time is:

$$k = v_{max} \left| \mathbf{r} - \mathbf{r}_G \right| \tag{2.8}$$

This has some advantages over the function defined in Eq. (2.6.b).

2.3.2 Conic-well

The conic potential well is defined as in Eq. (2.1) with the exponent m = 1, Fig. 2.2. This definition ensures constant velocity over the entire workspace as the potential function is defined as:

$$V_{att,trans} = \lambda_p \sqrt{(\mathbf{r} - \mathbf{r}_G).(\mathbf{r} - \mathbf{r}_G)} \tag{2.9}$$

The time derivative of the proposed function will be:

$$W_{trans} = \boldsymbol{\lambda}_p \frac{\dot{\mathbf{r}}.(\mathbf{r} - \mathbf{r}_G)}{|\mathbf{r} - \mathbf{r}_G|} \tag{2.10}$$

The manoeuvring object velocity is defined from the gradient of the potential as:

$$\dot{\mathbf{r}} = -k \frac{\mathbf{r} - \mathbf{r}_G}{|\mathbf{r} - \mathbf{r}_G|} \tag{2.10}$$

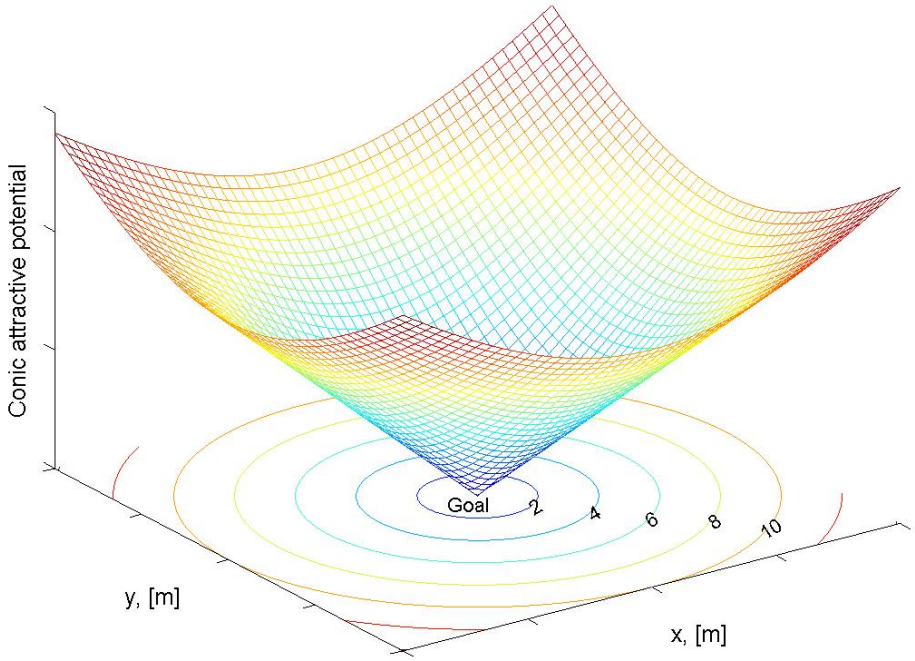

Fig. 2.2 Conic-well attractive potential

Again, the time derivative of the conic potential is shown to be negative definite as:

$$W_{trans} = -\boldsymbol{\lambda}_p k(\mathbf{r} - \mathbf{r}_G).\frac{(\mathbf{r} - \mathbf{r}_G)}{|\mathbf{r} - \mathbf{r}_G|} \tag{2.11}$$

As the conic-well is singular at the goal point, global stability is not ensured. Unlike the case of the parabolic well attractive potential, the manoeuvring object velocity at the goal is non-zero. Therefore, soft contact is not guaranteed (Ge and Cui, 2002).

2.3.3 Parabolic-well attractive potential with velocity term

An attractive parabolic potential including a velocity term using Eq. (2.2) is introduced by choosing m = 2, and n = 2 as:

$$V_{att,trans} = \frac{\lambda_p}{2}(\mathbf{r} - \mathbf{r}_G).(\mathbf{r} - \mathbf{r}_G) + \frac{\lambda_v}{2}\dot{\mathbf{r}}.\dot{\mathbf{r}} \tag{2.12}$$

In order to guarantee global stability, the time derivative should be negative definite so that:

$$W_{att,trans} = \lambda_p \dot{\mathbf{r}}.(\mathbf{r} - \mathbf{r}_G) + \lambda_v \dot{\mathbf{r}}.\ddot{\mathbf{r}} \tag{2.13}$$

The required manoeuvring object acceleration is then defined as:

$$\ddot{\mathbf{r}} = -\frac{\lambda_p}{\lambda_v}(\mathbf{r} - \mathbf{r}_G) - \lambda\dot{\mathbf{r}} \tag{2.14}$$

Substituting in Eq. (2.13) we obtain:

$$W_{att,trans} = -\lambda_v \lambda\, \dot{\mathbf{r}}.\dot{\mathbf{r}} \le 0 \tag{2.15}$$

The proposed function could be used as a potential function, but the acceleration is unbounded as the distance from the goal increases. In order to obtain smooth contact

at the goal position, this function is best used within a certain range around the goal. This range is proportional to the force capability of the actuators.

2.3.4 Conic-well attractive potential with velocity term

An attractive conic potential including a velocity term using Eq. (2.2) is introduced by choosing m = 1, and n = 2 as:

$$V_{att,trans} = \lambda_p \left|\mathbf{r} - \mathbf{r}_G\right| + \frac{\lambda_v}{2}\dot{\mathbf{r}}.\dot{\mathbf{r}} \tag{2.16}$$

The time derivative of the proposed potential function is:

$$W_{att,trans} = \lambda_p \dot{\mathbf{r}}.\frac{\mathbf{r} - \mathbf{r}_G}{\left|\mathbf{r} - \mathbf{r}_G\right|} + \lambda_v \dot{\mathbf{r}}.\ddot{\mathbf{r}} \tag{2.17}$$

To render $W_{att,trans}$ negative definite, the required acceleration is defined as:

$$\ddot{\mathbf{r}} = -\frac{\lambda_p}{\lambda_v}\frac{\mathbf{r} - \mathbf{r}_G}{\left|\mathbf{r} - \mathbf{r}_G\right|} - \lambda\dot{\mathbf{r}} \tag{2.18}$$

Substituting in Eq. (2.17) we obtain:

$$W_{att,trans} = -\lambda_v \lambda\, \dot{\mathbf{r}}.\dot{\mathbf{r}} \le 0 \tag{2.19}$$

Hence the proposed function in Eq. (2.16) is a *Lyapunov* function providing the acceleration is defined by Eq. (2.18). As can be seen from Eq. (2.18) the required acceleration remains bounded.

2.3.5 Hyperbolic attractive potential

The advantages of both the parabolic and conic potentials are merged in the hyperbolic attractive well. Stability at the goal point is guaranteed as its surface becomes smooth within some range from the goal, while the hyperboloid surface asymptotes to a cone away from the goal. Figure 2.3 shows the hyperbolic attractive potential for a manoeuvring object in 2D. The hyperbolic potential is defined as:

$$V_{att,trans} = \lambda_p \left(\sqrt{1 + (\mathbf{r} - \mathbf{r}_G).(\mathbf{r} - \mathbf{r}_G)} - 1 \right) \tag{2.20}$$

The time derivative of the proposed potential function is:

$$W_{att,trans} = \boldsymbol{\lambda}_p \dot{\mathbf{r}}. \frac{\mathbf{r} - \mathbf{r}_G}{\sqrt{1 + (\mathbf{r} - \mathbf{r}_G).(\mathbf{r} - \mathbf{r}_G)}} \tag{2.21}$$

To render $W_{att,trans}$ negative definite, the required velocity is defined as:

$$\dot{\mathbf{r}} = -k \frac{\mathbf{r} - \mathbf{r}_G}{\sqrt{1 + (\mathbf{r} - \mathbf{r}_G).(\mathbf{r} - \mathbf{r}_G)}} \tag{2.22}$$

Substituting in Eq. (2.21) we obtain:

$$W_{att,trans} = -\boldsymbol{\lambda}_v k \frac{(\mathbf{r} - \mathbf{r}_G).(\mathbf{r} - \mathbf{r}_G)}{1 + (\mathbf{r} - \mathbf{r}_G).(\mathbf{r} - \mathbf{r}_G)} \leq 0 \tag{2.23}$$

The proposed potential function therefore ensures convergence.

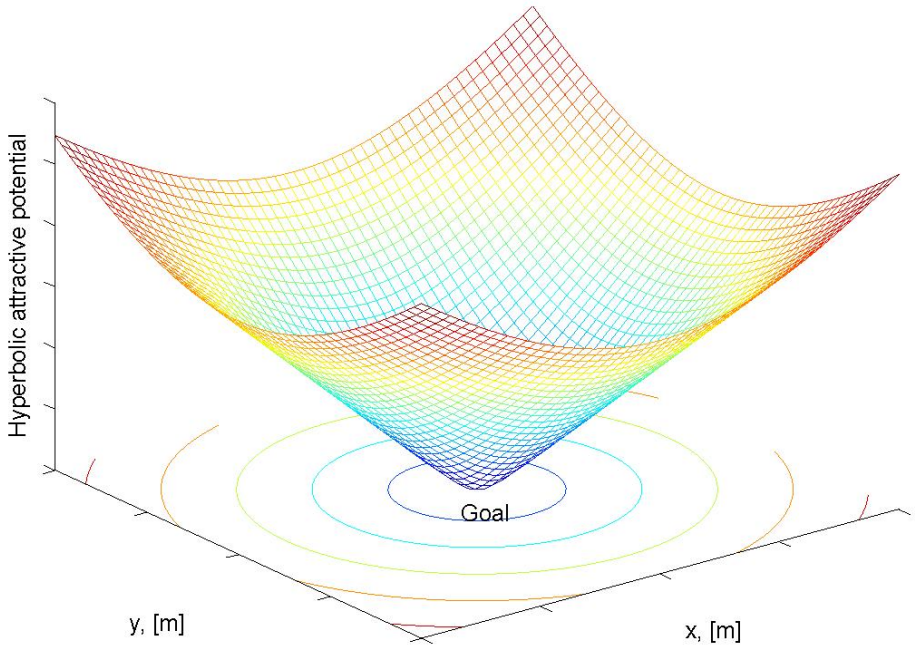

Fig. 2.3 Hyperbolic-well attractive potential

2.3.6 Hyperbolic attractive potential with velocity term

Adding a velocity term to Eq. (2.20) leads to a potential function suitable for acceleration control using:

$$V_{att,trans} = \boldsymbol{\lambda}_p \left(\sqrt{1 + (\mathbf{r} - \mathbf{r}_G).(\mathbf{r} - \mathbf{r}_G)} - 1 \right) + \frac{1}{2} \boldsymbol{\lambda}_v \dot{\mathbf{r}}.\dot{\mathbf{r}} \tag{2.24}$$

To derive the required acceleration, the time derivative of the proposed potential function is determined as:

$$W_{att,trans} = \lambda_p \dot{\mathbf{r}}. \frac{\mathbf{r} - \mathbf{r}_G}{\sqrt{1 + (\mathbf{r} - \mathbf{r}_G).(\mathbf{r} - \mathbf{r}_G)}} + \lambda_v \dot{\mathbf{r}}.\ddot{\mathbf{r}} \tag{2.25}$$

To ensure the time derivative function is negative definite the acceleration is then defined as:

$$\ddot{\mathbf{r}} = -\frac{\lambda_p}{\lambda_v} \frac{\mathbf{r} - \mathbf{r}_G}{\sqrt{1 + (\mathbf{r} - \mathbf{r}_G).(\mathbf{r} - \mathbf{r}_G)}} - \lambda \dot{\mathbf{r}} \tag{2.26}$$

which again remains bounded, but is smooth at the goal and non-singular.

2.4 Rotational Attractive Potential

In structural assembly, elements constituting the structure are defined as rigid bodies with various shapes and sizes. They must be assembled in a predefined configuration to form the final structure. Therefore, the translational attractive potentials must be augmented by rotational potentials. Before defining the rotational attractive potentials, methods of defining orientation are discussed in the following subsection.

2.4.1 Orientation definition

A) *Euler angles*

A scheme for orienting a rigid body to a desired attitude is called a body axis rotation. It involves three successive rotations about the axes of the rotated

body-fixed reference frame. The first rotation is about any of the three axes. The second is about any of the two axes that are not used in the first rotation. The third is about any of the axes that are not used in the second rotation. There are 12 sets of possible schemes defining so-called "Euler angles". The transformation matrix of Euler angles depends on the chosen rotation sequence (Wie, 1998).

B) *Direction cosines matrix*

A unit vector attached to a manoeuvring object has three components, which are equal to the cosines of the angles formed between the body and the inertial frame of reference. These angles are termed direction cosines and provide an alternative method to specify a unit direction vector.

C) Quaternions

Quaternions are a type of higher complex number first suggested by *William Hamilton* in 1843 (Quaternion, 2002). Quaternions have many important applications in mechanics, control, and space (Appendix A). The definition of orientation transformations in terms of quaternions instead of Euler angles has many advantages as:

1. The attitude estimation process with Euler angles is computationally more expensive as compared to quaternions (no trigonometric functions used in the transformation matrix).
2. Quaternions can define the minimal path of rotation between two reference frames, so that attitude manoeuvres with quaternions can be time optimal (Mukundan and Ramakrishnan, 1995).
3. Quaternions are more convenient to use for numerical computation since there is no singularity, which appears with Euler angles.

D) Error quaternions

Error quaternions, or unit quaternions, are the difference between the quaternion of an object and a reference quaternion. Hence at the reference

quaternion, the error quaternion is always $\lceil 0 \quad 0 \quad 0 \quad 1 \rceil^T$. The reference quaternion in our case is the goal orientation. Let the goal quaternion $\mathbf{q}_G = \lceil q_{g1} \; q_{g2} \; q_{g3} \; q_{g4} \rceil^T$, and the current quaternion $\mathbf{q}_c = \lceil q_{c1} \; q_{c2} \; q_{c3} \; q_{c4} \rceil^T$. The error quaternion will then be expressed as:

$$\begin{bmatrix} q_1 \\ q_2 \\ q_3 \\ q_4 \end{bmatrix} = \begin{bmatrix} q_{4g} & -q_{3g} & q_{2g} & q_{1g} \\ q_{3g} & q_{4g} & -q_{1g} & q_{2g} \\ -q_{2g} & q_{1g} & q_{4g} & q_{3g} \\ -q_{1g} & -q_{2g} & -q_{3g} & q_{4g} \end{bmatrix} \begin{bmatrix} q_{1c} \\ q_{2c} \\ q_{3c} \\ q_{4c} \end{bmatrix} \tag{2.27}$$

2.4.2 Rotational potential function

The rotational potential function will be expressed in terms of error quaternions, since they provide a direct relation between the current attitude and the goal attitude. The potential function is expressed as:

$$V_{att,rot} = \frac{\lambda_q}{2}(\overline{\mathbf{q}}.\overline{\mathbf{q}}) \tag{2.28}$$

where λ_q is constant, and $\overline{\mathbf{q}}$ is the vector of the error quaternion $\lceil q_1 \, q_2 \, q_3 \rceil^T$. The fourth quaternion parameter, $q_4 = \sqrt{1 - q_1^2 - q_2^2 - q_3^2}$, will reach its goal value, $q_4 = 1$, as the first three terms reach zero. The proposed function forms a *Lyapunov* function so that:

$$W_{att,rot} = \lambda_q \overline{\mathbf{q}}.\dot{\overline{\mathbf{q}}} \tag{2.29}$$

setting

$$\dot{\overline{\mathbf{q}}} = -k_q \frac{\nabla^q V_{att,rot}}{\left| \nabla^q V_{att,rot} \right|} \tag{2.30}$$

where $$\nabla^q = \lceil \partial/\partial q_1 \;\; \partial/\partial q_2 \;\; \partial/\partial q_3 \rceil^T \tag{2.31}$$

It can be seen from Eq. (2.29) and (2.30) that:

$$W_{att,rot} = -k_q \frac{\overline{\mathbf{q}}.\overline{\mathbf{q}}}{|\overline{\mathbf{q}}|} \leq 0 \tag{2.32}$$

The positive function k_q is chosen in the two possible ways discussed for the translational attractive potential for asymptotic or finite time approach as:

$$k_q = \omega_{max}\left(1 - e^{\beta_q |\overline{q}|^2}\right) \tag{2.33-a}$$

or

$$k_q = \omega_{max}|\overline{q}| \tag{2.33-b}$$

where ω_{max} is the maximum controlled angular velocity of the manoeuvring object.

2.4.3 Rotational potential function with angular velocity term

Consider a rigid body which performs pure rotation, with the body frame of reference aligned with the principal axes of inertia of the rigid body. The body rotates with angular velocity, $\boldsymbol{\omega} = \lceil \omega_1 \ \omega_2 \ \omega_3 \rceil^T$, with respect to the inertial frame of reference. The product moments of inertia vanish and the mass moment of inertia of the rigid body is constant. The inertia matrix, *I,* is then

$$I = \begin{bmatrix} I_1 & 0 & 0 \\ 0 & I_2 & 0 \\ 0 & 0 & I_3 \end{bmatrix} \tag{2.34}$$

The angular momentum, **H**, is then defined as:

$$\mathbf{H} = \mathbf{I}\boldsymbol{\omega} \tag{2.35}$$

with the external torque, **T**, acting on the rigid body defined as:

$$\mathbf{T} = \dot{\mathbf{H}} \tag{2.36}$$

$$\mathbf{T} = \mathbf{I}\dot{\boldsymbol{\omega}} + \boldsymbol{\omega} \times \mathbf{I}\boldsymbol{\omega} \tag{2.37}$$

The rotational attractive potential function will be defined as:

$$V_{att,rot} = \lambda_q \left(\bar{\mathbf{q}}^T \bar{\mathbf{q}}\right) + \frac{\lambda_\omega}{2} \boldsymbol{\omega}^T \mathbf{I} \boldsymbol{\omega} \tag{2.38}$$

where λ_ω is constant. The proposed function satisfies the condition of a *Lyapunov* function such as:

1. $V_{att,rot} = 0$ at the goal position where $\boldsymbol{\omega}$ and $\bar{\mathbf{q}}$ are both zero.
2. $V_{att,rot} > 0$ for every state vector except at the goal position.

The time derivative of the proposed function needs some discussion to prove that it is negative definite as the function itself is positive definite. The time derivative of the function $V_{att,rot}$ is defined as:

$$W_{att,rot} = 2\lambda_q \left(\dot{\bar{\mathbf{q}}}^{\mathbf{T}} \bar{\mathbf{q}}\right) + \lambda_\omega \boldsymbol{\omega}^{\mathbf{T}} \mathbf{I} \dot{\boldsymbol{\omega}} \tag{2.39}$$

The first derivative of the quaternion is however defined as (Wie, 1998):

$$\dot{\bar{\mathbf{q}}} = \frac{1}{2} \mathbf{Q} \boldsymbol{\omega} \tag{2.40}$$

where $\mathbf{Q}$ is the matrix of quaternion components and is defined as:

$$\mathbf{Q} = \begin{bmatrix} q_4 & q_3 & -q_2 \\ -q_3 & q_4 & q_1 \\ q_2 & -q_1 & q_4 \end{bmatrix} \tag{2.41}$$

Substituting in Eq. (2.39) it can be seen that

$$W_{att,rot} = \boldsymbol{\lambda}_q \boldsymbol{\omega}^{\mathbf{T}} \mathbf{Q}^{\mathbf{T}} \bar{\mathbf{q}} + \boldsymbol{\omega}^{\mathbf{T}} \mathbf{I} \dot{\boldsymbol{\omega}}$$

$$W_{att,rot} = \boldsymbol{\omega}^{\mathbf{T}} \left(\lambda_q \mathbf{Q}^{\mathbf{T}} \bar{\mathbf{q}} + \lambda_\omega \mathbf{I} \dot{\boldsymbol{\omega}}\right) \tag{2.42}$$

Simplifying the term $\mathbf{Q}^{\mathbf{T}} \bar{\mathbf{q}}$ it can be seen that:

$$\mathbf{Q}^{\mathbf{T}}\bar{\mathbf{q}} = \begin{bmatrix} q_4 & -q_3 & q_2 \\ q_3 & q_4 & -q_1 \\ -q_2 & q_1 & q_4 \end{bmatrix} \begin{bmatrix} q_1 \\ q_2 \\ q_3 \end{bmatrix} = q_4\bar{\mathbf{q}} \tag{2.43}$$

Then substituting for the time derivative of the proposed potential function Eq. (2.42), we obtain:

$$W_{att,rot} = \boldsymbol{\omega}^{\mathbf{T}}\left(\lambda_q q_4\bar{\mathbf{q}} + \lambda_\omega \mathbf{I}\dot{\boldsymbol{\omega}}\right) \tag{2.44}$$

and from Eq. (2.37) we obtain:

$$W_{att,rot} = \boldsymbol{\omega}^{\mathbf{T}}\left(\lambda_q q_4\bar{\mathbf{q}} + \lambda_\omega \mathbf{T} - \lambda_\omega \boldsymbol{\omega}\times\mathbf{I}\boldsymbol{\omega}\right) \tag{2.45}$$

The control torque, **T**, can therefore be defined as:

$$\mathbf{T} = -\frac{\lambda_q}{\lambda_\omega} q_4\bar{\mathbf{q}} - \lambda_\omega^*\boldsymbol{\omega} \tag{2.46}$$

where λ_ω^* is the total angular velocity gain. Substituting in Eq. (2.45) we obtain:

$$W_{att,rot} = \boldsymbol{\omega}^{\mathbf{T}}\left(-\lambda_\omega\lambda_\omega^*\boldsymbol{\omega} - \lambda_\omega\boldsymbol{\omega}\times\mathbf{I}\boldsymbol{\omega}\right) \tag{2.47}$$

However, $\boldsymbol{\omega}^{\mathbf{T}}\left(\boldsymbol{\omega}\times\mathbf{I}\boldsymbol{\omega}\right) = 0$ so that:

$$W_{att,rot} = -\lambda\boldsymbol{\omega}^{\mathbf{T}}\boldsymbol{\omega} \tag{2.48}$$

where λ is constant. It is now guaranteed that, $W_{att,rot} < 0$, is satisfied for all states except at the goal, so the proposed function can be considered as a *Lyapunov* function providing the following relation is valid:

$$\dot{\boldsymbol{\omega}} = -\mathbf{I}^{-1}\left(\lambda_q/\lambda_\omega\, q_4\bar{\mathbf{q}} + \lambda_\omega^*\boldsymbol{\omega} + \boldsymbol{\omega}\times\mathbf{I}\boldsymbol{\omega}\right) \tag{2.49}$$

where the ratio λ_q/λ_ω is the total rotation gain.

2.5 Global Attractive Potential

The overall attractive potential is the summation of both the translational and rotational attractive potentials. The translational attractive potential aims to null the Euclidian distance between a manoeuvring object and its goal position, while the rotational attractive potential aims to bring the error quaternion to $\lceil 0 \;\; 0 \;\; 0 \;\; 1 \rceil^T$, relative to the required final orientation. The attractive potential guides each extended manoeuvring object, considered as rigid body, toward its goal configuration, both in position and orientation through impulses or continuous force and continuous torque commands. The attractive potential is therefore defined as:

$$V_{att} = V_{att,trans} + V_{att,rot} \tag{2.50}$$

Adding a translational potential to a rotational potential in a single global potential field leads to full 6 degree-of-freedom manoeuvring control, as will be seen later. The controller is able to choose between translation and/or rotation to reach its goal (Badawy and McInnes, 2006b). Examples of global attractive potentials are presented in the following subsection using the two translational types of attractive potentials defined in Eqs. (2.1) and (2.2) along with the two types of rotational attractive potentials defined in Eqs. (2.28) and (2.38). The purpose of these examples is to demonstrate the convergence process of one manoeuvring object to its goal configuration.

2.5.1 Example I

The conventional parabolic-well attractive translational potential without a velocity term is introduced in this example along with the rotational attractive potential with the angular velocity term. Asymptotic convergence will be used to guarantee a bounded maximum velocity. The global attractive potential is defined as:

$$V_{att} = \frac{\lambda_p}{2}\left|\mathbf{r} - \mathbf{r}_G\right|^2 + \lambda_p\left(\bar{\mathbf{q}}^T\bar{\mathbf{q}}\right) + \frac{\lambda_\omega}{2}\boldsymbol{\omega}^T\mathbf{I}\boldsymbol{\omega} \tag{2.51}$$

Using Eqs. (2.5) and (2.6) the required object velocity is defined as:

$$\dot{\mathbf{r}} = -\lambda_p v_{max}\left(1 - e^{-\beta|\mathbf{r}-\mathbf{r}_G|^2}\right)\frac{\mathbf{r}-\mathbf{r}_G}{|\mathbf{r}-\mathbf{r}_G|} \qquad \text{if } W \geq 0 \tag{2.52}$$

while the required control toque is obtained from Eq. (2.46).

The initial object configuration is defined with a state vector as $[10\ 10\ 5,\ 0\ 0.7071\ 0\ 0.7071,\ 0\ 0\ 0]^T$, where the first three elements represent the Cartesian coordinates in an inertial frame of reference with respect to *x, y,* and *z* directions respectively, whereas the elements from four to seven are the initial quaternion parameters. These parameters represent an initial rotation of 90^o about the *y*-axis as discussed in Appendix A. Finally, the last three terms are the initial angular velocity vector which is null.

At the goal configuration, the manoeuvring object should come again to rest with a final configuration defined as $[1\ 0\ -2,\ 0\ 0\ 0.5\ 0.866,\ 0\ 0\ 0]^T$ where it will have a final rotation of 60^o with respect to the *x*-axis. The maximum controlled velocity is chosen to be 0.05 m sec^{-1}. The resulting manoeuvre is shown in Fig. 2.4. The overall cost of the translational motion is 0.10179 m sec^{-1}, while the manoeuvring object impulses are shown in Fig. 2.5. Moreover, Fig. 2.6 shows the rotational control parameters of the manoeuvring object. The total rotational gain is chosen to be 0.02, while the angular velocity gain is 0.5. The manoeuvring object is a cylinder of length 1 m, radius 0.1 m and mass 4 kg.

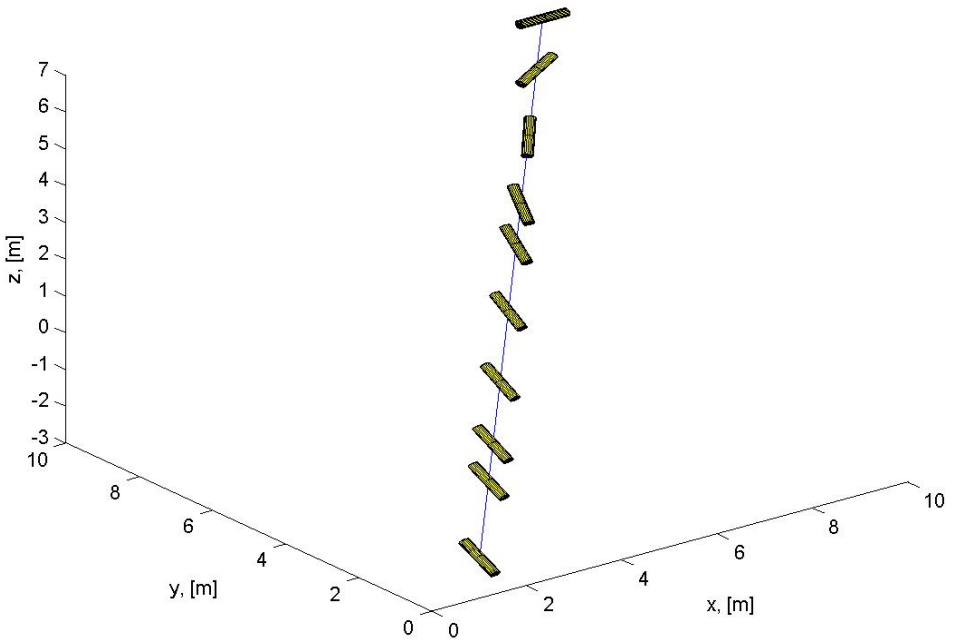

Fig. 2.4 Manoeuvring object motion in 3D

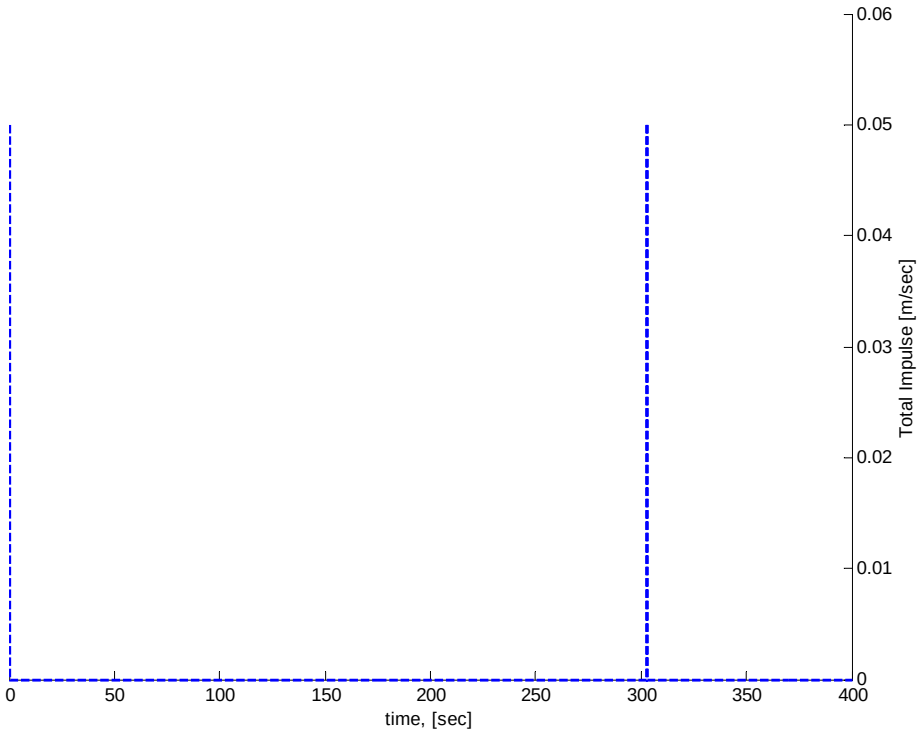

Fig. 2.5.a) Manoeuvring object total impulses

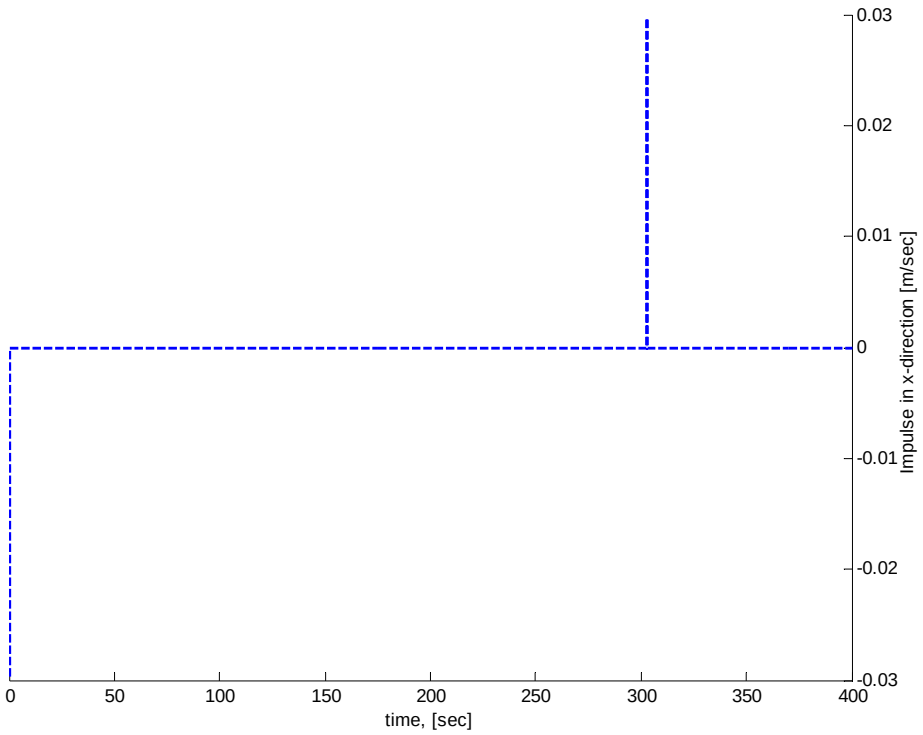

Fig. 2.5.b) Manoeuvring object impulses in the *x*-direction

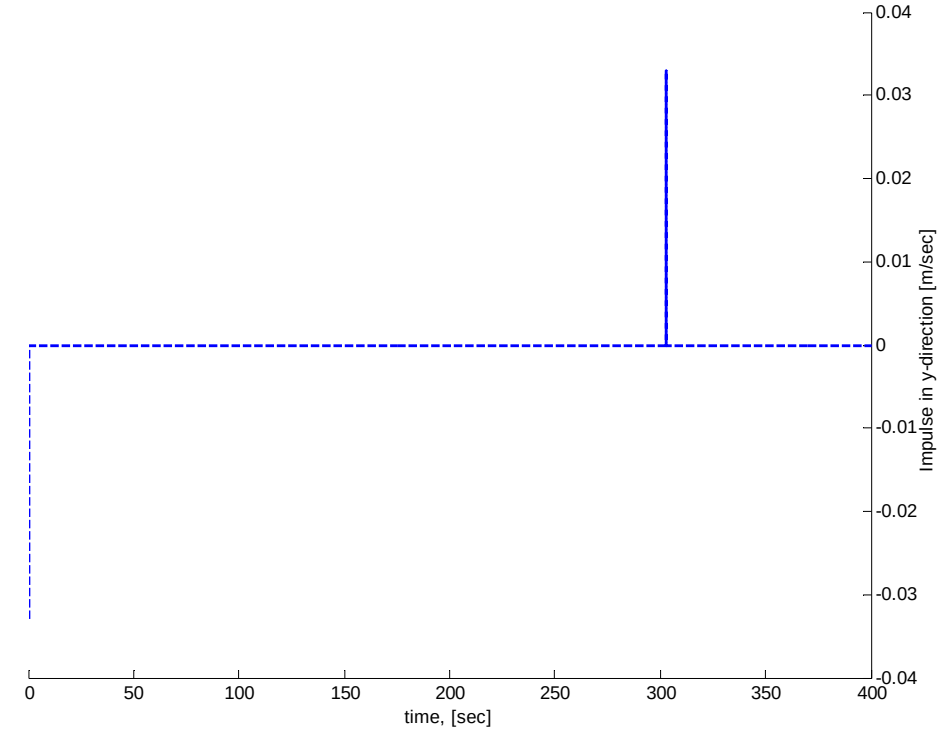

Fig. 2.5.c) Manoeuvring object impulses in the *y*-direction

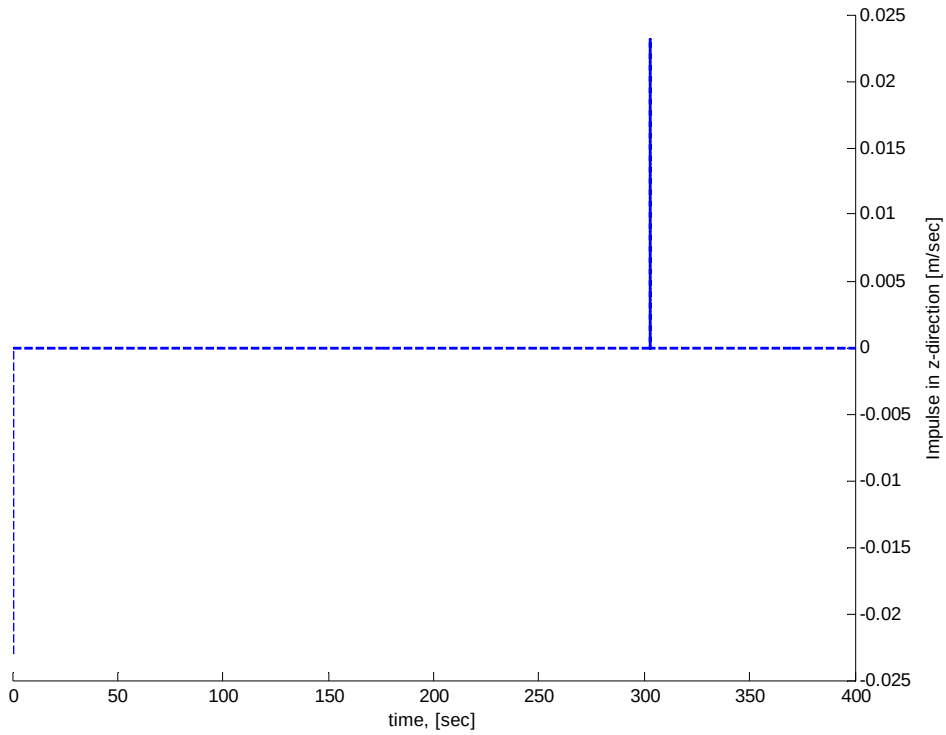

Fig. 2.5.d) Manoeuvring object impulses in the *z*-direction

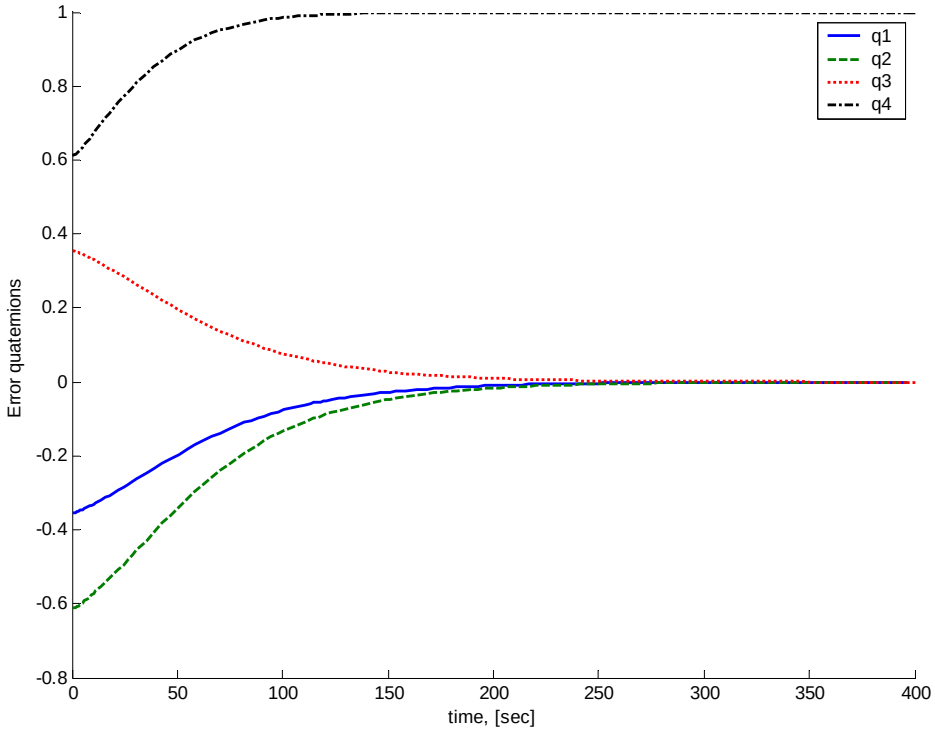

Fig. 2.6.a) Manoeuvring object error quaternion

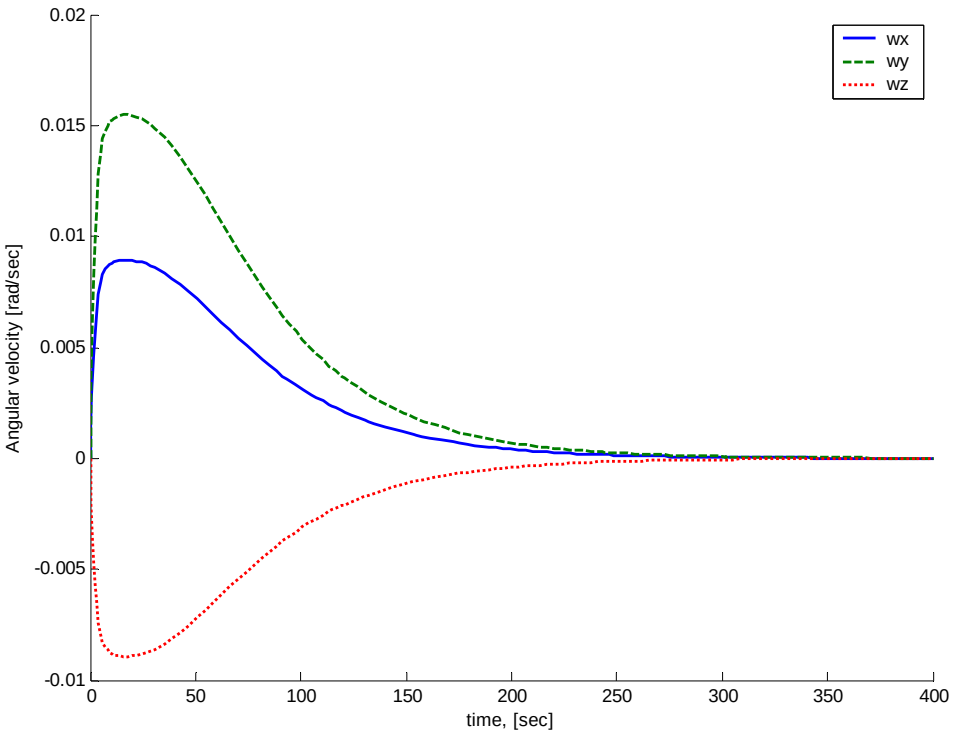

Fig. 2.6.b) Manoeuvring object angular velocities

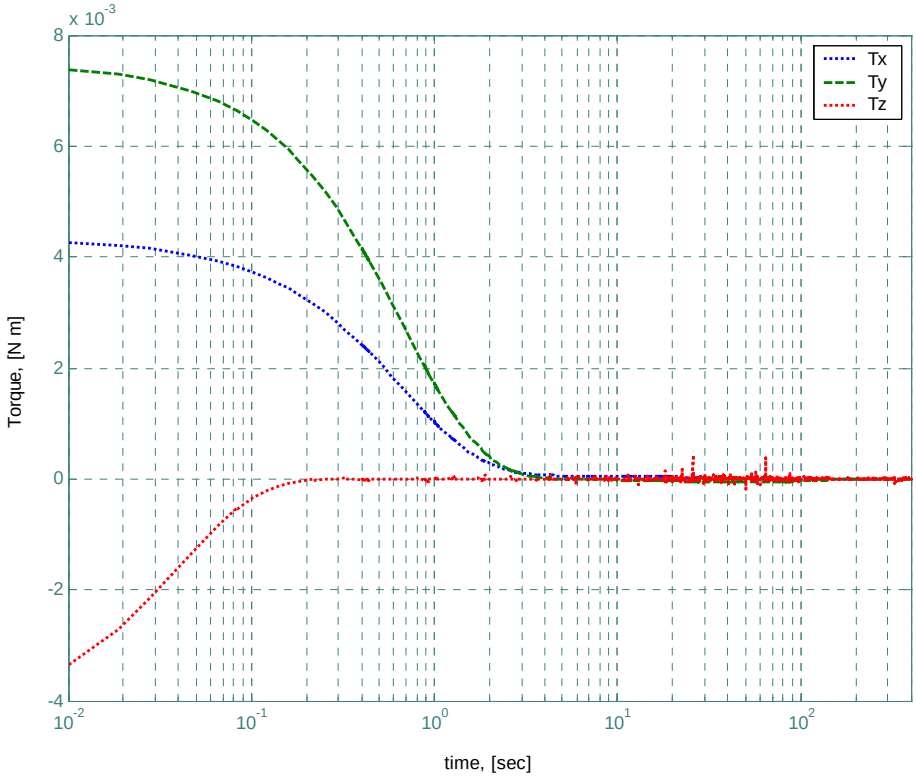

Fig. 2.6.c) Manoeuvring object torques

Since only one object moves in the workspace, its motion is similar to that of two-impulse motion: the first is used for motion initiation, while the second is used to null the manoeuvring object velocity as it reaches its goal position. As a result of momentum conservation, the two impulses are equal in magnitude, opposite in direction.

2.5.2 Example II

A more sophisticated potential function is introduced in this example as a combination of the parabolic and conical potential for translation control, and rotational potential with angular velocity. A different control law will be used in this example to show the flexibility of the potential field method. The proposed attractive potential function is defined as:

$$V_{att} = \begin{cases} \lambda_p \left|\mathbf{r}-\mathbf{r}_G\right| + 0.5\lambda_v \dot{\mathbf{r}}.\dot{\mathbf{r}} + \lambda_q \overline{\mathbf{q}}.\overline{\mathbf{q}} + 0.5\lambda_\omega \boldsymbol{\omega}.\boldsymbol{\omega} & \text{if } \left|\mathbf{r}-\mathbf{r}_G\right| > R \\ 0.5\lambda_p (\mathbf{r}-\mathbf{r}_G).(\mathbf{r}-\mathbf{r}_G) + 0.5\lambda_v \dot{\mathbf{r}}.\dot{\mathbf{r}} + \lambda_q \overline{\mathbf{q}}.\overline{\mathbf{q}} + 0.5\lambda_\omega \boldsymbol{\omega}.\boldsymbol{\omega} & \text{if } \left|\mathbf{r}-\mathbf{r}_G\right| \le R \end{cases} \quad (2.53)$$

The time derivative of the global potential is defined as:

$$W_{att} = \begin{cases} \dot{\mathbf{r}}.\left(\lambda_p (\mathbf{r}-\mathbf{r}_G)/\left|\mathbf{r}-\mathbf{r}_G\right| + \lambda_v \ddot{\mathbf{r}}\right) + 2\lambda_q \dot{\overline{\mathbf{q}}}.\overline{\mathbf{q}} + \lambda_\omega \dot{\boldsymbol{\omega}}.\boldsymbol{\omega} & \text{if } \left|\mathbf{r}-\mathbf{r}_G\right| > R \\ \dot{\mathbf{r}}.\left(\lambda_p (\mathbf{r}-\mathbf{r}_G) + \lambda_v \ddot{\mathbf{r}}\right) + 2\lambda_q \dot{\overline{\mathbf{q}}}.\overline{\mathbf{q}} + \lambda_\omega \dot{\boldsymbol{\omega}}.\boldsymbol{\omega} & \text{if } \left|\mathbf{r}-\mathbf{r}_G\right| \le R \end{cases} \quad (2.54)$$

Therefore from Eqs. (2.40) and (2.43) we obtain:

$$W_{att} = \begin{cases} \dot{\mathbf{r}}.\left(\lambda_p (\mathbf{r}-\mathbf{r}_G)/\left|\mathbf{r}-\mathbf{r}_G\right| + \lambda_v \ddot{\mathbf{r}}\right) + \boldsymbol{\omega}.\left(\lambda_q q_4 \overline{\mathbf{q}} + \lambda_\omega \dot{\boldsymbol{\omega}}\right) & \text{if } \left|\mathbf{r}-\mathbf{r}_G\right| > R \\ \dot{\mathbf{r}}.\left(\lambda_p (\mathbf{r}-\mathbf{r}_G) + \lambda_v \ddot{\mathbf{r}}\right) + \boldsymbol{\omega}.\left(\lambda_q q_4 \overline{\mathbf{q}} + \lambda_\omega \dot{\boldsymbol{\omega}}\right) & \text{if } \left|\mathbf{r}-\mathbf{r}_G\right| \le R \end{cases} \quad (2.55)$$

To set the time derivative of the potential function to be negative definite the control laws will be defined as in order to minimize Eq. (2.53):

$$\ddot{\mathbf{r}} = \begin{cases} -\left(\dfrac{\lambda_p}{\lambda_v}\dfrac{\mathbf{r}-\mathbf{r}_G}{\left|\mathbf{r}-\mathbf{r}_G\right|} + \lambda_v^* \dot{\mathbf{r}}\right) & \text{if } \left|\mathbf{r}-\mathbf{r}_G\right| > R \\ -\left(\dfrac{\lambda_p}{\lambda_v}(\mathbf{r}-\mathbf{r}_G) + \lambda_v^* \dot{\mathbf{r}}\right) & \text{if } \left|\mathbf{r}-\mathbf{r}_G\right| \le R \end{cases} \quad (2.56)$$

where λ_v^* is the velocity gain, while the rotational control law is then defined as:

$$\dot{\boldsymbol{\omega}} = -\left(\frac{\lambda_q}{\lambda_\omega} q_4 \overline{\mathbf{q}} + \lambda_\omega^* \boldsymbol{\omega} \right) \tag{2.57}$$

Using the same initial and goal configurations defined in example I with the parabolic zone radius equals 1 m, the results are illustrated in Fig. 2.7. The manoeuvring object velocities and accelerations are shown in Fig. 2.8. Constant linear velocities are obtained as a result of the new combination of the parabolic and conical attractive potentials. Rotational parameters are shown in Fig. 2.9 as the error quaternions, angular velocities, angular accelerations, and finally the required control torques. As a result of unequal mass moment of inertia about the three axes, the required torque about the *z*-axis is much less than those about *x* and *y*-axes.

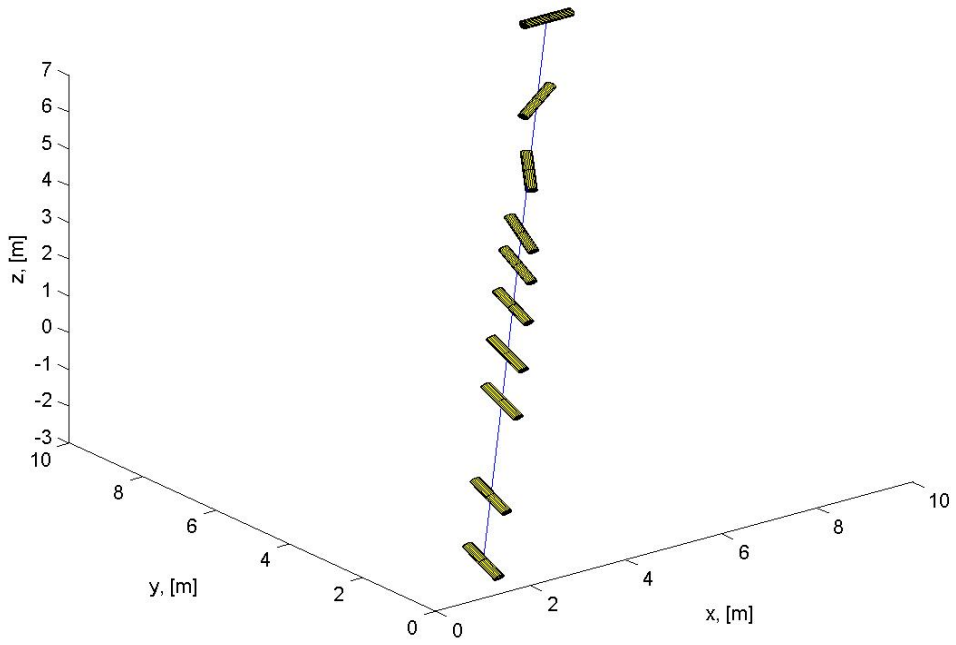

Fig. 2.7 Manoeuvring object motion in 3D

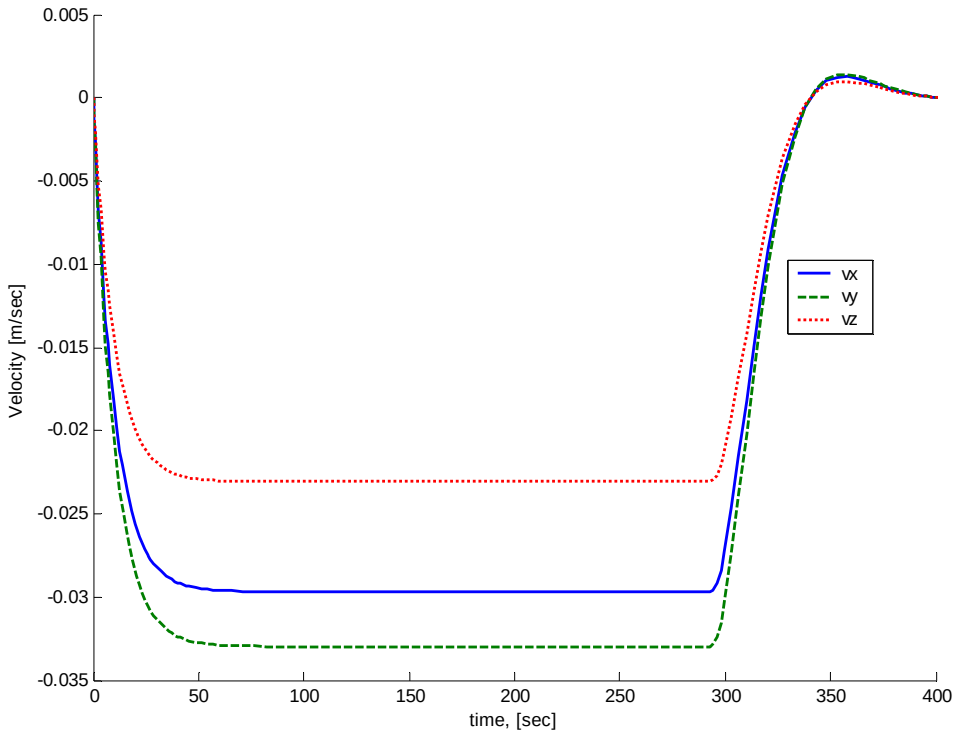

Fig. 2.8.a) Manoeuvring object velocity

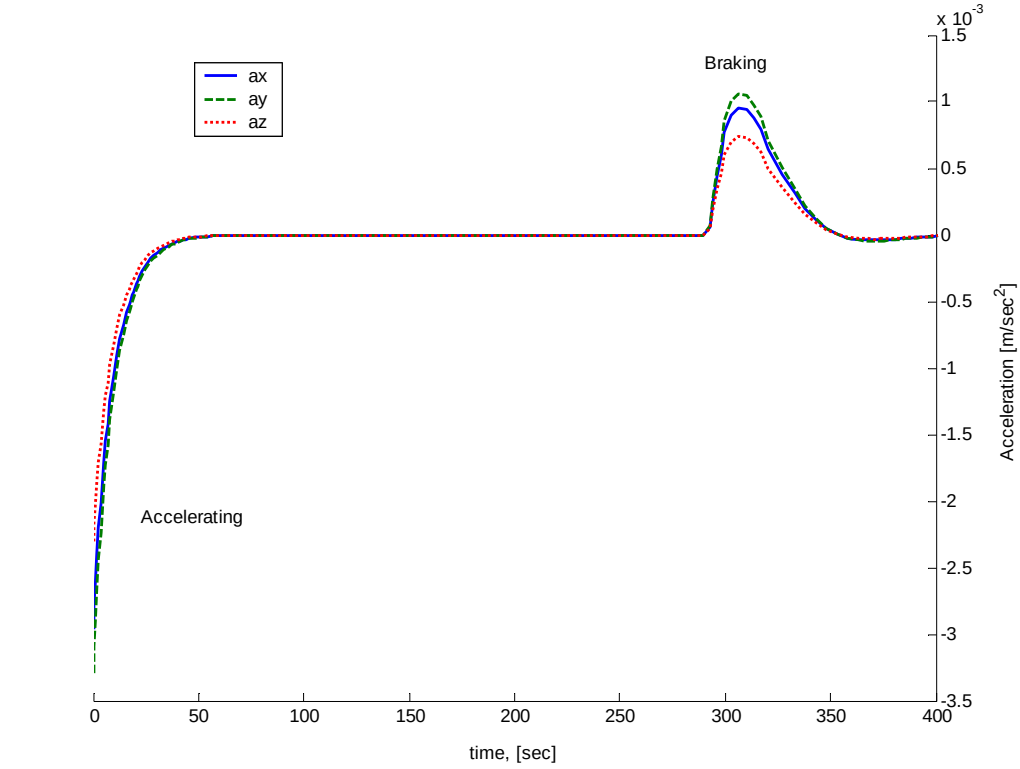

Fig. 2.8.b) Manoeuvring object acceleration

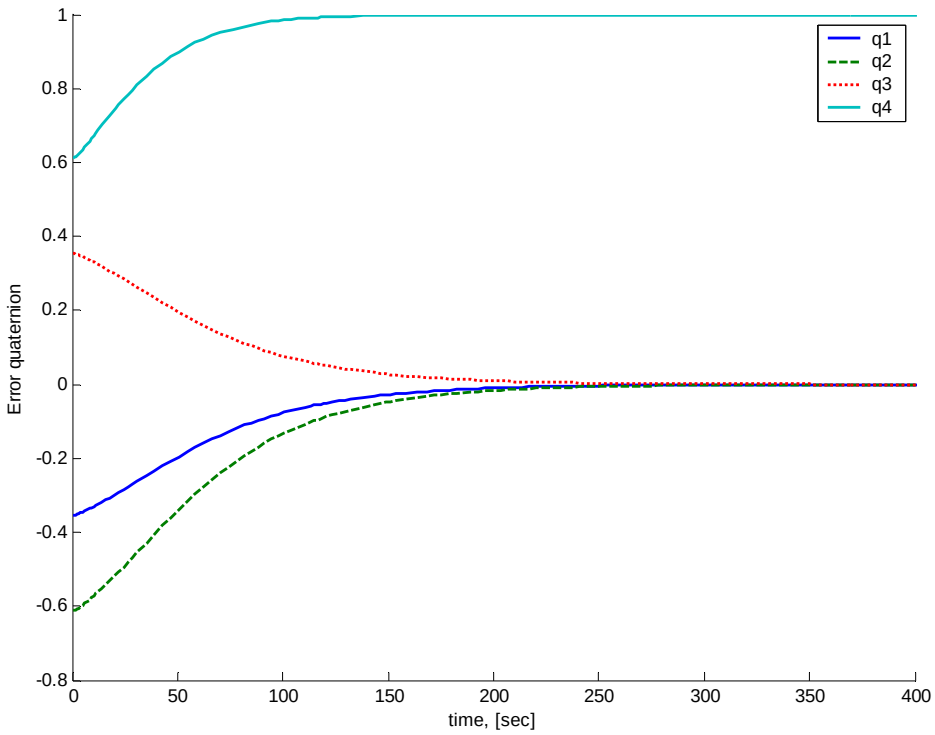

Fig. 2.9.a) Manoeuvring object error quaternions

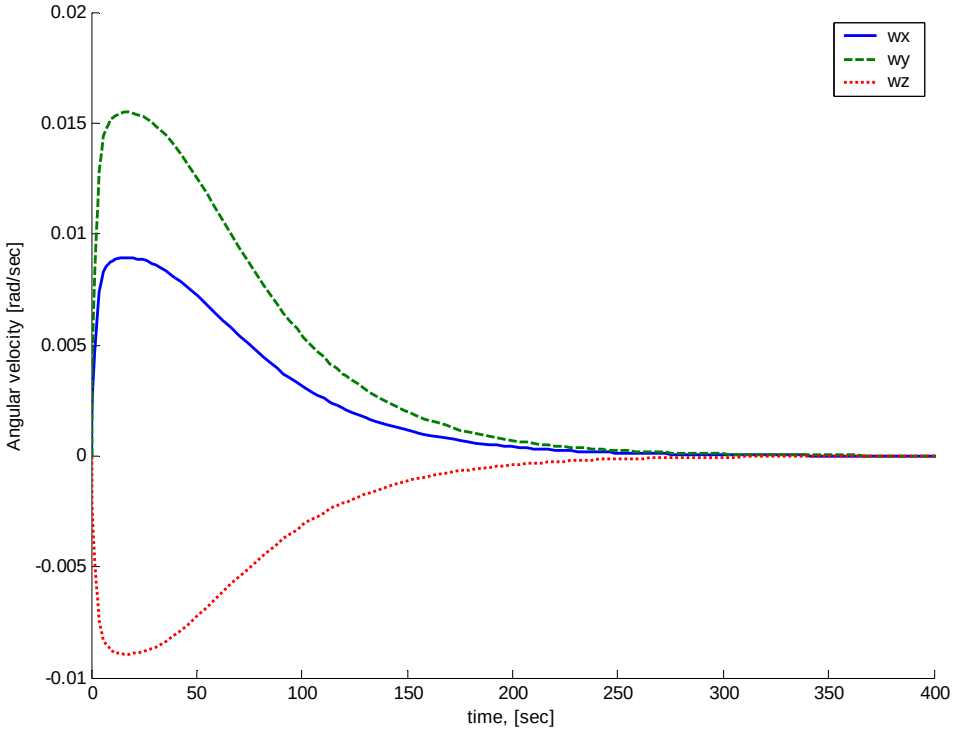

Fig. 2.9.b) Manoeuvring object angular velocity

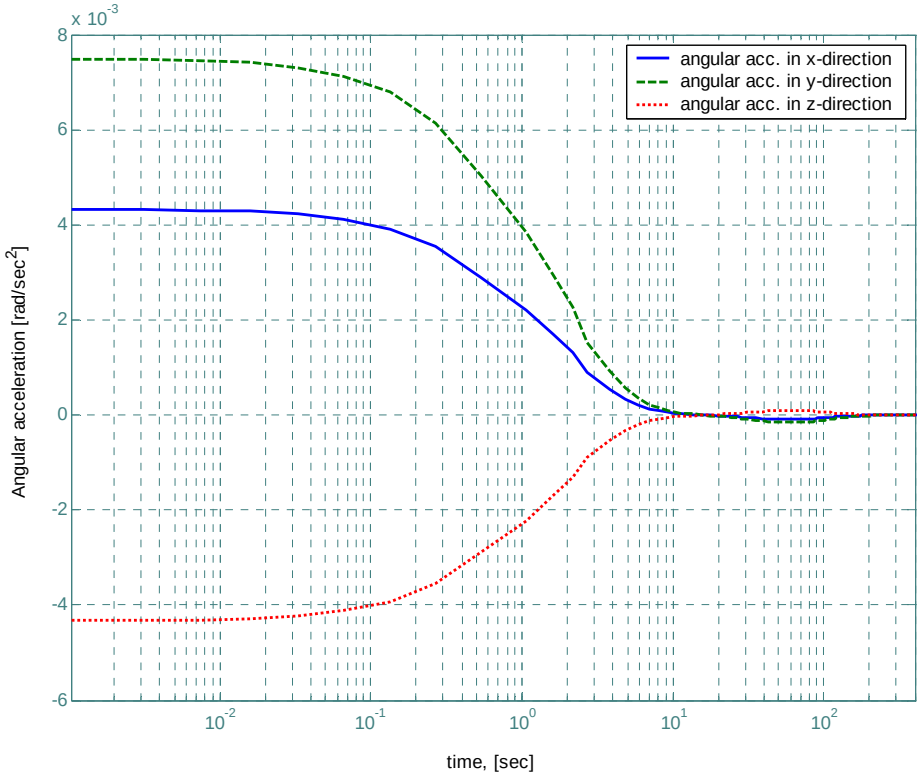

Fig. 2.9.c) Manoeuvring object angular acceleration

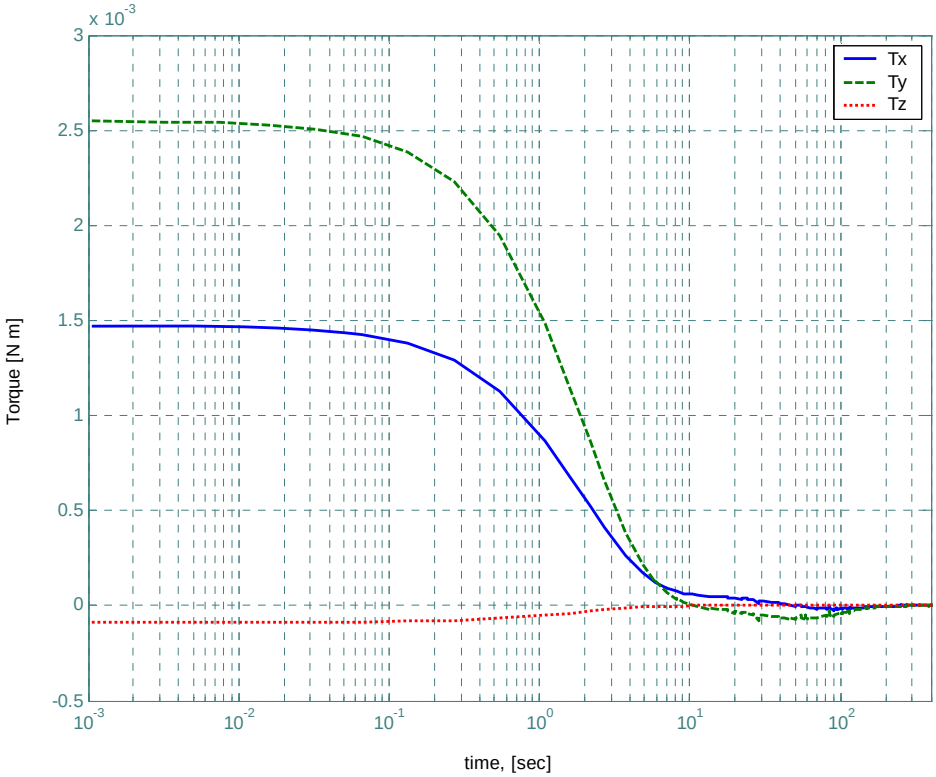

Fig. 2.9.d) Manoeuvring object control torque

2.6 Conclusions

Constructing an attractive potential combining both translational and rotational terms provides the controller with the ability to chose which motion translation and/or rotation is more convenient especially in the presence of obstacles, as will be seen later. The definition of the attractive potential depends on the type of control algorithm used. Potential functions without a velocity term produce the required velocity profile; hence it is more suited to an impulsive control methodology. While those with a velocity term generate the required acceleration and so are suited to continuous control.

Potential functions with a conical well provide a constant control force throughout the workspace, which is preferable from the point of view of actuator sizing and saturation. However it suffers from a singularity problem at the goal configuration and whenever the manoeuvring object velocity relative to the goal is zero. These problems are removed with the parabolic well potential function. Mixing both types of attractive potentials, gives enhanced characteristics for the control scheme in the impulsive control methodology. A hyperbolic potential function provides the same behaviour as the mixing between parabolic and conic wells as it provides a constant gradient away from the goal with a smooth approach to it.

3. SUPERQUADRIC OBSTACLE REPRESENTATION

"It is neither round nor rectangular, but in between"

Piet Hein

3.1 Introduction

The superquadric function represents a family of complex object shape representations that include the super-ellipsoids and the super-hyperboloids of one and two sheets. The shape representation used in this thesis is the superellipsoid, used in the context of the general term superquadric. The simplest superquadric shape is termed the super-ellipse which has morphology similar to a rectangle and ellipse. The super-ellipse is a special case of a *Lame'* curve, which is defined as:

$$\left|\frac{x}{a}\right|^n + \left|\frac{y}{b}\right|^n = 1 \tag{3.1}$$

where $n > 0$, and a, b are the radii of the super-ellipse. Changing the parameter n, results in a change of the global shape of the super-ellipse. For example, setting $n = 2$ produces an ellipse; increasing n beyond 2 yields the hyper-ellipse, as $n \rightarrow \infty$ the function resembles a rectangle; decreasing n below 2 yields a hypo-ellipse which develops a star shape and increasingly resembles a cross.

In the 1960s, *Hein* used these curves for design purpose (Jaklic et al., 2000). He generalized the super-ellipse form into a three-dimensional version and termed it then supereggs or super-ellipsoids. Two decades later, *Barr* made a major advance in generalization of the super-ellipsoids into a new family of 3D shapes termed superquadrics (Barr, 1981; Barr, 1984). The importance of his work appears in computer graphics. He presented a compact description of three-dimensional shapes with rounded edges, which can be easily rendered to other shapes.

Superquadrics are mathematical representations of solid objects. They are a set of parametric functions that have great utility in object modelling. Their parametric characteristics enable the creation of a range of object shapes by manipulating the roundness and shape parameters. A generic superquadric function is defined in body axes as:

$$\mathbf{r}(\eta,\psi)=\begin{bmatrix} a\cos^{\epsilon_1}(\eta)\cos^{\epsilon_2}(\psi) \\ b\cos^{\epsilon_1}(\eta)\sin^{\epsilon_2}(\psi) \\ c\sin^{\epsilon_1}(\eta) \end{bmatrix}, \qquad \begin{matrix} -\pi/2 \le \eta \ge\le \pi/2 \\ -\pi \le \psi \le \pi \end{matrix} \tag{3.2}$$

The surface vector **r** originates in the object centre, body frame of reference, and defines the surface of a superquadric. The latitude angle, ψ, is the angle between the x_B-axis and the projection of the vector **r** on the x_B-y_B plane, while the altitude angle, η, is formed between the vector **r** and the *x*-*y* plane as shown in Fig. 3.1.

The parameters *a*, *b*, and *c* determine the size of superquadric in the x_B, y_B, and z_B axes respectively. The two parameters ϵ_1 and ϵ_2 are used to determine the roundness of the solid shape. The first determines the roundness in a plane containing the z_B-axis whereas the second determines the roundness in a plane parallel to the x_B-y_B plane. Variation of the roundness parameters defines the superquadric as:

$\epsilon << 1$: square shape

$\epsilon \sim 1$: round shape

$\epsilon \sim 2$: flat shape

$\epsilon > 2$: pinched shape

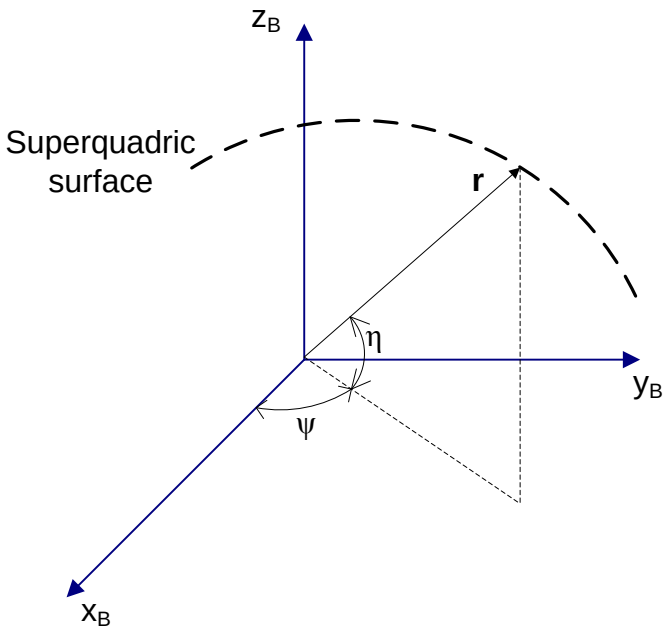

Fig. 3.1 Superquadric surface vector

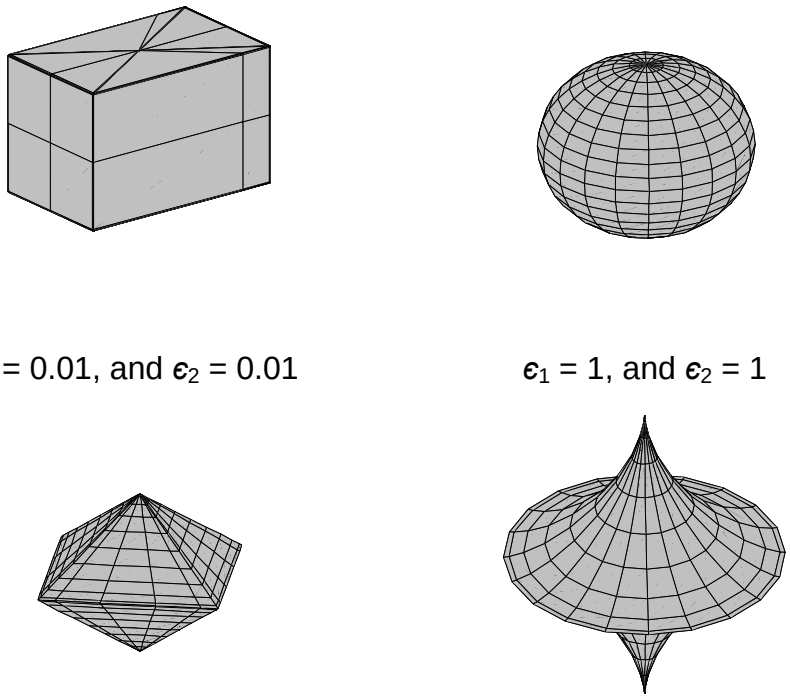

Fig. 3.2 Superquadric shapes

The above figure, Fig. 3.2, shows the effect of roundness parameter variation on superquadric surfaces while the size parameters remain unchanged.

3.2 Inside-Outside Function

The inside-outside function, F, defines whether a point lies inside, on the surface or outside the superquadric shape. It is constructed by eliminating the parameters η, and ψ to form an implicit equation written as (Solina and Bajcsy, 1990):

$$F(\mathbf{a}, \mathbf{x}_B) = \left[\left(\frac{x_B}{a} \right)^{\frac{2}{\varepsilon_2}} + \left(\frac{y_B}{b} \right)^{\frac{2}{\varepsilon_2}} \right]^{\frac{\varepsilon_2}{\varepsilon_1}} + \left(\frac{z_B}{c} \right)^{\frac{2}{\varepsilon_1}} \tag{3.3}$$

The superquadric surface therefore satisfies the equation (Leonardis et al., 1997):

$$F(\mathbf{a}, \mathbf{x}_B) = 1 \tag{3.4}$$

where the vector **a**, represents superquadric radii a, b, and c and the roundness parameters ϵ_1, and ϵ_2. The vector $\mathbf{x}_B$ is the position vector with respect to the body frame of reference. Consider any point P with coordinates (x_B, y_B, z_B) with respect to a set of body axes attached to the superquadric. If $F < 1$, the point P lies inside the superquadric whereas if $F = 1$, the point lies on the superquadric surface, and finally if $F > 1$, the point lies outside the superquadric.

3.3 Superquadrics and Motion Planning

New techniques to deal with motion planning and obstacle avoidance have been introduced using potential field functions as discussed in chapter 1. Some of these methods are constructed to avoid the formation of local minima in the case of many adjacent obstacles. The major advantage of using superquadrics as an obstacle representation in calculating the obstacle potential field is the change of the obstacle shape from its actual geometric shape near the obstacle edges to a sphere by using the deformable superquadric function. The parametric properties of deformable superquadrics make the smooth change of obstacle shape suitable to be represented in a potential function. This can avoid formation of local minima that would be produced by the addition of a goal potential to an obstacle potential, especially for obstacles with straight edges (Volpe, 1990).

The compact object representation that led to the popularity of superquadric use in computer graphics is used herein in the autonomous assembly problem. Assembly of structures requires many objects with different shapes and sizes to be considered. This variety needs a function that is suitable to represent all assembled objects. No function does that in a compact way other than the superquadric.

McQuade presented an autonomous assembly method using potential functions by representing each object as a sphere. Although his work made a great contribution to the field of autonomous assembly of complex structures, he did not deal with objects with different shapes or sizes (McQuade, 1997). Imagine for example, a long, slender beam. It should be surrounded by an obstacle potential sphere of size equal to the beam length. However, less space is available for object manoeuvring. The

superquadric provides a compact but geometrically accurate means of representing obstacles.

3.4 Separation Distance

The main requirement to calculate the obstacle potential is to define the distance between any point in space and the superquadric surface, taking into consideration that the origin of the Cartesian coordinate system will be the centre of the obstacle. Hence, before defining the obstacle potential it is necessary to define the distance between any point and the superquadric surface.

The minimum separation distance between two objects (manoeuvring object and obstacle) is crucial in the application of potential field algorithms to autonomous motion control. The minimum distance between a point and a superquadric surface is computationally very expensive to obtain (Harden, 1997; Chevalieret et al., 2003). Consequently, many approximate definitions were investigated as an alternative. Unlike previous work, position, orientation, and body dimensions will be taken into consideration for the distance calculation. The more accurate distance calculation presented here helps in decreasing an unnecessary obstacle potential strength and providing a larger available free workspace. Consequently, the more accurate distance calculation available, the less manoeuvring is required. Mathematical formulations of different methods are discussed in this section, whereas their applications will be discussed later.

3.4.1 Approximate Euclidian distance

An approximate estimation of the Euclidian distance is still computationally expensive. This estimation, based on Taubin's approach, can be expressed as (Chevalier et al., 2003):

$$d(\mathbf{a}, \mathbf{x}_B) = \left| F(\mathbf{a}, \mathbf{x}_B) - 1 \right| / \left\| \nabla F(\mathbf{a}, \mathbf{x}_B) \right\| \tag{3.5}$$

The gradient calculation will be expensive due to the dependency of the coordinate parameters on both the relative position and orientation of the obstacles (quaternion

parameters). This difficulty may reduce the speed of the calculation, which will affect the online control process.

3.4.2 Pseudo-distance

The pseudo-distance function has been used in object shape representations in the field of computer vision (Bajcsy and Solina, 1987; Solina and Bajcsy, 1990). It was then used in the motion planning problem to determine the separation distance, *d*, between a manoeuvring object centre and an obstacle surface represented by a superquadratic as (Khosla and Volpe, 1988):

$$d(\mathbf{a}, \mathbf{x}_B) = F(\mathbf{a}, \mathbf{x}_B)^{\frac{\varepsilon_1}{2}} - 1 \tag{3.6}$$

The exact Euclidian distance is found to be relatively far from the corresponding pseudo-distance; since it increases slowly compared with the increase in the Euclidian distance, as seen in iso-potential contour plots in the literature (Volpe and Khosla, 1990). Consequently, the high potential range around the obstacle increases and excess manoeuvres are required to avoid the high potential zone.

Another disadvantage of the pseudo-distance function is its high sensitivity to any change in the superquadric size parameters *a*, *b*, and *c* (Chevalier et al., 2003). This can be enhanced by multiplying the pseudo distance function by the norm of the position vector of the manoeuvring object centre with respect to the centre of the superquadric, $\left|\mathbf{r}_{obj/obs}\right|$, to form the modified pseudo distance function defined as:

$$d(\mathbf{a}, \mathbf{x}_B) = \left|\mathbf{r}_{obj/obs}\right|\left(F(\mathbf{a}, \mathbf{x}_B)^{\frac{\varepsilon_1}{2}} - 1 \right) \tag{3.7}$$

Examples of contour plots for the modified pseudo distance function will be presented later when considering certain obstacle shapes to define the required parameters used in the inside-outside function.

3.4.3 Radial Euclidian distance

A new utilization of the radial Euclidian distance in the field of motion planning is now discussed. Calculating the radial Euclidian separation distance between a point and the superquadric surface is more sophisticated than the pseudo distance (Bardinet et al., 1995; Katsoulas and Jaklič, 2002; Zhang, 2003a; Zhang, 2003b).

The radial Euclidian distance of a point, P, is defined as the distance between the point P and the point of intersection of the line OP and the superquadric, where O is the centre of the superquadric. The radial Euclidian distance is always greater or equal to the radial distance $|PM|$, Fig. 3.3. Let $|OP_o| = \mu|OP|$, $0 < \mu < 1$, and the Cartesian coordinates of points P and P_o in the superquadric body frame of reference are (x_B, y_B, z_B) and (x_{oB}, y_{oB}, z_{oB}) respectively.

Therefore $(x_{oB}, y_{oB}, z_{oB}) = (\mu\, x_B, \mu\, y_B, \mu\, z_B)$ and let:

$$g(\mathbf{a}, \mathbf{x}_B) = F(\mathbf{a}, \mathbf{x}_B)^{\frac{\varepsilon_1}{2}} = \left[\left[\left(\frac{x_B}{a} \right)^{\frac{2}{\varepsilon_2}} + \left(\frac{y_B}{b} \right)^{\frac{2}{\varepsilon_2}} \right]^{\frac{\varepsilon_2}{\varepsilon_1}} + \left(\frac{z_B}{c} \right)^{\frac{2}{\varepsilon_1}} \right]^{\frac{\varepsilon_1}{2}} \tag{3.8}$$

then

$$g(\mathbf{a}, \mathbf{x}_{B,o}) = \left[\left[\left(\frac{\mu\, x_B}{a} \right)^{\frac{2}{\varepsilon_2}} + \left(\frac{\mu\, y_B}{b} \right)^{\frac{2}{\varepsilon_2}} \right]^{\frac{\varepsilon_2}{\varepsilon_1}} + \left(\frac{\mu\, z_B}{c} \right)^{\frac{2}{\varepsilon_1}} \right]^{\frac{\varepsilon_1}{2}} = \mu\, g(\mathbf{a}, \mathbf{x}_B) \tag{3.9}$$

Since the point P_o lies on the superquadric, $g(\mathbf{a}, \mathbf{x}_{B,o}) = 1$, then

$$\mu = \frac{1}{g(\mathbf{a}, \mathbf{x}_B)} \tag{3.10}$$

Hence, the radial Euclidian distance is:

$$\|PP_o\| = |1 - \mu| \|OP\| = \left| \frac{g(\mathbf{a}, \mathbf{x}_B) - 1}{g(\mathbf{a}, \mathbf{x}_B)} \right| \|OP\| \tag{3.11}$$

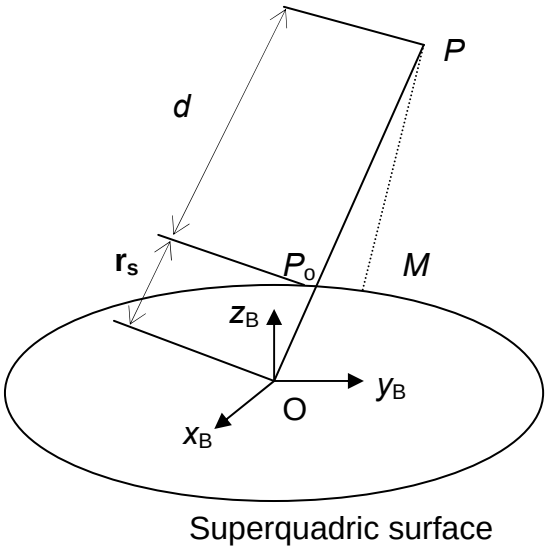

Fig. 3.3 Radial Euclidian distance

Therefore, it is now possible to calculate the radial Euclidian distance between a point and a superquadric as:

$$d(\mathbf{a}, \mathbf{x}_B) = \left|\mathbf{r}_{obj/obs}\right|\left(1 - F(\mathbf{a}, \mathbf{x}_B)^{\frac{-\varepsilon_1}{2}}\right) \tag{3.12}$$

This method still suffers from the drawback of limiting its estimation to the manoeuvring object centre rather than its edge.

3.4.4 Rigid body radial Euclidian distance

Another new improvement of the method is now discussed. Other than spherically symmetric objects, all previous methods fail to predict collision possibilities in cases such as in Fig. 3.4. Considering the distance between a manoeuvring object centre and an obstacle surface only is not sufficient in the case of extended rigid body objects.

The new method involves subtracting the distance inside the superquadric which lies on the line joining the two centres. This is the length of the segment $\|OP_o\|$, but inside the manoeuvring object.

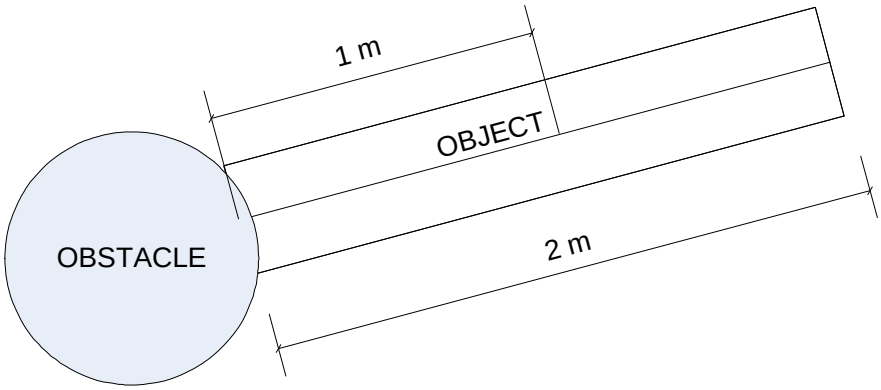

Fig. 3.4 Possible collision configuration

Since $|OP_o| = \mu|OP|$, and from Eq. (3.11), the radial Euclidian distance will now be written as:

$$\|PP_o\| = \left|\frac{1-\mu}{\mu}\right| \|OP_o\| = |g(\mathbf{a}, \mathbf{x}_B) - 1| \|OP_o\| \tag{3.13}$$

The distance $\|OP_o\|$ will be termed $|\mathbf{r}_s|_{obj}$ for generality, hence from Eqs. (3.8), (3.12) and (3.13) the part of the radial Euclidian distance inside the manoeuvring object is defined as:

$$|\mathbf{r}_s|_{obj} = |\mathbf{r}_{obj/obs}| \frac{1 - F_{obj}(\mathbf{a}, \mathbf{x})^{\frac{-\varepsilon_1}{2}}}{F_{obj}(\mathbf{a}, \mathbf{x})^{\frac{\varepsilon_1}{2}} - 1} \tag{3.14}$$

Hence, the separation distance can now be expressed as:

$$d(\mathbf{a}_{obs}, \mathbf{a}_{obj}, \mathbf{x}_{obs,B}, \mathbf{x}_{obj,B}) = |\mathbf{r}_{obj/obs}| \left(1 - F(\mathbf{a}, \mathbf{x}_B)^{\frac{-\varepsilon_1}{2}} \right)\Big|_{obs} - |\mathbf{r}_s|_{obj} \tag{3.15}$$

Finally, it can be seen that:

$$d(\mathbf{a}_{obs}, \mathbf{a}_{obj}, \mathbf{x}_{obs,B}, \mathbf{x}_{obj,B}) = |\mathbf{r}_{obj/obs}| \left[1 - F(\mathbf{a}_{obs}, \mathbf{x}_{obs,B})^{\frac{-\varepsilon_{1,obs}}{2}} - F_{obj}(\mathbf{a}_{obj}, \mathbf{x}_{obj,B})^{\frac{-\varepsilon_{1,obj}}{2}} \right] \tag{3.16}$$

The new proposed distance function in Eq. (3.16) takes into consideration the possible difference between the obstacle and manoeuvring object shapes and sizes as

the inside-outside function, F, is calculated for each object. The exact Euclidian distance is found in special cases, mainly when the object edges are parallel.

3.5 Attitude-Distance Effect

Although the previously discussed separation distance functions do not explicitly determine the effect of object orientation on the distance estimation, this effect implicitly exists. Figure 3.5 shows the necessity of considering orientation in the distance estimation, as the distance varies as a result of object orientation as shown in the two cases (1) and (2).

The orientation using the real quaternion, not the error quaternion discussed earlier in chapter 2, implicitly affects the position vector $\mathbf{x}_B$ as described by the homogeneous transformation in the absence of translation as (Appendix A):

$$\begin{bmatrix} x \\ y \\ z \end{bmatrix}_B = \begin{bmatrix} q_1^2 - q_2^2 - q_3^2 + q_4^2 & 2(q_1 q_2 + q_3 q_4) & 2(q_1 q_3 - q_2 q_4) \\ 2(q_1 q_2 - q_3 q_4) & -q_1^2 + q_2^2 - q_3^2 + q_4^2 & 2(q_2 q_3 + q_1 q_4) \\ 2(q_1 q_3 + q_2 q_4) & 2(q_2 q_3 - q_1 q_4) & -q_1^2 - q_2^2 + q_3^2 + q_4^2 \end{bmatrix}_{real} \begin{bmatrix} x_{obj} - x_{obs} \\ y_{obj} - y_{obs} \\ z_{obj} - z_{obs} \end{bmatrix}_I \quad (3.17)$$

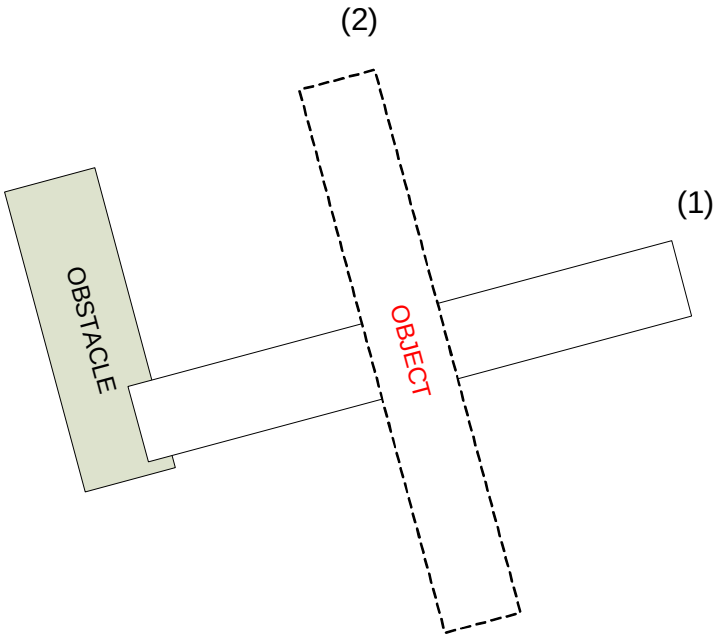

Fig. 3.5 Orientation effect on separation distance

The quaternion parameters in the transformation matrix are for the object on which the body frame of reference is attached. The subscript, *I*, refers to the chosen inertial frame of reference for the motion planning analysis. The error quaternions are the difference between the real quaternions and goal. Since error quaternions are used more frequently in this thesis, no subscript is used with error quaternions. The real quaternions are calculated as:

$$\begin{bmatrix} q_1 \\ q_2 \\ q_3 \\ q_4 \end{bmatrix}_{real} = \begin{bmatrix} q_4 & q_3 & -q_2 & -q_1 \\ -q_3 & q_4 & q_1 & -q_2 \\ q_2 & -q_1 & q_4 & -q_3 \\ q_1 & q_2 & q_3 & q_4 \end{bmatrix}_{goal,real} \begin{bmatrix} q_1 \\ q_2 \\ q_3 \\ q_4 \end{bmatrix} \tag{3.18}$$

Figure 3.7 shows the dependency of the separation distance on the quaternion parameters about the *z*-axis of the two objects illustrated in Fig. 3.6. The dependence of distance on object orientation can clearly be seen.

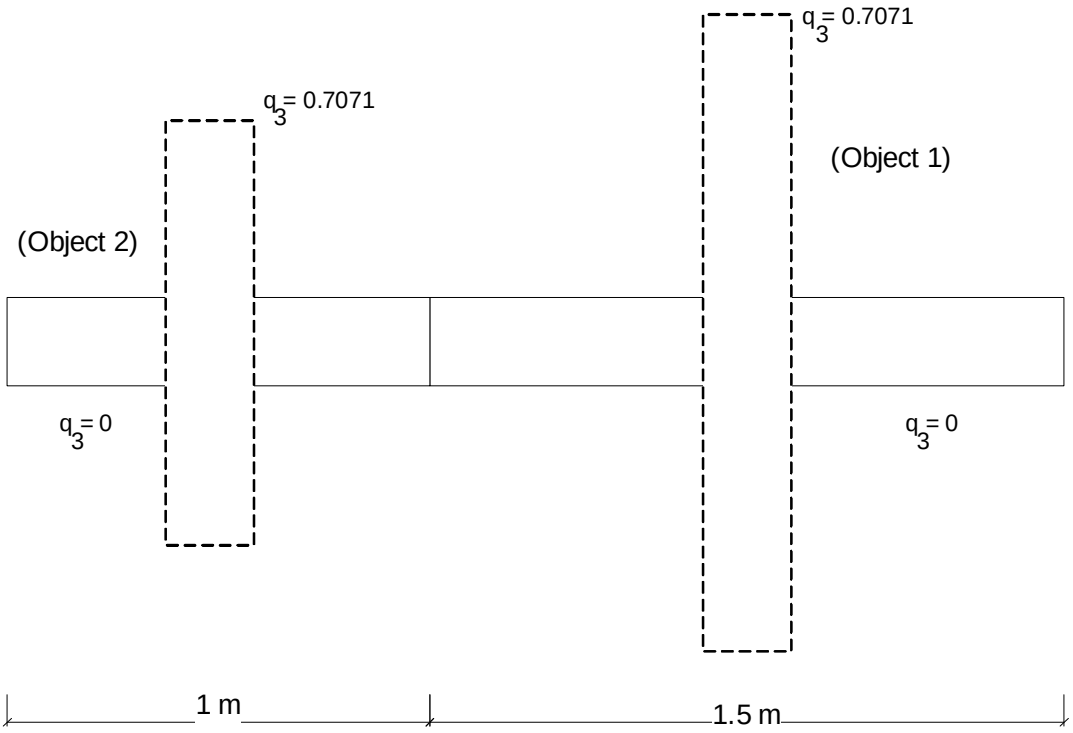

Fig. 3.6 Two object configuration

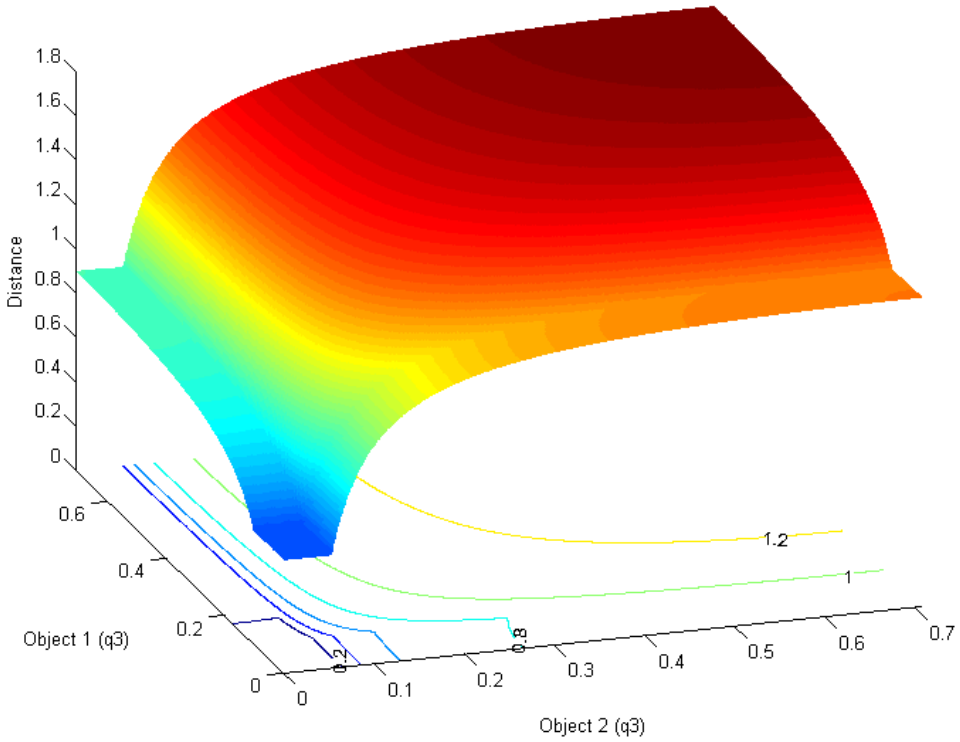

Fig. 3.7 Separation distance vs. quaternion parameter about *z*-axis

3.6 Superquadric Obstacle Representation

Various obstacle shapes can now be represented using the superquadric methodology by adjusting the five parameters defined in Eq. (3.3). For example, in order to define a spherical shape, the shape parameters ε_1, and ε_2 should be unity. As will be seen, through the appropriate choice of shape parameters the precise geometric form of objects can be captured in proximity to them, but smoothed away from the object to allow for collision avoidance with less likelihood of local minima formation.

3.6.1 Parallelepiped shape (cuboid)

The parallelepiped shape is common in structural assembly problems. Columns and plates can be modelled by fixed parameters, while triangles and trapezoids can be modelled by a variable set of parameters. Parallelepiped obstacles were first

investigated by *Volpe* as static objects for collision avoidance during manipulator control (Volpe and Khosla, 1990).

To form a parallelepiped shape the values of ϵ_1 and ϵ_2 are chosen to approach zero in proximity to the object to have a sharp edged parallelepiped. On the other hand, their values should approach unity far from the obstacle edges to form a smooth ellipsoid. Deformable superquadric surfaces are represented by introducing a new shaping parameter, n, related to each surface. This parameter replaces both ϵ_1 and ϵ_2 with $n \rightarrow \infty$ near the object edges (to ensure sharp edges) while $n \rightarrow 1$ away from the object (to ensure smoothness) to form an n-ellipsoid with semi-axes a, b, and c. Figure 3.8 shows a superquadric model for such a cuboid element. The most general form of an implicit function for a parallelepiped object is defined as:

$$\left(\frac{x_B}{f_1(x_B, y_B, z_B)}\right)^{2n} + \left(\frac{y_B}{f_2(x_B, y_B, z_B)}\right)^{2n} + \left(\frac{z_B}{f_3(x_B, y_B, z_B)}\right)^{2n} = 1 \tag{3.19}$$

where the scaling functions f_1, f_2 and f_3 are used to define the required geometric form of the parallelepiped.

For example, the scaling functions for a column and a plate are constants. They can then be set to a, b, and c, the semi-major axis in x_B, y_B, and z_B directions respectively such that:

$$\left(\frac{x_B}{a}\right)^{2n} + \left(\frac{y_B}{b}\right)^{2n} + \left(\frac{z_B}{c}\right)^{2n} = 1 \tag{3.20}$$

It is now possible to modify the nested level surfaces defined by Eq. (3.20) to form a sphere away from the object rather than an ellipsoid by adjusting the coefficients as:

$$\left(\frac{x_B}{a}\right)^{2n} + \left(\frac{b}{a}\right)^{2}\left(\frac{y_B}{b}\right)^{2n} + \left(\frac{c}{a}\right)^{2}\left(\frac{z_B}{c}\right)^{2n} = 1 \tag{3.21}$$

The inside-outside function is then expressed as:

$$F(\mathbf{a}, \mathbf{x}_B) = \left(\frac{x_B}{a}\right)^{2n} + \left(\frac{b}{a}\right)^{2}\left(\frac{y_B}{b}\right)^{2n} + \left(\frac{c}{a}\right)^{2}\left(\frac{z_B}{c}\right)^{2n} \tag{3.22}$$

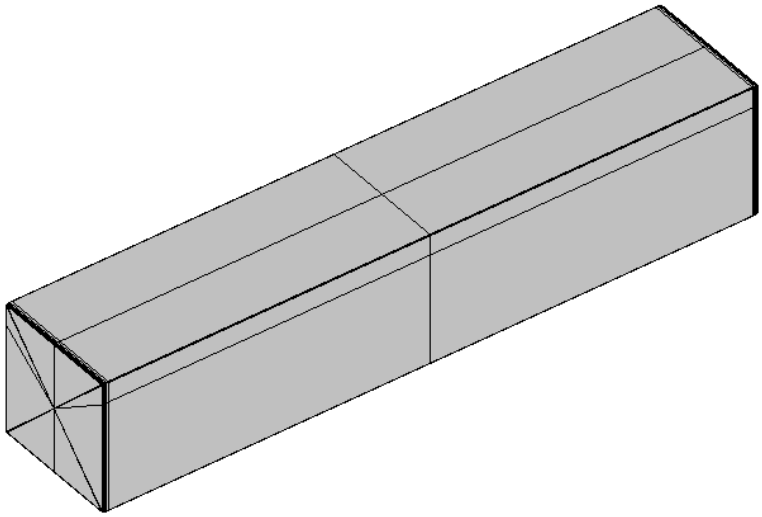

Fig. 3.8 Cuboid element representation using a superquadric function

Following *Volpe*, n can be defined as (Volpe, 1990):

$$n = \frac{1}{1 - exp(-\alpha d)} \tag{3.23}$$

where d is the distance function defined by Eqs. (3.7), (3.12) and (3.16). The parameter α has a major influence on the transition from sharp to rounded superquadric surfaces. Increasing the value of α increases the sharpness of the transition, this limits the range of influence of the object. Figure 3.9 shows the effect of α on the object iso-distance contours through estimating the separation distance using the modified pseudo-distance, radial Euclidian distance, and rigid body radial Euclidian distance using Eqs. (3.7), (3.12) and (3.16) respectively. Plotting the iso-distance contour lines indicate that points of equal distance from an obstacle will have equal obstacle potential, as will be discussed later.

These figures show that the appropriate choice of α reduces the possibility of the formation of local minima since the potential has spherical symmetry at small distance from the object for large α. In addition, the improvement in distance estimation can be seen between the various estimation methods.

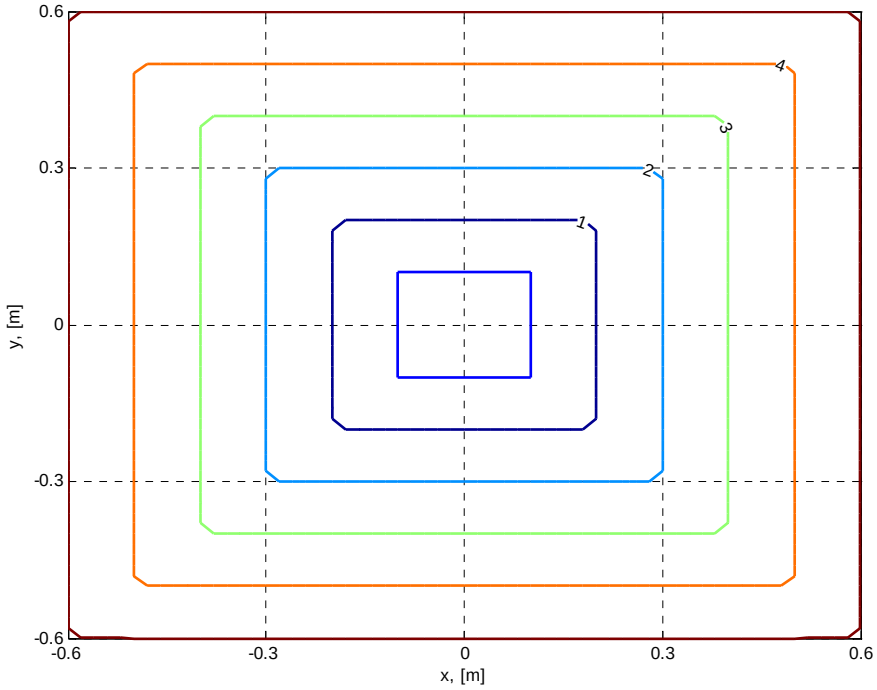

Fig. 3.9.a) Cuboid iso-distance contours, [m], using modified pseudo distance method, Eq. (3.7), (α = 1)

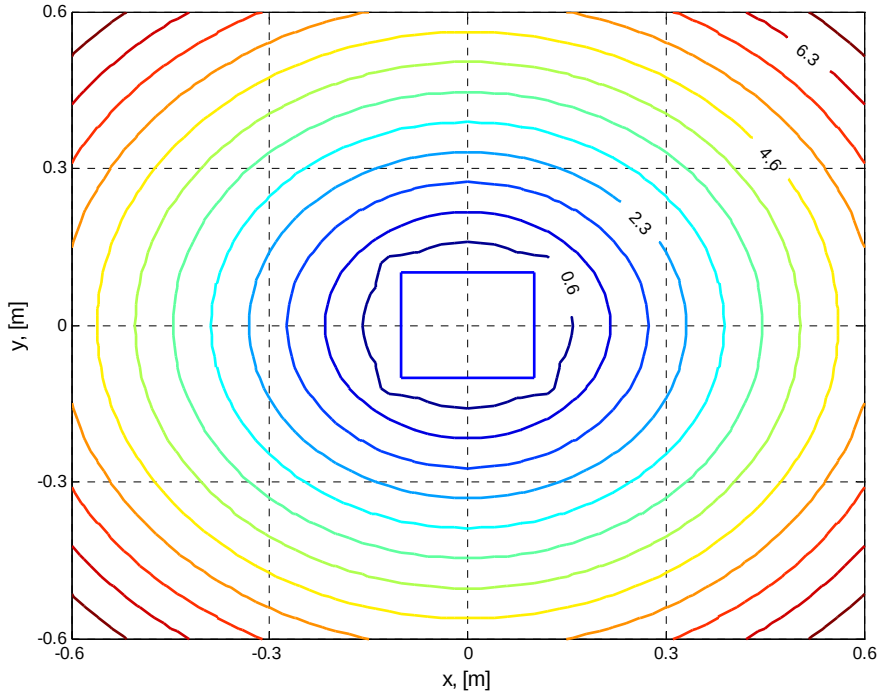

Fig. 3.9.b) Cuboid iso-distance contours, [m], using modified pseudo distance method (α = 100)

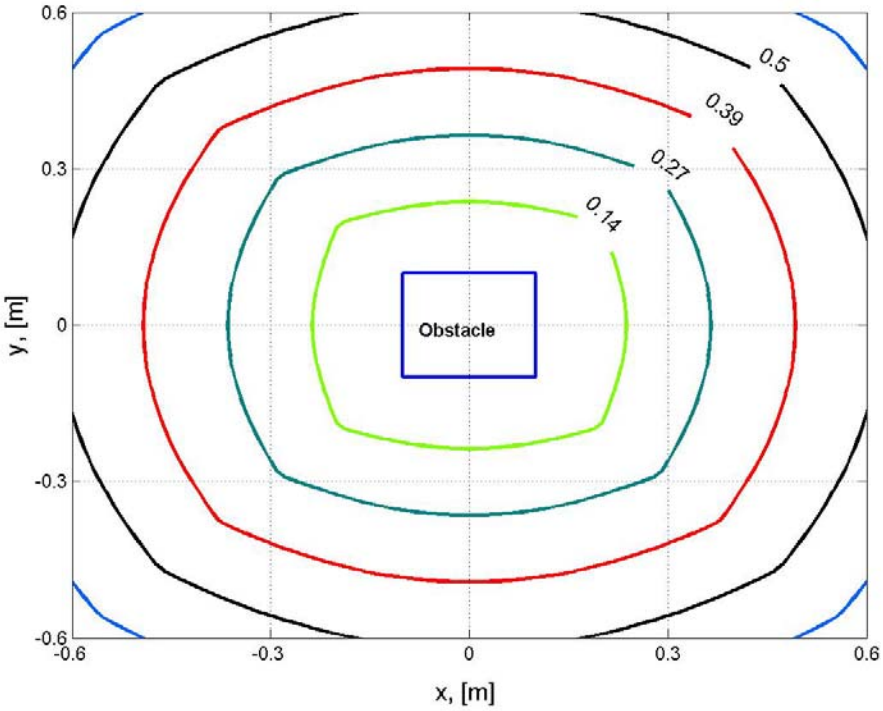

Fig. 3.9.c) Cuboid iso-distance contours, [m] using radial distance method, Eq. (3.12), (α = 1)

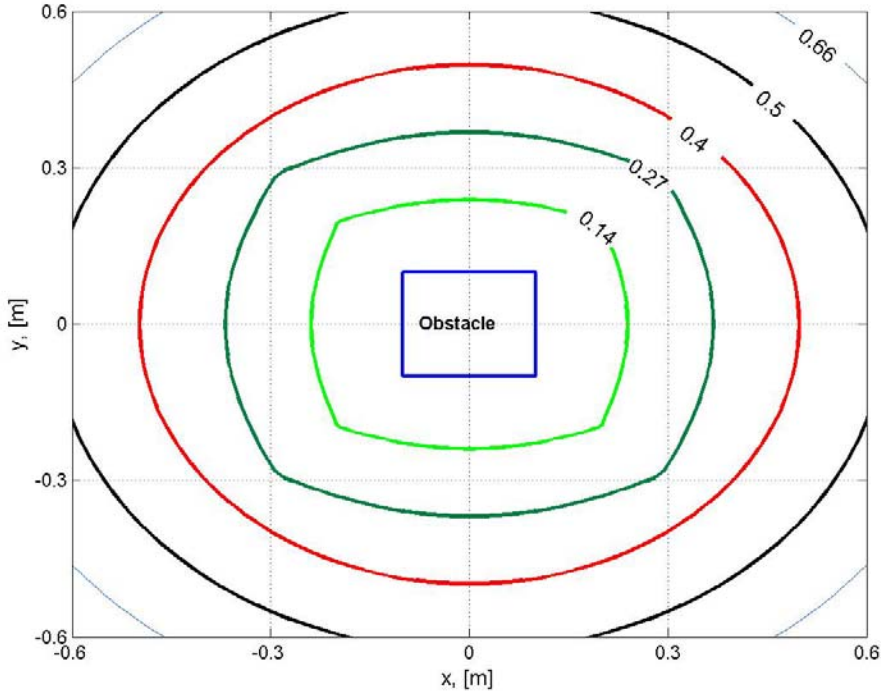

Fig. 3.9.d) Cuboid iso-distance contours using radial distance method (α = 100)

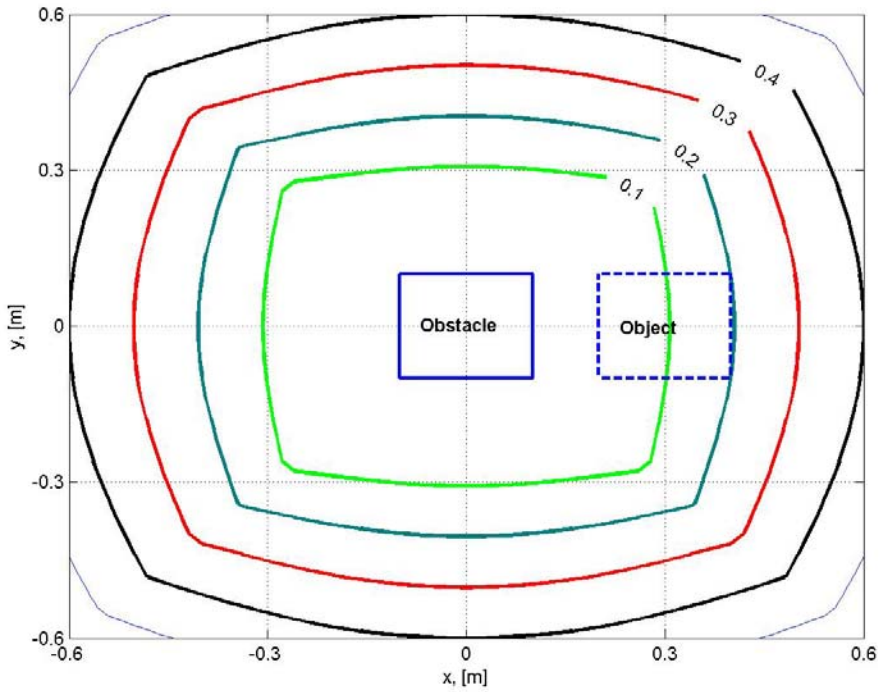

Fig. 3.9.e) Cuboid iso-distance contours, [m], using rigid body radial distance method, Eq. (3.16), (α = 1)

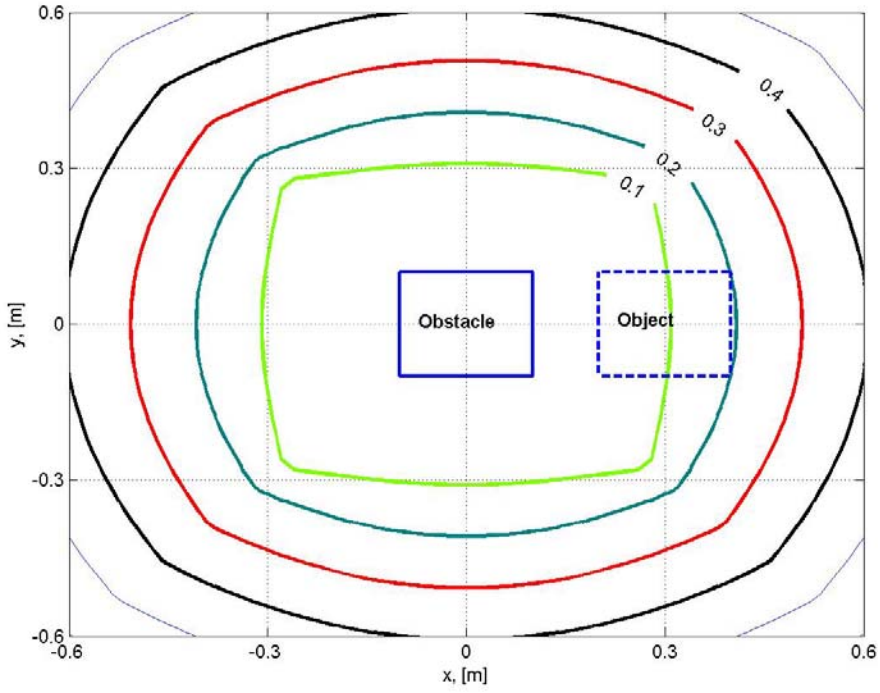

Fig. 3.9.f) Cuboid iso-distance contours using rigid body radial distance method (α=100)

3.6.2 Cylindrical obstacle (beam)

Beam elements are again widely used in structural assembly problems, especially in truss-type structures. Cylinders can be represented by a superquadric function by setting the shape parameter $\epsilon_1 \rightarrow 0$, and $\epsilon_2 = 1$. Figure 3.10 shows the superquadric model for a cylindrical element.

The objective of having spherical symmetry away from the obstacle edges will be guaranteed by deforming the superquadric shape from a cylinder to a sphere. For a spherical shape both ϵ_1 and ϵ_2 should be set to unity, hence the parameter ϵ_2 will remain unchanged throughout the workspace, while the parameter ϵ_1 should be gradually changed from zero at the beam edge to unity. It is then inversely proportional to the contour parameter n. Hence, for a cylinder of radius r and length c, the superquadric model can be adapted to the following form as:

$$\left[\left(\frac{x_B}{r}\right)^2 + \left(\frac{y_B}{r}\right)^2\right]^n + \left(\frac{c}{r}\right)^2\left(\frac{z_B}{c}\right)^{2n} = 1 \tag{3.24}$$

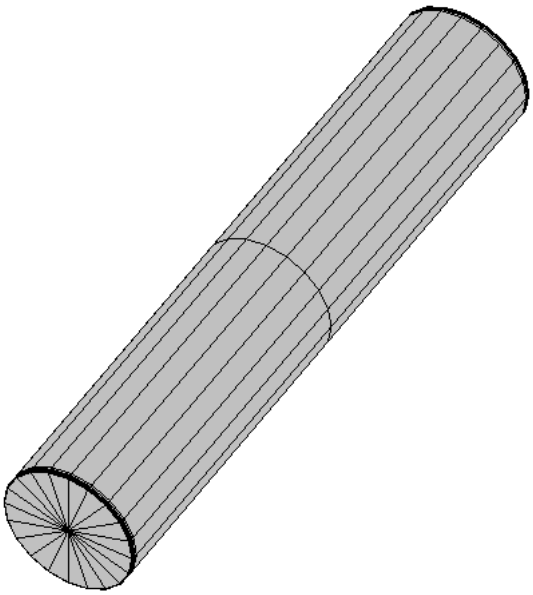

Fig. 3.10 Cylindrical element representation using a superquadric function

The corresponding inside-outside function is then expressed as:

$$F(\mathbf{a},\mathbf{x}_B)=\left[\left(\frac{x_B}{r}\right)^2+\left(\frac{y_B}{r}\right)^2\right]^n+\left(\frac{c}{r}\right)^2\left(\frac{z_B}{c}\right)^{2n} \tag{3.25}$$

The beam element iso-distance contours using the modified pseudo-distance, the radial Euclidian distance, and the rigid body radial Euclidian distance methods are shown in Fig. 3.11 using Eqs. (3.7), (3.12), and (3.16). The iso-distance in the circular cross-section plane remains unchanged, whereas those in the longitudinal plane change their shape in the same way as those of the cuboid element to provide sharp edges close to the beam and spherically symmetric contours away from the beam. Again such spherical symmetry will avoid the formation of local minima after the addition of the goal potential.

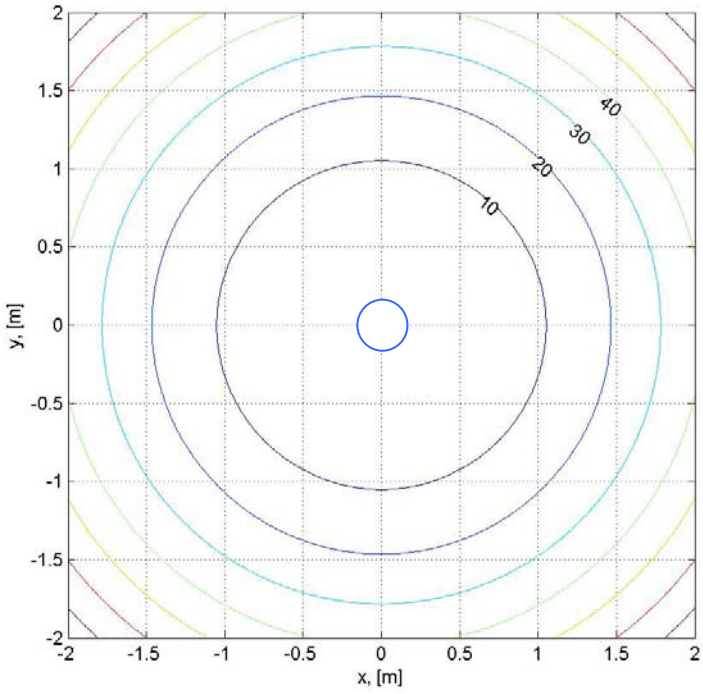

Fig. 3.11.a) Beam iso-potential contours, [m], using pseudo distance method, Eq. (3.7), (cross section)

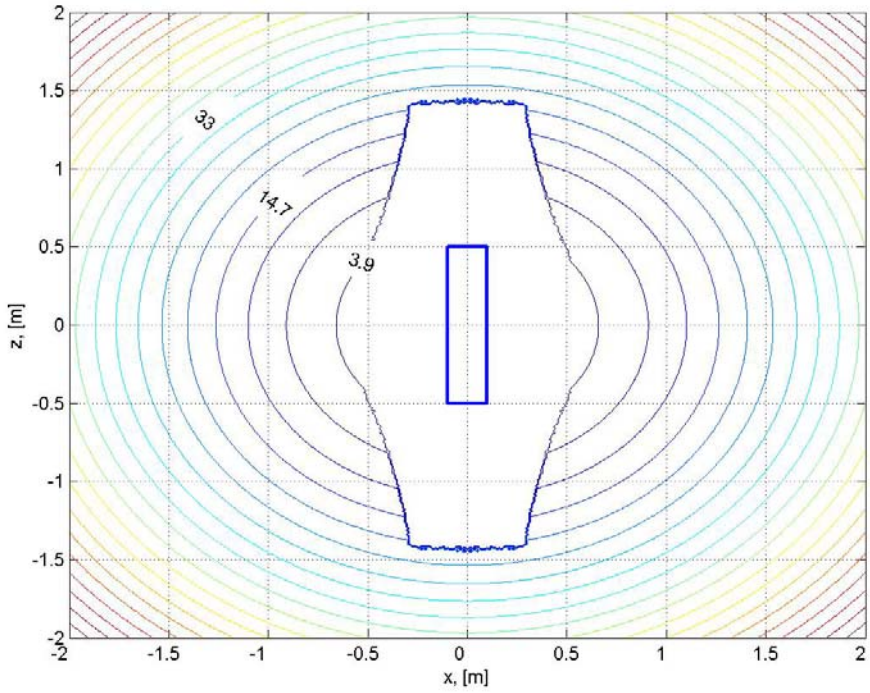

Fig. 3.11.b) Beam iso-potential contours, [m], using pseudo distance method (longitudinal section)

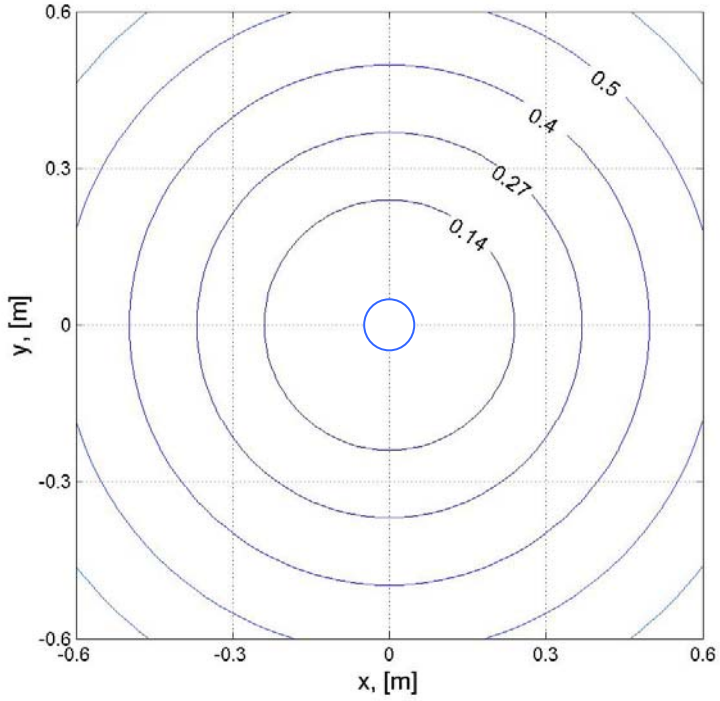

Fig. 3.11.c) Beam iso-distance contours, [m], using radial distance method, Eq. (3.12), (cross section)

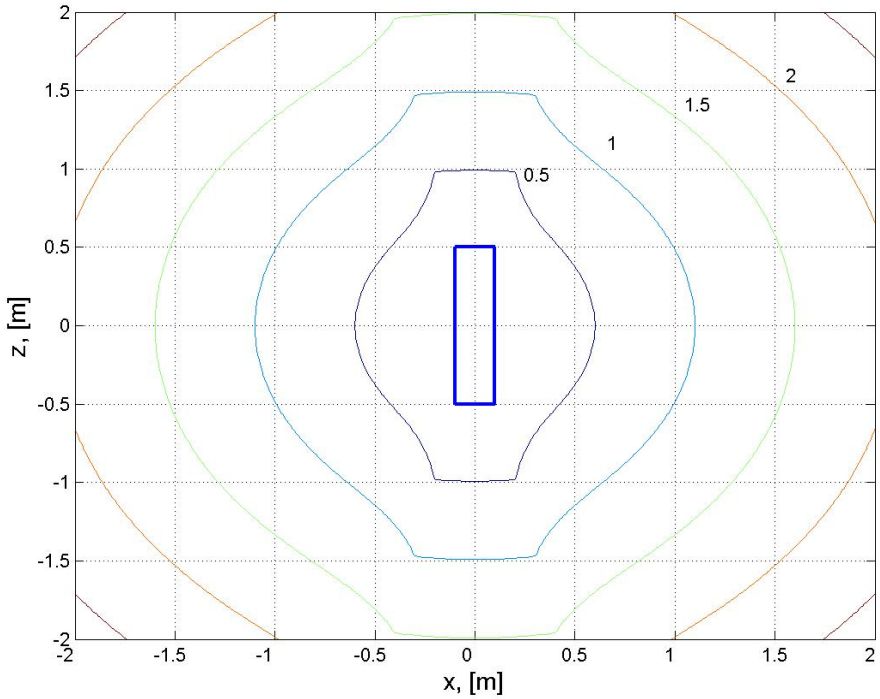

Fig. 3.11.d) Beam iso-distance contours, [m], using radial distance method (longitudinal section)

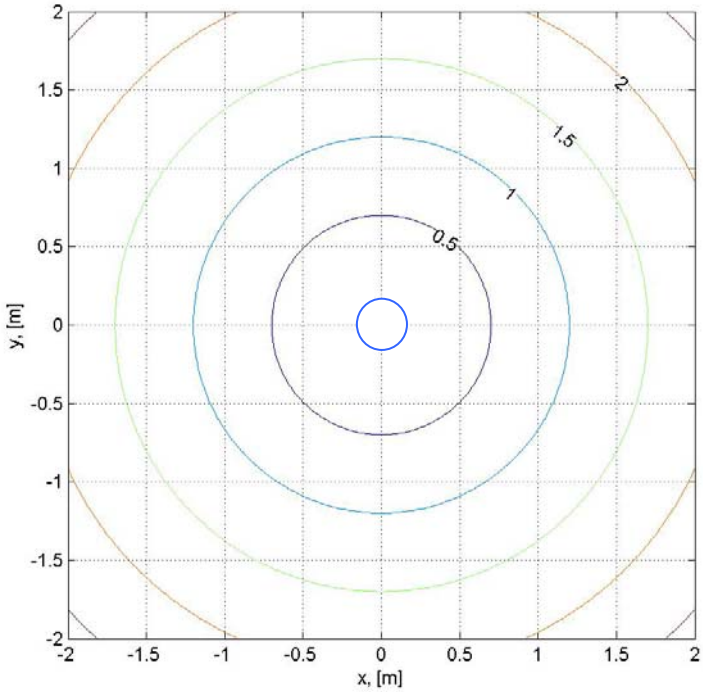

Fig. 3.11.e) Beam iso-distance contours, [m], using radial distance for rigid body method, Eq. (3.16), (cross section)

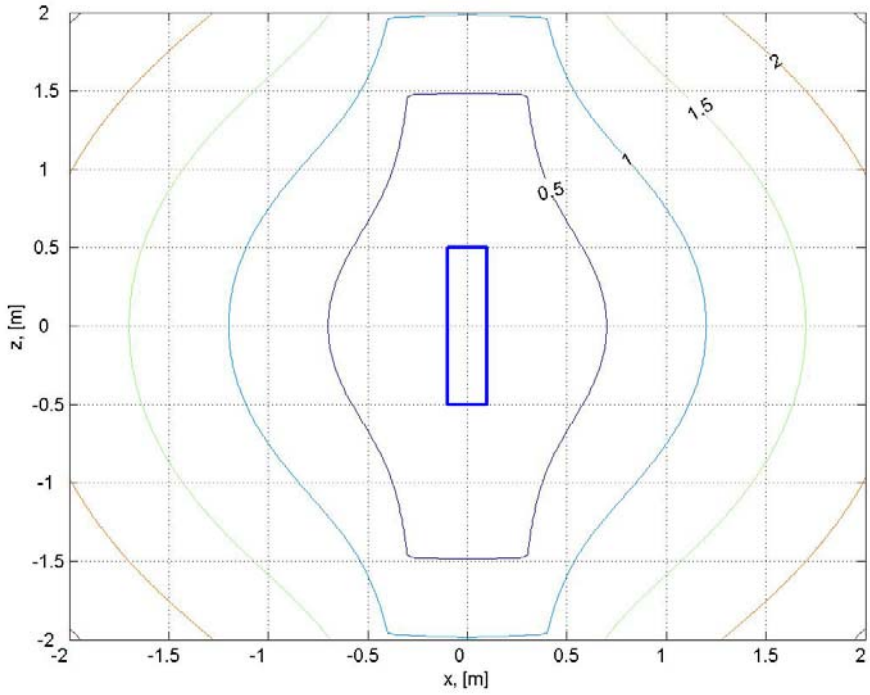

Fig. 3.11.f) Beam iso-distance contours, [m], radial distance for rigid body method (longitudinal section)

3.7 Conclusions

The superquadric function has proved its ability to represent various object shapes in a suitable manner for motion planning problems through the potential field method as it converges to the object shape near its edges while it converts to a sphere at some distance from them. The potential contours approximate the shape of the obstacle at its surface hence decreasing the occupied volume in the workspace. Introducing the constant α, affects the rate of deformation of iso-potential contour lines from the actual object shape to a spherical one. Objects with different shapes and sizes are handled with the same algorithm by changing only a few parameters, without changing the model itself.

New more accurate approximate distance estimation methods were discussed in this chapter. The separation distance produced from the first of them, the modified pseudo distance, gives better results compared to the original method suggested by *Volpe*. Adding the effect of the object attitude to the distance estimation, the new

rigid body radial Euclidian distance method presented, gives a new method to determine the distance in the case of autonomous mobile robots of different shapes.

4. SUPERQUADRIC OBSTACLE POTENTIAL

4.1 Introduction

The superquadric functions provide an efficient and flexible means of representing geometric shapes. They are able to overcome the deficiencies of other representations such as spherically symmetric Gaussian or power law functions where objects are represented as spheres of diameter equal to the maximum physical object dimension. Rather than a simple spherical form, the superquadric potential can be moulded to represent the geometric shape of an object by attaching the potential to the object body axes. In this way the obstacle potential becomes a function of both the obstacle position and orientation. Transformations with quaternion parameters are then used to define the dependency of Cartesian coordinates in the body frame of reference, where the element superquadric function is defined, and an inertial frame of reference where the attractive potential is defined. Obstacles potentials are then summed together in addition to the attractive goal potential in the inertial frame.

Local minima appear in some obstacle representation like FIRAS (discussed in section 1.5.1) due to the interaction between the iso-potential contours of both goal and obstacle, where one is spherical while the other has straight edges. The superquadric potential proposed by *Volpe* (Volpe, 1990) overcomes this problem of local minimum with a single obstacle.

4.2 Types of Obstacle Potential

The formulation of the repulsive potential depends on the required controlled object behaviour whilst approaching the obstacle. Two types of repulsive potential function are used herein termed avoidance and approach potentials; each is defined over a certain domain around the obstacle. The idea of the avoidance potential is to prevent collision between the controlled object and the surrounding obstacles by introducing infinite repulsive potential around the obstacle to force the controlled object to move away from the obstacle regardless of the kinetic energy of each of

them. The approach potential objective is to decrease the kinetic energy of the moving object when approaching the obstacle to within a certain range to reduce the contact velocity.

4.2.1 Avoidance potential

The avoidance potential is defined by the measurement of the minimum distance between the two objects, as discussed in chapter 3. It is possible to use the *Born* approximation for a *Yukawa* potential (Cohen et al., 1997; Chuang, 1998) in which the exponential term reaches zero faster than the d^{-1} term:

$$V_{obs} = A\frac{exp(-\alpha d)}{d} \quad , \quad d \geq d_{\min} \tag{4.1}$$

where $d_{\min}$ is a pre-defined range around each obstacle, in which the approach potential is defined.

4.2.2 Approach potential

The approach potential is used to reduce the manoeuvring object velocity to generate smooth contact between objects. Smooth contact is required in the goal position to achieve perfect assembly. The approach potential is defined as (Volpe, 1990) :

$$V_{obs} = A\, exp\left(-\alpha\, d^{1+\frac{1}{\alpha}}\right) \quad , \quad d < d_{\min} \tag{4.2}$$

The use of the parameter α helps in controlling both the sharpness of the obstacle potential shape and the iso-potential contour shape change from the actual obstacle shape to a spherical one, as discussed in detail earlier in chapter 3. Increasing the value of α, increases the sharpness of the potential decay, limiting the distance of influence of the obstacle on the overall potential. Figure 4.1 shows the effect of α on both the avoidance and the approach obstacle potentials respectively. The potentials

will switch according to $d \geq d_{min}$ and $d < d_{min}$ as discussed earlier. The avoidance potential is unbounded, while the approach potential is smooth and finite.

The parameter A, defined in the obstacle potential definition Eqs. (4.1) and (4.2), is termed the repulsive amplitude. It is used to define the maximum repulsive potential between objects. It is crucial in the case of the structural assembly problem. It will be expressed as a function of the object configuration allowing the obstacle potential to decay to zero at the goal configuration to allow smooth contact, which is required for connection of the structure elements (McQuade, 1997; Ge and Cui, 2000) and to avoid shifting the goal position due to the presence of obstacles nearby.

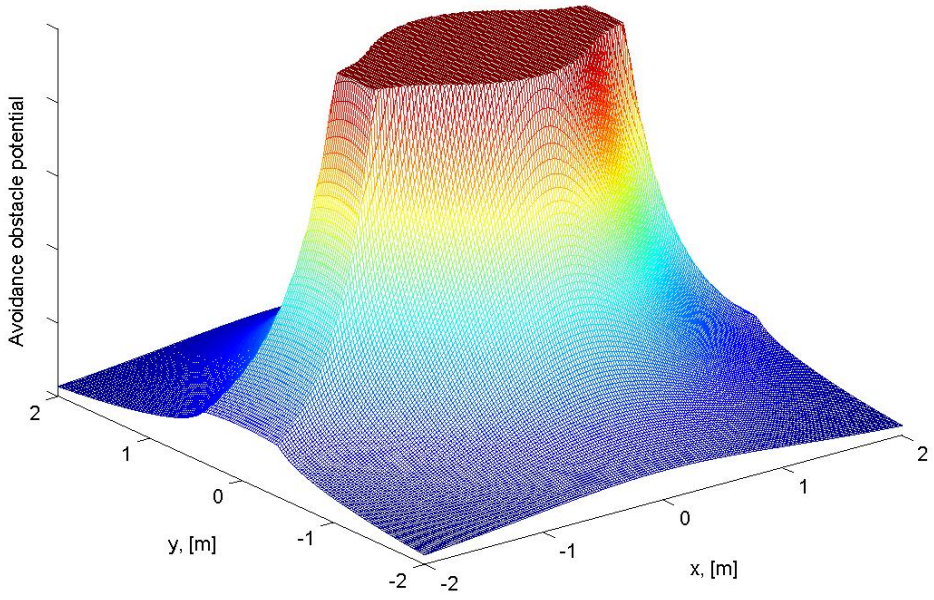

Fig. 4.1.a) Avoidance potential function (α = 1)

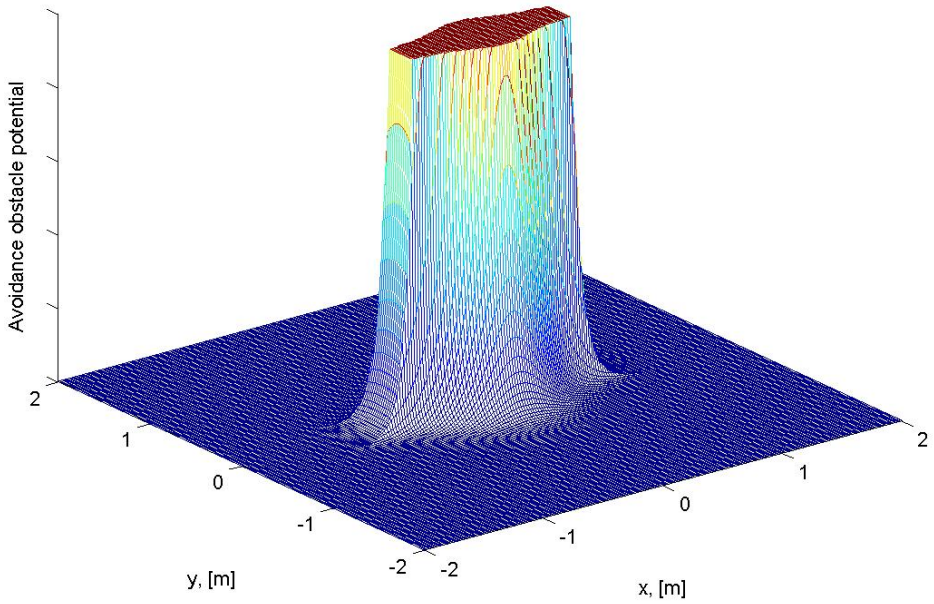

Fig. 4.1.b) Avoidance potential function (α = 10)

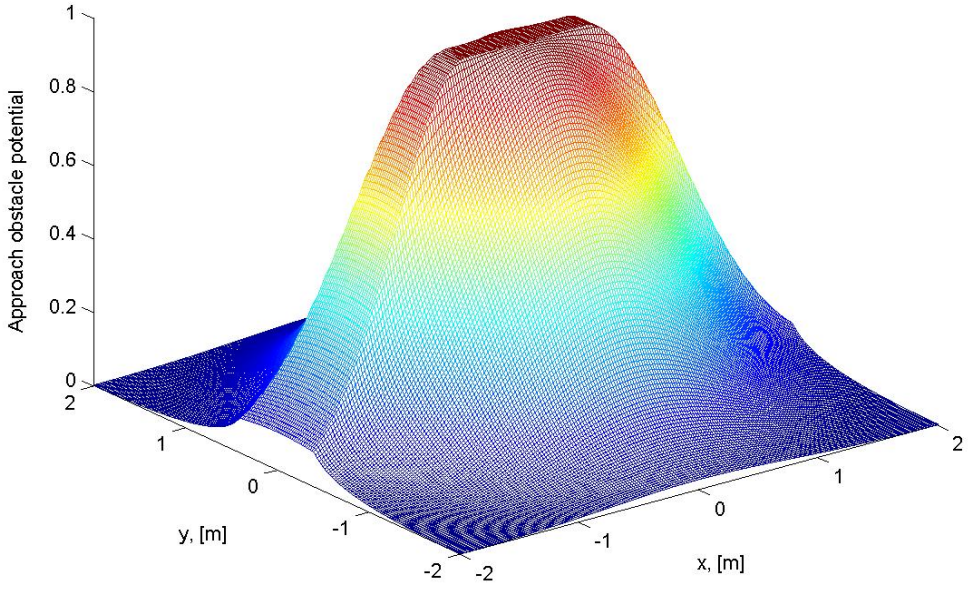

Fig. 4.1.c) Approach potential function (α = 1)

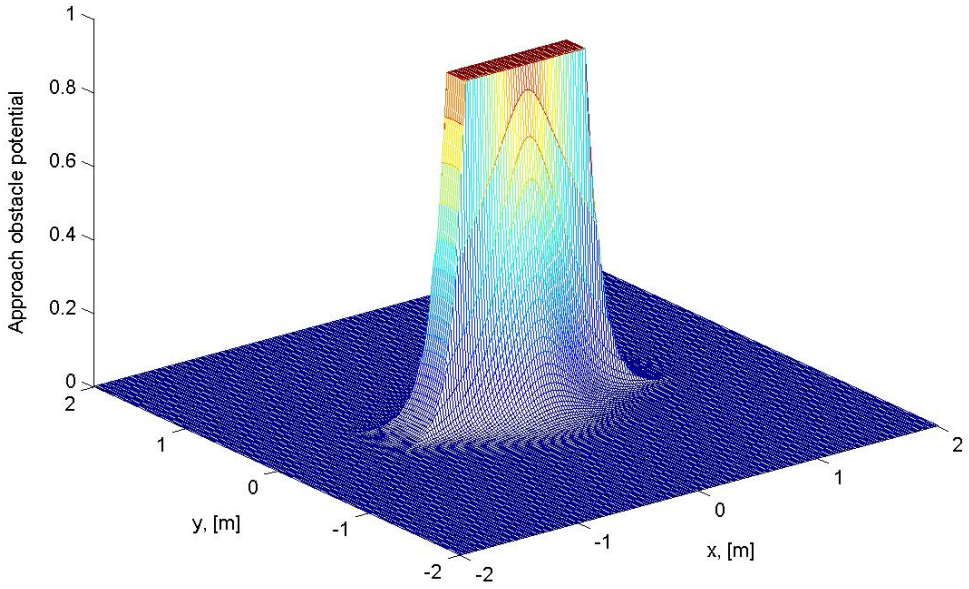

Fig. 4.1.d) Approach potential function (α = 10)

The obstacle potentials affect the manoeuvring object motion, which is already moving along the negative gradient of the attractive potential, by changing the shape of the overall potential field and consequently changing its gradient. The objective is to calculate the gradient of the obstacle potential which can be expressed from Eqs. (4.1) and (4.2) as :

$$\nabla V = \begin{cases} -A\dfrac{e^{-\alpha d}}{d}\left(\alpha + \dfrac{1}{d}\right)\nabla d & , d \geq d_{min} \\ A(\alpha+1)d^{\frac{1}{\alpha}}\, exp\left(-\alpha\, d^{1+\frac{1}{\alpha}}\right)\nabla d & , d < d_{min} \end{cases} \tag{4.3}$$

As these gradients depend on the obstacle shape, the following sections describe how the gradient of the separation distance for cuboid and beam elements are calculated.

4.3 Obstacle Potential of Parallelepiped Element

The inside-outside function of a parallelepiped element, discussed in section 3.6.2, is expressed as:

$$F(\mathbf{a},\mathbf{x}_B)=\left(\frac{x}{a}\right)^{2n}+\left(\frac{b}{a}\right)^{2}\left(\frac{y}{b}\right)^{2n}+\left(\frac{c}{a}\right)^{2}\left(\frac{z}{c}\right)^{2n} \tag{4.4}$$

4.3.1 Cuboid obstacle potential using the modified pseudo distance

The modified pseudo distance function, discussed in section 3.4.2, is expressed for a parallelepiped element as:

$$d(\mathbf{a},\mathbf{x}_B)=\left|\mathbf{r}_{obj/obs}\right|\left(F(\mathbf{a},\mathbf{x}_B)^{\frac{1}{2n}}-1\right) \tag{4.5}$$

Using the homogeneous transformation, the manoeuvring object coordinates with respect to the obstacle body frame of reference are defined as:

$$\begin{bmatrix}x_{obj}\\ y_{obj}\\ z_{obj}\end{bmatrix}_B=\begin{bmatrix}q_1^2-q_2^2-q_3^2+q_4^2 & 2(q_1q_2+q_3q_4) & 2(q_1q_3-q_2q_4)\\ 2(q_1q_2-q_3q_4) & -q_1^2+q_2^2-q_3^2+q_4^2 & 2(q_2q_3+q_1q_4)\\ 2(q_1q_3+q_2q_4) & 2(q_2q_3-q_1q_4) & -q_1^2-q_2^2+q_3^2+q_4^2\end{bmatrix}\begin{bmatrix}x_{obj}-x_{obs}\\ y_{obj}-y_{obs}\\ z_{obj}-z_{obs}\end{bmatrix}_I \tag{4.6}$$

To have a compact formulation let;

$$H_{obs,1}=\frac{(x_{obj}-x_{obs})(q_1^2-q_2^2-q_3^2+q_4^2)+2(y_{obj}-y_{obs})(q_1q_2+q_3q_4)+2(z_{obj}-z_{obs})(q_1q_3-q_2q_4)}{a_{obs}} \tag{4.7.a}$$

$$H_{obs,2}=\frac{2(x_{obj}-x_{obs})(q_1q_2-q_3q_4)+(y_{obj}-y_{obs})(-q_1^2+q_2^2-q_3^2+q_4^2)+2(z_{obj}-z_{obs})(q_2q_3+q_1q_{4_4})}{b_{obs}} \tag{4.7.b}$$

$$H_{obs,3}=\frac{2(x_{obj}-x_{obs})(q_1q_3+q_2q_4)+2(y_{obj}-y_{obs})(q_2q_3-q_1q_4)+(z_{obj}-z_{obs})(-q_1^2-q_2^2+q_3^2+q_4^2)}{c_{obs}} \tag{4.7.c}$$

$$H_{obs} = \left(H_{obs,1}^{2n} + \left(\frac{b_{obs}}{a_{obs}} \right)^2 H_{obs,2}^{2n} + \left(\frac{c_{obs}}{a_{obs}} \right)^2 H_{obs,3}^{2n} \right)^{\frac{-2n-1}{2n}} \tag{4.8}$$

Substituting in Eq. (4.5) for the pseudo distance we obtain:

$$d(\mathbf{a}, \mathbf{x}_B) = \left| \mathbf{r}_{obj/obs} \right| \left[\left(H_{obs,1}^{2n} + \left(\frac{b}{a} \right)^2 H_{obs,2}^{2n} + \left(\frac{c}{a} \right)^2 H_{obs,3}^{2n} \right)^{\frac{1}{2n}} - 1 \right] \tag{4.9}$$

To determine the effect of the proposed potential function on the path of a manoeuvring object, the gradient of the distance function will be defined from Eq. (4.5) as:

$$\nabla^* d = \nabla^* \left| \mathbf{r}_{obj/obs} \right| \left(F(\mathbf{a}, \mathbf{x}_B)^{\frac{1}{2n}} - 1 \right) + \frac{1}{2n} \left| \mathbf{r}_{obj/obs} \right| F(\mathbf{a}, \mathbf{x}_B)^{\frac{1}{2n}-1} \nabla^* F(\mathbf{a}, \mathbf{x}_B) \tag{4.10}$$

where $\nabla^* = \left[\partial/\partial x \;\; \partial/\partial y \;\; \partial/\partial z \;\; \partial/\partial q_1 \;\; \partial/\partial q_2 \;\; \partial/\partial q_3 \right]^T$, then the gradient of the inside-outside function is defined as:

$$\nabla^* F_{obs} = H_{obs} \begin{bmatrix} aH_{obs,1}^{2n-1}\left(q_1^2 - q_2^2 - q_3^2 + q_4^2\right)_{obs} + 2\frac{b^3}{a^2} H_{obs,2}^{2n-1}\left(q_1 q_2 - q_3 q_4\right)_{obs} \\ + 2\frac{c^3}{a^2} H_{obs,3}^{2n-1}\left(q_1 q_3 + q_2 q_4\right)_{obs} \\ \hline 2aH_{obs,1}^{2n-1}\left(q_1 q_2 + q_3 q_4\right)_{obs} + \frac{b^3}{a^2} H_{obs,2}^{2n-1}\left(-q_1^2 + q_2^2 - q_3^2 + q_4^2\right)_{obs} \\ + 2\frac{c^3}{a^2} H_{obs,3}^{2n-1}\left(q_2 q_3 - q_1 q_4\right)_{obs} \\ \hline 2aH_{obs,1}^{2n-1}\left(q_1 q_3 - q_2 q_4\right)_{obs} + 2\frac{b^3}{a^2} H_{obs,2}^{2n-1}\left(q_2 q_3 + q_1 q_4\right)_{obs} \\ + \frac{c^3}{a^2} H_{obs,3}^{2n-1}\left(-q_1^2 - q_2^2 + q_3^2 + q_4^2\right)_{obs} \\ \hline 2aH_{obs,1}^{2n-1}\left(q_1\left(x_{obj} - x_{obs}\right) + q_2\left(y_{obj} - y_{obs}\right) + q_3\left(z_{obj} - z_{obs}\right)\right) \\ + 2\frac{b^3}{a^2} H_{obs,2}^{2n-1}\left(q_2\left(x_{obj} - x_{obs}\right) - q_1\left(y_{obj} - y_{obs}\right) + q_4\left(z_{obj} - z_{obs}\right)\right) + \\ 2\frac{c^3}{a^2} H_{obs,3}^{2n-1}\left(q_3\left(x_{obj} - x_{obs}\right) - q_4\left(y_{obj} - y_{obs}\right) - q_1\left(z_{obj} - z_{obs}\right)\right) \\ \hline 2aH_{obs,1}^{2n-1}\left(-q_2\left(x_{obj} - x_{obs}\right) + q_1\left(y_{obj} - y_{obs}\right) - q_4\left(z_{obj} - z_{obs}\right)\right) \\ + 2\frac{b^3}{a^2} H_{obs,2}^{2n-1}\left(q_1\left(x_{obj} - x_{obs}\right) + q_2\left(y_{obj} - y_{obs}\right) + q_3\left(z_{obj} - z_{obs}\right)\right) \\ + 2\frac{c^3}{a^2} H_{obs,3}^{2n-1}\left(q_4\left(x_{obj} - x_{obs}\right) + q_3\left(y_{obj} - y_{obs}\right) - q_2\left(z_{obj} - z_{obs}\right)\right) \\ \hline 2aH_{obs,1}^{2n-1}\left(-q_3\left(x_{obj} - x_{obs}\right) + q_4\left(y_{obj} - y_{obs}\right) + q_1\left(z_{obj} - z_{obs}\right)\right) \\ + 2\frac{b^3}{a^2} H_{obs,2}^{2n-1}\left(-q_4\left(x_{obj} - x_{obs}\right) - q_3\left(y_{obj} - y_{obs}\right) + q_2\left(z_{obj} - z_{obs}\right)\right) \\ + 2\frac{c^3}{a^2} H_{obs,3}^{2n-1}\left(q_1\left(x_{obj} - x_{obs}\right) + q_2\left(y_{obj} - y_{obs}\right) + q_3\left(z_{obj} - z_{obs}\right)\right) \end{bmatrix} \quad (4.11)$$

Using Eq. (4.3) and (4.11), it is possible to estimate the effect of the obstacle on the manoeuvring object motion through the gradient of obstacle potential. The following examples will show how to calculate this gradient.

Example I: in the *y*-direction

From Eq. (4.10):

$$\frac{\partial d}{\partial y}=\frac{\partial\left|\mathbf{r}_{obj/obs}\right|}{\partial y}\left(F\left(\mathbf{a},\mathbf{x}_B\right)_{obs}^{\frac{1}{2n}}-1\right)+\frac{1}{2n}\left|\mathbf{r}_{obj/obs}\right|F\left(\mathbf{a},\mathbf{x}_B\right)^{\frac{1}{2n}-1}\frac{\partial}{\partial y}F\left(\mathbf{a},\mathbf{x}_B\right)_{obs} \tag{4.12}$$

$$\frac{\partial d}{\partial y}=\frac{\left|y_{obj}-x_{obs}\right|}{\left|\mathbf{r}_{obj/obs}\right|}\left[\left(F\left(\mathbf{a},\mathbf{x}_B\right)\right)_{obs}^{\frac{1}{2n}}-1\right]+$$

$$\frac{\left|\mathbf{r}_{obj/obs}\right|}{2n}\left(F\left(\mathbf{a},\mathbf{x}_B\right)\right)_{obs}^{\frac{-1}{2n}-1}\left[2aH_{obs,1}^{2n-1}\left(q_1q_2+q_3q_4\right)+\frac{b^3}{a^2}H_{obs,2}^{2n-1}\left(-q_1^2+q_2^2-q_3^2+q_4^2\right)\right. \tag{4.13}$$

$$\left.+2\frac{c^3}{a^2}H_{obs,3}^{2n-1}\left(q_2q_3-q_1q_4\right)\right]$$

To calculate the original pseudo distance rather than the modified one, simply let $\left|\mathbf{r}_{obj/obs}\right|=1$.

4.3.2 Cuboid obstacle potential using the rigid body radial Euclidian distance

The rigid body radial Euclidian distance, Fig. 4.2, is discussed earlier in section 3.4.4 as:

$$d\left(\mathbf{a}_{obs},\mathbf{a}_{obj},\mathbf{x}_{obs},\mathbf{x}_{obj}\right)=\left|\mathbf{r}_{obj/obs}\right|\left(d_1-d_2\right) \tag{4.14}$$

Therefore, using the distance estimation function:

$$d\left(\mathbf{a}_{obs},\mathbf{a}_{obj},\mathbf{x}_{obs,B},\mathbf{x}_{obj,B}\right)=\left|\mathbf{r}_{obj/obs}\right|\left[1-F\left(\mathbf{a},\mathbf{x}_B\right)_{obs}^{\frac{-1}{2n}}-F_{obj}\left(\mathbf{a},\mathbf{x}_B\right)_{obj}^{\frac{-1}{2n}}\right] \tag{4.15}$$

Let the orientations of both the manoeuvring object and obstacle be defined as $\mathbf{q}_{obj}$, and $\mathbf{q}_{obs}$ respectively. The homogeneous transformation is used to find the position of the manoeuvring object centre, $(x,y,z)_{obj,B}$, with respect to the body frame of reference attached with the obstacle under consideration as:

$$\begin{bmatrix} x \\ y \\ z \end{bmatrix}_{obj,B} = \begin{bmatrix} q_1^2 - q_2^2 - q_3^2 + q_4^2 & 2(q_1 q_2 + q_3 q_4) & 2(q_1 q_3 - q_2 q_4) \\ 2(q_1 q_2 - q_3 q_4) & -q_1^2 + q_2^2 - q_3^2 + q_4^2 & 2(q_2 q_3 + q_1 q_4) \\ 2(q_1 q_3 + q_2 q_4) & 2(q_2 q_3 - q_1 q_4) & -q_1^2 - q_2^2 + q_3^2 + q_4^2 \end{bmatrix}_{obs} \begin{bmatrix} x_{obj} - x_{obs} \\ y_{obj} - y_{obs} \\ z_{obj} - z_{obs} \end{bmatrix}_I \quad (4.16)$$

The same procedure is carried out to find the obstacle centre position, $(x,y,z)_{obs,B}$, with respect to the manoeuvring object body frame of reference as:

$$\begin{bmatrix} x \\ y \\ z \end{bmatrix}_{obs,B} = \begin{bmatrix} q_1^2 - q_2^2 - q_3^2 + q_4^2 & 2(q_1 q_2 + q_3 q_4) & 2(q_1 q_3 - q_2 q_4) \\ 2(q_1 q_2 - q_3 q_4) & -q_1^2 + q_2^2 - q_3^2 + q_4^2 & 2(q_2 q_3 + q_1 q_4) \\ 2(q_1 q_3 + q_2 q_4) & 2(q_2 q_3 - q_1 q_4) & -q_1^2 - q_2^2 + q_3^2 + q_4^2 \end{bmatrix}_{obj} \begin{bmatrix} x_{obs} - x_{obj} \\ y_{obs} - y_{obj} \\ z_{obs} - z_{obj} \end{bmatrix}_I \quad (4.17)$$

The inside-outside functions will be:

$$F(\mathbf{a}, \mathbf{x}_B)_{obs} = H_{obs,1}^{2n} + \left(\frac{b_{obs}}{a_{obs}}\right)^2 H_{obs,2}^{2n} + \left(\frac{c_{obs}}{a_{obs}}\right)^2 H_{obs,3}^{2n} \quad (4.18)$$

$$F(\mathbf{a}, \mathbf{x}_B)_{obj} = H_{obj,1}^{2n} + \left(\frac{b_{obj}}{a_{obj}}\right)^2 H_{obj,2}^{2n} + \left(\frac{c_{obj}}{a_{obj}}\right)^2 H_{obj,3}^{2n} \quad (4.19)$$

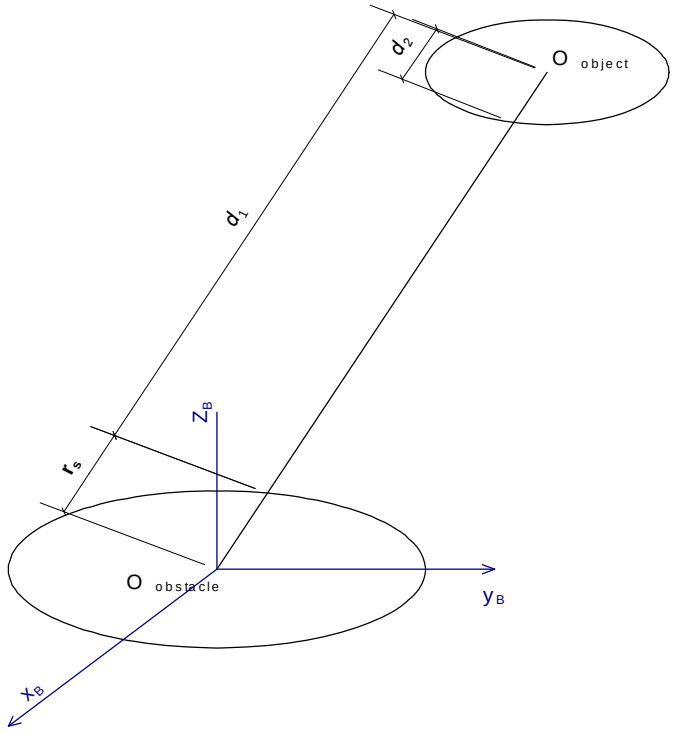

Fig. 4.2 Radial Euclidian distance

By substituting $F(\mathbf{a},\mathbf{x}_B)_{obs}$ and $F(\mathbf{a},\mathbf{x}_B)_{obj}$ in Eq. (4.15), it is possible to define the separation distance as a function of *x, y, z*, q_1, q_2, q_3, and q_4 of both the manoeuvring object and the obstacles as:

$$d(\mathbf{a}_{obs},\mathbf{a}_{obj},\mathbf{x}_{obs,B},\mathbf{x}_{obj,B}) = |\mathbf{r}_{obj/obs}| \left[1 - \left[H_{obs,1}^{2n} + \left(\frac{b_{obs}}{a_{obs}}\right)^2 H_{obs,2}^{2n} + \left(\frac{c_{obs}}{a_{obs}}\right)^2 H_{obs,3}^{2n} \right]^{\frac{-1}{2n}} - \left[H_{obj,1}^{2n} + \left(\frac{b_{obj}}{a_{obj}}\right)^2 H_{obj,2}^{2n} + \left(\frac{c_{obj}}{a_{obj}}\right)^2 H_{obj,3}^{2n} \right]^{\frac{-1}{2n}} \right] \tag{4.20}$$

The gradient of the distance function expressed in Eq. (4.15) is found to be:

$$\nabla^* d = \nabla^* |\mathbf{r}_{obj/obs}| \left[1 - F(\mathbf{a},\mathbf{x}_B)_{obs}^{\frac{-1}{2n}} - F(\mathbf{a},\mathbf{x}_B)_{obj}^{\frac{-1}{2n}} \right] + |\mathbf{r}_{obj/obs}| \nabla^* \left[1 - F(\mathbf{a},\mathbf{x}_B)_{obs}^{\frac{-1}{2n}} - F(\mathbf{a},\mathbf{x}_B)_{obj}^{\frac{-1}{2n}} \right] \tag{4.21}$$

The following examples will demonstrate how to calculate the distance function gradient that will be used in the obstacle potential gradient calculation.

Example (II): In the *x*-direction

$$\frac{\partial d}{\partial x} = \frac{\partial |\mathbf{r}_{obj/obs}|}{\partial x} \left[1 - F(\mathbf{a},\mathbf{x}_B)_{obs}^{\frac{-1}{2n}} - F(\mathbf{a},\mathbf{x}_B)_{obj}^{\frac{-1}{2n}} \right] + |\mathbf{r}_{obj/obs}| \frac{\partial}{\partial x} \left[1 - F(\mathbf{a},\mathbf{x}_B)_{obs}^{\frac{-1}{2n}} - F(\mathbf{a},\mathbf{x}_B)_{obj}^{\frac{-1}{2n}} \right] \tag{4.22}$$

$$\frac{\partial d}{\partial x} = \frac{|x_{obj} - x_{obs}|}{|\mathbf{r}_{obj/obs}|} \left[1 - F(\mathbf{a},\mathbf{x}_B)_{obs}^{\frac{-1}{2n}} - F(\mathbf{a},\mathbf{x}_B)_{obj}^{\frac{-1}{2n}} \right] + |\mathbf{r}_{obj/obs}| \left[\frac{1}{2n} F(\mathbf{a},\mathbf{x}_B)_{obs}^{\frac{-1}{2n}-1} \frac{\partial}{\partial x} F(\mathbf{a},\mathbf{x}_B)_{obj} + \frac{1}{2n} F(\mathbf{a},\mathbf{x}_B)_{obs}^{\frac{-1}{2n}-1} \frac{\partial}{\partial x} F(\mathbf{a},\mathbf{x}_B)_{obj} \right] \tag{4.23}$$

$$\frac{\partial d}{\partial x}=\frac{\left|x_{obj}-x_{obs}\right|}{\left|\mathbf{r}_{obj/obs}\right|}\left[1-F\left(\mathbf{a},\mathbf{x}_B\right)_{obs}^{\frac{-1}{2n}}-F\left(\mathbf{a},\mathbf{x}_B\right)_{obj}^{\frac{-1}{2n}}\right]+\left|\mathbf{r}_{obj/obs}\right|\mathrm{x}$$

$$\left[\frac{1}{2n}F\left(\mathbf{a},\mathbf{x}_B\right)_{obs}^{\frac{-1}{2n}-1}\left[aH_{obs,1}^{2n-1}\left(q_1^2-q_2^2-q_3^2+q_4^2\right)_{obs}+2\frac{b^3}{a^2}H_{obs,2}^{2n-1}\left(q_1q_2-q_3q_4\right)_{obs}\right.\right. \tag{4.24}$$

$$\left.+2\frac{c^3}{a^2}H_{obs,3}^{2n-1}\left(q_1q_3+q_2q_4\right)_{obs}\right]+\frac{1}{2n}F\left(\mathbf{a},\mathbf{x}_B\right)_{obj}^{\frac{-1}{2n}-1}\left[aH_{obj,1}^{2n-1}\left(q_1^2-q_2^2-q_3^2+q_4^2\right)_{obj}\right.$$

$$\left.\left.+2\frac{b^3}{a^2}H_{obj,2}^{2n-1}\left(q_1q_2-q_3q_4\right)_{obj}+2\frac{c^3}{a^2}H_{obj,3}^{2n-1}\left(q_1q_3+q_2q_4\right)_{obj}\right]\right]$$

Example (III): With respect to q_1

$$\frac{\partial d}{\partial q_1}=\frac{\partial\left|\mathbf{r}_{obj/obs}\right|}{\partial q_1}\left[1-F\left(\mathbf{a},\mathbf{x}_B\right)_{obs}^{\frac{-1}{2n}}-F\left(\mathbf{a},\mathbf{x}_B\right)_{obj}^{\frac{-1}{2n}}\right] \tag{4.25}$$

$$+\left|\mathbf{r}_{obj/obs}\right|\frac{\partial}{\partial q_1}\left[1-F\left(\mathbf{a},\mathbf{x}_B\right)_{obs}^{\frac{-1}{2n}}-F\left(\mathbf{a},\mathbf{x}_B\right)_{obj}^{\frac{-1}{2n}}\right]$$

$$\frac{\partial d}{\partial q_1}=\left|\mathbf{r}_{obj/obs}\right|\left[\frac{1}{2n}F\left(\mathbf{a},\mathbf{x}_B\right)_{obs}^{\frac{-1}{2n}-1}\frac{\partial}{\partial q_1}F\left(\mathbf{a},\mathbf{x}_B\right)_{obs}+\frac{1}{2n}F\left(\mathbf{a},\mathbf{x}_B\right)_{obj}^{\frac{-1}{2n}-1}\frac{\partial}{\partial q_1}F\left(\mathbf{a},\mathbf{x}_B\right)_{obj}\right] \tag{4.26}$$

$$\frac{\partial d}{\partial q_1}=\left|\mathbf{r}_{obj/obs}\right|\left[\frac{1}{2n}F\left(\mathbf{a},\mathbf{x}_B\right)_{obs}^{\frac{-1}{2n}-1}\left[2aH_{obs,1}^{2n-1}\left(q_1\left(x_{obj}-x_{obs}\right)+q_2\left(y_{obj}-y_{obs}\right)+q_3\left(z_{obj}-z_{obs}\right)\right)_{obs}\right.\right.$$

$$+2\frac{b^3}{a^2}H_{obs,2}^{2n-1}\left(q_2\left(x_{obj}-x_{obs}\right)-q_1\left(y_{obj}-y_{obs}\right)+q_4\left(z_{obj}-z_{obs}\right)\right)_{obs}$$

$$\left.+2\frac{c^3}{a^2}H_{obs,3}^{2n-1}\left(q_3\left(x_{obj}-x_{obs}\right)-q_4\left(y_{obj}-y_{obs}\right)-q_1\left(z_{obj}-z_{obs}\right)\right)_{obs}\right]$$

$$+\frac{1}{2n}F\left(\mathbf{a},\mathbf{x}_B\right)_{obj}\left[2aH_{obj,1}^{2n-1}\left(q_1\left(x_{obs}-x_{obj}\right)+q_2\left(y_{obs}-y_{obj}\right)+q_3\left(z_{obs}-z_{obj}\right)\right)_{obj}\right.$$

$$+2\frac{b^3}{a^2}H_{obj,2}^{2n-1}\left(q_2\left(x_{obs}-x_{obj}\right)-q_1\left(y_{obs}-y_{obj}\right)+q_4\left(z_{obs}-z_{obj}\right)\right)_{obj}$$

$$\left.\left.+2\frac{c^3}{a^2}H_{obj,3}^{2n-1}\left(q_3\left(x_{obs}-x_{obj}\right)-q_4\left(y_{obs}-y_{obj}\right)-q_1\left(z_{obs}-z_{obj}\right)\right)_{obj}\right]\right] \tag{4.27}$$

4.4 Obstacle Potential of a Cylindrical Element

The inside-outside function for a cylindrical element was expressed as:

$$F(\mathbf{a},\mathbf{x}_B)=\left[\left(\frac{x}{r}\right)^2+\left(\frac{y}{r}\right)^2\right]^n+\left(\frac{c}{r}\right)^2\left(\frac{z}{c}\right)^{2n} \tag{4.28}$$

using the modified pseudo-distance method to estimate the distance between a point and a beam represented by the superquadric method. Substituting in Eq. (4.5) with the previous inside-outside function, the modified pseudo-distance will be expressed as:

$$\begin{aligned} &d(\mathbf{a},\mathbf{x})=\left|\mathbf{r}_{obj/obs}\right|\cdot \\ &\left[\left[\left(\frac{\left(q_1^2-q_2^2-q_3^2+q_4^2\right)(x-x_{obs})+2\left(q_1q_2+q_3q_4\right)(y-y_{obs})+2\left(q_1q_3-q_2q_4\right)(z-z_{obs})}{r}\right)_{obs}^2\right. \\ &+\left(\frac{2\left(q_1q_2-q_3q_4\right)(x-x_{obs})-\left(q_1^2+q_2^2-q_3^2+q_4^2\right)(y-y_{obs})+2\left(q_2q_3+q_1q_4\right)(z-z_{obs})}{r}\right)_{obs}^2 \\ &\left.+\left(\frac{c}{r}\right)^2\left(\frac{2\left(q_1q_3+q_2q_4\right)(x-x_{obs})+2\left(q_2q_3-q_1q_4\right)(y-y_{obs})-\left(q_1^2-q_2^2+q_3^2+q_4^2\right)(z-z_{obs})}{c}\right)_{obs}^{2n}\right]^{\frac{1}{2n}}-1\Bigg] \end{aligned} \tag{4.29}$$

Using the same procedure as done before in the modified-pseudo distance for the parallelepiped element:

$$\nabla d=\nabla\left|\mathbf{r}_{obj/obs}\right|\left(F(\mathbf{a},\mathbf{x}_B)^{\frac{1}{2n}}-1\right)+\frac{1}{2n}\left|\mathbf{r}_{obj/obs}\right|F(\mathbf{a},\mathbf{x}_B)^{\frac{1}{2n}-1}\nabla F(\mathbf{a},\mathbf{x}_B) \tag{4.30}$$

The gradient of the corresponding inside-outside function is defined as:

$$\nabla^* F = \begin{bmatrix} 2\frac{n}{r}\left(H_1^2+H_2^2\right)^{n-1}\left[H_1\left(q_1^2-q_2^2-q_3^2+q_4^2\right)+2H_2\left(q_1q_2-q_3q_4\right)\right] \\ +4n\frac{c^3}{a^2}H_3^{2n-1}\left(q_1q_3+q_2q_4\right) \\ \hdashline 2\frac{n}{r}\left(H_1^2+H_2^2\right)^{n-1}\left[2H_1\left(q_1q_2+q_3q_4\right)+H_2\left(-q_1^2+q_2^2-q_3^2+q_4^2\right)\right] \\ +4n\frac{c^3}{a^2}H_3^{2n-1}\left(q_2q_3-q_1q_4\right) \\ \hdashline 2\frac{n}{r}\left(H_1^2+H_2^2\right)^{n-1}\left[2H_1\left(q_1q_3-q_2q_4\right)+2H_2\left(q_2q_3+q_1q_4\right)\right] \\ +4n\frac{c^3}{a^2}H_3^{2n-1}\left(-q_1^2-q_2^2+q_3^2+q_4^2\right) \\ \hline 4\frac{n}{r}\left(H_1^2+H_2^2\right)^{n-1}\begin{bmatrix} H_1\left(q_1\left(x-x_o\right)+q_2\left(y-y_o\right)+q_3\left(z-z_o\right)\right)+ \\ H_2\left(q_2\left(x-x_o\right)-q_1\left(y-y_o\right)+q_4\left(z-z_o\right)\right) \end{bmatrix} \\ 4n\frac{c^3}{r^2}H_3^{2n-1}\left(q_3\left(x-x_o\right)-q_4\left(y-y_o\right)-q_1\left(z-z_o\right)\right) \\ \hdashline 4\frac{n}{r}\left(H_1^2+H_2^2\right)^{n-1}\begin{bmatrix} H_1\left(-q_2\left(x-x_o\right)+q_1\left(y-y_o\right)-q_4\left(z-z_o\right)\right)+ \\ H_2\left(q_1\left(x-x_o\right)+q_2\left(y-y_o\right)+q_3\left(z-z_o\right)\right) \end{bmatrix} \\ 4n\frac{c^3}{r^2}H_3^{2n-1}\left(q_4\left(x-x_o\right)+q_3\left(y-y_o\right)-q_2\left(z-z_o\right)\right) \\ \hdashline 4\frac{n}{r}\left(H_1^2+H_2^2\right)^{n-1}\begin{bmatrix} H_1\left(-q_3\left(x-x_o\right)+q_4\left(y-y_o\right)+q_1\left(z-z_o\right)\right)+ \\ H_2\left(-q_4\left(x-x_o\right)-q_3\left(y-y_o\right)+q_2\left(z-z_o\right)\right) \end{bmatrix} \\ 4n\frac{c^3}{r^2}H_3^{2n-1}\left(q_1\left(x-x_o\right)+q_2\left(y-y_o\right)+q_3\left(z-z_o\right)\right) \end{bmatrix} \tag{4.31}$$

The same procedure can be used for the radial Euclidian distance.

4.5 Conclusions

Superquadric repulsive potentials have shown their flexibility. They can form a steep decay in the obstacle potential to a smooth ramp by changing the parameter α. If the workspace is dense, a large value of α is required to minimize the range of each obstacle to allow the manoeuvring objects to pass through narrow passages

between them. However, the objects will suffer from sudden changes in direction as the repulsive potentials suddenly increase. Small values of α result in a smooth change in motion at the expense of increasing the range of the obstacles. The dependency of the superquadric repulsive potentials on both the position and orientation of the objects lead to their gradients being defined in terms of both position and quaternion parameters.

5. GLOBAL POTENTIAL FUNCTION

5.1 Introduction

Potential function elements were discussed in the previous chapters separately as attractive and repulsive functions. Formation of the global potential will be discussed in this chapter as a superposition of its elements. The global potential function allows a manoeuvring object to be attracted toward its goal while being repelled from obstacles. The selected functions should satisfy *Lyapunov*'s stability criteria to guarantee the global stability and convergence. Two control strategy types are discussed in this chapter, termed continuous and impulsive control strategies. The continuous control strategy produces continuous forces which act as the main control force for the manoeuvring object. The impulsive control strategy produces discrete control action to maintain continuous approach to the required goal (Schaub and Alfriend, 2001). In both strategies, potential field elements are summed together; hence some drawbacks are produced (Koren and Borenstein, 1991):

1. Local minimum due to the interference between the spherically symmetric attractive potential and the repulsive potentials produced from a single sharp edged object.
2. Local minima due to the existence of multiple obstacles close to each other.
3. The "goal non-reachable due to obstacle nearby" problem which exists when an obstacle is located near the goal position. Consequently the global minimum of the potential function may be shifted from the desired location.

However, all these problems were in fact found to be overcome through the use of the superquadric obstacle representation by virtue of its spherical symmetry even for sharp edge objects, and through the decay of the obstacle potential amplitude when approaching the goal configuration. The mathematical models of the two strategies are discussed with examples in the rest of this chapter.

5.2 Continuous Control

The continuous control concept is to apply bounded control forces to drive the manoeuvring object toward its goal. The original potential function, defined through proportionality with the distance between the manoeuvring object and its goal, provides simple control forces as a relation from the potential function gradient (Latombe, 1991). The potential functions defined in this thesis are used to derive the control force in a more sophisticated way explained in this section. The derived control laws provide the required accelerations which the manoeuvring objects should generate.

A global potential function suitable for the continuous control strategy with a stationary goal position is defined by adding the attractive potential defined in Eq. (2.53) to the repulsive potential defined by Eqs. (4.1) and (4.2) as (Badawy and McInnes, 2007c):

$$V = \begin{cases} \lambda_p \left|\mathbf{r}-\mathbf{r}_G\right| + \frac{1}{2}\lambda_v \dot{\mathbf{r}}.\dot{\mathbf{r}} + \lambda_q \overline{\mathbf{q}}.\overline{\mathbf{q}} + \frac{1}{2}\lambda_\omega \boldsymbol{\omega}.\boldsymbol{\omega} + V_{obs} & \text{if } \left|\mathbf{r}-\mathbf{r}_G\right| > R \\ \frac{1}{2}\lambda_p \left(\mathbf{r}-\mathbf{r}_G\right).\left(\mathbf{r}-\mathbf{r}_G\right) + \frac{1}{2}\lambda_v \dot{\mathbf{r}}.\dot{\mathbf{r}} + \lambda_q \overline{\mathbf{q}}.\overline{\mathbf{q}} + \frac{1}{2}\lambda_\omega \boldsymbol{\omega}.\boldsymbol{\omega} + V_{obs} & \text{if } \left|\mathbf{r}-\mathbf{r}_G\right| \le R \end{cases} \tag{5.1}$$

The time derivative of the potential function will be:

$$W = \begin{cases} \dot{\mathbf{r}}.\left(\lambda_p \left(\mathbf{r}-\mathbf{r}_G\right)/\left|\mathbf{r}-\mathbf{r}_G\right| + \lambda_v \ddot{\mathbf{r}} + \nabla V_{obs}\right) + 2\lambda_q \dot{\overline{\mathbf{q}}}.\overline{\mathbf{q}} + \lambda_\omega \dot{\boldsymbol{\omega}}.\boldsymbol{\omega} + \dot{\overline{\mathbf{q}}}.\nabla^q V_{obs} & \text{if } \left|\mathbf{r}-\mathbf{r}_G\right| > R \\ \dot{\mathbf{r}}.\left(\lambda_p \left(\mathbf{r}-\mathbf{r}_G\right) + \lambda_v \ddot{\mathbf{r}} + \nabla V_{obs}\right) + 2\lambda_q \dot{\overline{\mathbf{q}}}.\overline{\mathbf{q}} + \lambda_\omega \dot{\boldsymbol{\omega}}.\boldsymbol{\omega} + \dot{\overline{\mathbf{q}}}.\nabla^q V_{obs} & \text{if } \left|\mathbf{r}-\mathbf{r}_G\right| \le R \end{cases} \tag{5.2}$$

where the terms ∇ and ∇^q are defined as Eqs. (2.6.a) and (2.31) respectively, therefore from Eqs. (2.40) and (2.43) we obtain:

$$W = \begin{cases} \dot{\mathbf{r}}.\left(\lambda_p \left(\mathbf{r}-\mathbf{r}_G\right)/\left|\mathbf{r}-\mathbf{r}_G\right| + \lambda_v \ddot{\mathbf{r}} + \nabla V_{obs}\right) + \boldsymbol{\omega}.\left(\lambda_q q_4 \overline{\mathbf{q}} + \lambda_\omega \dot{\boldsymbol{\omega}} + 0.5\mathbf{Q}\nabla^q V_{obs}\right) & \text{if } \left|\mathbf{r}-\mathbf{r}_G\right| > R \\ \dot{\mathbf{r}}.\left(\lambda_p \left(\mathbf{r}-\mathbf{r}_G\right) + \lambda_v \ddot{\mathbf{r}} + \nabla V_{obs}\right) + \boldsymbol{\omega}.\left(\lambda_q q_4 \overline{\mathbf{q}} + \lambda_\omega \dot{\boldsymbol{\omega}} + 0.5\mathbf{Q}\nabla^q V_{obs}\right) & \text{if } \left|\mathbf{r}-\mathbf{r}_G\right| \le R \end{cases} \tag{5.3}$$

To set the time derivative of the potential function to be negative definite, the control laws as in Eqs. (2.56) and (2.57) are then defined as:

$$\ddot{\mathbf{r}} = \begin{cases} -\left(\dfrac{\lambda_p}{\lambda_v} \dfrac{\mathbf{r} - \mathbf{r}_G}{|\mathbf{r} - \mathbf{r}_G|} + \lambda_v^* \dot{\mathbf{r}} + \dfrac{1}{\lambda_v} \nabla V_{obs} \right) & \text{if } |\mathbf{r} - \mathbf{r}_G| > R \\ -\left(\dfrac{\lambda_p}{\lambda_v} (\mathbf{r} - \mathbf{r}_G) + \lambda_v^* \dot{\mathbf{r}} + \dfrac{1}{\lambda_v} \nabla V_{obs} \right) & \text{if } |\mathbf{r} - \mathbf{r}_G| \le R \end{cases} \tag{5.4}$$

and

$$\dot{\boldsymbol{\omega}} = -\left(\frac{\lambda_q}{\lambda_\omega} q_4 \overline{\mathbf{q}} + \lambda_\omega^* \boldsymbol{\omega} + \frac{1}{2\lambda_\omega} \mathbf{Q} \nabla^q V_{obs} \right) \tag{5.5}$$

The following example demonstrates this method using two different object shapes, two parallelepipeds of dimensions 1 x 1 x 0.1 m and of 1 kg mass and two discs of 1 m diameter, 0.1 m thickness and 1.2 kg mass. The repulsive parameters are defined as $\alpha = 4$, $A_o = 5$, $\sigma = 0.1$, and $\beta = 1$. The control law parameters, λ_p, λ_q, λ_ω, λ_v^*, and λ_ω^* are selected as unity, while λ_v is selected to be 3. The parabolic zone radius, *R,* is chosen to be 0.5. The objects will swap their positions while avoiding collision with each other. Mutual object dependency on position and orientation is illustrated. The initial object configurations are shown in Fig. 5.1 while subsequent configurations are illustrated in Fig. 5.2. Object trajectories are shown in Fig. 5.3. It can be seen that both translational and rotational manoeuvres are used for collision avoidance. The proposed potential function enables the controller to act with a constant velocity as seen in Fig. 5.4 until reaching a certain range from the goal position. At this range, the controller reduces the object velocity to perform smooth motion to the goal position allowing smooth contact in the case of assembly. It can be seen from Figs. 5.4.c and 5.4.d that an initial pulse is produced to generate constant translational velocities, followed by collision avoidance and braking manoeuvres. Finally, the object angular velocities and angular accelerations are shown in Fig. 5.5.

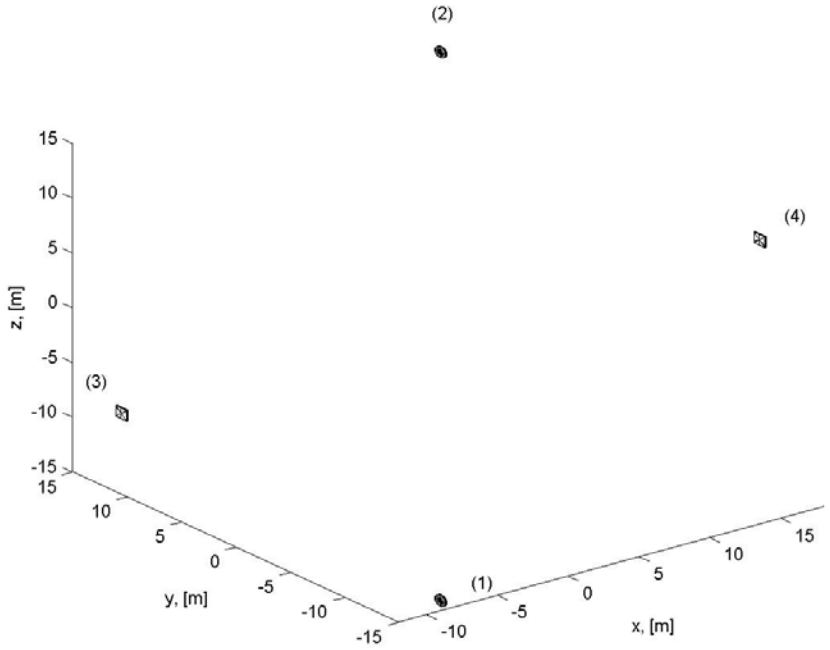

Fig. 5.1 Initial configuration

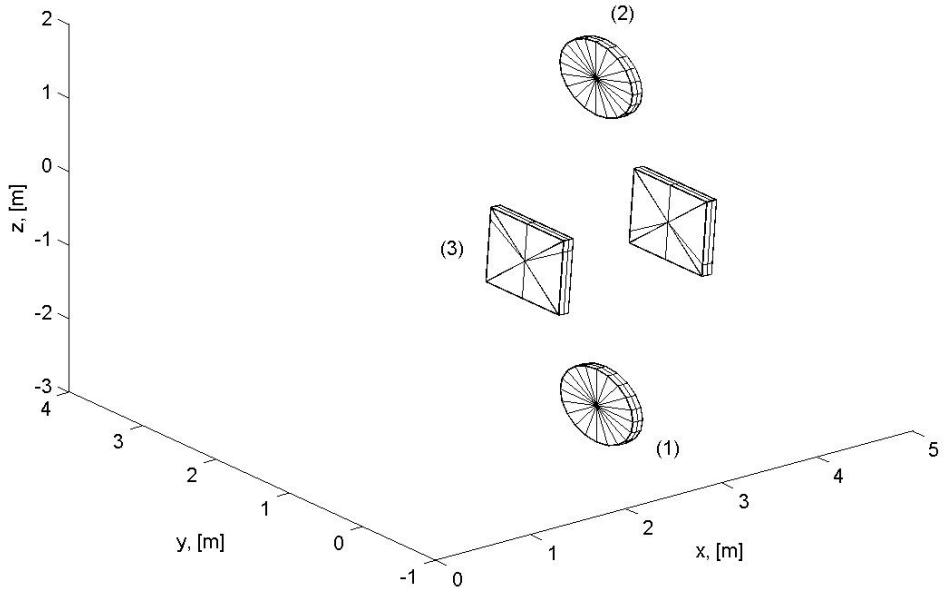

Fig. 5.2.a) Object configuration at t = 70 sec

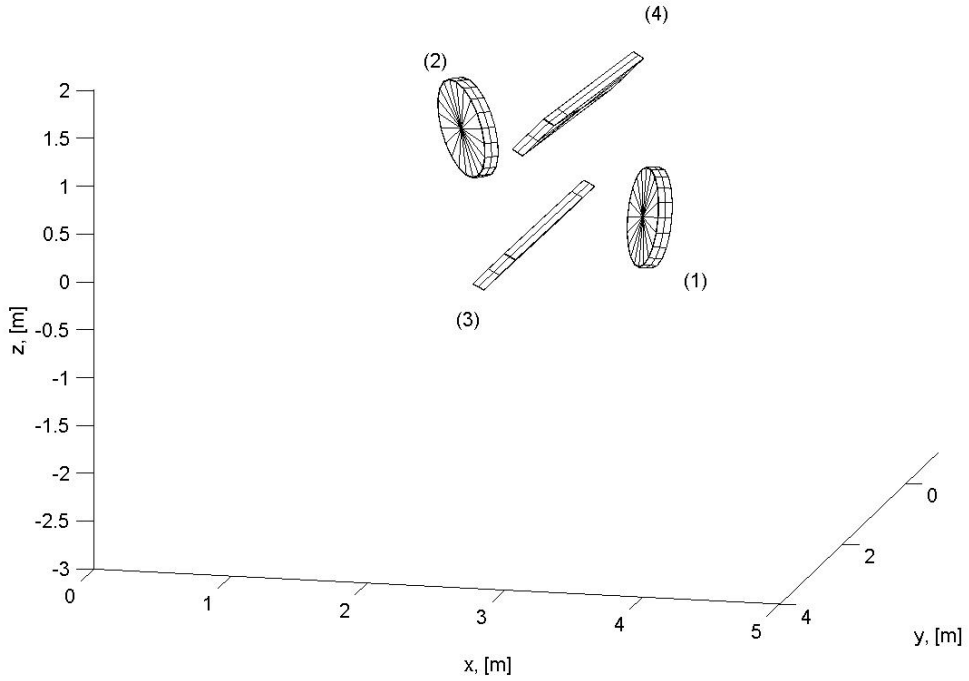

Fig. 5.2.b) Object configuration at t = 80 sec

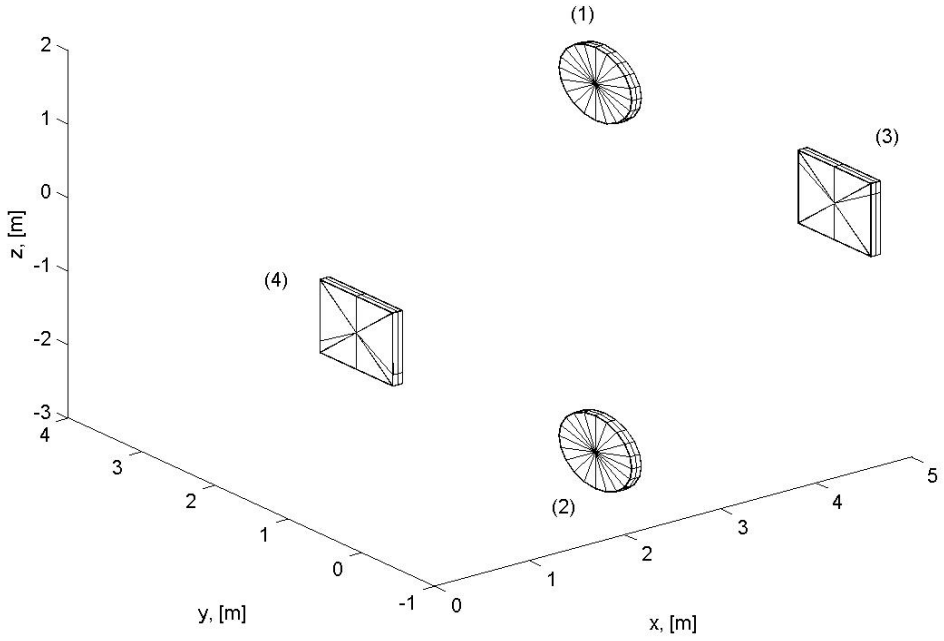

Fig. 5.2.c) Final object configuration at t = 130 sec

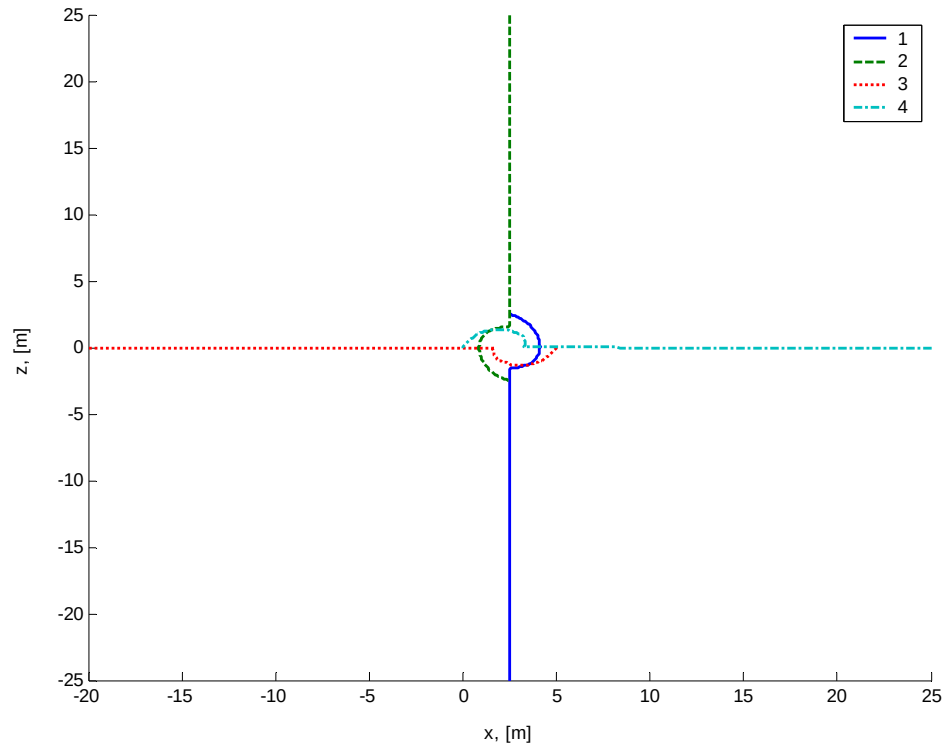

Fig. 5.3 Object trajectories

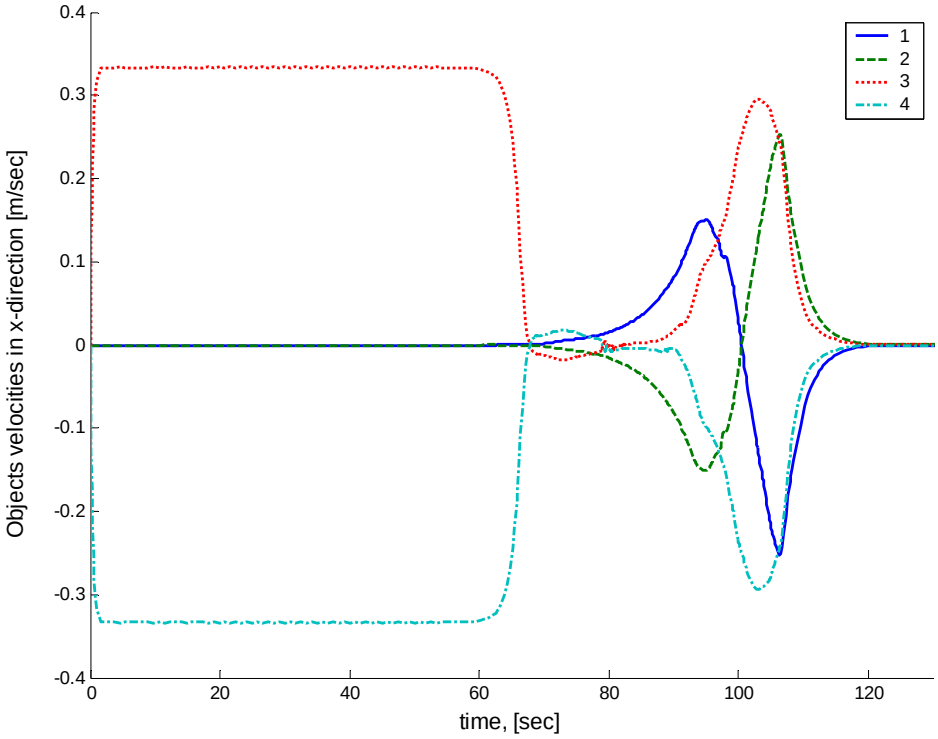

Fig. 5.4.a) Object velocities in *x*-direction

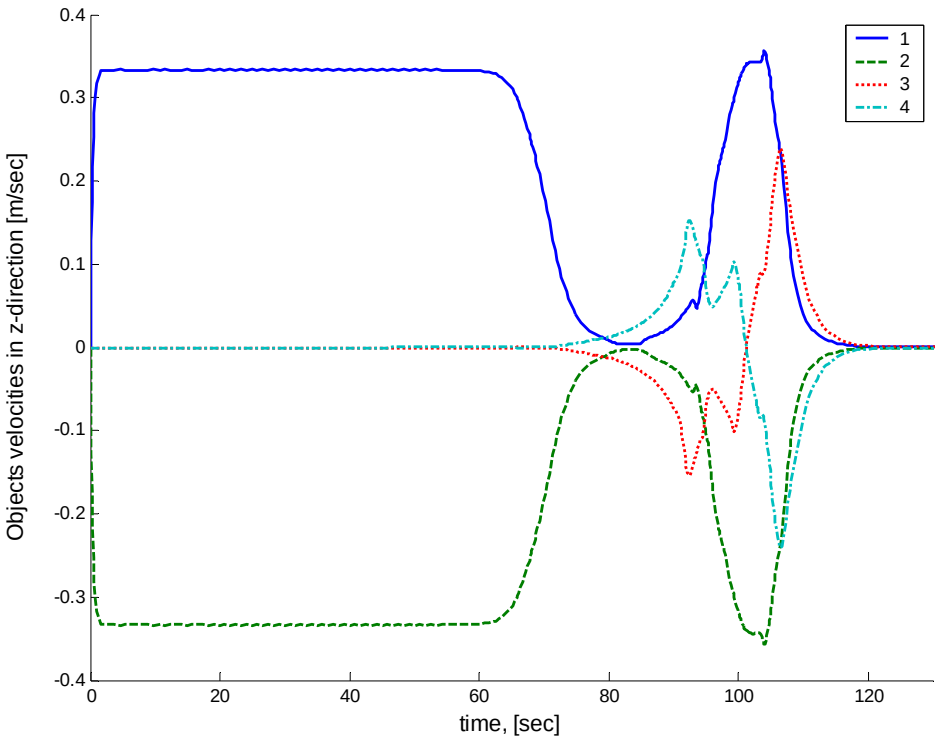

Fig. 5.4.b) Object velocities in *z*-direction

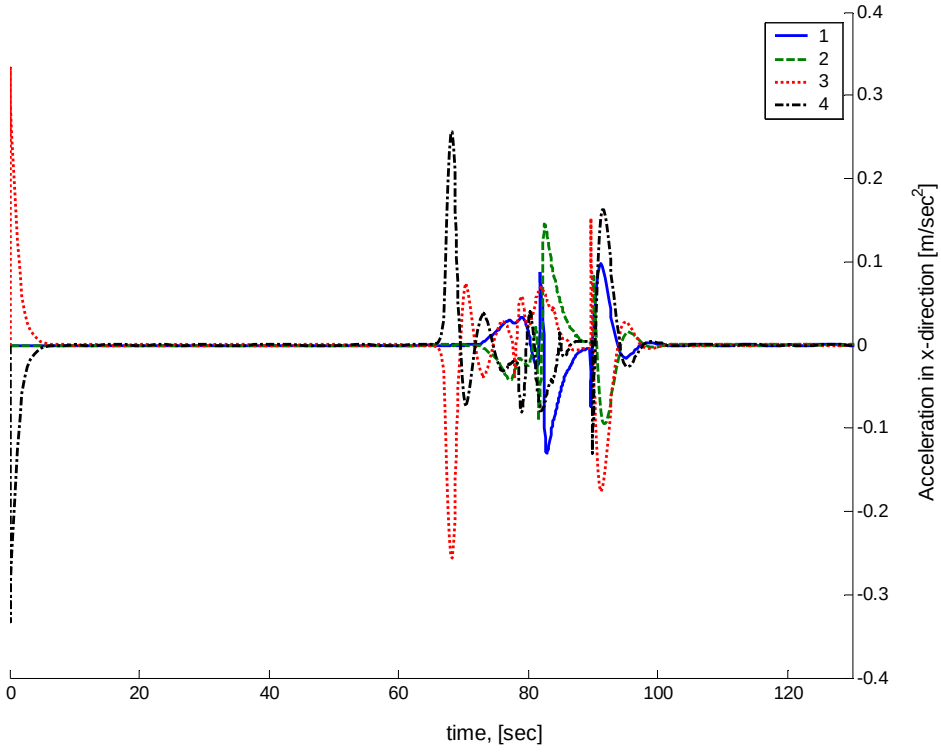

Fig. 5.4.c) Object accelerations in *x*-direction

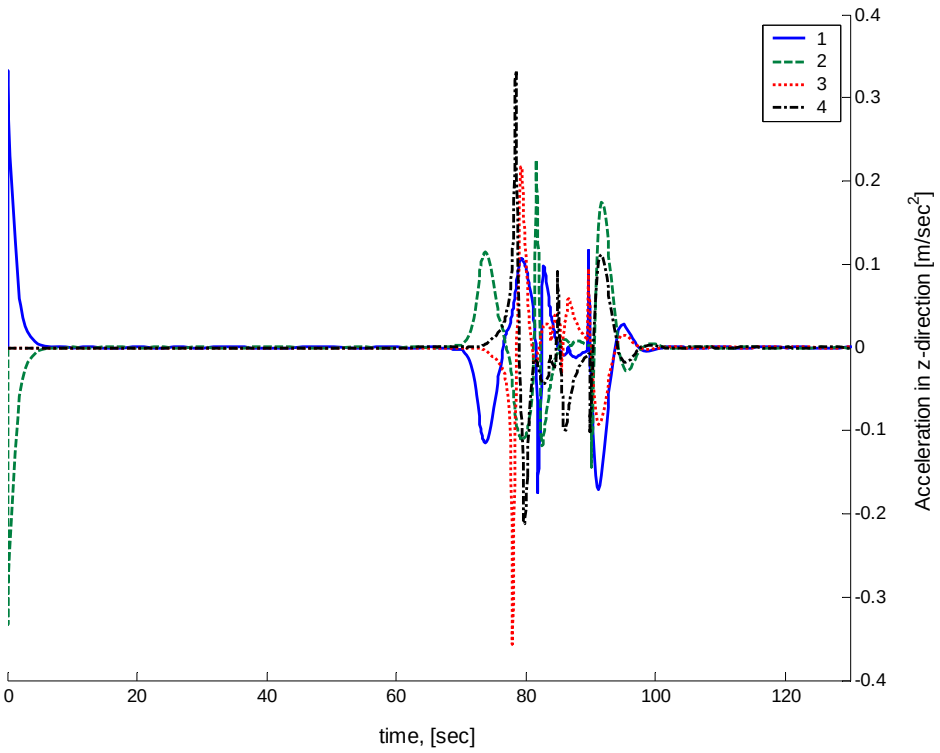

Fig. 5.4.d) Object accelerations in *z*-direction

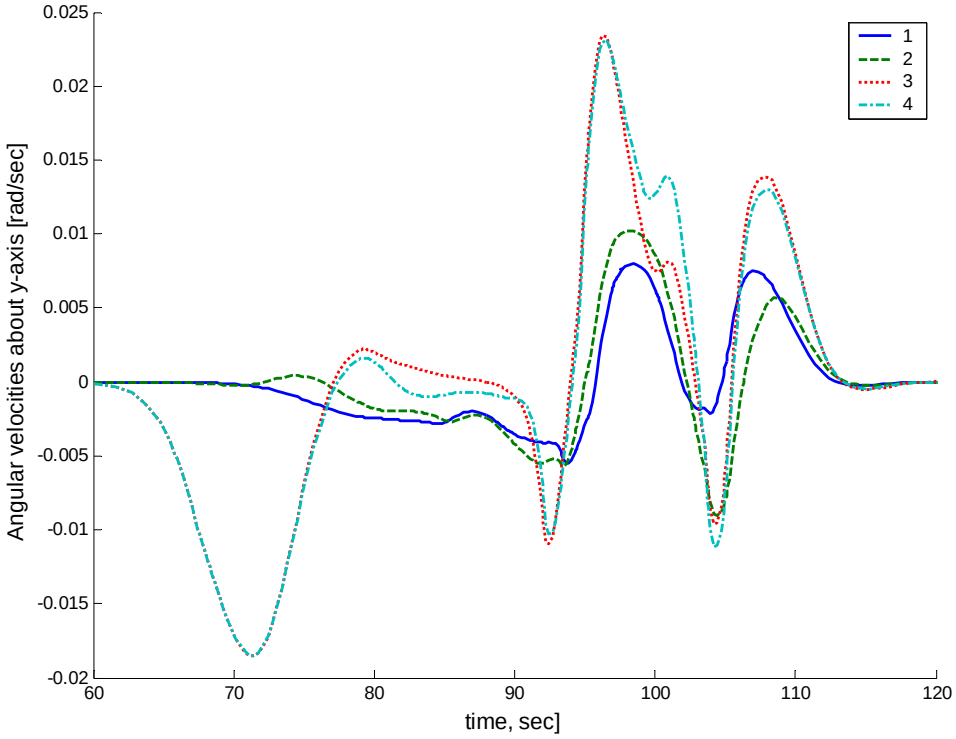

Fig. 5.5.a) Object angular velocities about *y*-axis

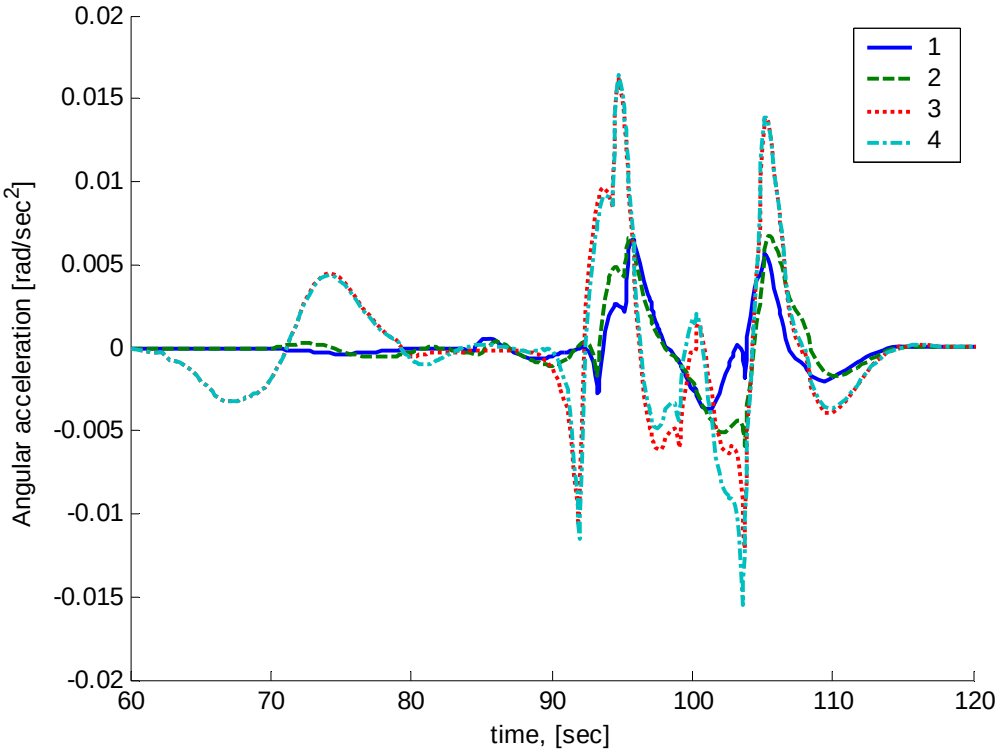

Fig. 5.5.b) Object angular accelerations about *y*-axis

5.3 Impulsive Control

The impulsive control strategy utilizes high thrust to produce impulsive forces able to maintain continuous approach to the goal. This control intervention is used only to amend the manoeuvring object trajectory as it diverges from the goal. Since the impulse is defined as a step change in the object velocity, the control law should be constructed to define the required control velocity profile.

A modification to Eq. (5.1) for this different control strategy is discussed. The stability criteria defined in section 5.2 are not adequate for impulsive control as the control laws should deal with objects velocities rather than accelerations. The proposed global potential function is then expressed as:

$$V = \frac{\lambda_p}{2}(\mathbf{r}-\mathbf{r}_G).(\mathbf{r}-\mathbf{r}_G) + \lambda_q \bar{\mathbf{q}}.\bar{\mathbf{q}} + \frac{\lambda_\omega}{2}\boldsymbol{\omega}.\boldsymbol{\omega} + V_{obs} \tag{5.6}$$

The time derivative of the potential function will be:

$$W = \dot{\mathbf{r}}.\left(\lambda_p\left(\mathbf{r}-\mathbf{r}_G\right)+\nabla V_{obs}\right)+2\lambda_q\dot{\bar{\mathbf{q}}}.\bar{\mathbf{q}}+\lambda_\omega\dot{\boldsymbol{\omega}}.\boldsymbol{\omega}+\dot{\bar{\mathbf{q}}}.\nabla^q V_{obs} \tag{5.7}$$

The rotational motion will be defined using continuous control as discussed in the previous section, hence the attitude control law will be the same as in Eq. (5.5). The object velocity will be defined as:

$$\dot{\mathbf{r}} = -v_{max}\left(1-exp\left(-\beta\left|\mathbf{r}-\mathbf{r}_G\right|^2\right)\right)\frac{\nabla V}{\left|\nabla^* V\right|} \qquad \text{if} \quad W \geq c_f \tag{5.8}$$

where the control trigger constant, c_f, is a non-positive number used to decide when the control action is needed. It should be set to zero to satisfy the *Lyapunov* stability criteria, however a negative constant is also applicable to anticipate advance control action. Rewriting Eq. (2.5) with added repulsive potential leads to:

$$\dot{\mathbf{r}} = -v_{max}\left(1-exp\left(-\boldsymbol{\beta}\left|\mathbf{r}-\mathbf{r}_G\right|^2\right)\right)\frac{\lambda_p\left(\mathbf{r}-\mathbf{r}_G\right)+\nabla V_{obs}}{\left|\nabla^* V\right|} \quad \text{if} \quad W \geq c_f \tag{5.9}$$

Now, substituting with Eq. (5.9) into Eq. (5.7) for the translation term only we obtain:

$$W = -v_{max}\left(1-exp\left(-\beta\left|\mathbf{r}-\mathbf{r}_G\right|^2\right)\right)\frac{\lambda_p\left(\mathbf{r}-\mathbf{r}_G\right)+\nabla V_{obs}}{\left|\nabla^* V\right|}.\left(\lambda_p\left(\mathbf{r}-\mathbf{r}_G\right)+\nabla V_{obs}\right)\leq 0 \tag{5.10}$$

Hence, the proposed impulsive control law ensures stability. The same motion planning problem discussed with the continuous motion planning strategy in the previous section is repeated using the impulsive control strategy. The maximum controlled velocity is 0.01 m/sec, with the control trigger constant equal zero as it produces the most difficult motion planning problem with no anticipation. The initial object configuration is shown in Fig. 5.6, while proximity motion is illustrated in Fig. 5.7. Figure 5.8 shows the object trajectories whereas Fig. 5.9 shows the required impulses. Rotation parameters are shown in Fig. 5.10 as error quaternions, angular velocities, and the required control torques about the *y*-axis. Finally, the total translation cost is shown in Table 5.1.

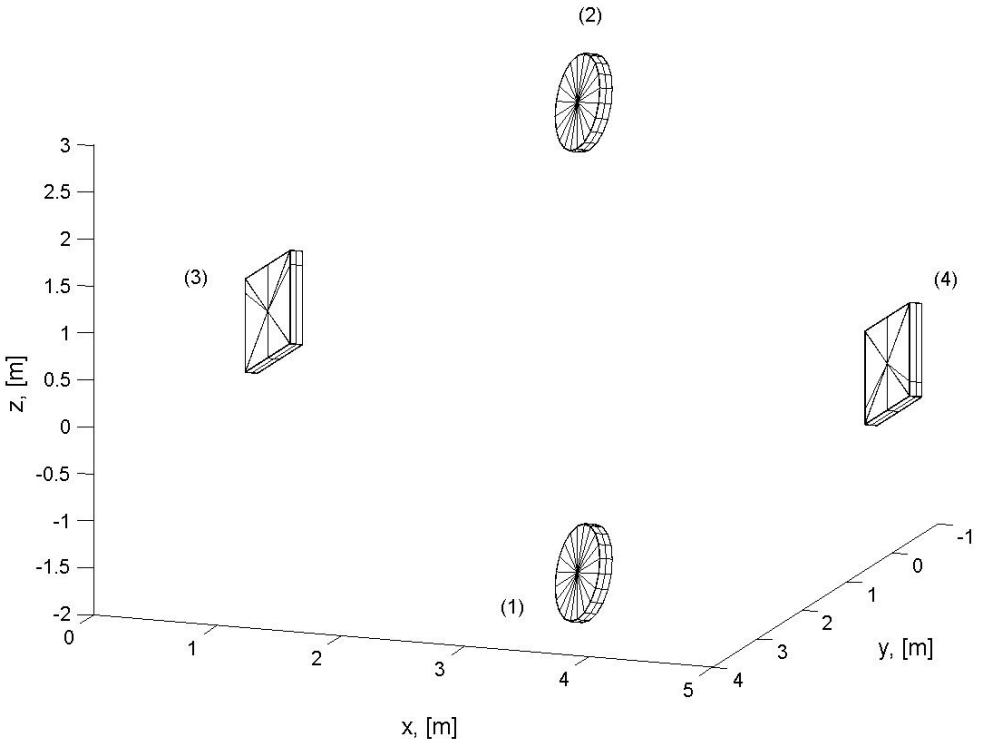

Fig. 5.6 Initial object configuration

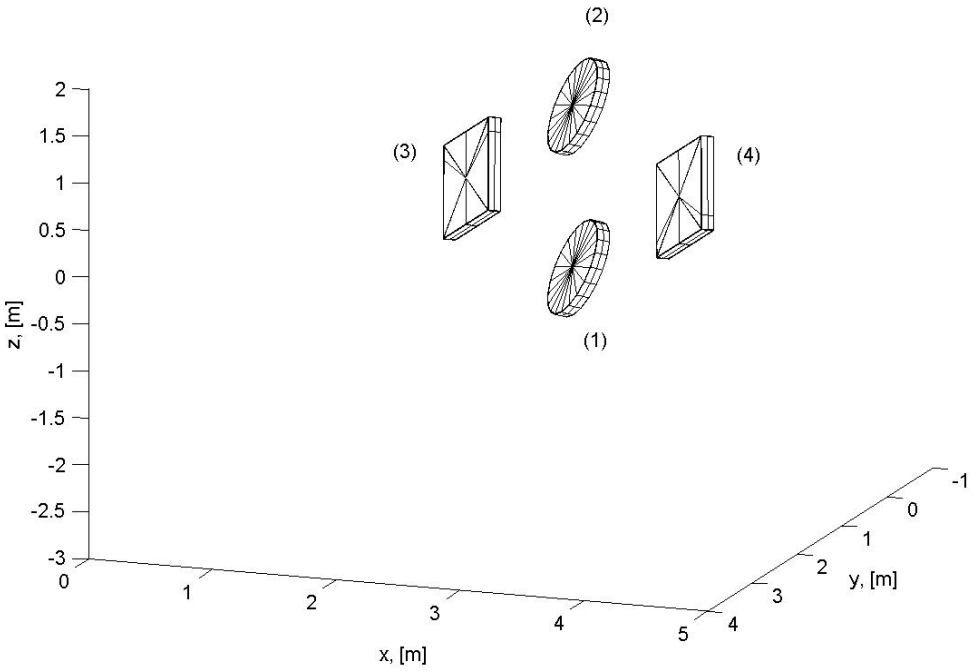

Fig. 5.7.a) Object configuration at t = 165 sec

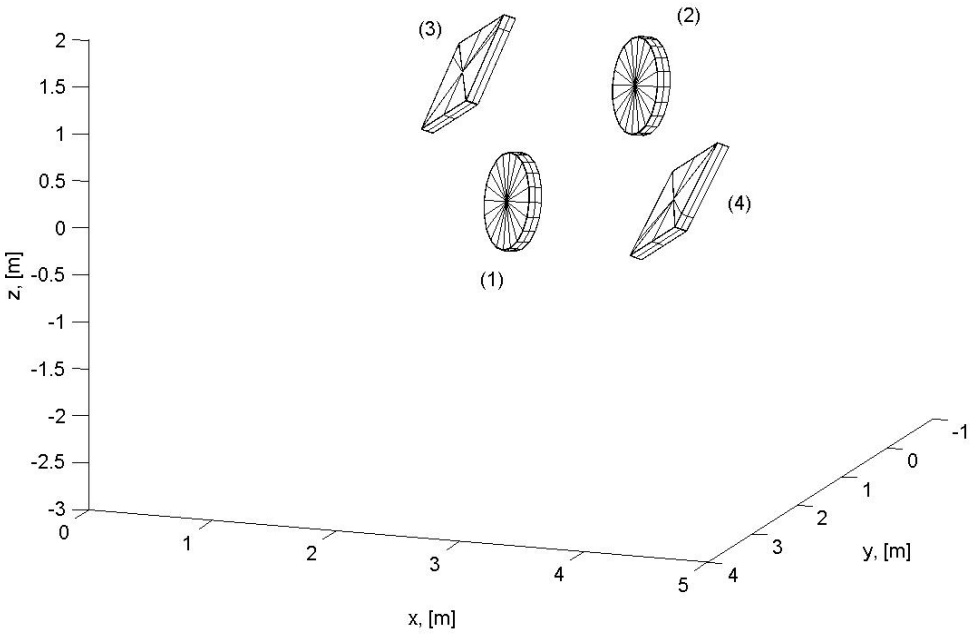

Fig. 5.7.b) Object configuration at t = 220 sec

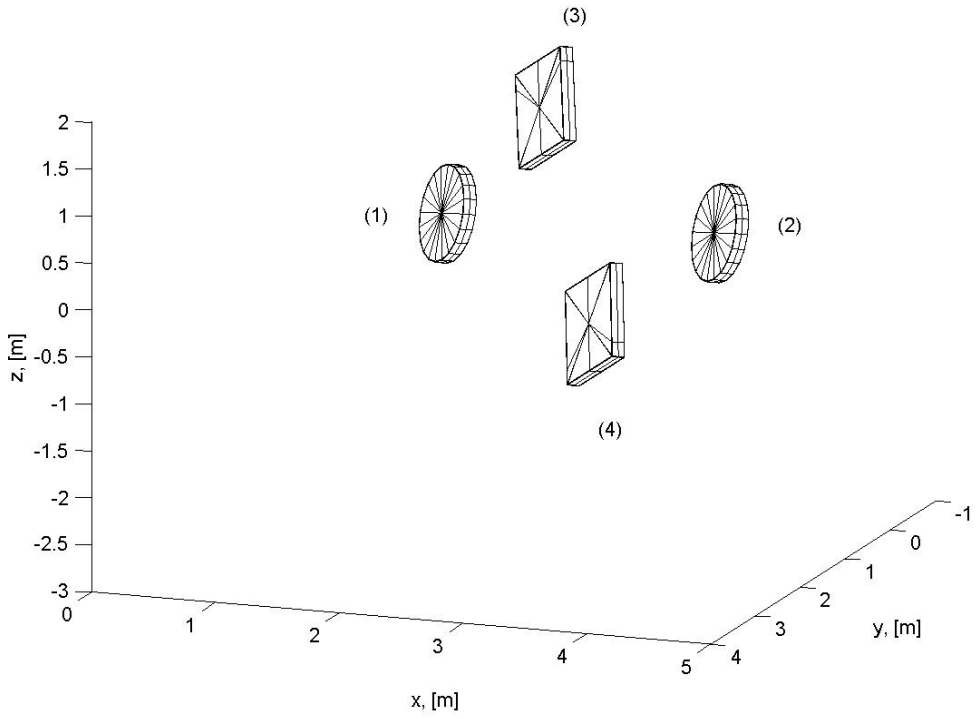

Fig. 5.7.c) Object configuration at t = 310 sec

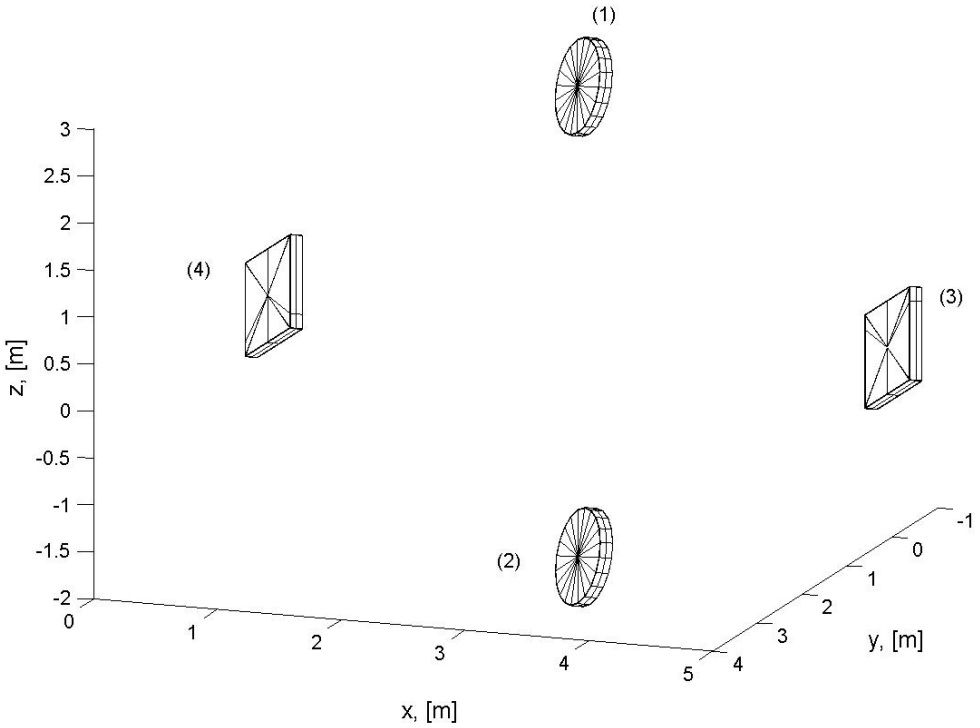

Fig. 5.7.d) Final object configuration at t = 1000 sec

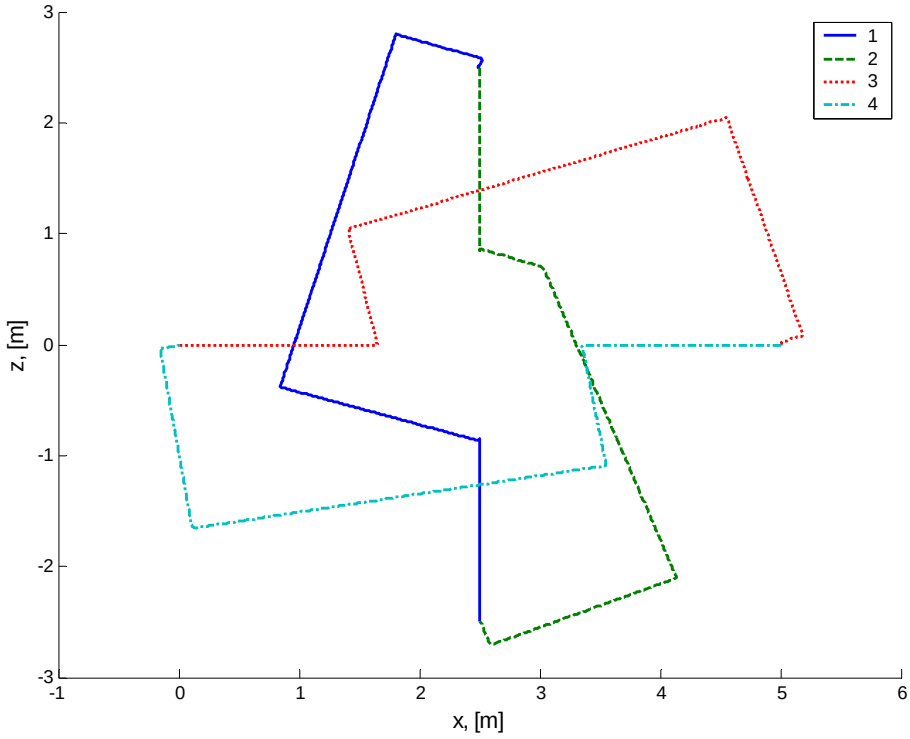

Fig. 5.8 Object trajectories

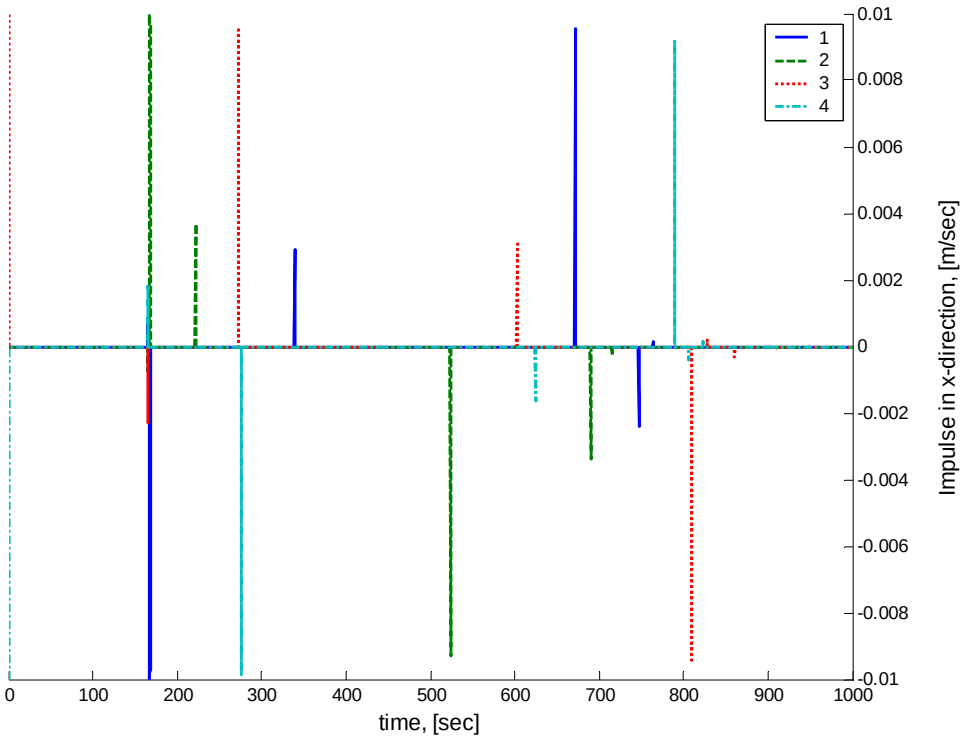

Fig. 5.9.a) Object impulses in *x*-direction

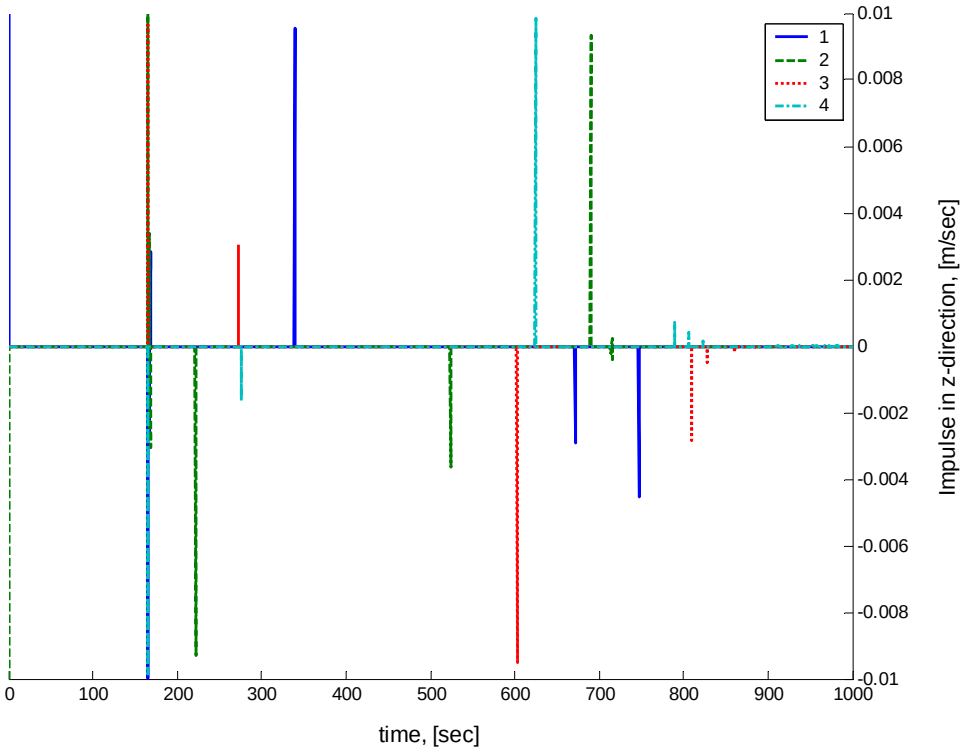

Fig. 5.9.b) Object impulses in *z*-direction

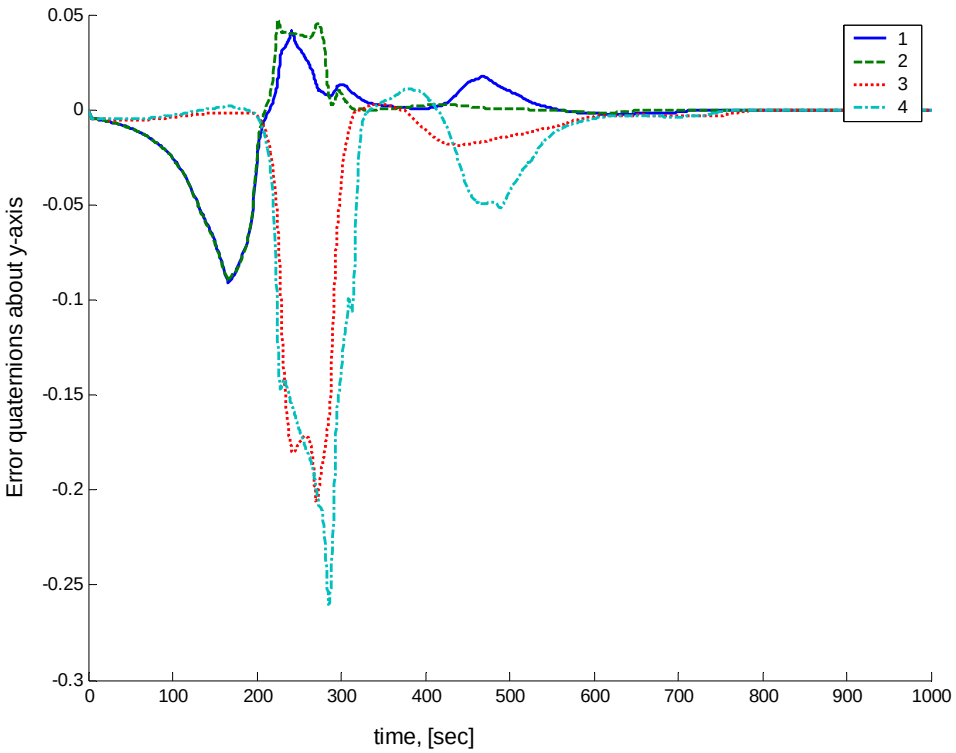

Fig. 5.10.a) Object error quaternion about *y*-axis

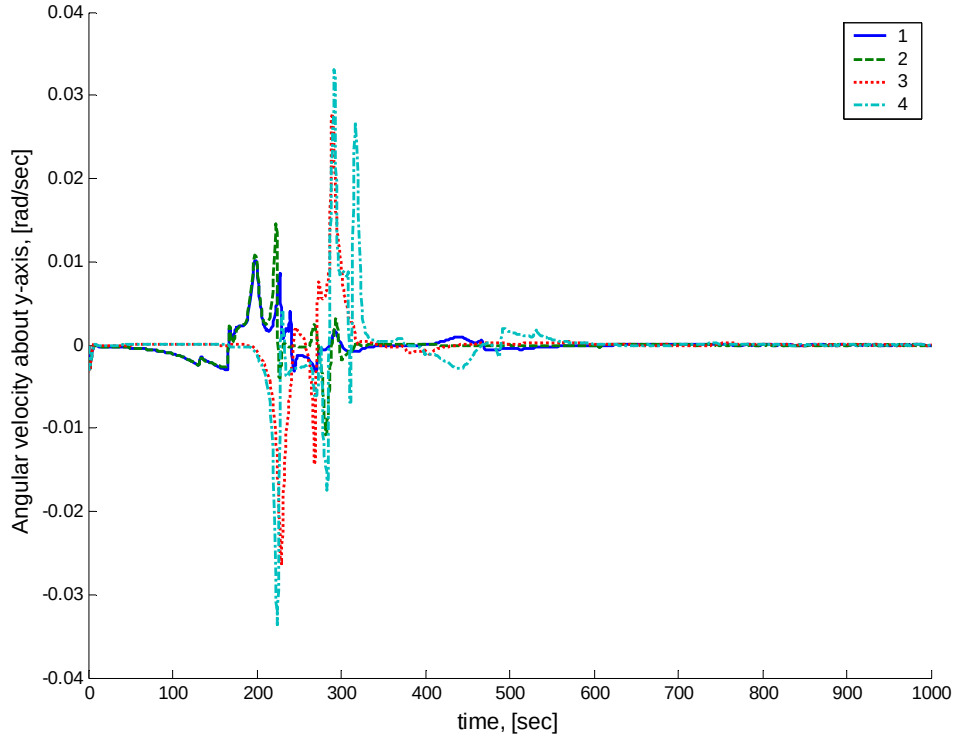

Fig. 5.10.b) Object angular velocities about *y*-axis

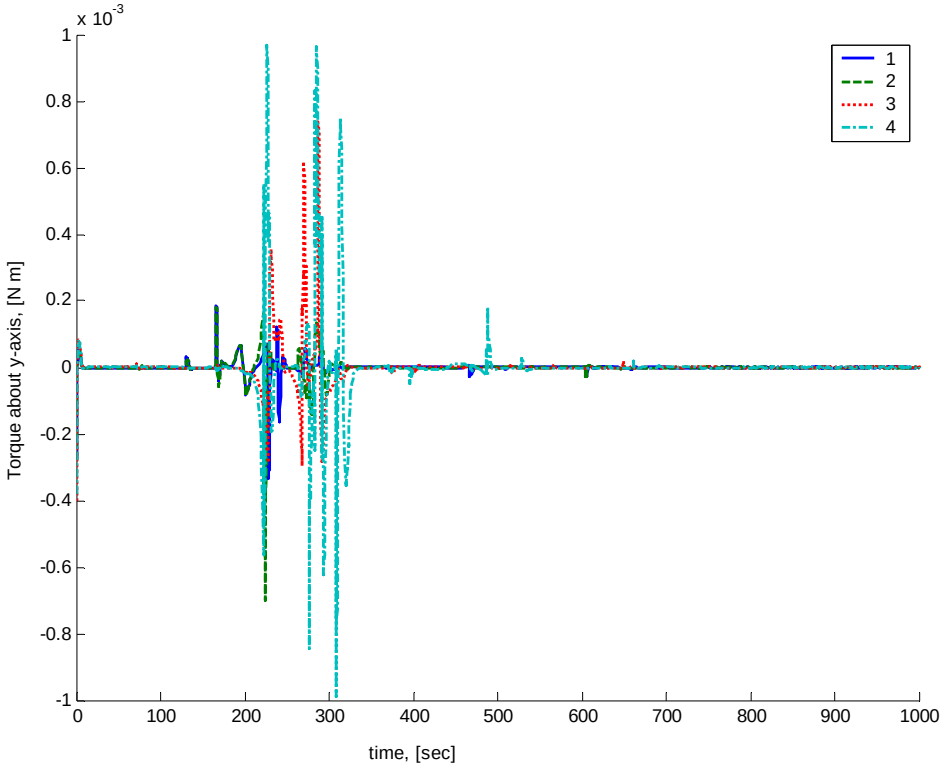

Fig. 5.10.c) Object torques about *y*-axis

element no.	Δ*v* [m/sec]	element no.	Δ*v* [m/sec]	element no.	Δ*v* [m/sec]	element no.	Δ*v* [m/sec]
1	0.24531	2	0.31099	3	0.051858	4	0.050021

Table 5.1 Element translation cost

5.4 Conclusions

The global potential functions proposed in this chapter proved their ability to solve a motion planning problem successfully. The continuous control motion planning strategy is constructed such that velocity and angular velocity states along with position and orientation states of all elements are used. Construction of a potential function containing a velocity term using the original parabolic function leads to unbounded control force that actuators will fail to provide. By using the method described in this chapter to combine parabolic and conical functions this problem is removed. The potential function for the impulsive control strategy limits the

required states to position, orientation, and angular velocity only. The key difference between the two strategies is based on translational motion. The rotational motion for both strategies is continuous. The continuous control strategy enables the control actuators to produce constant force all the entire workspace away from the goal position and the obstacles.

6. ORBITAL ASSEMBLY

6.1 Introduction

The main applications of orbital mechanics include ascent trajectories, re-entry and landing, rendezvous, lunar and interplanetary trajectories (Graham, 1995). The aim of this chapter is to perform on-orbit assembly in a circular low Earth orbit (LEO). Only one speed will produce a circular orbit at a given altitude, termed the local circular speed. The orbital angular velocity, Ω, for such a circular orbit is given as:

$$\Omega = \sqrt{GM/\rho^3} \tag{6.1}$$

where G is the gravitational constant (6.67300×10^{-11} m^3 kg^{-1} s^{-2}), M is the mass of the Earth (5.9742×10^{24} kg), and ρ is the orbit radius. Relative motion between a manoeuvring object and its goal point is described as a rendezvous and docking operation or proximity operation. Many rendezvous and docking operations have been undertaken through the assembly, re-supply, and crew exchange of the International Space Station (ISS) (Fehse, 2005).

Reaction thrusters and gravity are considered the two forces which define proximity motion. Thrusters are used to either initiate relative motion between the manoeuvring object and its goal, to avoid collision with other objects, or to bring a manoeuvring object to rest at its goal.

Typically two main types of thrusters are used in on-orbit manoeuvres: high- or low-thrust systems based on the magnitude of the thrust force relative to the local gravitational force (Prussing and Conway, 1993). Consequently, the rendezvous process can take different forms as:

1. *Continuous control* such that thrusters are always on during the manoeuvre.
2. *Discrete control* performed by using on-off thrusters with powered and coast arcs.
3. *Impulsive control* with (assumed) step changes, to the spacecraft velocity.

6.2 Proximity Motion

The equations of motion describing the transfer of an object from some initial point on a circular orbit toward a goal are described by the two-body model. In this model, only the gravitational force of a central body is taken into consideration, in addition to the representation of both bodies as point masses (Roy, 2005).

In the two-body model, an object of mass, *m,* is in orbit about the Earth, the central body, with an orbital angular velocity vector $\mathbf{\Omega}$, and a position vector $\mathbf{r}_{o,i}$ with respect to an inertial frame of reference centred at the Earth. It is required to bring this element to its goal which is placed at a position vector $\mathbf{r}_{G,i}$ with respect to a local orbiting frame of reference. The origin of the local orbiting frame of reference is placed at a position vector $\boldsymbol{\rho}$ with respect to the inertial frame. The local frame axes directions are described in Fig. 6.1. The position vector of the i^{th} manoeuvring object, $\mathbf{r}_{o,i}$, is given as:

$$\mathbf{r}_{o,i} = \boldsymbol{\rho} + \mathbf{r}_i \tag{6.2}$$

Describing these vectors in the inertial frame of reference is difficult, hence it is better to express them in the rotating frame as:

$$\mathbf{r}_{o,i} = x_i \boldsymbol{i} + y_j \boldsymbol{j} + (z_i + \rho)\boldsymbol{k} \tag{6.3}$$

where x_i, y_i, and z_i define the i^{th} object coordinates relative to the local orbiting frame. The object velocity, $\mathbf{v}_i$, is then given as:

$$\begin{aligned} \mathbf{v}_i &= \mathbf{v}_o + \mathbf{v}_{i/o} \\ &= \mathbf{\Omega} \times (\boldsymbol{\rho} + \mathbf{r}_i) + \dot{\mathbf{r}}_i \end{aligned}$$

so that in component form:

$$\mathbf{v}_i = \left(\dot{x}_i + \Omega(\rho + z_i)\right)\boldsymbol{i} + \dot{y}_i \boldsymbol{j} + (\dot{z}_i - \Omega x_i)\boldsymbol{k} \tag{6.4}$$

The i^{th} object acceleration, $\mathbf{a}_i$, is then given as:

$$\mathbf{a}_i = \ddot{\boldsymbol{\rho}} + \ddot{\mathbf{r}}_i + 2(\mathbf{\Omega} \times \dot{\mathbf{r}}_i) + \dot{\mathbf{\Omega}} \times \mathbf{r}_i + \mathbf{\Omega} \times (\mathbf{\Omega} \times \mathbf{r}_i) \tag{6.5}$$

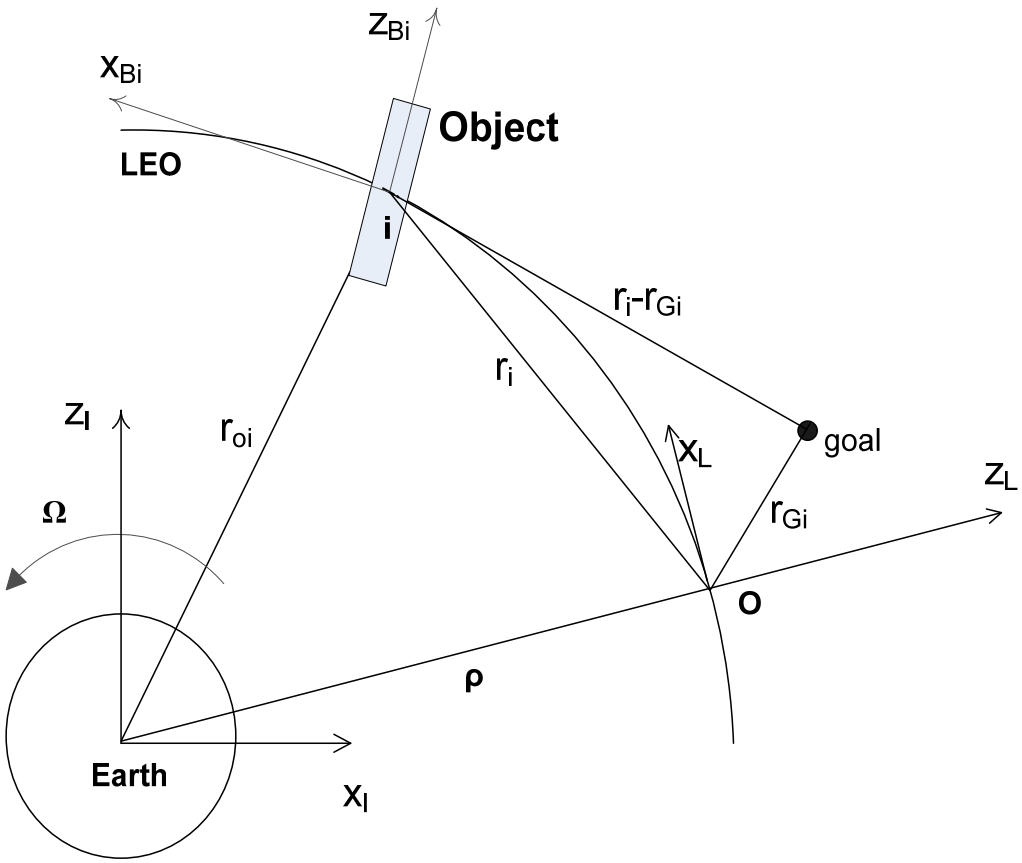

Fig. 6.1 Inertial, local orbiting and body frames for the i^{th} manoeuvring object

The gravitational force is always directed toward the centre of the Earth, hence the local gravitational acceleration at the origin *O* of the local frame, $\ddot{\boldsymbol{\rho}}$, is defined as:

$$\ddot{\boldsymbol{\rho}} = -g_O \boldsymbol{k} \tag{6.6}$$

where g_o is the local gravity at the origin *O*. The acceleration of the object, $\mathbf{a}_i$, is also defined as:

$$\mathbf{a}_i = \frac{-g_i}{\left\|\mathbf{r}_{o,i}\right\|}\mathbf{r}_{o,i} + \boldsymbol{\Gamma}_i \tag{6.7}$$

where $\mathbf{\Gamma}_i$ is the thruster acceleration vector acting upon the i^{th} manoeuvring object. Simplifying Eq. (6.5) we obtain:

In the *x*-direction $$\frac{-g_i}{\|\mathbf{r}_{o,i}\|} x_i + \Gamma_{i,x} = \ddot{x}_i + \dot{\Omega}\, z_i - \Omega^2 x_i + 2\Omega\, \dot{z}_i \tag{6.8.a}$$

In the *y*-direction $$\frac{-g_i}{\|\mathbf{r}_{o,i}\|} y_i + \Gamma_{i,y} = \ddot{y}_i \tag{6.8.b}$$

In the z-direction $$\frac{-g_i}{\|\mathbf{r}_{o,i}\|} (\rho + z_i) + \Gamma_{i,z} = -g_O + \ddot{z}_i - \dot{\Omega}\, z_i - \Omega^2 z_i - 2\Omega\, \dot{x}_i \tag{6.8.c}$$

For a circular orbit $|\mathbf{\Omega}|$ is constant. If the thrusters are off during the coast period, further simplification of Eq. (6.8) can be expressed as:

In the *x*-direction $$\frac{-g_i}{\|\mathbf{r}_{o,i}\|} x_i = \ddot{x}_i - \Omega^2 x_i + 2\Omega\, \dot{z}_i \tag{6.9.a}$$

In the *y*-direction $$\frac{-g_i}{\|\mathbf{r}_{o,i}\|} y_i = \ddot{y}_i \tag{6.9.b}$$

In the *z*-direction $$\frac{-g_i}{\|\mathbf{r}_{o,i}\|} (\rho + z_i) = -g_O + \ddot{z}_i - \Omega^2 z_i - 2\Omega\, \dot{x}_i \tag{6.9.c}$$

In all cases, $\|\rho\| >> \|\mathbf{r}_i\|$, hence (McQuade, 1997):

$$\frac{-g_i}{\|\mathbf{r}_{o,i}\|} x_i \approx -g_O \frac{x_i}{\rho} \tag{6.10.a}$$

$$\frac{-g_i}{\|\mathbf{r}_{o,i}\|} y_i \approx -g_O \frac{y_i}{\rho} \tag{6.10.b}$$

$$\frac{-g_i}{\|\mathbf{r}_{o,i}\|} (\rho + z_i) \approx -g_O \left(1 - \frac{2z_i}{\rho}\right) \tag{6.10.c}$$

The acceleration at the origin of the local frame is defined as:

$$g_O = \Omega^2 \rho \tag{6.11}$$

The linearised equations of motion of the i^{th} object are then defined as:

$$\ddot{x}_i = -2\Omega\, \dot{z}_i \tag{6.12.a}$$

$$\ddot{y}_i = -\Omega^2 y_i \tag{6.12.b}$$

$$\ddot{z}_i = 3\Omega^2 z_i + 2\Omega\, \dot{x}_i \tag{6.12.c}$$

which are the so-called *Clohessy-Wiltshire* equations. Solving Eq. (6.12.b), which is uncoupled from any other differential equations and defines simple harmonic motion, the general solution is expressed as:

$$y_i = C_1 \cos(\Omega t) + C_2 \sin(\Omega t)$$

where the constants C_1 and C_2 can be determined from the initial conditions. Then, the solution will then be expressed as:

$$y_i = y_{o,i} \cos(\Omega t) + \frac{\dot{y}_{o,i}}{\Omega} \sin(\Omega t) \tag{6.13}$$

Integrating Eq. (6.12.a) with respect to time, t, gives:

$$\dot{x}_i = -2\Omega\, z_i + C_3$$

Again, the constant C_3 can be determined from initial conditions as:

$$C_3 = \dot{x}_{o,i} + 2\Omega\, z_{o,i}$$

Hence it can be seen that

$$\dot{x}_i = -2\Omega\, z_i + \dot{x}_{o,i} + 2\Omega\, z_{o,i} \tag{6.14}$$

Substituting from Eq. (6.14) in Eq. (6.12.c) we obtain:

$$\ddot{z}_i = -\Omega^2 z_i + 2\Omega\,\dot{x}_{o,i} + 4\Omega^2 z_{o,i} \tag{6.15}$$

This equation has a general solution as forced harmonic motion as:

$$z_i = C_4\,cos(\Omega t) + C_5\,sin(\Omega t) + C_6$$

By determining the constants C_4, C_5 and C_6 from the initial conditions, it is possible to define $z_i(t)$ as:

$$z_i = \frac{2}{\Omega}(1\text{-}cos(\Omega t))\dot{x}_{o,i} + (4 - 3cos(\Omega t))z_{o,i} + \frac{sin(\Omega t)}{\Omega}\dot{z}_{o,i} \tag{6.16}$$

Substituting from Eq. (6.16) in Eq. (6.14), the time derivative of the x-coordinate will be:

$$\dot{x}_i = 6\Omega(cos(\Omega t) - 1)z_{o,i} + (4\,cos(\Omega t) - 3)\dot{x}_{o,i} - 2\,sin(\Omega t)\dot{z}_{o,i} \tag{6.17}$$

Integrating, the x-coordinate is then obtained as:

$$x_i = 6\Omega\left(\frac{sin(\Omega t)}{\Omega} - t\right)z_{o,i} + (4\frac{sin(\Omega t)}{\Omega} - 3t)\dot{x}_{o,i} + 2\frac{cos(\Omega t)}{\Omega}\dot{z}_{o,i} + C_7$$

where from the initial conditions, the constant C_7 will be:

$$C_7 = x_{o,i} - \frac{2}{\Omega}\dot{z}_{o,i}$$

Hence:

$$x_i = x_{o,i} + 6\Omega\left(\frac{sin(\Omega t)}{\Omega} - t\right)z_{o,i} + \left(4\frac{sin(\Omega t)}{\Omega} - 3t\right)\dot{x}_{o,i} + \frac{2}{\Omega}(cos(\Omega t) - 1)\dot{z}_{o,i} \tag{6.18}$$

The motion of the manoeuvring object can then be represented using a state transition matrix $\mathbf{\Phi}(t)$ as:

$$\mathbf{s}(t) = \mathbf{\Phi}(t)\mathbf{s}(0) \tag{6.19}$$

where $\mathbf{s}(t) = \lceil x \;\; y \;\; z \;\; \dot{x} \;\; \dot{y} \;\; \dot{z} \rceil^T$, and $\mathbf{s}(0)$ is the initial conditions for the current coast period between impulses. The state transition matrix can then be defined from the above as:

$$\mathbf{\Phi}(t) = \begin{bmatrix} 1 & 0 & 6(sin(\Omega t) - \Omega t) & \frac{1}{\Omega}(4\,sin(\Omega t) - 3\Omega t) & 0 & \frac{2}{\Omega}(cos(\Omega t) - 1) \\ 0 & cos(\Omega t) & 0 & 0 & \frac{sin(\Omega t)}{\Omega} & 0 \\ 0 & 0 & 4 - 3\,cos(\Omega t) & \frac{2}{\Omega}(1 - cos(\Omega t)) & 0 & \frac{sin(\Omega t)}{\Omega} \\ 0 & 0 & 6\Omega(cos(\Omega t) - 1) & 4\,cos(\Omega t) - 3 & 0 & -2\,sin(\Omega t) \\ 0 & -\Omega\,sin(\Omega t) & 0 & 0 & cos(\Omega t) & 0 \\ 0 & 0 & 3\Omega\,sin(\Omega t) & 2\,sin(\Omega t) & 0 & cos(\Omega t) \end{bmatrix} \tag{6.20}$$

6.3 On-Orbit Assembly Strategies

Many future large space structures will be unable to be launched as a single assembly. Carrying unassembled structural elements in several launch vehicles and then assembling them in-orbit will be required for both large mechanical structures, such as trusses, and for large science missions using multiple spacecraft for formation-flying as a reconfiguration problem.

It is assumed that all the elements for the structure are initially on a circular orbit in some initial configuration. Natural orbital motion can bring the structure elements toward their goals or away from them depending on their relative positions and relative velocities. Therefore control actuation is required when the global potential field is not monotonically decreasing. A limitation on the initial element configuration is that they should have sufficient Δv to accomplish the assembly process. Two types of control strategies are then used as discussed in detail in chapter 5 for on-orbit assembly termed:

1. *Continuous control strategy*, in which continuous thrust exists over the entire assembly manoeuvre.

2. *Impulsive control strategy,* in which object trajectories are modified through impulses in order to ensure continuous approach to the goals.

These two strategies will be discussed in the following sections using the potential functions discussed in chapter 5 and adding natural orbit motion.

6.4 On-Orbit Continuous Control

6.4.1 Continuous assembly using conic and parabolic potentials

Continuous control force and moments for on-orbit assembly are demonstrated in this section. Rotational motion is assumed to be performed using control moment gyros. Translations are performed through continuous thrust control. A manoeuvring object is under the influence of both control and gravitational forces. Therefore its acceleration is expressed using Eqs. (5.4) and (6.12) as:

$$\ddot{\mathbf{r}} = \begin{cases} -\left(\dfrac{\lambda_p}{\lambda_v}\dfrac{\mathbf{r}-\mathbf{r}_G}{|\mathbf{r}-\mathbf{r}_G|} + \lambda_v^*\dot{\mathbf{r}} + \dfrac{1}{\lambda_v}\nabla V_{obs}\right) - 2\Omega\,\dot{z}\boldsymbol{i} - \Omega^2 y\boldsymbol{j} + \left(3\Omega^2 z + 2\Omega\,\dot{x}\right)\boldsymbol{k} & \text{if } |\mathbf{r}-\mathbf{r}_G| > R \\ -\left(\dfrac{\lambda_p}{\lambda_v}(\mathbf{r}-\mathbf{r}_G) + \lambda_v^*\dot{\mathbf{r}} + \dfrac{1}{\lambda_v}\nabla V_{obs}\right) - 2\Omega\,\dot{z}\boldsymbol{i} - \Omega^2 y\boldsymbol{j} + \left(3\Omega^2 z + 2\Omega\,\dot{x}\right)\boldsymbol{k} & \text{if } |\mathbf{r}-\mathbf{r}_G| \le R \end{cases} \tag{6.21}$$

The following example demonstrates the on-orbit assembly process of twelve columns of dimensions 1x0.2x0.2 m to form a cube. The repulsive parameters are defined as $\alpha = 20$, $A_o = 5$, $\sigma = 0.1$, and $\beta = 1$. The control law parameters, $\lambda_p = 0.01$, $\lambda_q = 0.1$, $\lambda_v = 1, \lambda_\omega = 1, \lambda_v^* = 0.5$, and $\lambda_\omega^* = 1$. The parabolic zone radius, *R,* is chosen to be 0.1 m. The process takes place in a LEO with a circular altitude of 100 km. The elements are initially placed along the *x*-axis of the local orbiting frame, Fig. 6.2. The assembly progress is shown in successive positions until assembly after 5300 sec, Fig. 6.3. Object linear velocities and accelerations are shown in Fig. 6.4 where accelerating, coasting, and braking phases are produced using continuous force. Error quaternions, angular velocities, and control torques, are shown in Fig. 6.5.

It can be seen that although a continuous control force is used, acceleration and braking pulses are generated (with coast arcs). This is a key benefit of the method compared to conventional potential field approaches which generate continuously varying control forces. Similar behaviour is seen with the required control torques, where a log-linear scale is used to demonstrate the resulting behaviour of the method.

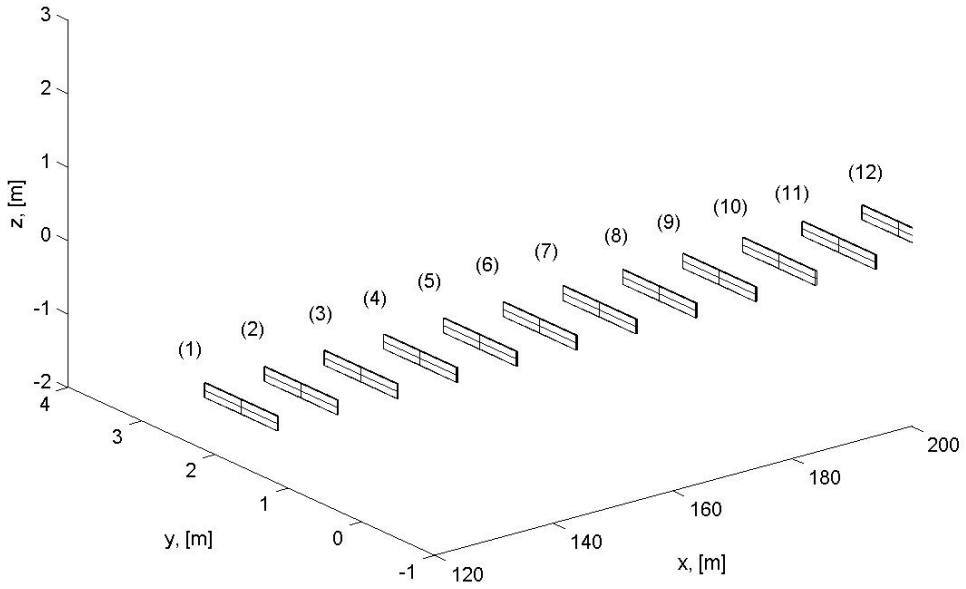

Fig. 6.2 Initial object configuration

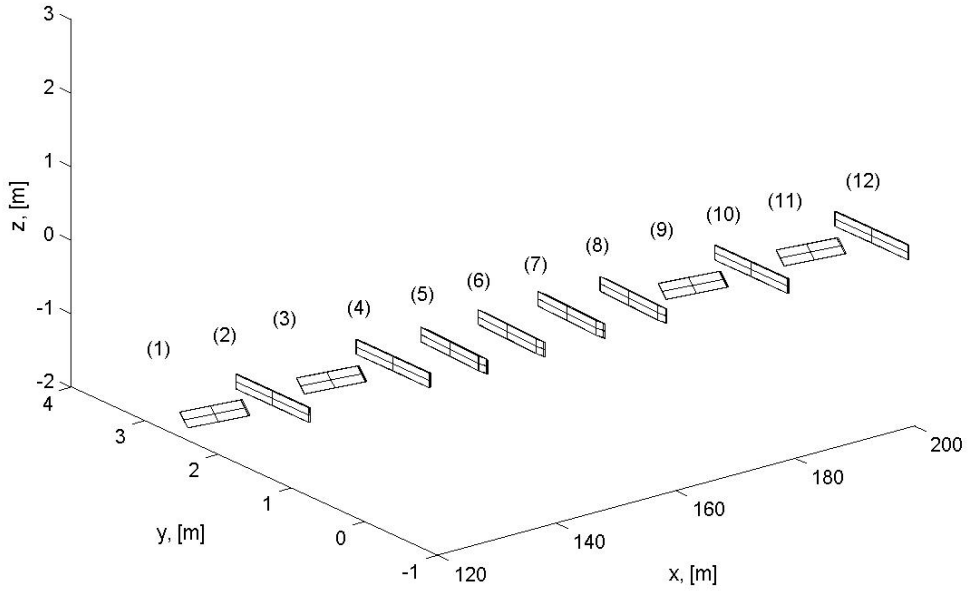

Fig. 6.3.a) Object configuration t = 124 sec

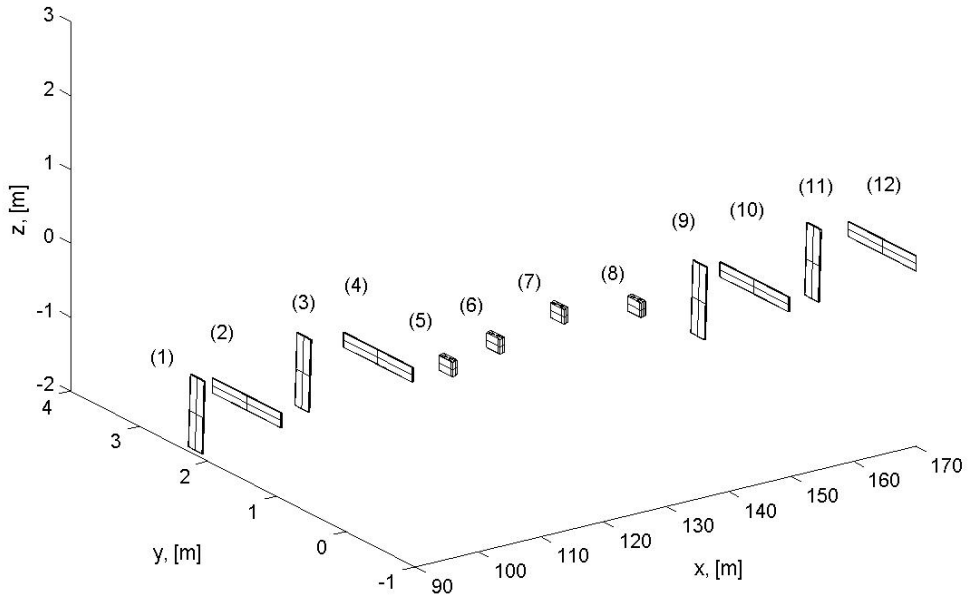

Fig. 6.3.b) Object configuration t= 838 sec (scale affects object shapes)

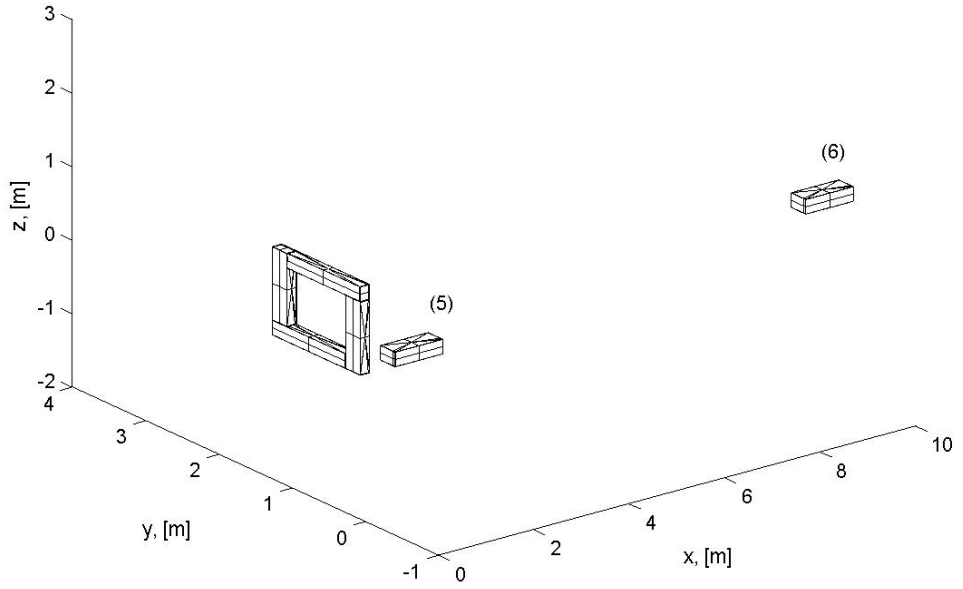

Fig. 6.3.c) Object configuration t = 3470 sec

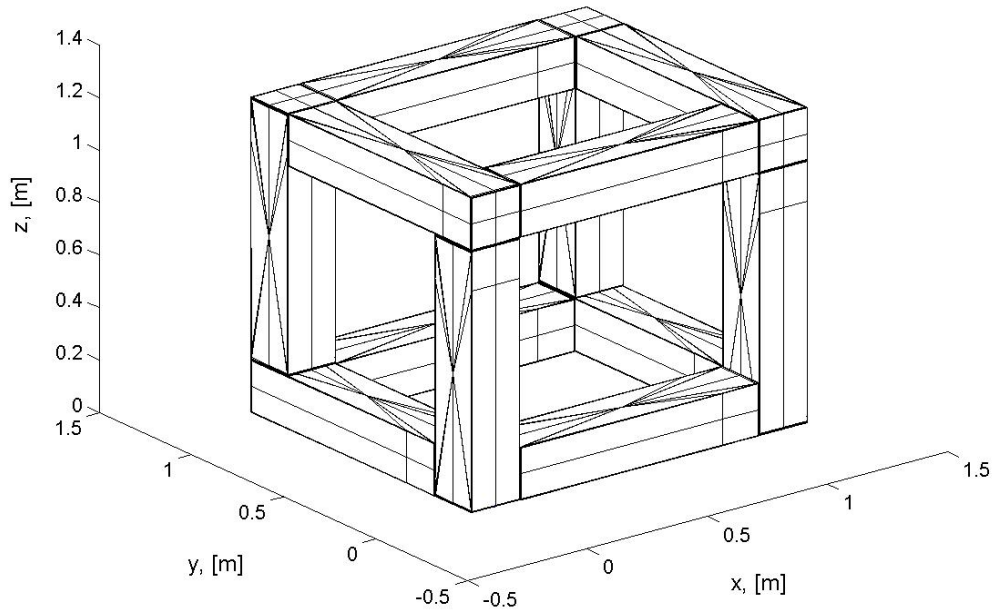

Fig. 6.3.d) Assembled structure t = 5300 sec

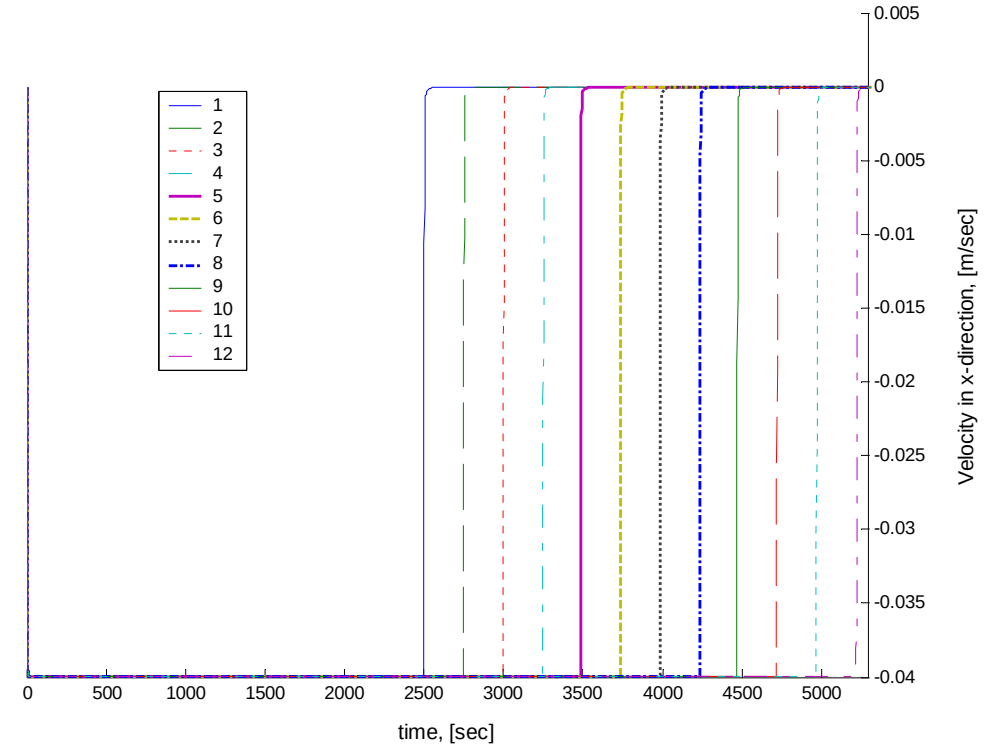

Fig. 6.4.a) Object velocities in the *x*-direction

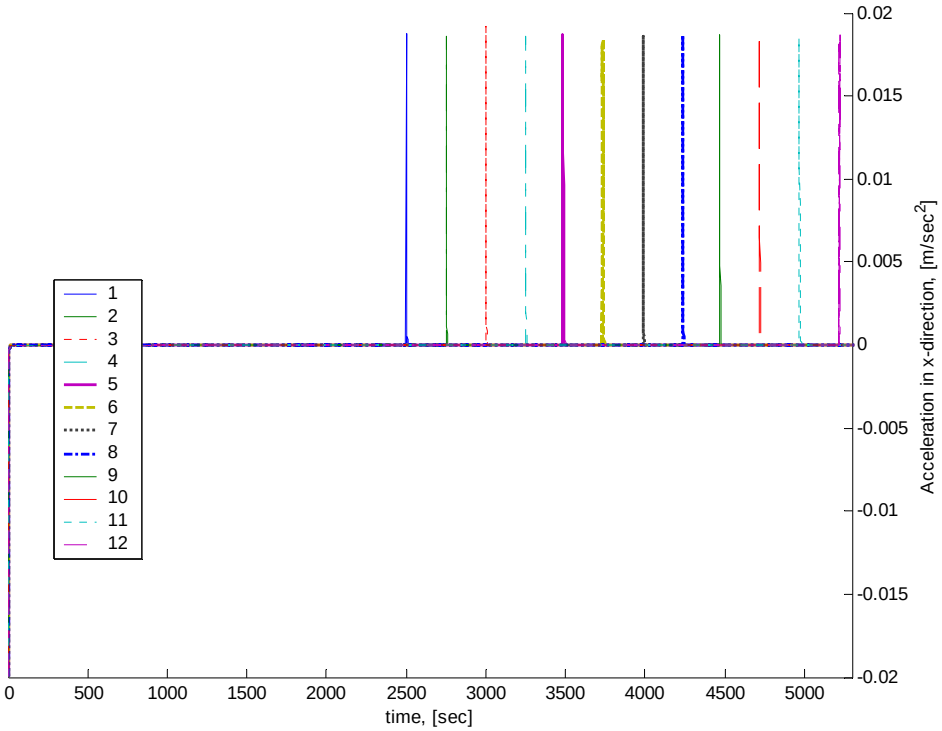

Fig. 6.4.b) Object accelerations in the *x*-direction

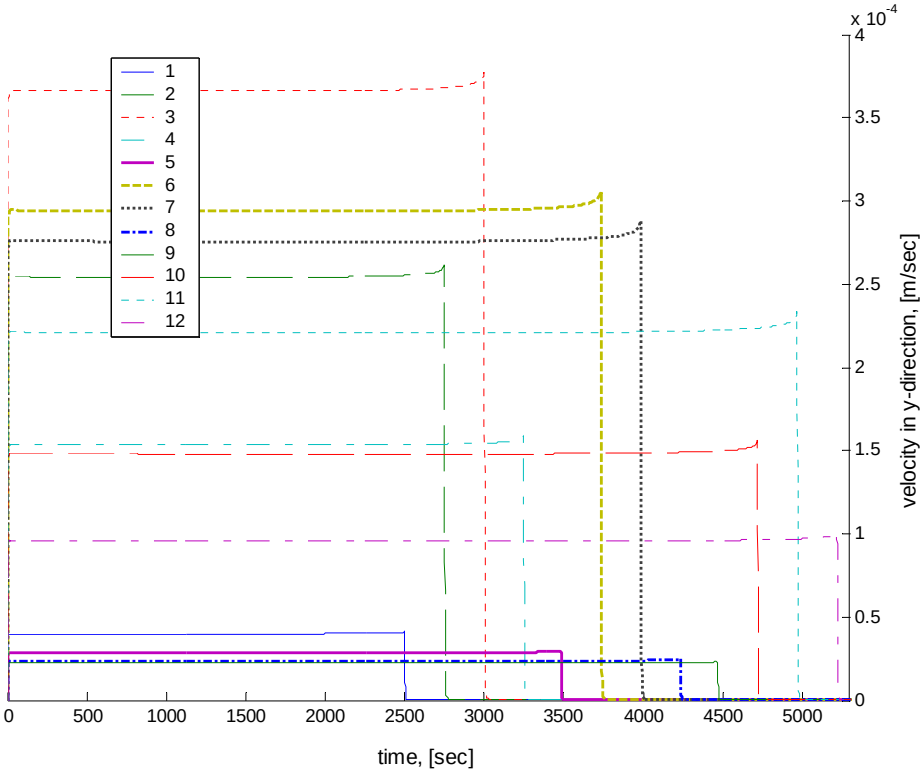

Fig. 6.4.c) Object velocities in the *y*-direction

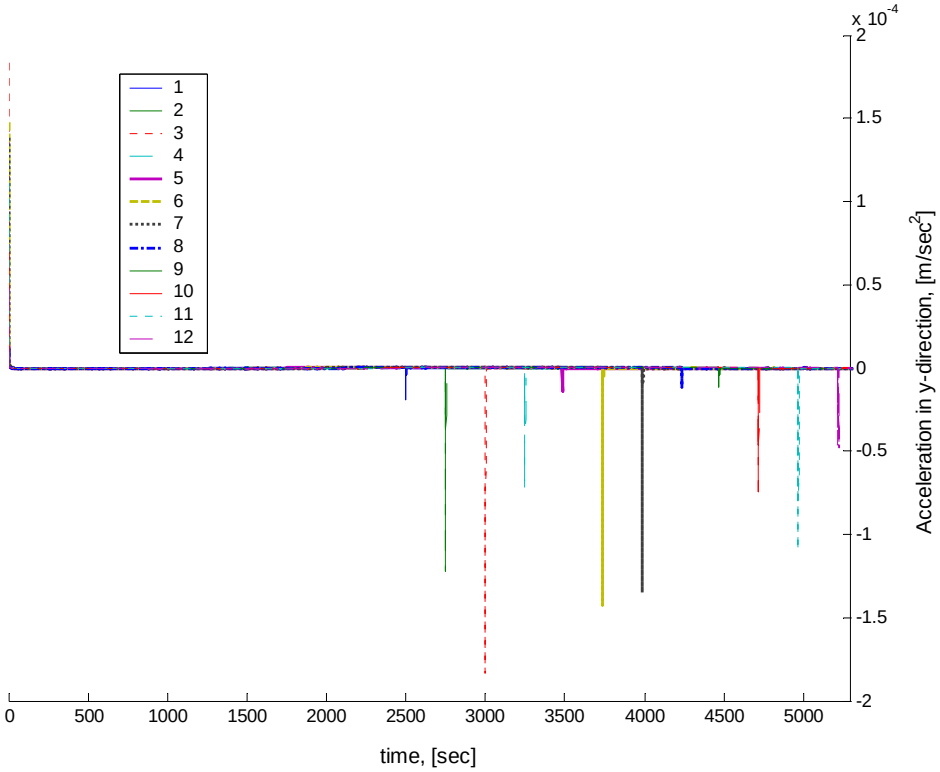

Fig. 6.4.d) Object accelerations in the *y*-direction

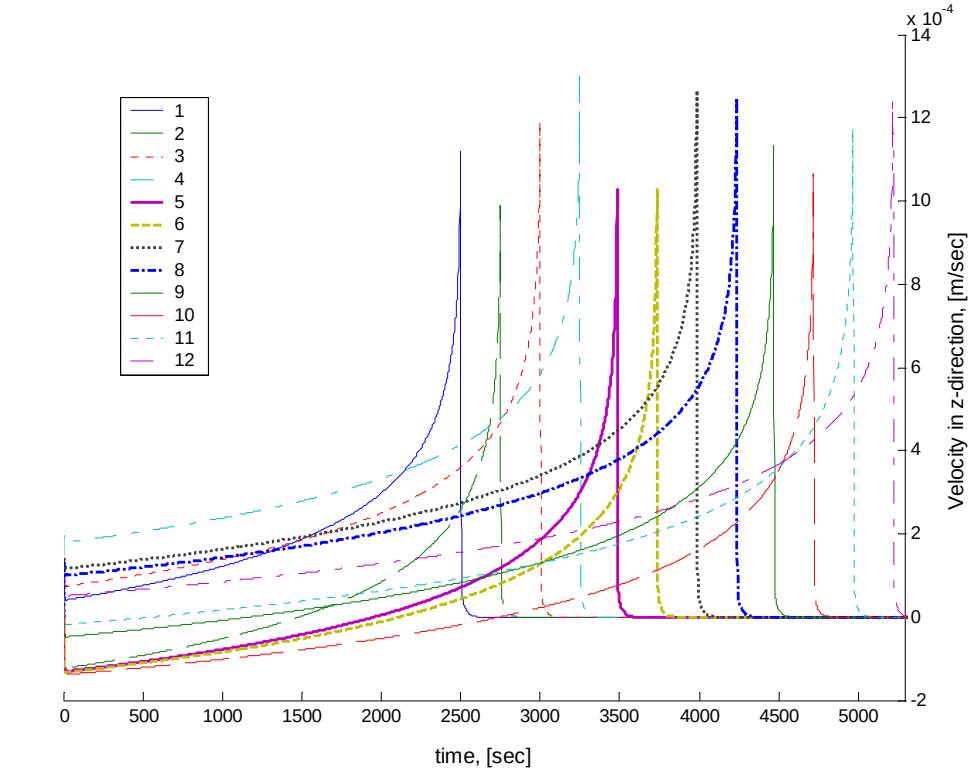

Fig. 6.4.e) Object velocities in the *z*-direction

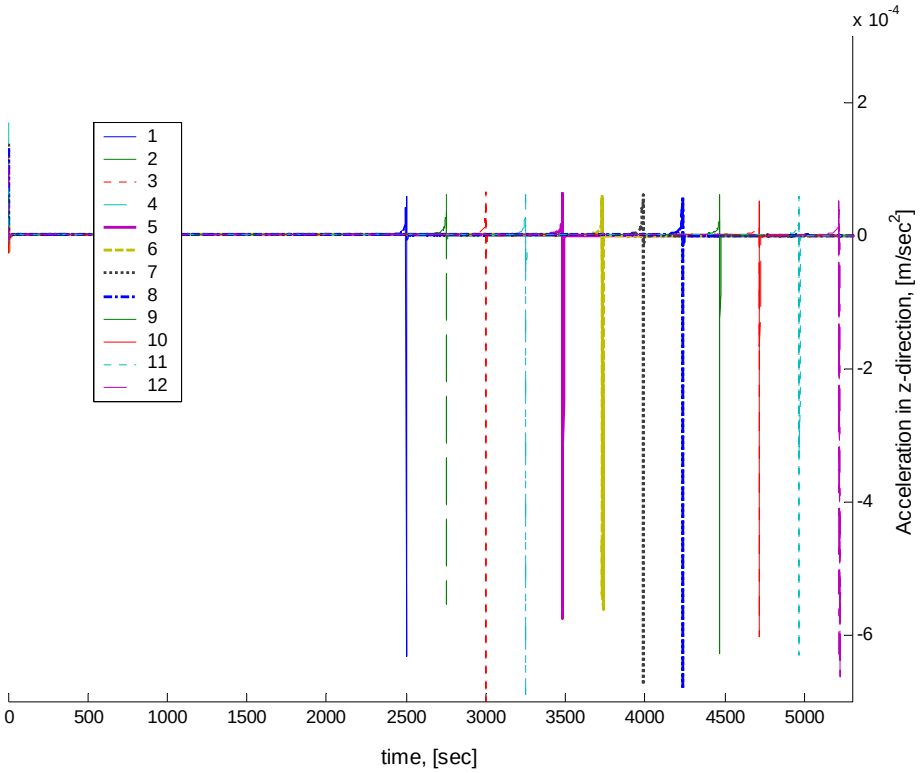

Fig. 6.4.f) Object accelerations in the *z*-direction

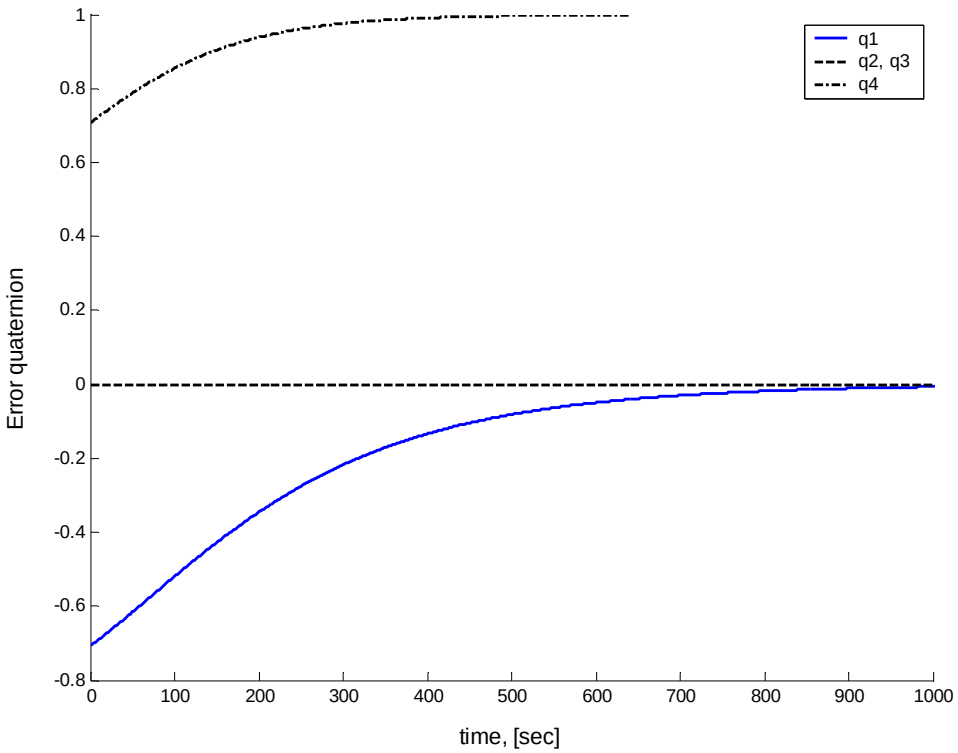

Fig. 6.5.a) Error quaternions of Objects 1, 3, 9, and 11

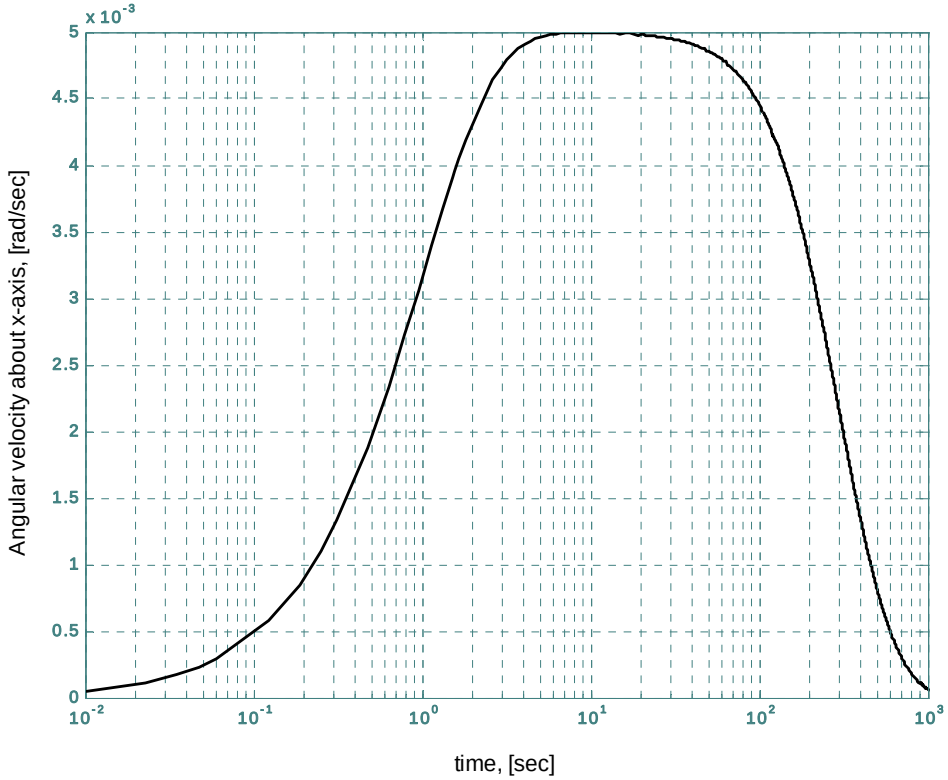

Fig. 6.5.b) Angular velocity about *x*-axis of objects 1, 3, 9, and 11

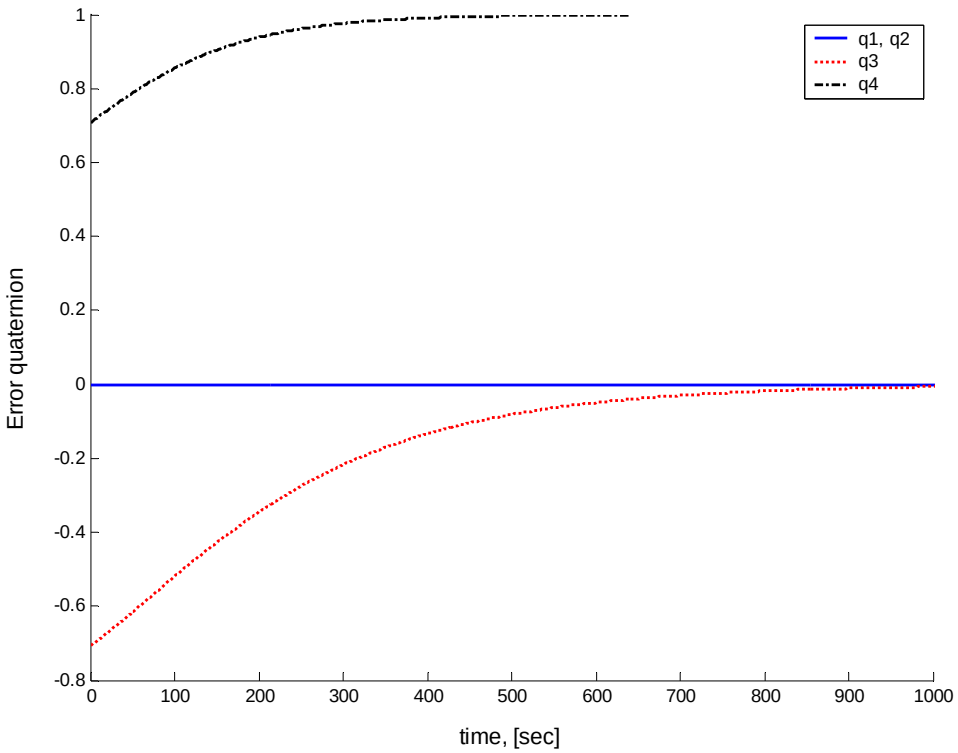

Fig. 6.5.c) Error quaternions of objects 5, 6, 7, and 8

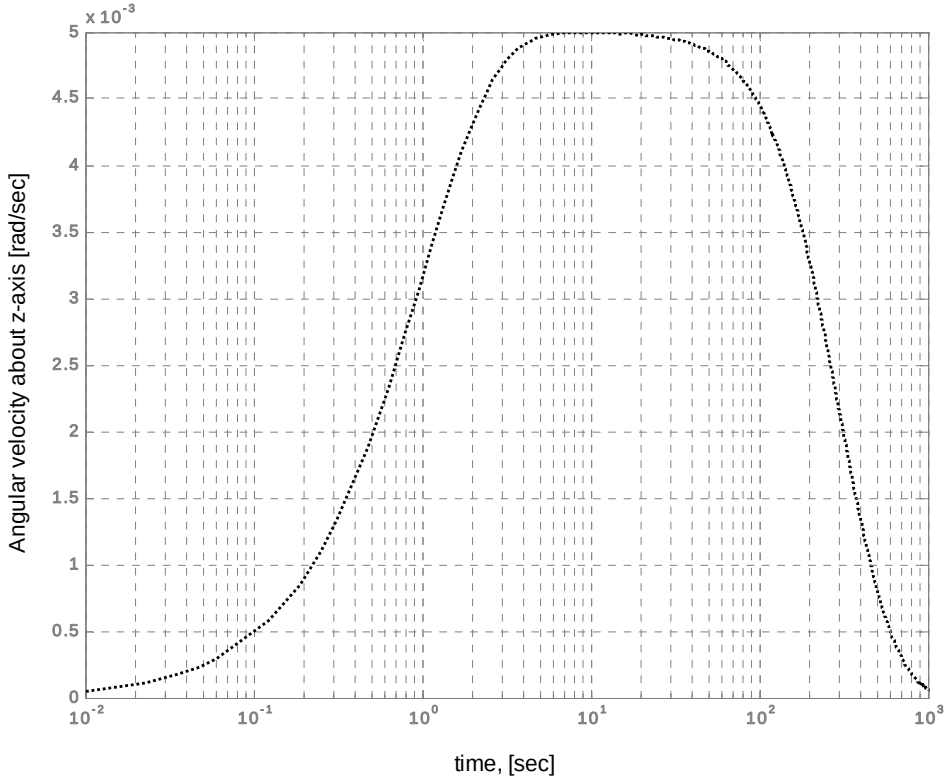

Fig. 6.5.d) Angular velocity about *z*-axis of objects 5, 6, 7, and 8

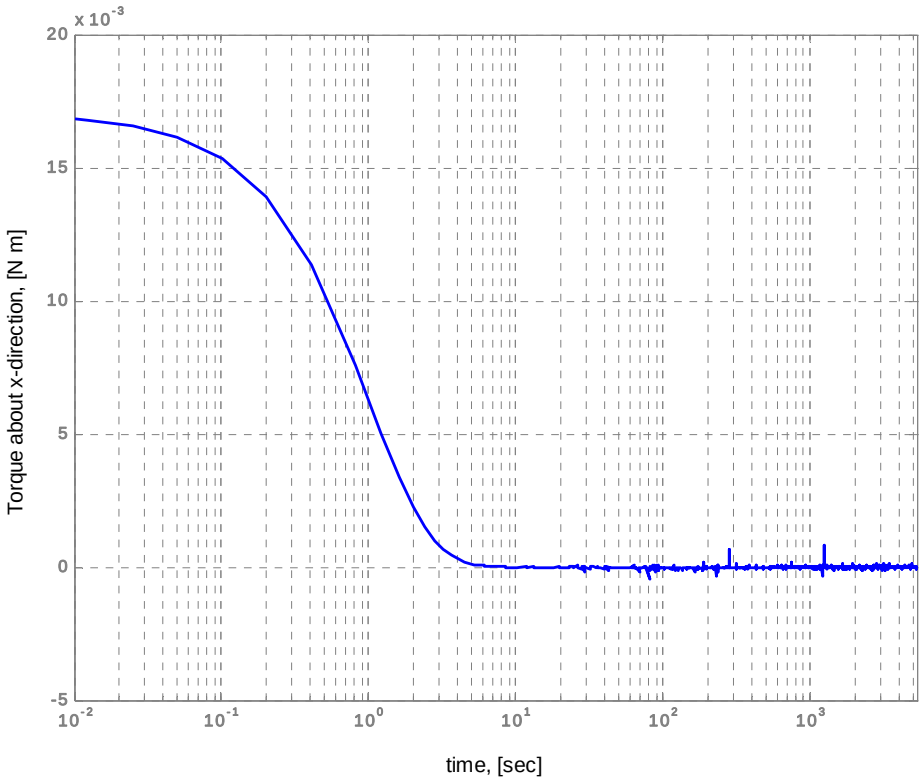

Fig. 6.5.e) Torque about *x*-axis of objects 1, 3, 9, and 11

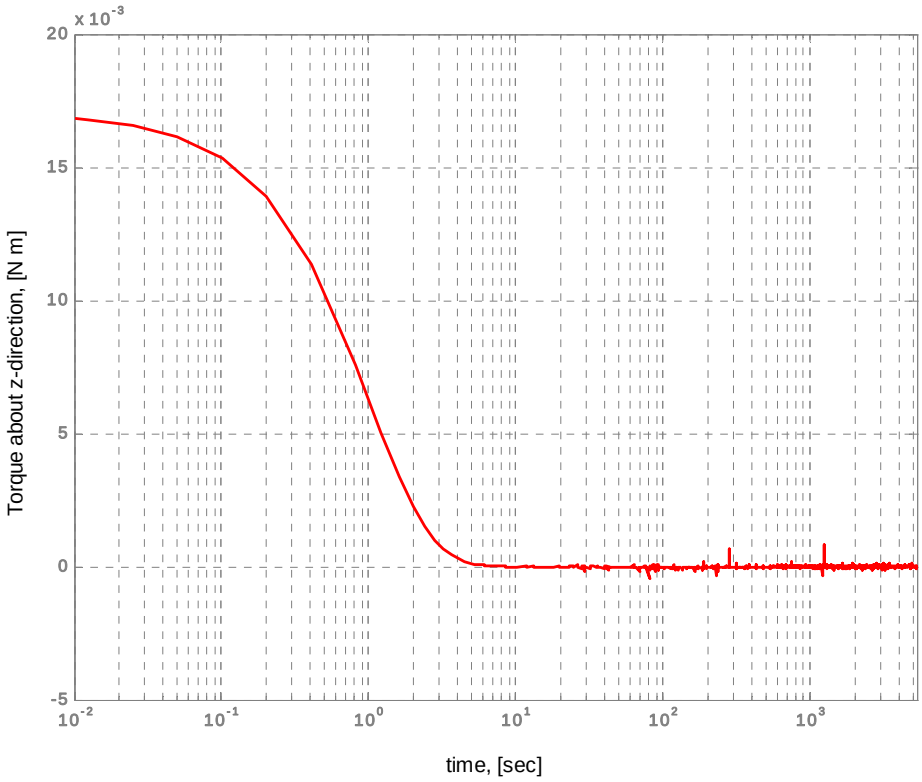

Fig. 6.5.f) Torque about *z*-axis of objects 5, 6, 7, and 8

6.4.2 Continuous assembly using hyperbolic potential

A new approach to motion planning problems is the use of hyperboloid functions as discussed in section 2.5.3. Unlike the parabolic potential function, where the control force increases with distance from the goal and is unbound, and the conic potential function where a singularity occurs at the goal, the hyperboloid potential function avoids both these drawbacks. They combine the advantages of both parabolic and conic potentials as the asymptotic property of the hyperbolic functions ensures constant control forces, while stability and smooth contact are guaranteed at the goal point.

In the previous section a merging of the parabolic and the conic potential, each over certain range, was discussed. However the hyperbolic potential function has the same advantages of this merging, but with less complexity. The formulation of the attractive hyperbolic potential was defined in chapter 2. The global hyperbolic potential of the i^{th} object in presence of m-1 obstacles is defined as:

$$V_i = \lambda_p\left(\sqrt{1+\left|\mathbf{r}_i-\mathbf{r}_{G,i}\right|^2}-1\right)+\frac{\lambda_v}{2}\left|\dot{\mathbf{r}}_i\right|^2+\lambda_q\bar{\mathbf{q}}_i.\bar{\mathbf{q}}_i+\frac{\lambda_\omega}{2}\boldsymbol{\omega}_i.\boldsymbol{\omega}_i+\sum_{j=1,j\neq i}^{m}V_{obs,ij} \tag{6.22}$$

The time derivative is then expressed as:

$$W_i=\dot{\mathbf{r}}_i.\left(\frac{\boldsymbol{\lambda}_p\left(\mathbf{r}_i-\mathbf{r}_{G,i}\right)}{\sqrt{1+\left|\mathbf{r}_i-\mathbf{r}_{G,i}\right|^2}}+\boldsymbol{\lambda}_v\ddot{\mathbf{r}}_i+\sum_{j=1,j\neq i}^{m}\nabla V_{obs,ij}\right)+2\boldsymbol{\lambda}_q\dot{\bar{\mathbf{q}}}_i.\bar{\mathbf{q}}_i+\boldsymbol{\lambda}_{\boldsymbol{\omega}}\dot{\boldsymbol{\omega}}_i.\boldsymbol{\omega}_i+\dot{\bar{\mathbf{q}}}_i.\sum_{j=1,j\neq i}^{m}\nabla^q V_{obs,ij} \tag{6.23}$$

Finally, using Eqs. (2.40) and (2.43), the potential function time derivative is expressed as:

$$W_i=\dot{\mathbf{r}}_i.\left(\frac{\boldsymbol{\lambda}_p\left(\mathbf{r}_i-\mathbf{r}_{G,i}\right)}{\sqrt{1+\left|\mathbf{r}_i-\mathbf{r}_{G,i}\right|^2}}+\boldsymbol{\lambda}_v\ddot{\mathbf{r}}_i+\sum_{j=1,j\neq i}^{m}\nabla V_{obs,ij}\right)+\boldsymbol{\omega}_i.\left(\boldsymbol{\lambda}_q q_{i,4}\bar{\mathbf{q}}_i+\boldsymbol{\lambda}_{\boldsymbol{\omega}}\dot{\boldsymbol{\omega}}_i+\frac{1}{2}\mathbf{Q}\sum_{j=1,j\neq i}^{m}\nabla^q V_{obs,ij}\right) \tag{6.24}$$

Suitable bounded, smooth and singularity-free control laws are expressed as (Badawy and McInnes, 2007b):

$$\ddot{\mathbf{r}}_i = -\frac{\lambda_p\left(\mathbf{r}_i - \mathbf{r}_{G,i}\right)}{\lambda_v\sqrt{1+\left|\mathbf{r}_i - \mathbf{r}_{G,i}\right|^2}} - \boldsymbol{\lambda}_v^*\dot{\mathbf{r}}_i - \frac{1}{\boldsymbol{\lambda}_v}\sum_{j=1, j\neq i}^{m}\nabla V_{obs,ij} \tag{6.25.a}$$

and

$$\dot{\boldsymbol{\omega}}_i = -\left(\frac{\boldsymbol{\lambda}_q}{\boldsymbol{\lambda}_{\boldsymbol{\omega}}} q_{i,4}\overline{\mathbf{q}}_i + \boldsymbol{\lambda}_{\boldsymbol{\omega}}^*\boldsymbol{\omega}_i + \frac{1}{2\boldsymbol{\lambda}_{\boldsymbol{\omega}}}\mathbf{Q}\sum_{j=1, j\neq i}^{m}\nabla^q V_{obs,ij}\right) \tag{6.25.b}$$

The hyperbolic potential field is then again used with continuous control to assemble seven beam elements to form a truss structure. In order to demonstrate the assembly process using the hyperbolic potential, a simple example of on-orbital assembly is discussed. Beam elements of diameter 0.2 m and 1 m length are initially placed along the *x*-axis, Fig. 6.6. The repulsive parameters are $\alpha = 7, A_o = 5$, and $\sigma = 0.1$. All control constants are chosen as unity except $\lambda_v = 10$. The assembly of the objects is demonstrated in Fig. 6.7, where Fig. 6.8 shows the evolution of the object dynamics. Again, it can be seen that accelerating and braking pulses are generated, with coast arcs.

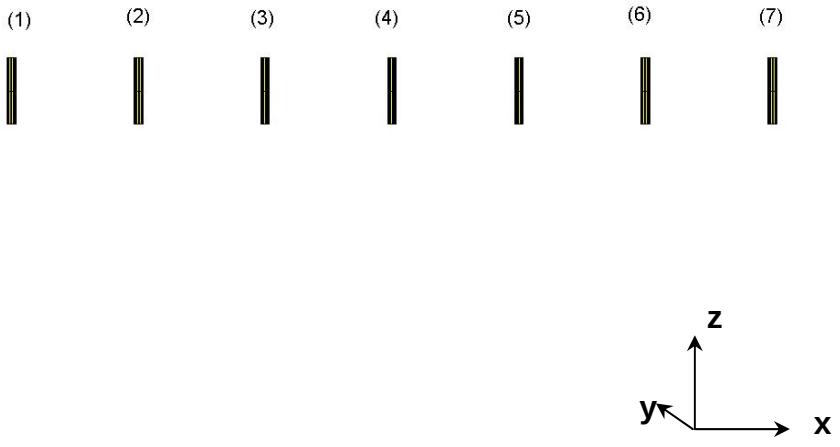

Fig. 6.6 Initial object configuration

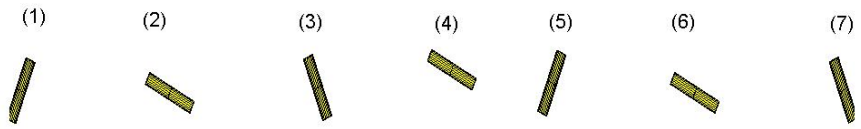

Fig. 6.7.a) Object configuration (t = 37 sec)

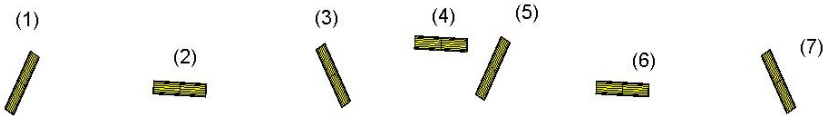

Fig. 6.7.b) Object configuration (t = 120 sec)

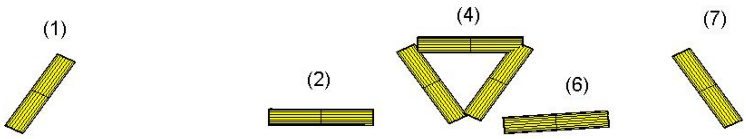

Fig. 6.7.c) Object configuration (t = 180 sec)

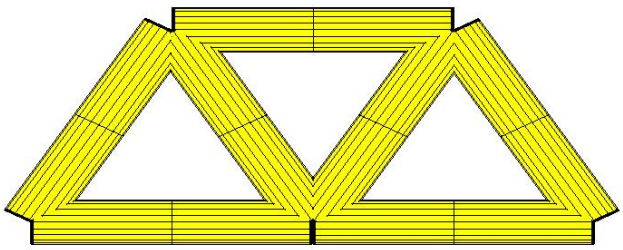

Fig. 6.7.d) Final object configuration (t = 300 sec)

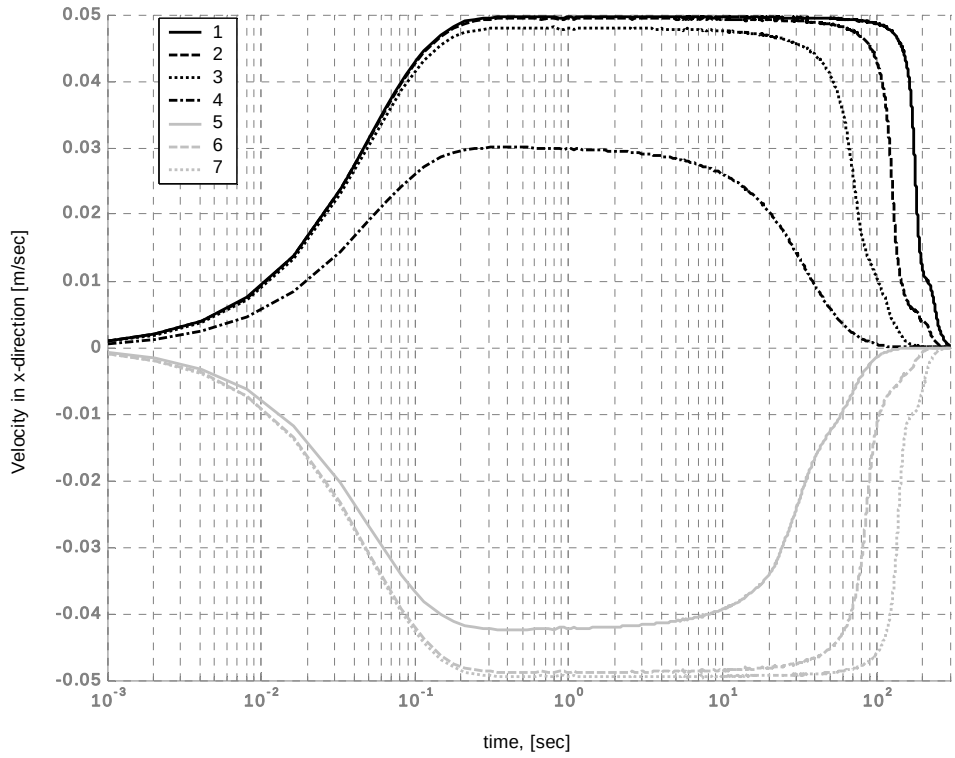

Fig. 6.8.a) Object velocities in *x*-direction

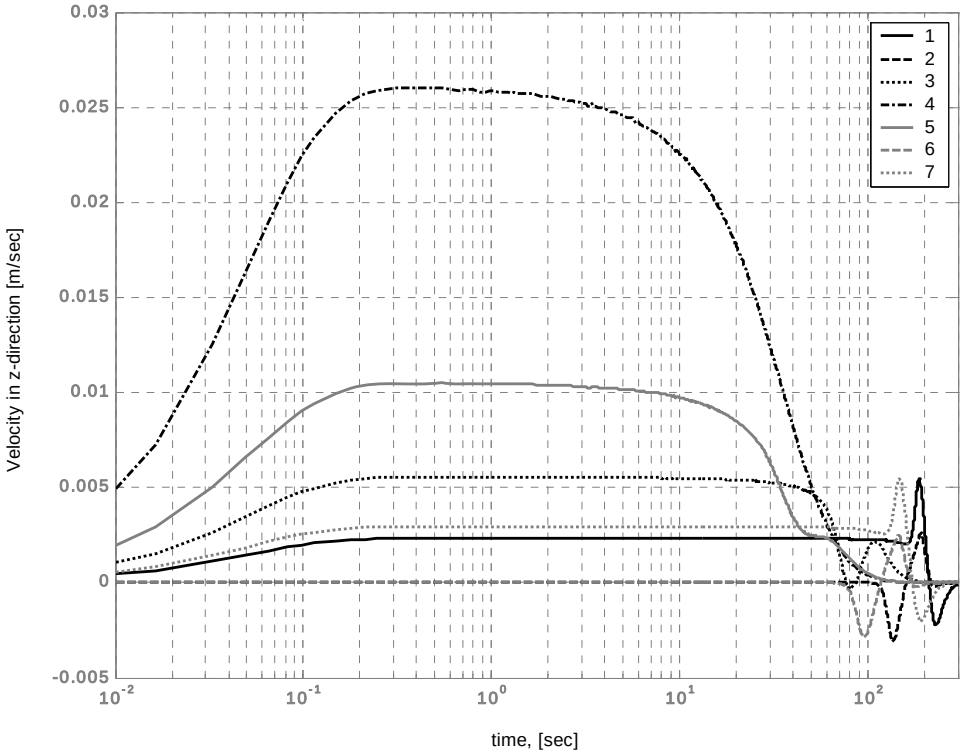

Fig. 6.8.b) Object velocities in *z*-direction

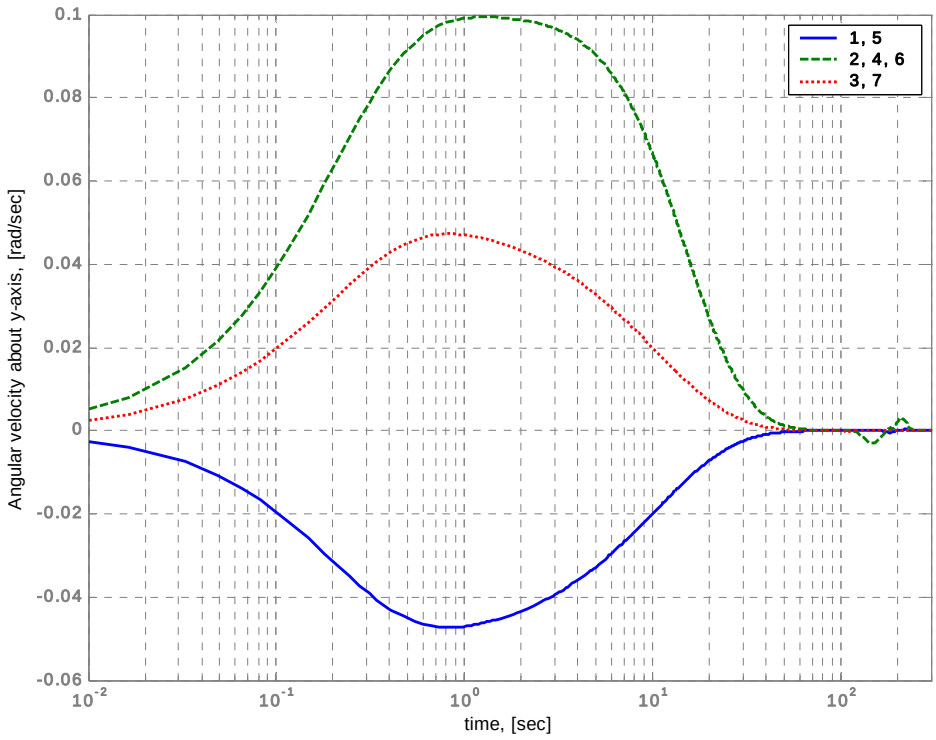

Fig. 6.8.c) Object angular velocities about *y*-axis

6.5 On-Orbit Impulsive Control

In this section impulsive control will be used for motion initiation, collision avoidance, and braking. The simplest form of impulsive motion is a two impulse rendezvous where the first impulse is used to initiate chaser vehicle motion which intersects the target. The second impulse brings the relative chaser-target velocity to zero to allow smooth contact. In the presence of other objects or obstacles, the solution is more complicated.

The potential functions, both attractive and repulsive, will again be described with respect to the local orbiting frame of reference, Fig. 6.1. Natural orbital motion can bring the elements toward the goal or drift them away depending on the initial position and velocity. Control interventions are then used to ensure that the potential is monotonically decreasing. The thrusters are active if the rate of change of the global potential field is more than some non-positive value. Control actuation is therefore required when:

$$W_i \geq c_f \tag{6.22}$$

The control trigger constant, c_f, can be set to zero for *Lyapunov*-like stability, however a negative value can be used in order to anticipate collision avoidance manoeuvres. The correct choice of the constant results in minimizing the required thruster activity and so minimizing propellant mass used for the assembly process. As long as the rate of change of potential is not positive, continuous approach to the goal point is guaranteed. The overall potential function was expressed before in Eq. (5.6) with the superquadric repulsive function expressed in Eqs. (4.1) and (4.2) as:

$$V_i = \frac{\lambda_p}{2}\left(\mathbf{r}_i - \mathbf{r}_{G,i}\right).\left(\mathbf{r}_i - \mathbf{r}_{G,i}\right) + \lambda_q \overline{\mathbf{q}}_i.\overline{\mathbf{q}}_i + \frac{\lambda_\omega}{2}\boldsymbol{\omega}_i.\boldsymbol{\omega}_i + \sum_{j=1, j\neq i}^{m} V_{obs,j} \tag{6.23}$$

Therefore, the required velocity for the i^{th} object in the presence of m-1 obstacles through impulsive approach to the goal is provided as in Eq. (5.8). The required translational velocity is found to be:

$$\dot{\mathbf{r}}_i = -v_{max}\left(1 - exp\left(-\boldsymbol{\beta}\left|\mathbf{r}_i - \mathbf{r}_{G,i}\right|^2\right)\right)\frac{\nabla V_i}{\left|\nabla^* V_i\right|} \qquad \text{if} \quad W_i > c_f \tag{6.24}$$

As the rate of change of potential becomes more than the specified constant, the thrusters are activated and consequently the object velocity is defined through Eq. (6.24), otherwise natural orbit motion describes the object manoeuvre. Rotational motion is always controlled by continuous control using control moment gyros as defined in Eq. (5.5).

6.5.1 Example I

An example of LEO assembly at an altitude of 1000 km is illustrated in the following demonstration of truss assembly. Seven beam elements of diameter 0.2 m and 1 m length are initially placed along the x-axis with 10 m separation distance between them. The maximum controlled change in velocity, $v_{\max}$, is chosen to be

0.03 m sec^{-1}. The control trigger, c_f, is set to -0.01, hence advance control intervention is obtained, while other control constants are unity. The repulsive parameters are $\alpha = 8, A_o = 5$, and $\sigma = 0.1$. Figure 6.9 shows the proximity motion of the components from their initial configuration to the assembled structure. Object translational and rotational parameters are shown in Fig. 6.10. The superquadric obstacle potential effect appears in Figs. 6.9.c and 6.9.e as translation, and in Figs. 6.10.b and 6.10.c as rotation. Impulses, measured as the required change in object velocity, and the overall potential function and its rate of change are shown in Fig. 6.11. The assembly process is completed in 9800 sec. Total object translation costs are listed in Table 6.1.

element no.	Δv [m/sec]	element no.	Δv [m/sec]	element no.	Δv [m/sec]	element no.	Δv [m/sec]
1	0.54103	2	0.63026	3	0.82694	4	0.81521
5	0.90176	6	1.0178	7	1.1958		

Table 6.1 Element translation cost

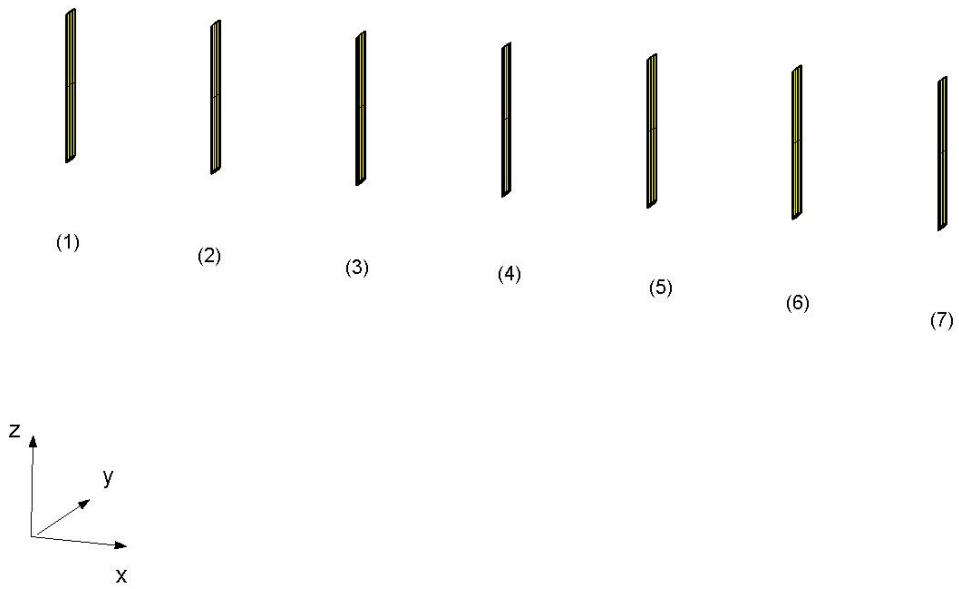

Fig. 6.9.a) Initial object configuration

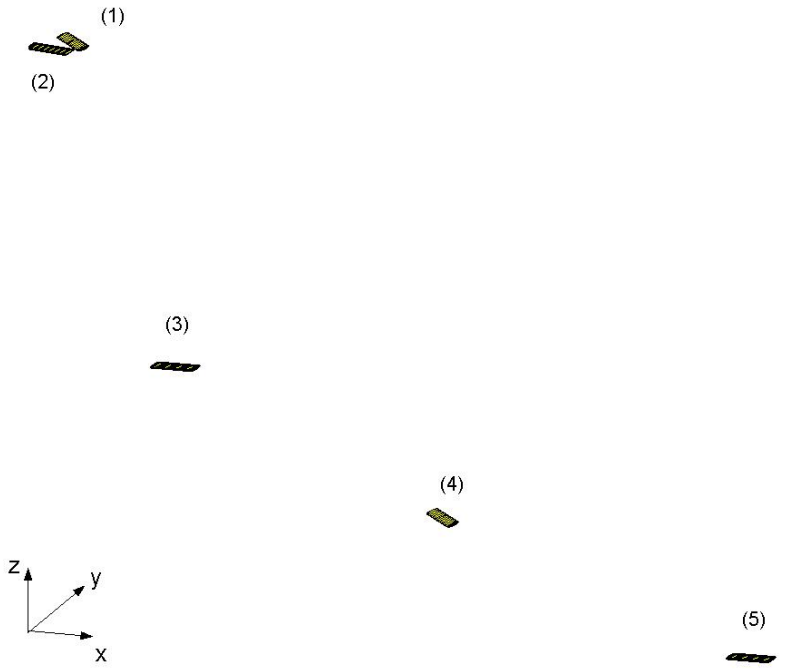

Fig. 6.9.b) Object configuration at t = 5800 sec

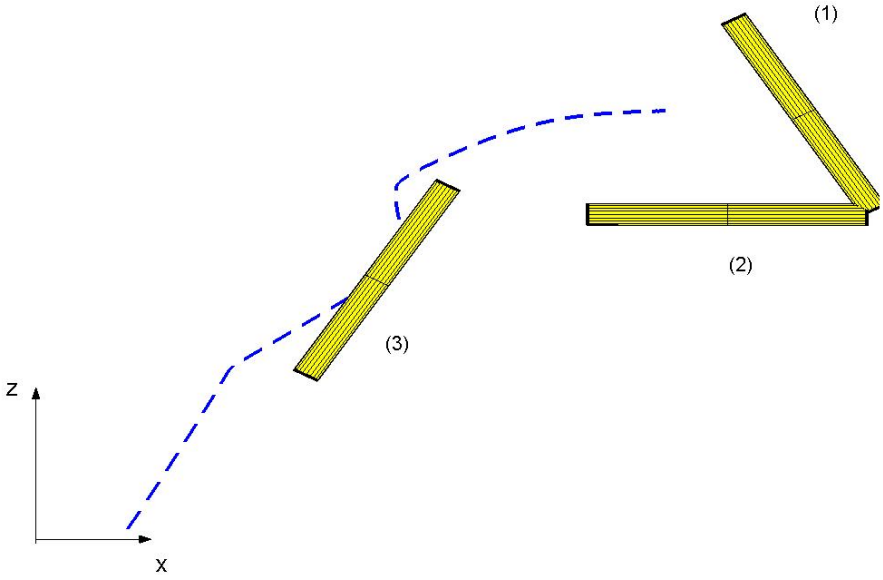

Fig. 6.9.c) Object configuration at t = 6370 sec

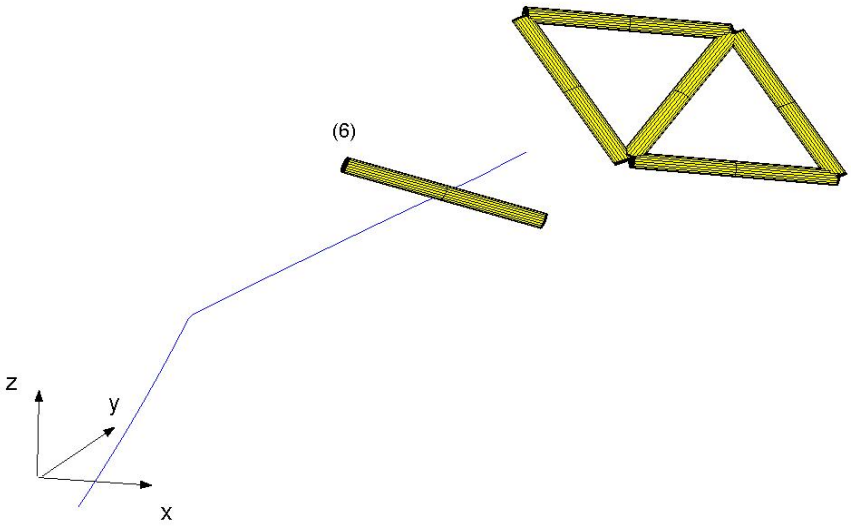

Fig. 6.9.d) Object configuration at t = 8300 sec

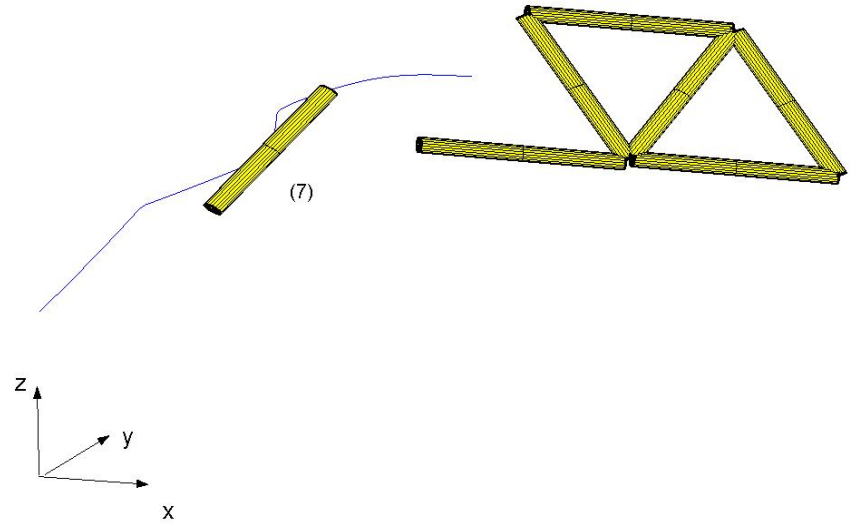

Fig. 6.9.e) Object configuration at t = 8900 sec

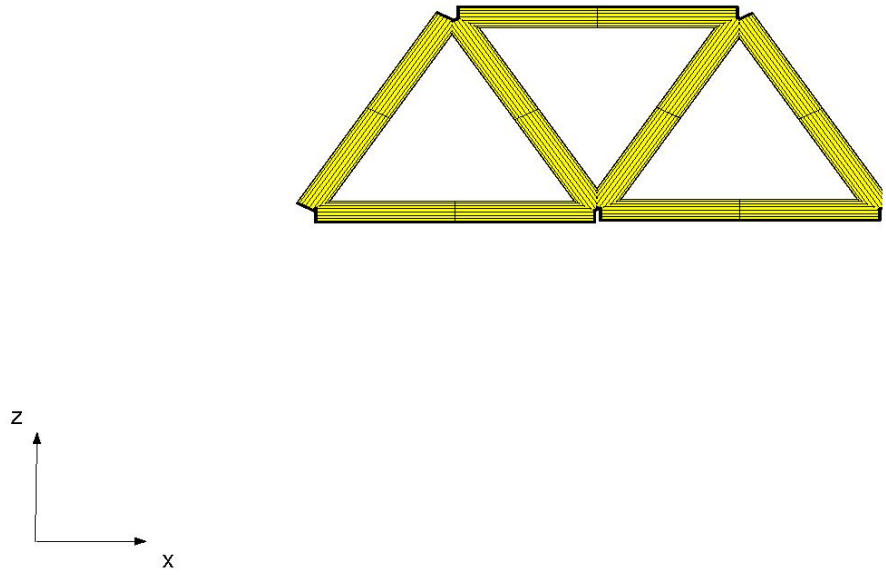

Fig. 6.9.f) Assembled structure at t = 9800 sec

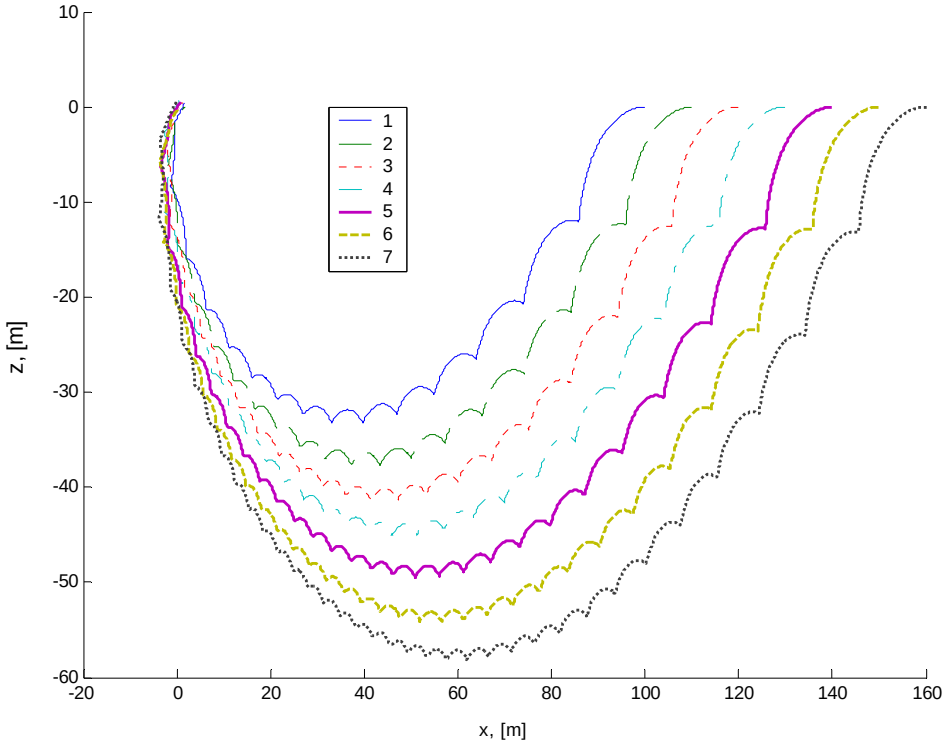

Fig. 6.10.a) Object trajectories

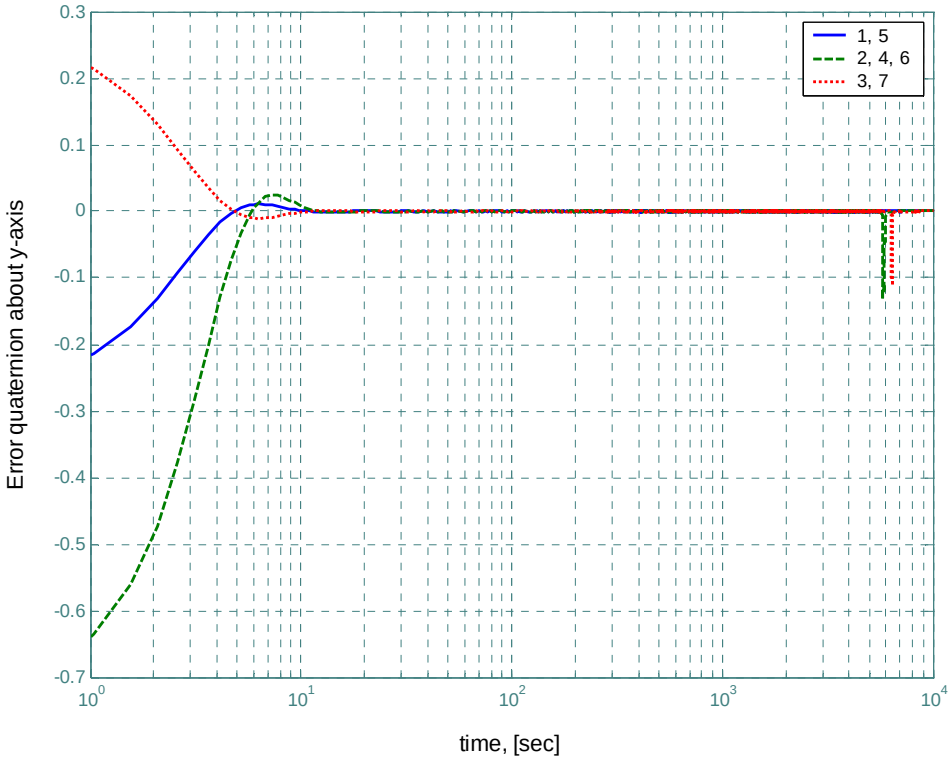

Fig. 6.10.b) Object error quaternions

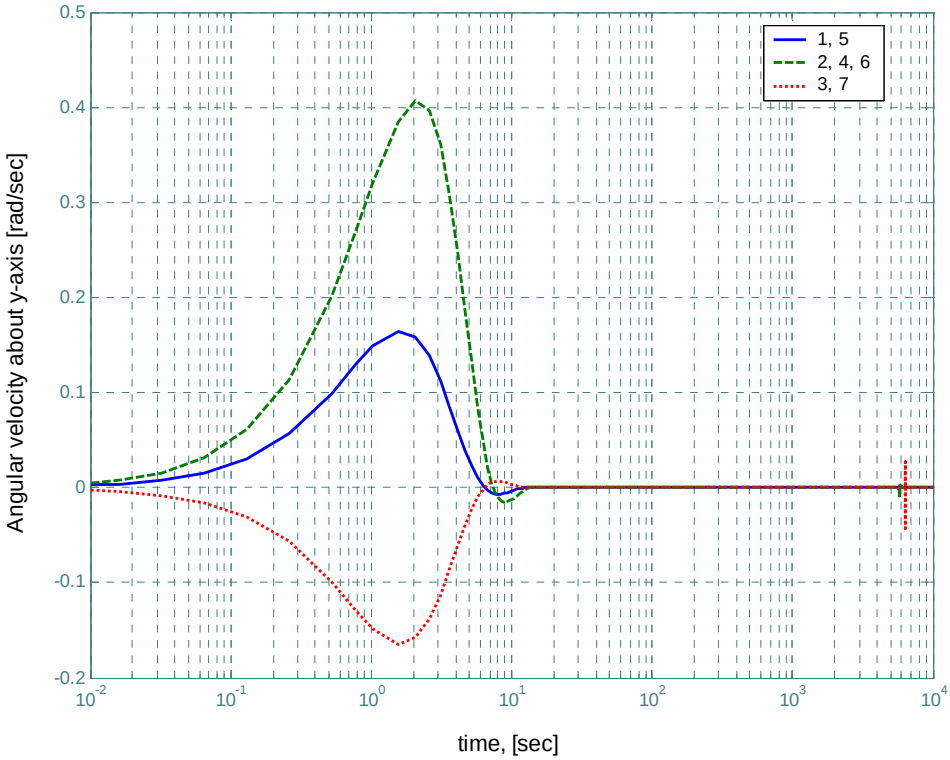

Fig. 6.10.c) Object angular velocities

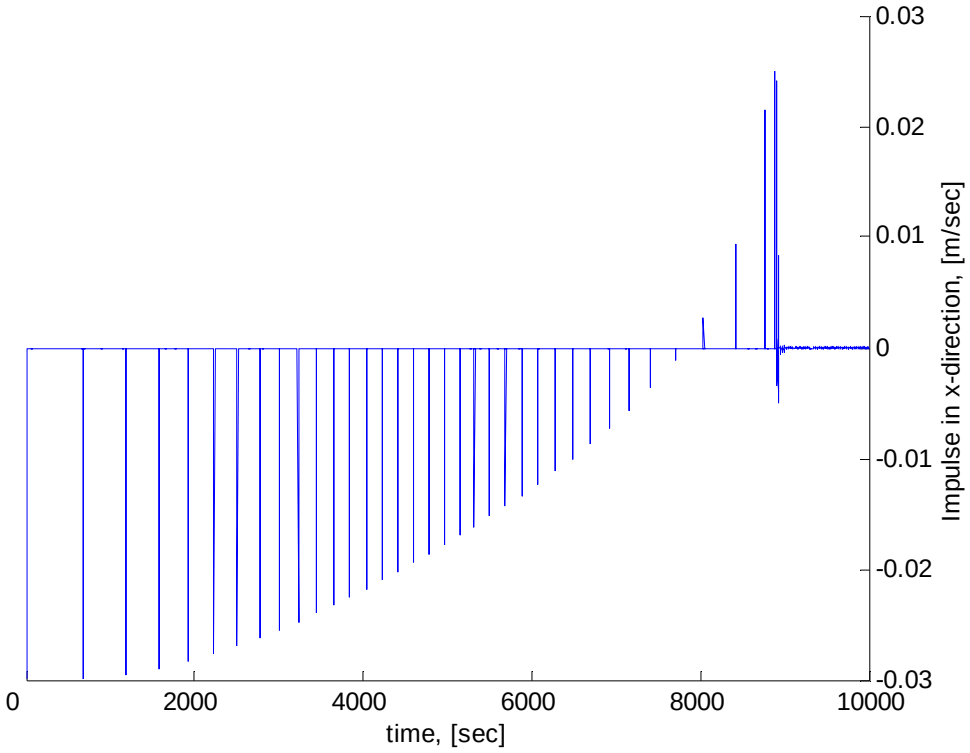

Fig. 6.11.a) Impulse in the *x*-direction (object 7)

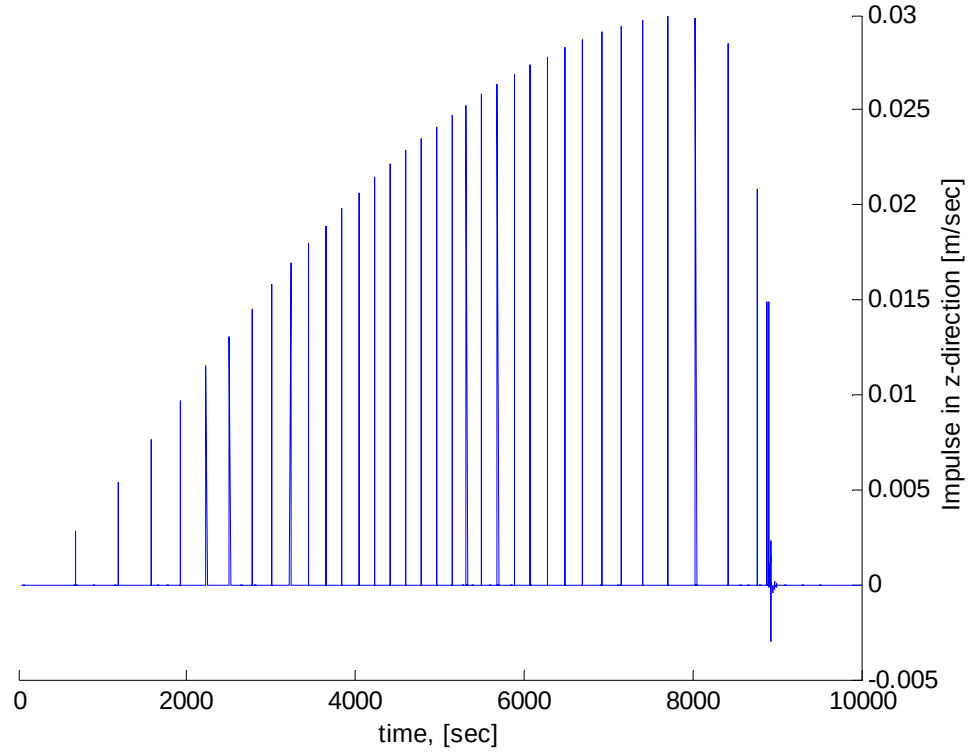

Fig. 6.11.b) Impulse in the *z*-direction (object 7)

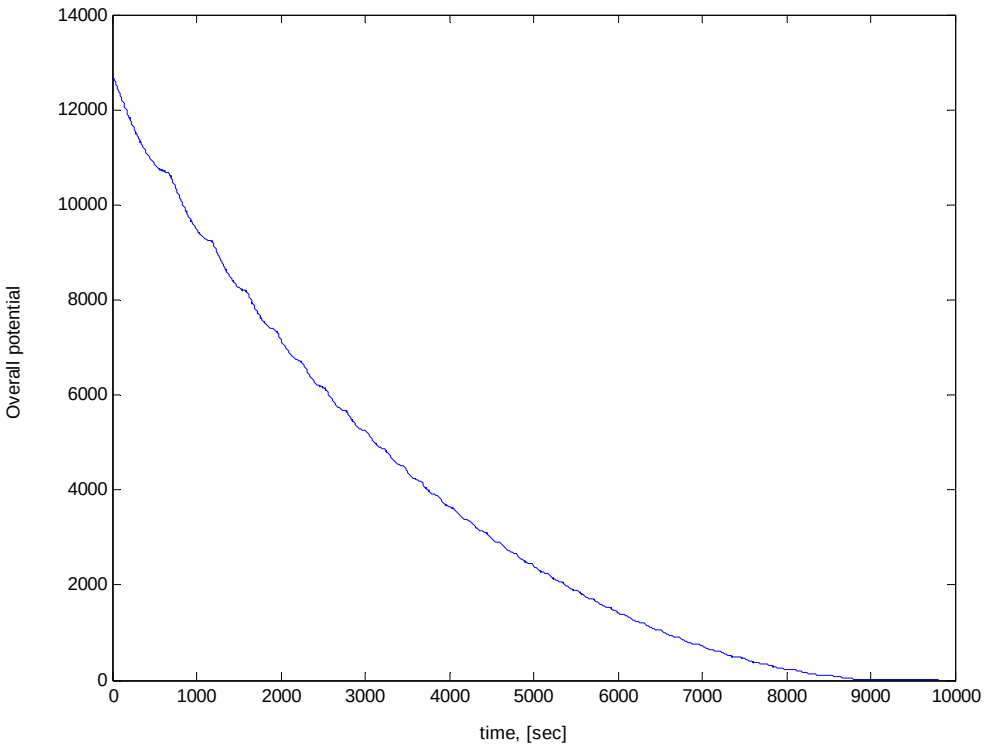

Fig. 6.11.c) Overall potential (object 7)

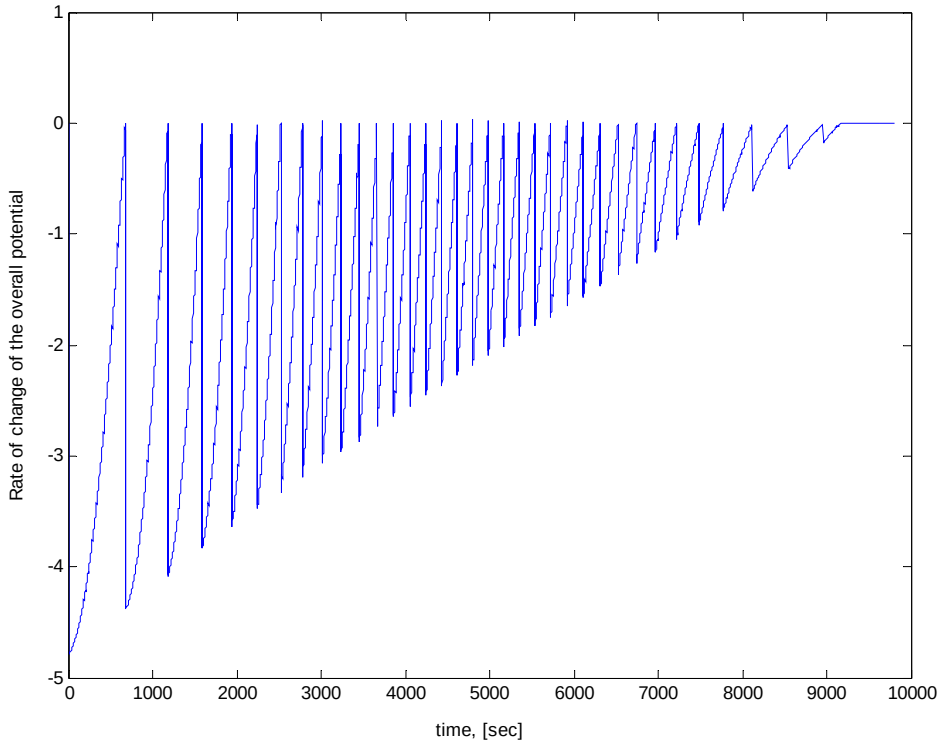

Fig. 6.11.d) Rate of change of the overall potential (object 7)

6.5.2 Example II

The above example of impulsive controlled assembly is re-produced with a maximum controlled velocity of 0.1 m sec^{-1}, rather than 0.03 m sec^{-1} in the previous example. This effect appears in Fig. 6.12 through reducing the number of impulses required. The assembly time is also decreased. The total translation cost is increased for some objects, however it is decreased for others, hence a trade-off can be done between assembly time and cost. Table 6.2 shows the new cost where the shaded cells show increased cost from to the example in section 6.5.1.

element no.	Δv [m/sec]	element no.	Δv [m/sec]	element no.	Δv [m/sec]	element no.	Δv [m/sec]
1	0.72828	2	0.59398	3	0.8291	4	0.67579
5	0.68594	6	0.77322	7	1.1031		

Table 6.2 Element translation cost

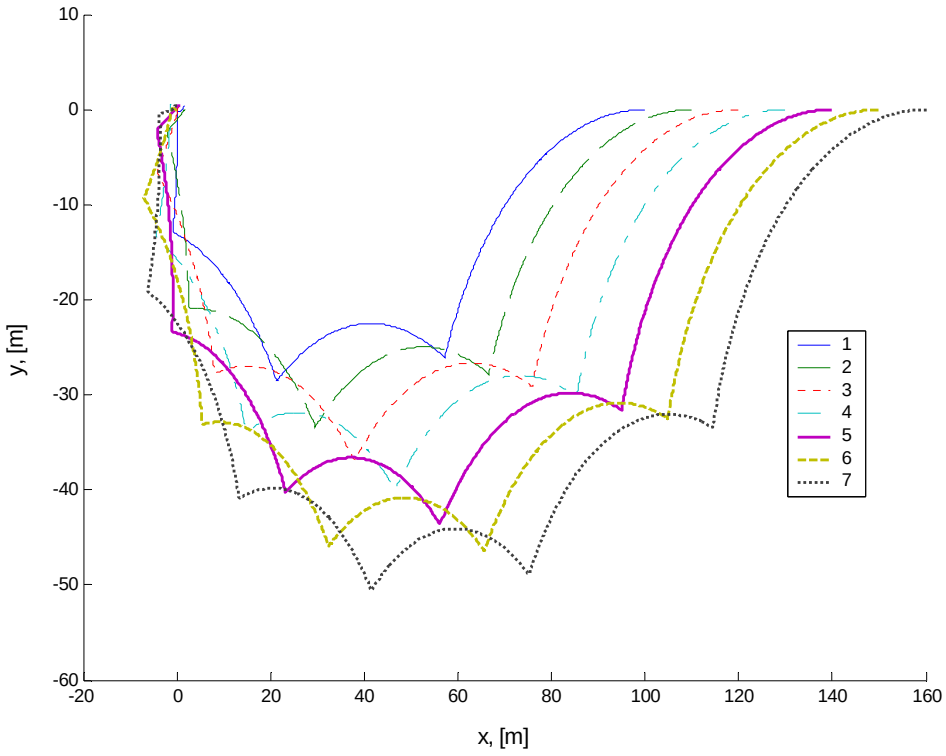

Fig. 6.12.a) Object trajectories

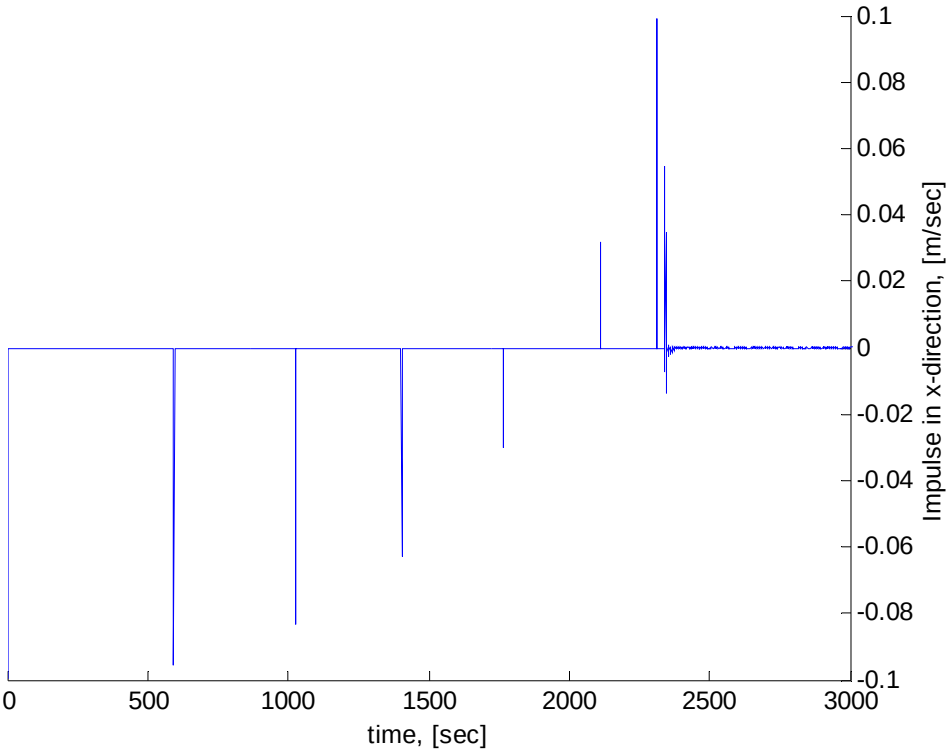

Fig. 6.12.b) Impulses in the *x*-direction (object 7)

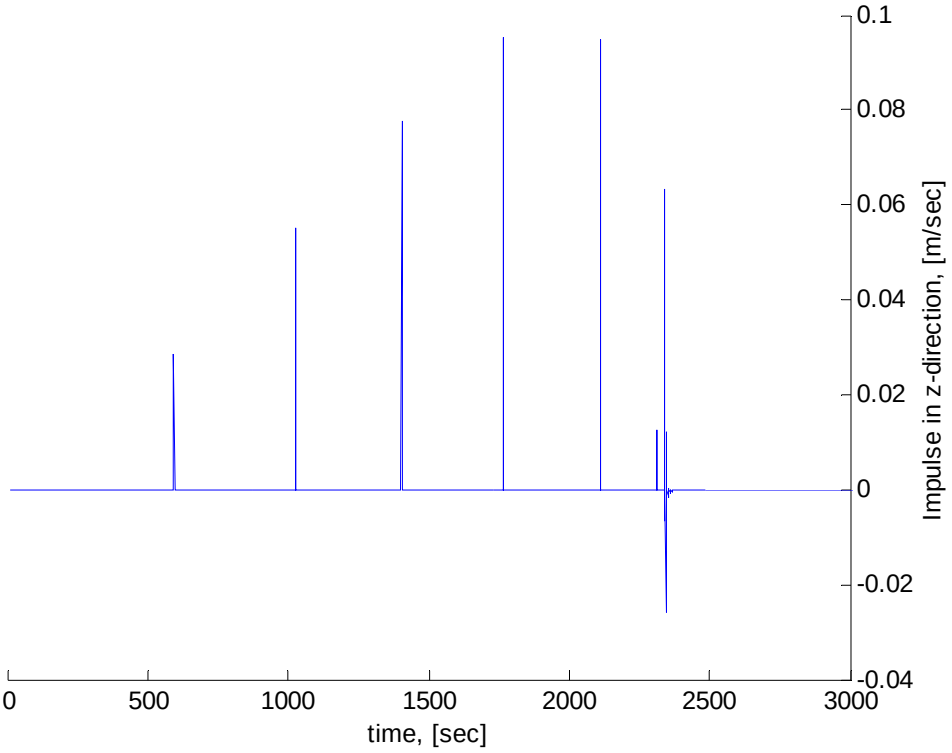

Fig. 6.12.c) Impulses in the *z*-direction (object 7)

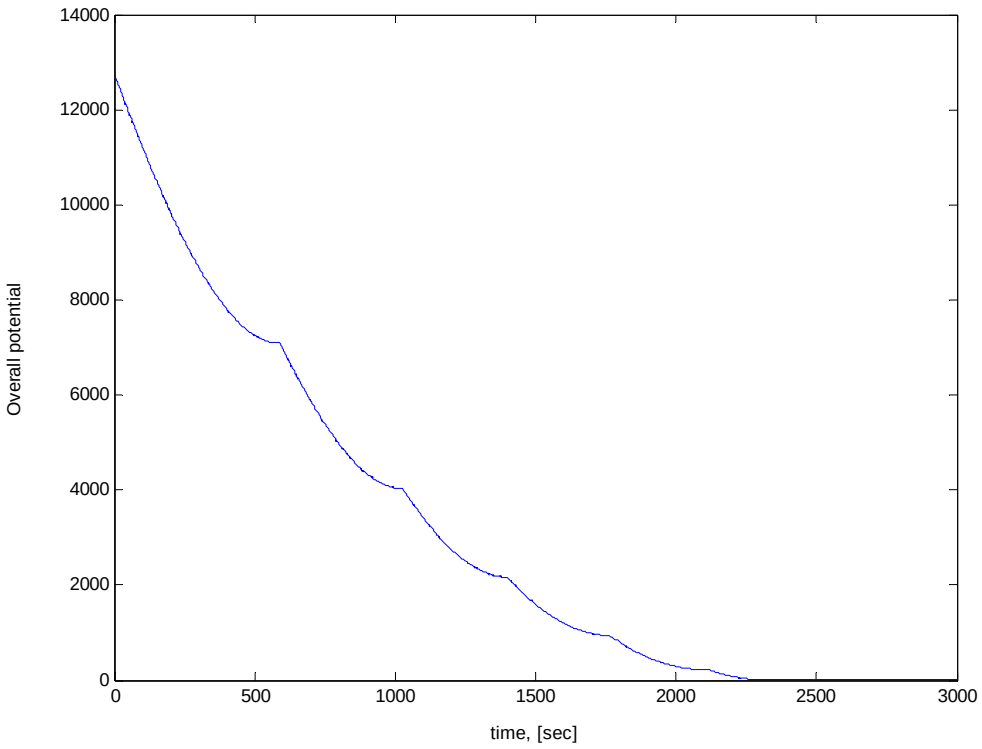

Fig. 6.12.d) Overall potential (object 7)

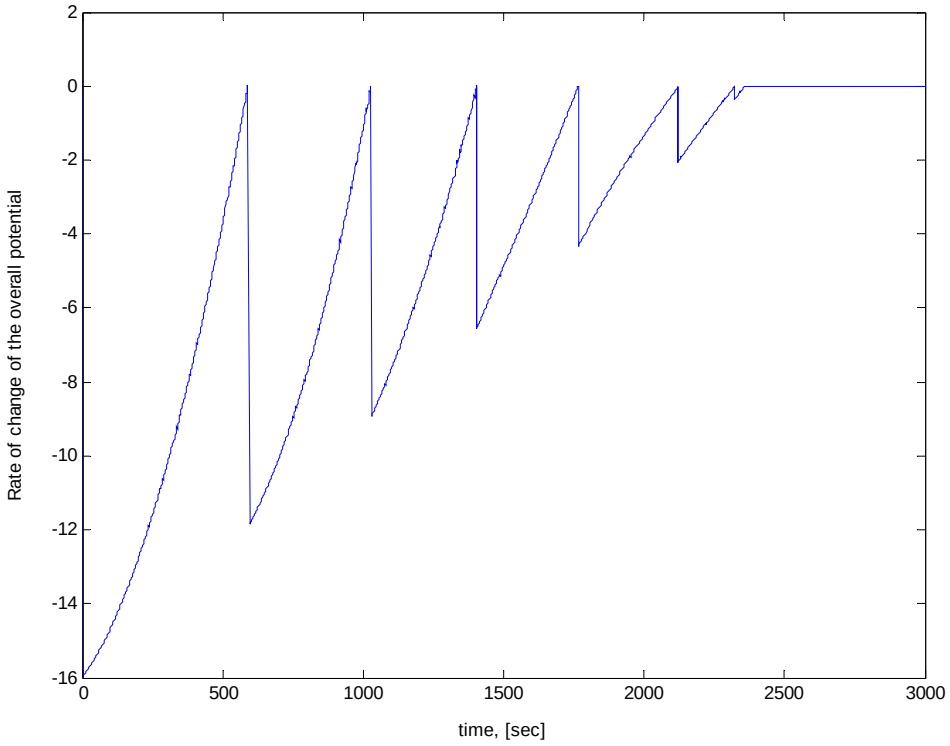

Fig. 6.12.e) Rate of change of the overall potential (object 7)

6.5.3 Complex structure assembly

A sixteen element structure is assembled at an altitude of 100 km using the impulsive control strategy. The structure is composed of 14 beam elements each of length 1 m, 0.1 m diameter, mass of 0.75 kg, and 2 plate elements of dimensions 1x1x0.2 m, mass of 2.5 kg and 2x12x0.4 m, mass of 10 kg. All control constants are unity except $\lambda_q = 0.1$. The repulsive parameters are $\alpha = 10, A_o = 5$, and $\sigma = 0.1$. Elements are initially placed parallel on two lines along the *x*-direction, Fig. 6.13.a. The control trigger is set to -0.01, hence advance control intervention is obtained. Figure 6.13 shows the proximity motion of the components from their initial configuration to the assembled structure. Object translational parameters including control impulses are shown in Fig. 6.14. Object rotational parameters including the control torque are shown in Fig. 6.15. The superquadric obstacle potential effect appears in Figs. 6.13.b, 6.13.c, 6.13.d, and 6.14.a as translation, and in Figs. 6.15.a, 6.15.b, and 6.15.c as rotation. The assembly process is completed in 4000 sec. Total object translation costs are listed in Table 6.3.

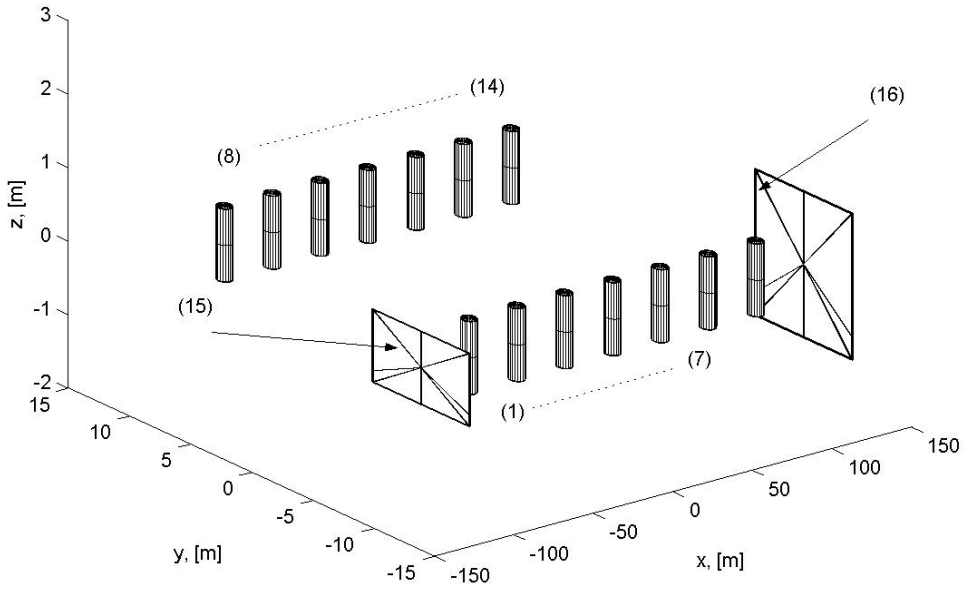

Fig. 6.13.a) Initial object configuration

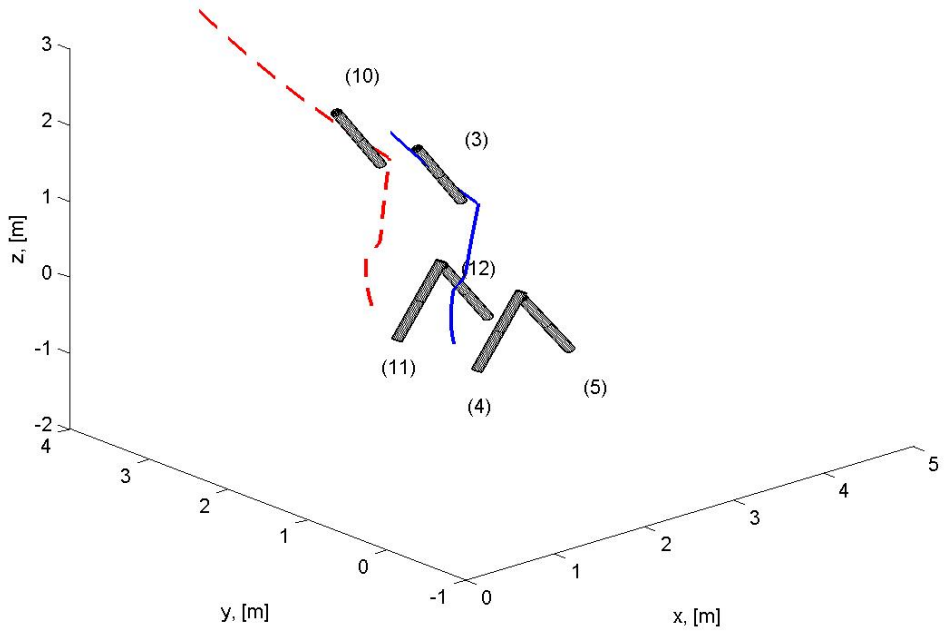

Fig. 6.13.b) Object configuration at t = 760 sec

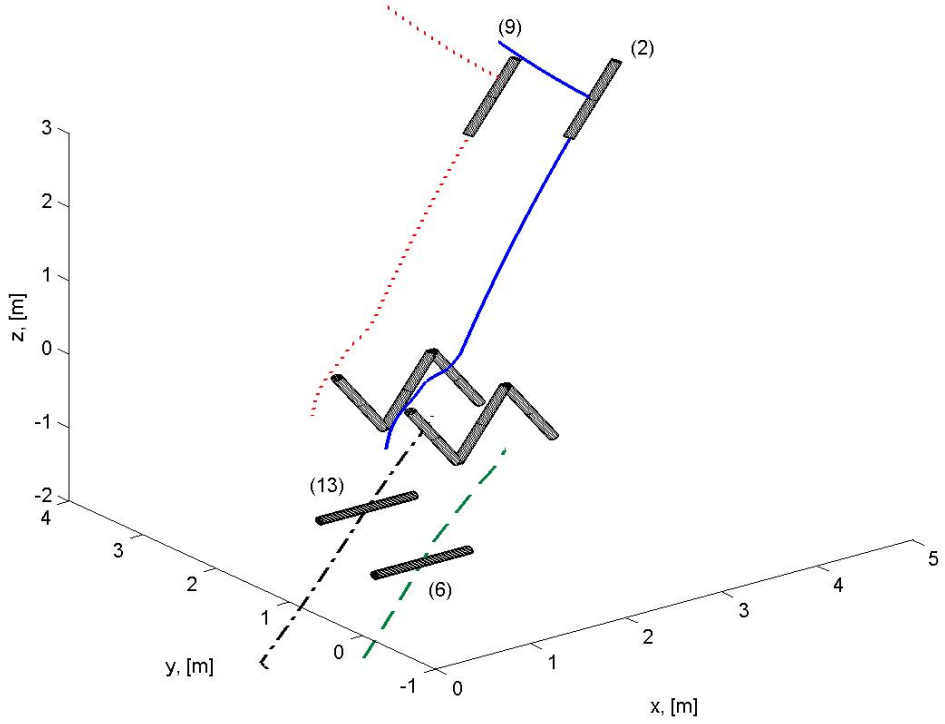

Fig. 6.13.c) Object configuration at t = 1630 sec

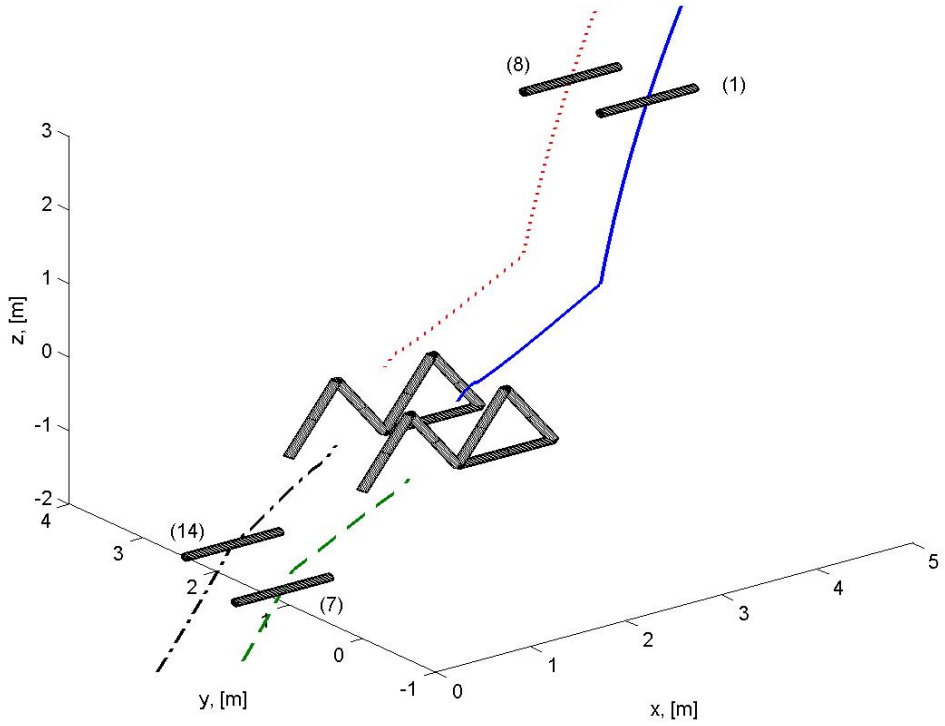

Fig. 6.13.d) Object configuration at t = 2670 sec

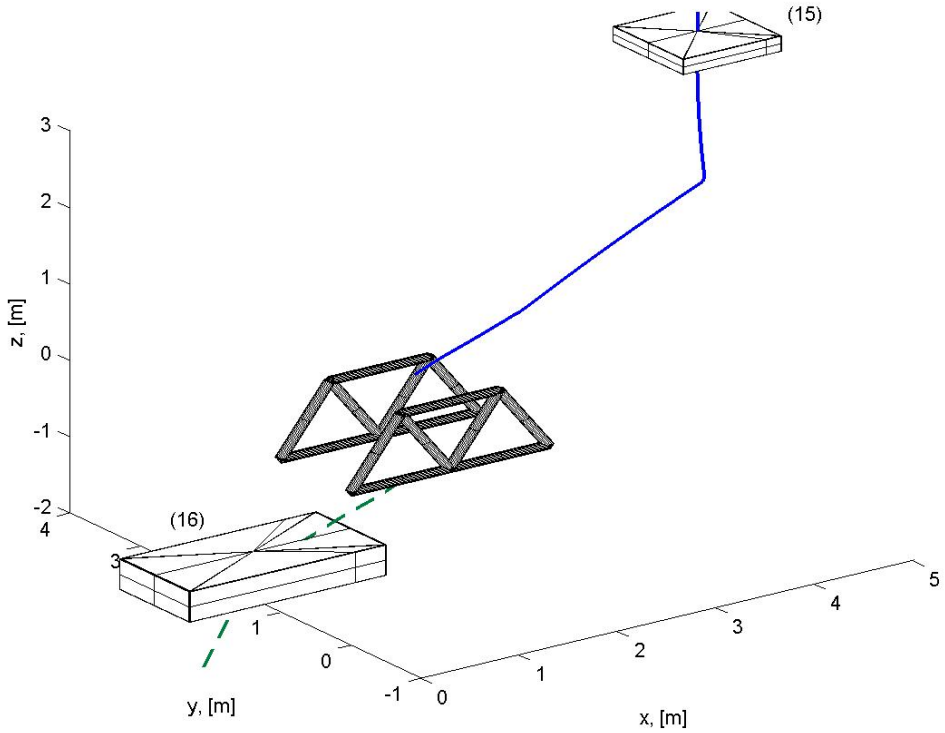

Fig. 6.13.e) Object configuration at t = 3725 sec

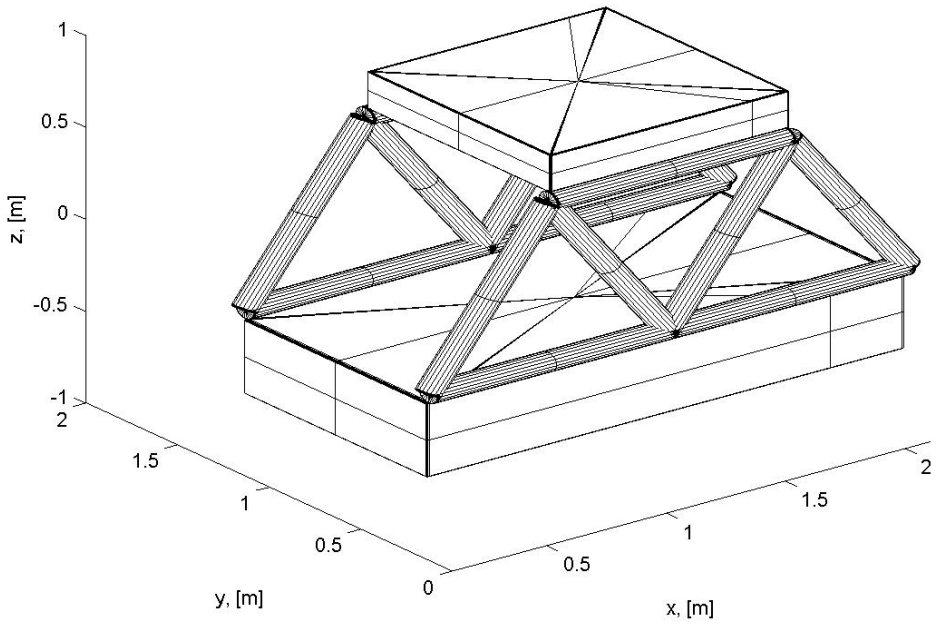

Fig. 6.13.f) Assembled structure at t = 4000 sec

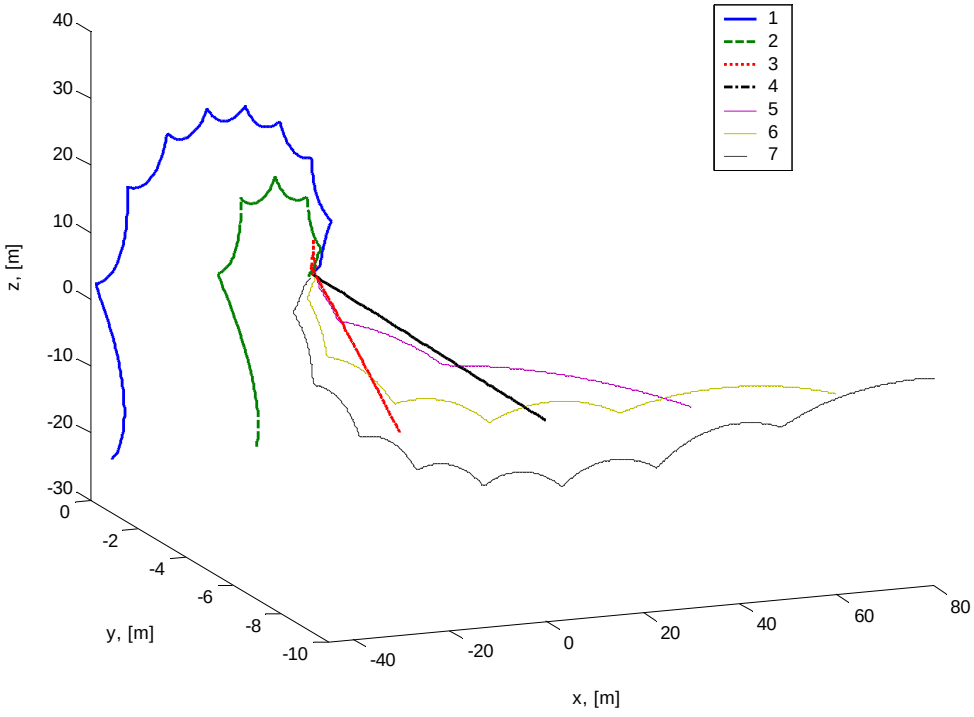

Fig. 6.14.a) Object trajectories (object 1 to 7)

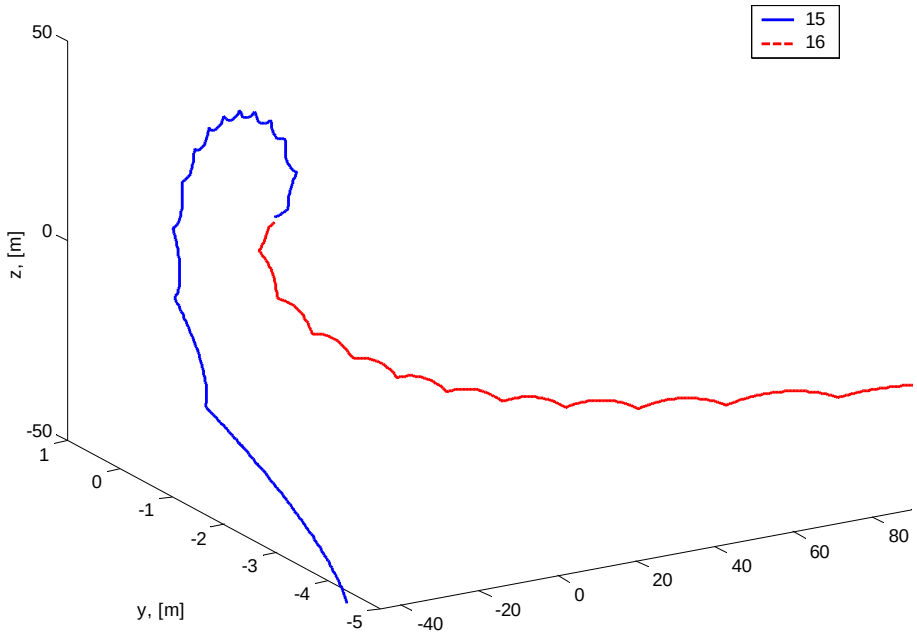

Fig. 6.14.b) Plate element trajectories (object 15 and 16)

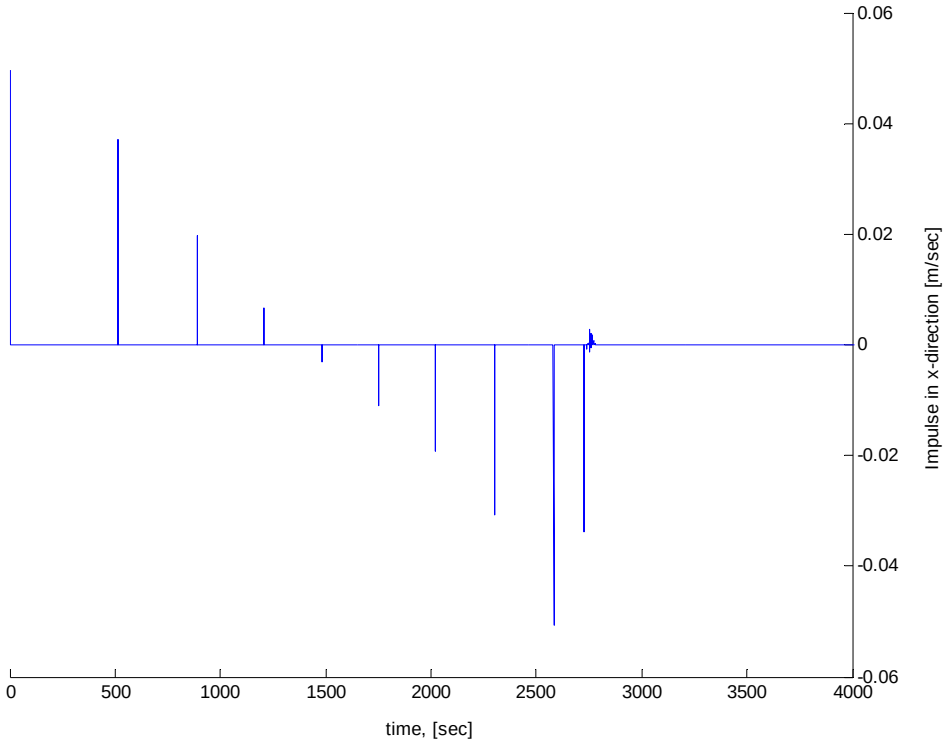

Fig. 6.14.c) Impulse in *x*-direction (object 1)

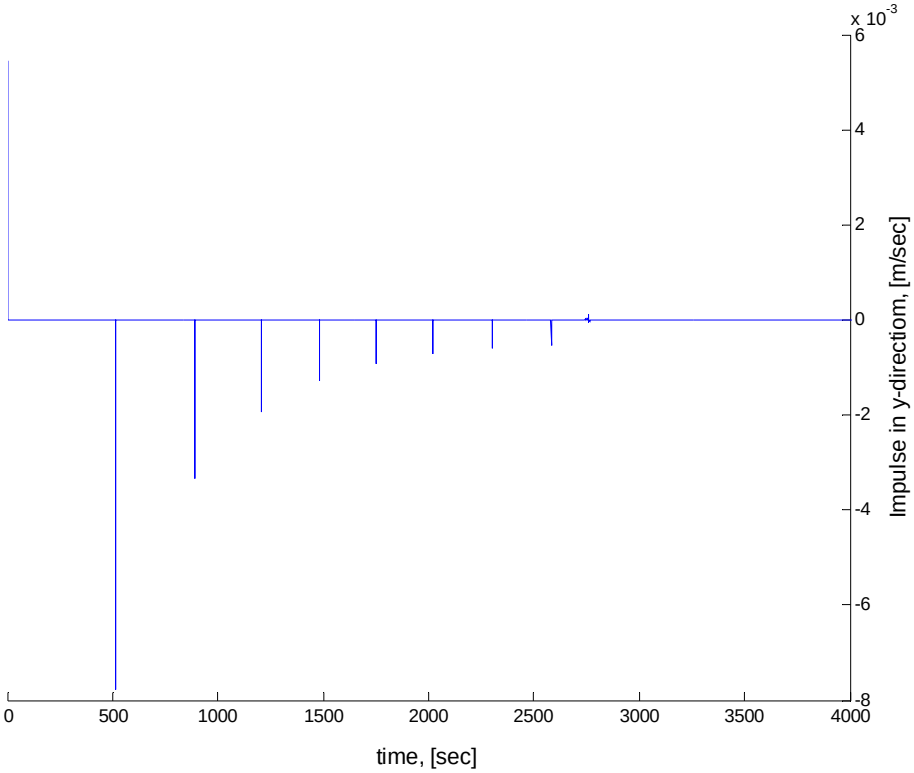

Fig. 6.14.d) Impulse in *y*-direction (object 1)

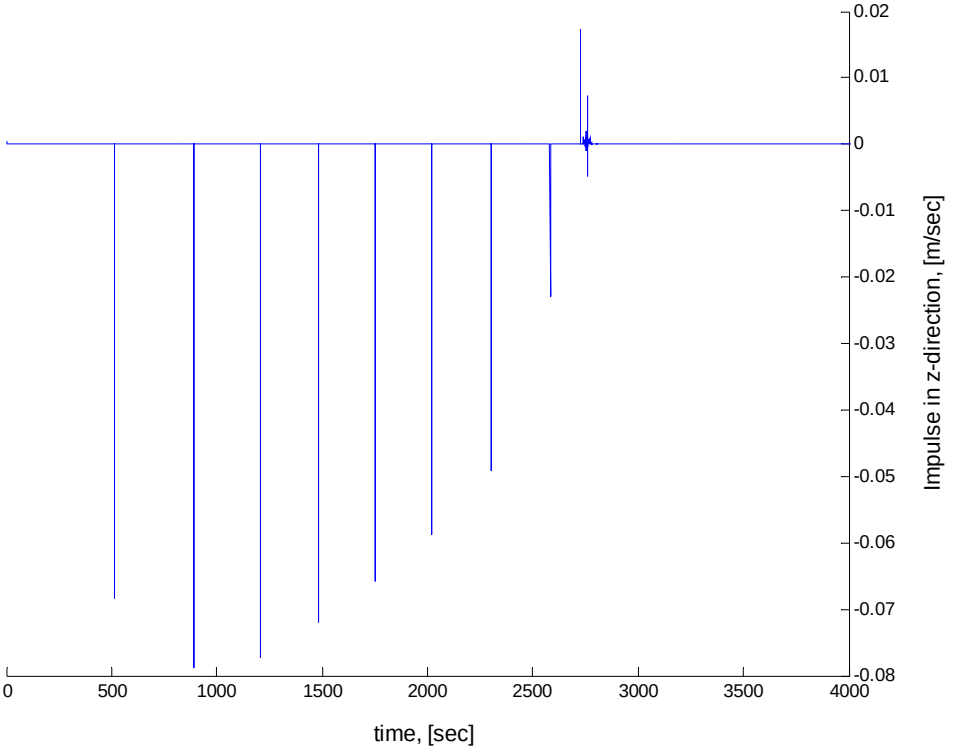

Fig. 6.14.e) Impulse in *z*-direction (object 1)

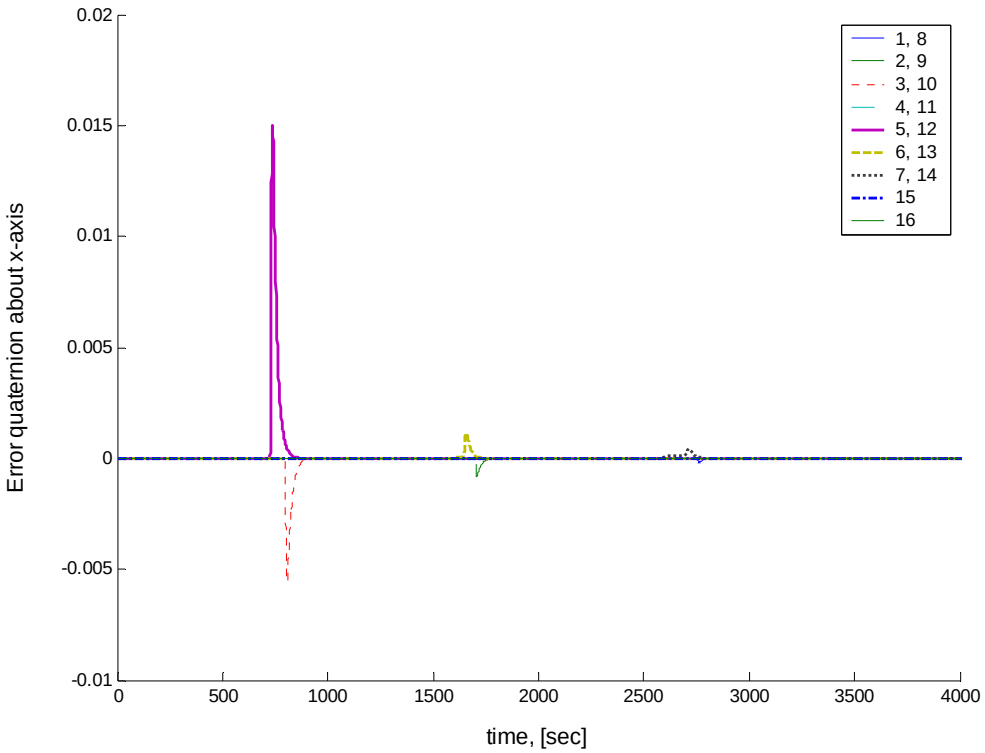

Fig. 6.15.a) Error quaternions about the *x*-axis

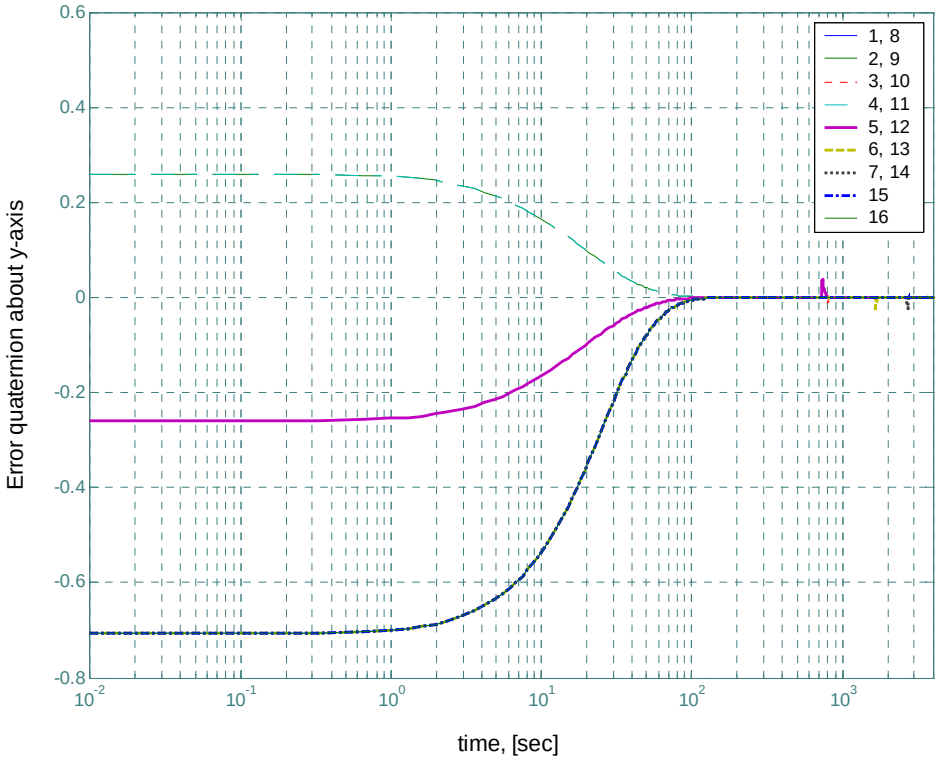

Fig. 6.15.b) Error quaternions about the *y*-axis

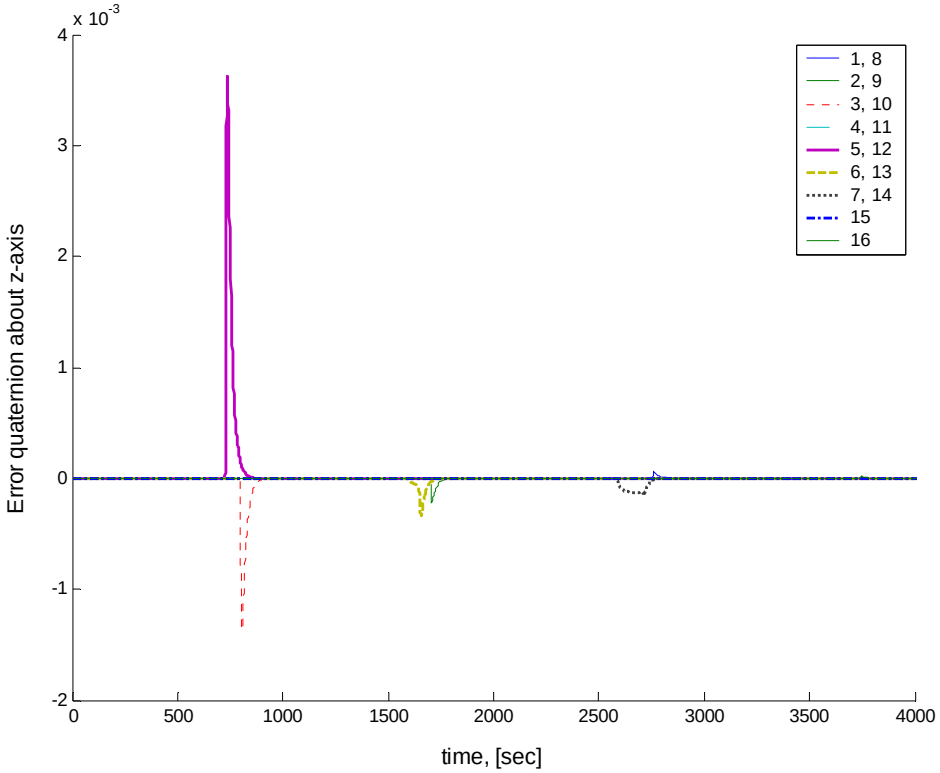

Fig. 6.15.c) Error quaternions about the *z*-axis

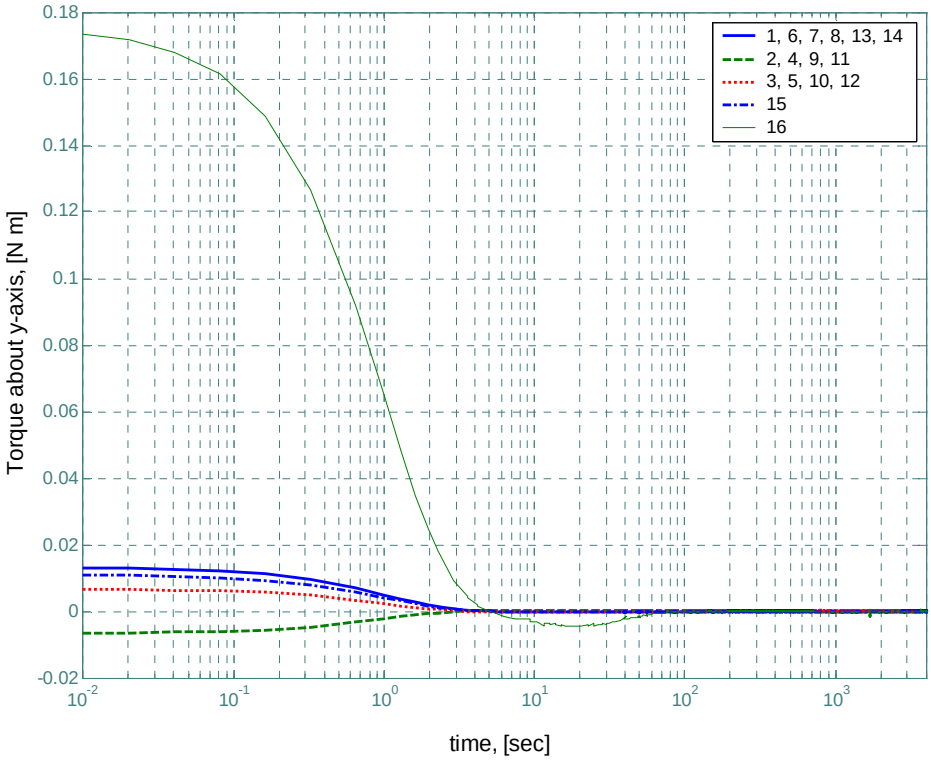

Fig. 6.15.d) Continuous control torque about the *y*-axis

element no.	Δv [m/sec]	element no.	Δv [m/sec]	element no.	Δv [m/sec]	element no.	Δv [m/sec]
1	0.73687	2	0.61377	3	0.48533	4	0.12892
5	0.4125	6	0.44357	7	0.68621	8	0.75072
9	0.56154	10	0.47197	11	0.13523	12	0.36982
13	0.4364	14	0.69376	15	1.0035	16	0.98077

Table 6.3 Element translation cost

6.6 Conclusions

Applying the potential field method with superquadric obstacle potentials succeeds in bringing structural components to their goal while avoiding collisions. Continuous control is presented through a new approach of using a combination of parabolic and conical functions, without which unbound control forces may arise. Excellent controller performance is obtained as the object velocities are near constant, hence little controller intervention is required. An assembly of twelve parallelepiped elements was performed using the continuous control scheme.

Adding a velocity term to a hyperbolic potential function provides successful continuous control with bounded control action. The resulting controlled velocities are nearly constant over the entire workspace, except in the neighbourhood of obstacles. Global stability and convergence of the system is proven and tested for a dense workspace. Proximity motion of the manoeuvring objects shows coupling between translational and rotational motion in the presence of obstacles.

Impulsive control also succeeds in on-orbit assembly of a truss structure composed of seven beams. Early controller intervention is required, especially, in a dense environment. Increasing the maximum impulse decreases the assembly time and affects the total translation cost. The maximum impulse should be chosen to optimize the trade-off between assembly duration and total manoeuvre cost.

7. ORBITAL RECONFIGURATION

7.1 Introduction

Changing the configuration of a space structure leads to changes in its position and/or orientation, which will be termed object reconfiguration. The reconfiguration process is required to achieve distinct configurations through kinematic constrains in order to produce a new or modified system configuration (Barfoot and Clark, 2004). This enables a system of limited functionality to accomplish various tasks (Shen et al., 2006). The term reconfiguration is defined as the set of necessary orbital manoeuvres to form a new formation, either to accomplish a new mission or after failure by replacing the faulty object with a replacement. The reconfiguration process allows new needs to be serviced that may arise over time.

Three general categories of object reconfiguration problem have been investigated: pure mathematical pattern development in cell-space, manually combined unit-structured system with fixed configuration, and unit-structured systems with dynamic reconfiguration ability (Murata et al., 1998).

Reconfiguration problems have been considered in case of satellite constellations using potential functions (McInnes, 1993; McQuade et al., 2003; Izzo and Pettazi, 2005; Izzo and Pettazi, 2007). Modular self-reconfigurable robots are another application of object reconfiguration in which the robot changes its shape to adapt to its surroundings (Ünsal and Khosla, 2000).

The reconfiguration strategy presented in this chapter is divided into two phases: disassembly and reassembly processes. Objects decouple from their initial configuration by virtue of the repulsive potential, and then reassemble in a new formation. Two cases are discussed in this chapter: free flyer manoeuvring and structure reconfiguration. The first problem discusses manoeuvring of one small body near another larger one, the International Space Station in this case. The second problem discusses the manoeuvring of multiple objects of the same size to form some formation from a starting position, and then decouple and reform another formation. A reconfigurable spacecraft can be envisaged which can change its morphology to be optimised to a particular mission phase.

7.2 Free Flyer Manoeuvring Near a Space Station

Free-flying robots enable flexible assembly and service facilities to work inside space facilities or operate in the free space. They serve in conjunction with redundant manipulators and astronauts with the advantage of flexibility over the first and safety over the second type.

A potential field incorporating both translational and rotational motion is used to control the dynamics of a free-flyer manoeuvring at the International Space Station, Fig. 7.1. The station modules use the same superquadric model, nevertheless shape and size differences are defined using the free parameters of the superquadric functions as discussed in chapter 3. The potential functions are formed in local body frames of reference, hence error quaternions are used to find relations between local and inertial parameters. The repulsive potentials depend on the relative distance between the free-flyer and the modules. As they have different sizes and orientations, a rigid body formulation is required, instead of considering only their centres to calculate the separation distances (Badawy and McInnes, 2006a).

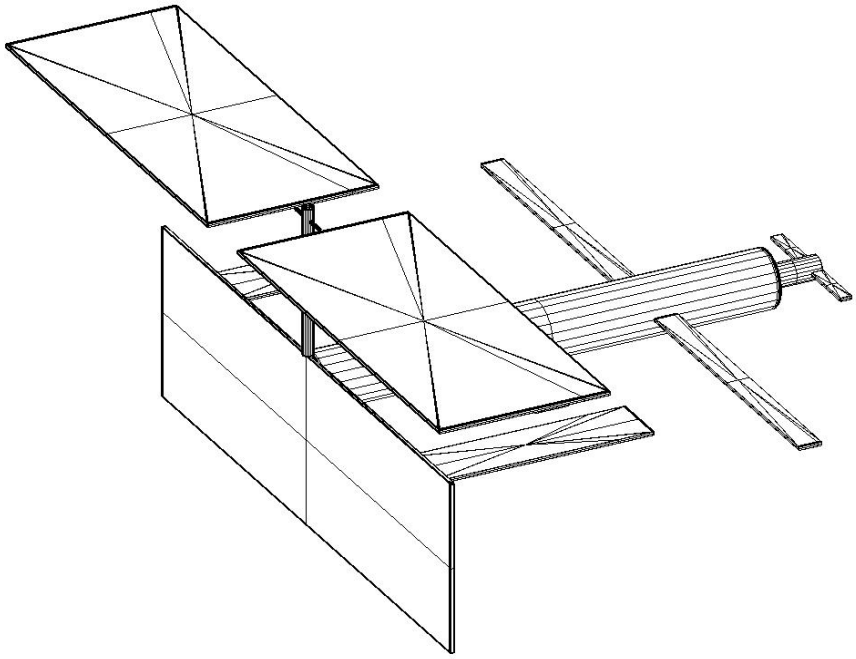

Fig. 7.1 International space station using superquadric model

The proposed global potential function is formulated to minimize on-board sensor requirements through the use of only kinematic data as the measured quantities. The required impulses are calculated on-board, then actuated by small thrusters, whereas a continuous control torque is assumed to be produced from control moment gyros (Badawy and McInnes, 2007a). The minimum formulation of the global potential function capable of performing the required control of both translation and rotation is produced by combining Eqs. (2.3) and (2.28) as the attractive potential along with the station module repulsive potentials defined by Eqs. (4.1) and (4.2). The proposed global function is expressed as:

$$V = \frac{\lambda_p}{2}(\mathbf{r} - \mathbf{r}_G).(\mathbf{r} - \mathbf{r}_G) + \frac{\lambda_q}{2}\overline{\mathbf{q}}.\overline{\mathbf{q}} + V_{obs} \tag{7.1}$$

The potential function time derivative is then defined as:

$$W = \lambda_p \dot{\mathbf{r}}.(\mathbf{r} - \mathbf{r}_G) + \lambda_q \dot{\overline{\mathbf{q}}}.\overline{\mathbf{q}} + \nabla V_{obs}.\dot{\mathbf{r}} + \nabla^q V_{obs}.\dot{\overline{\mathbf{q}}} \tag{7.2}$$

To set the time derivative of the potential function to be negative definite, the control laws will be defined as:

$$\dot{\mathbf{r}} = -v_{max}\left(1 - e^{-\beta V_{att}}\right)\frac{\nabla V}{\left|\nabla^* V\right|} \tag{7.3}$$

and

$$\dot{\overline{\mathbf{q}}} = -\omega_{max}\left(1 - e^{-\beta V_{att}}\right)\frac{\nabla^q V}{\left|\nabla^* V\right|} \tag{7.4}$$

where

$$\nabla = \left[\frac{\partial}{\partial x}\ \frac{\partial}{\partial y}\ \frac{\partial}{\partial z}\right]^T \tag{7.5-a}$$

$$\nabla^q = \left[\frac{\partial}{\partial q_1}\ \frac{\partial}{\partial q_2}\ \frac{\partial}{\partial q_3}\right]^T \tag{7.5-b}$$

$$\nabla^* = \left[\frac{\partial}{\partial x} \; \frac{\partial}{\partial y} \; \frac{\partial}{\partial z} \frac{\partial}{\partial q_1} \; \frac{\partial}{\partial q_2} \; \frac{\partial}{\partial q_3} \right]^T \tag{7.5-c}$$

Using Eqs. (7.3) and (7.4) this leads to the time rate of change of the potential function as:

$$W = -\left(1 - e^{-\beta V_{att}}\right) \left[v_{max} \lambda_p \frac{\left| \mathbf{r} - \mathbf{r}_G + \nabla V_{obs} \right|^2}{\left| \nabla^* V \right|} + \omega_{max} \lambda_q \frac{\left| \overline{\mathbf{q}} + \nabla^q V_{obs} \right|^2}{\left| \nabla^* V \right|} \right] \leq 0 \tag{7.6}$$

The angular velocity is calculated as (Wie, 1998):

$$\boldsymbol{\omega} = 2\mathbf{Q}^{-1}\dot{\overline{\mathbf{q}}} \tag{7.7}$$

A free-flyer parked on the station surface will manoeuvre to another point to perform certain operations such as inspection, installation, or repair. The free-flyer is equipped with thrusters to enable it to perform the required manoeuvre. The thrusters are on when the time derivative of the global potential function is larger than some non-positive value, c_f. Control actuation is then required when:

$$W_i \geq c_f \tag{7.8}$$

Between impulses the free-flyer will move according to the natural orbital mechanics equations using the *Clohessy-Wiltshire* approximation, since the relative distance between start and goal positions are much smaller than that distance to the Earth's centre, as discussed in chapter 6. Trajectory manoeuvres are shown at each impulse as shown in Fig. 7.2. Coupling between translation and rotation produces the quaternion change in Fig. 7.3 although initial and goal orientations are identical. The impulses required to perform the transfer described in Fig. 7.2 are shown in Fig.7.4. Finally, the required control torque about the *y*-axis is shown in Fig. 7.5, whereas the control torques about other axes are zeros.

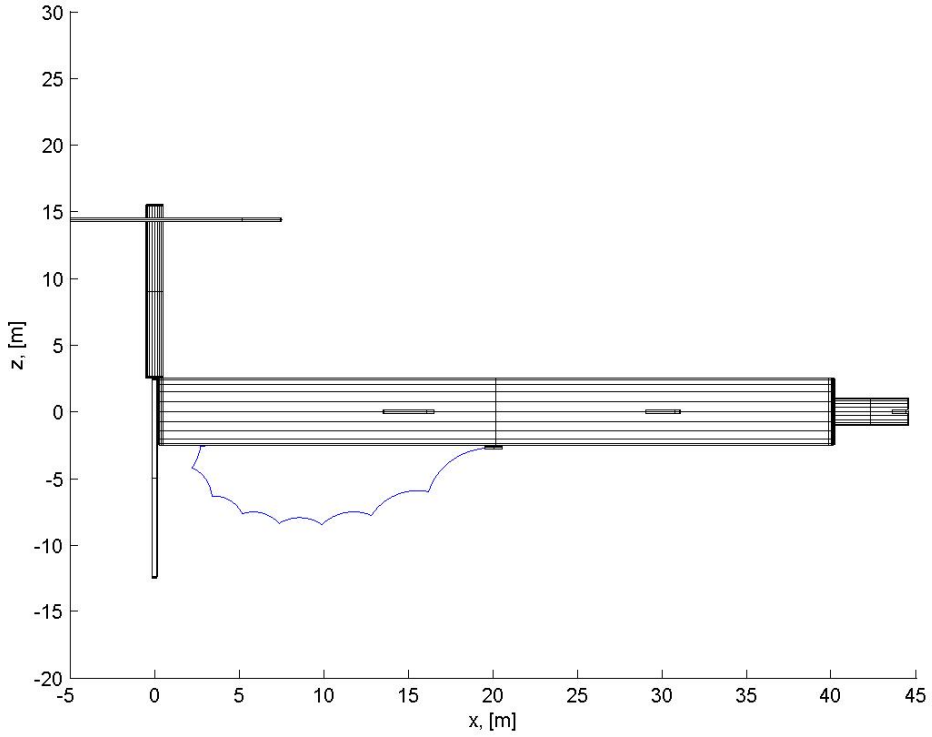

Fig. 7.2 Free-flyer trajectory

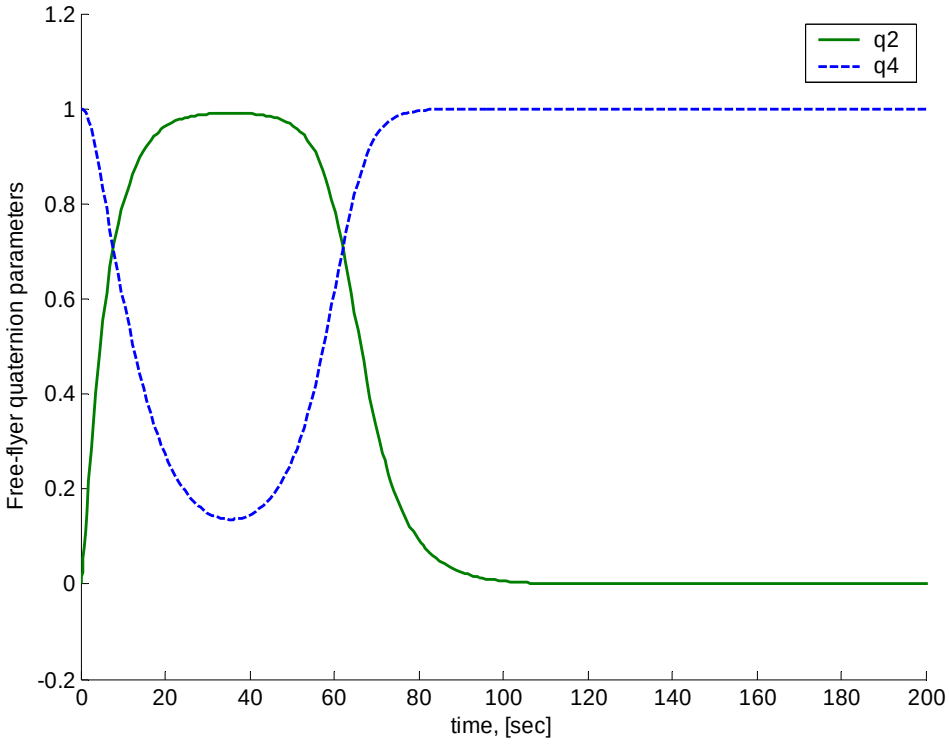

Fig. 7.3 Free-flyer rotation

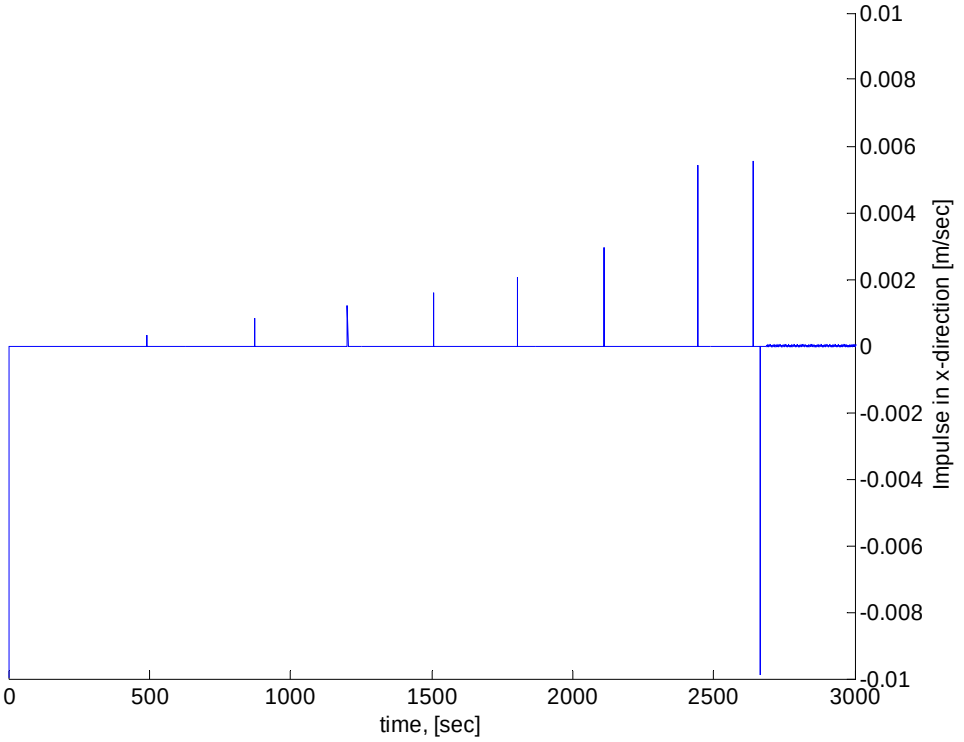

Fig. 7.4.a) Free-flyer thrust impulses in *x*-direction

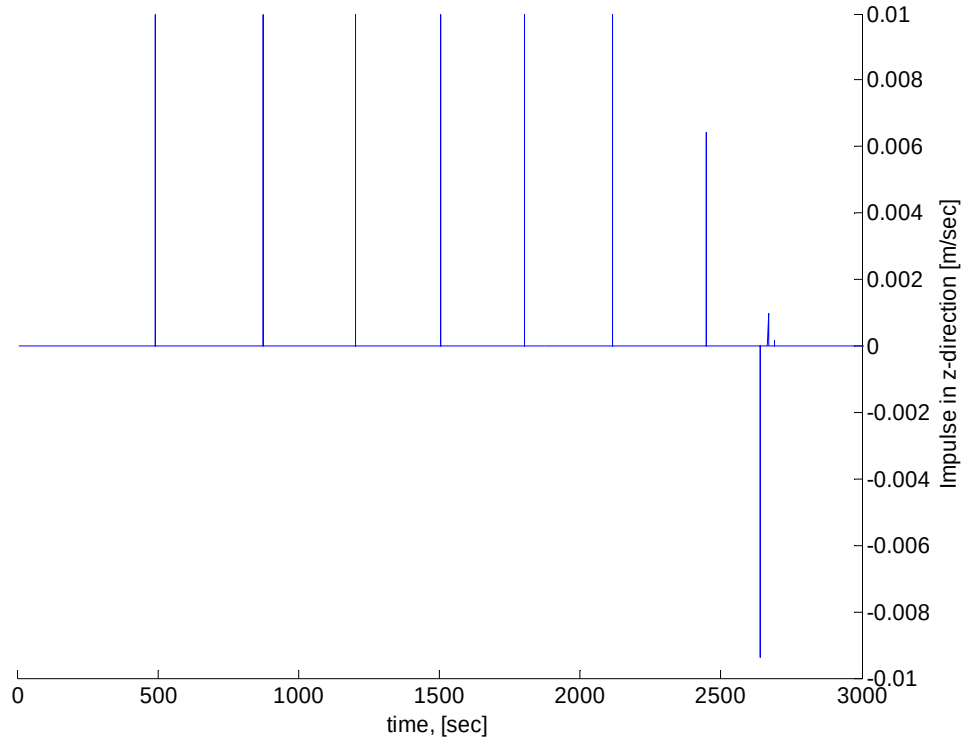

Fig. 7.4.b) Free-flyer thrust impulses in *z*-direction

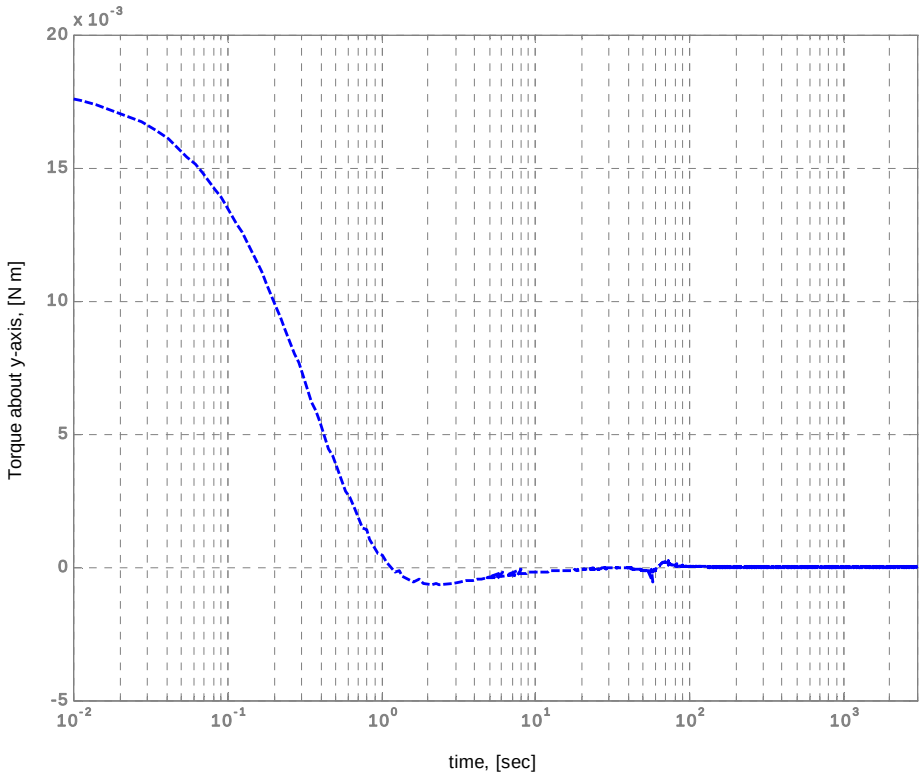

Fig. 7.5 Required control torque about *y*-axis

7.3 Structure Reconfiguration

Manoeuvring beam type objects of 0.1 m diameter and 1 m length are initially in a parking position with 1 m separation distance. They were then tasked to perform a manoeuvre to form a closed hexagonal formation. Later, the objects are disassembled and then form a line configuration. All control constants are unity except $\lambda_q = 0.1, \lambda_w = 0.8$. The repulsive parameters are defined as α = 6, A_o = 50, $\sigma = 0.1$, and $\beta = 1$.

During the 400 sec of the first task, coupled in/out of plane manoeuvres along with rotation manoeuvres are performed, except for the first object where its goal configuration is chosen to be the same as the initial one. Complex manoeuvres from the initial to goal configurations are shown in Fig. 7.6 using an impulsive control strategy with a maximum controlled velocity of 0.02 m sec^{-1} as shown in Fig. 7.7. Although the control constant, c_f, is chosen to be zero, it is noted for object (3) that there exists a similarity to continuous control due to the very close spacing of the

objects. Hence even after the impulsive intervention the rate of change of the potential function remains positive as other objects manoeuvre nearby. The objects also perform some rotational manoeuvres in three-dimensions to avoid collisions, as shown in Fig. 7.8, and in Fig. 7.9 as the required continuous control torques. The total translation costs are shown in Table 7.1.

element no.	Δv [m/sec]	element no.	Δv [m/sec]	element no.	Δv [m/sec]
1	0	2	0.035289	3	0.1118
4	0.20255	5	0.42914	6	0.1025

Table 7.1 First phase translation cost

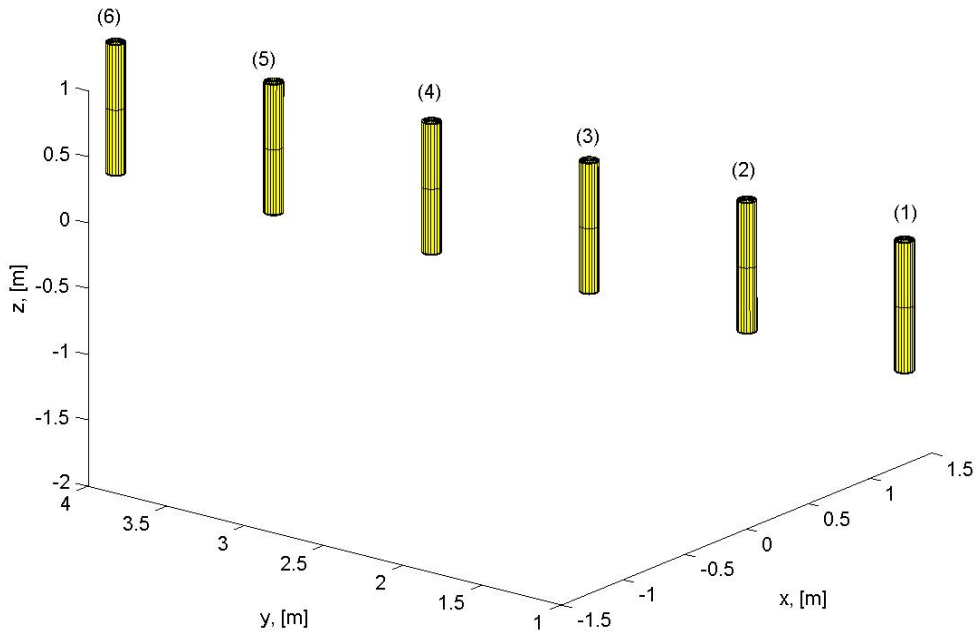

Fig. 7.6.a) Initial object configuration

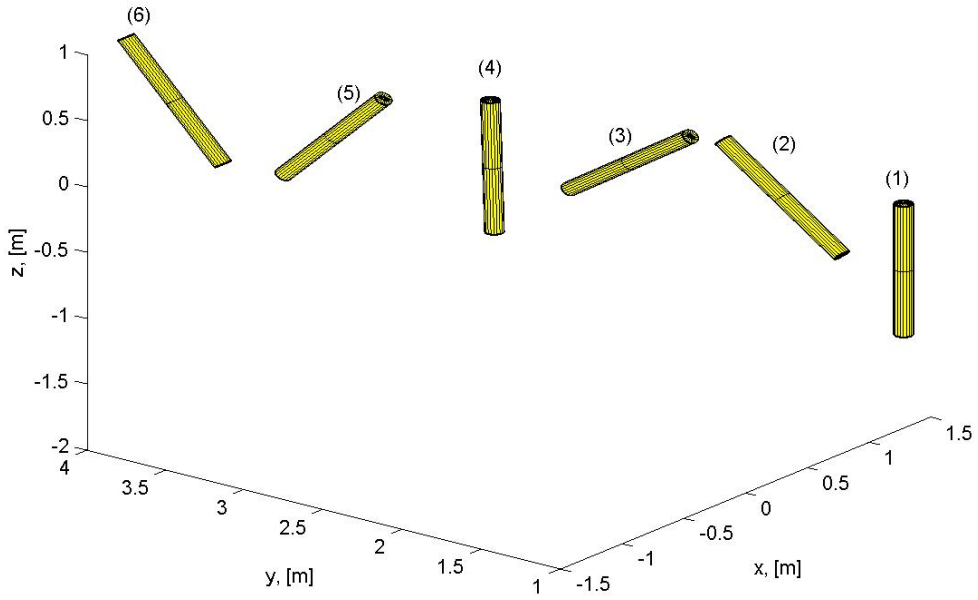

Fig. 7.6.b) Object configuration (t = 20 sec)

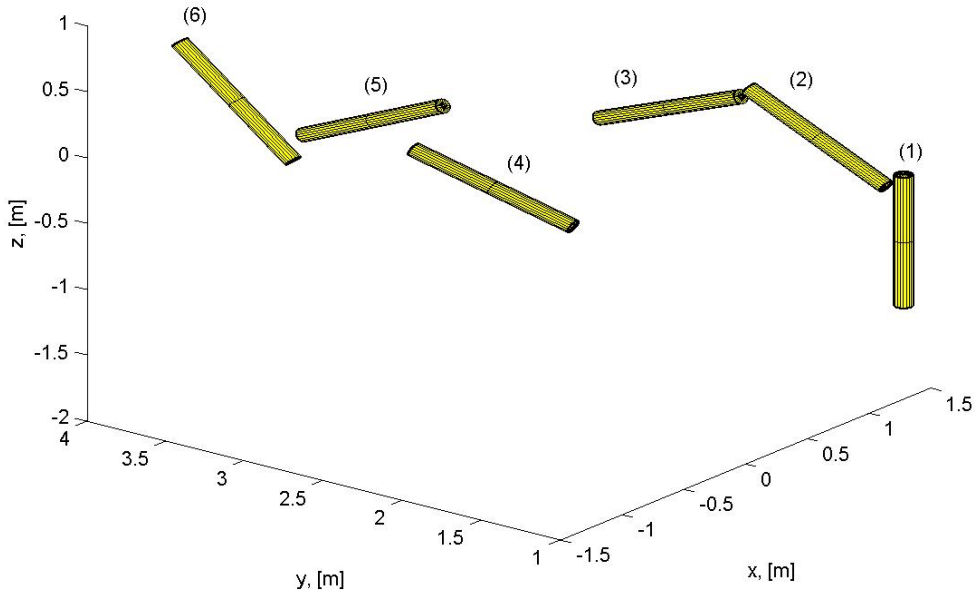

Fig. 7.6.c) Object configuration (t = 40 sec)

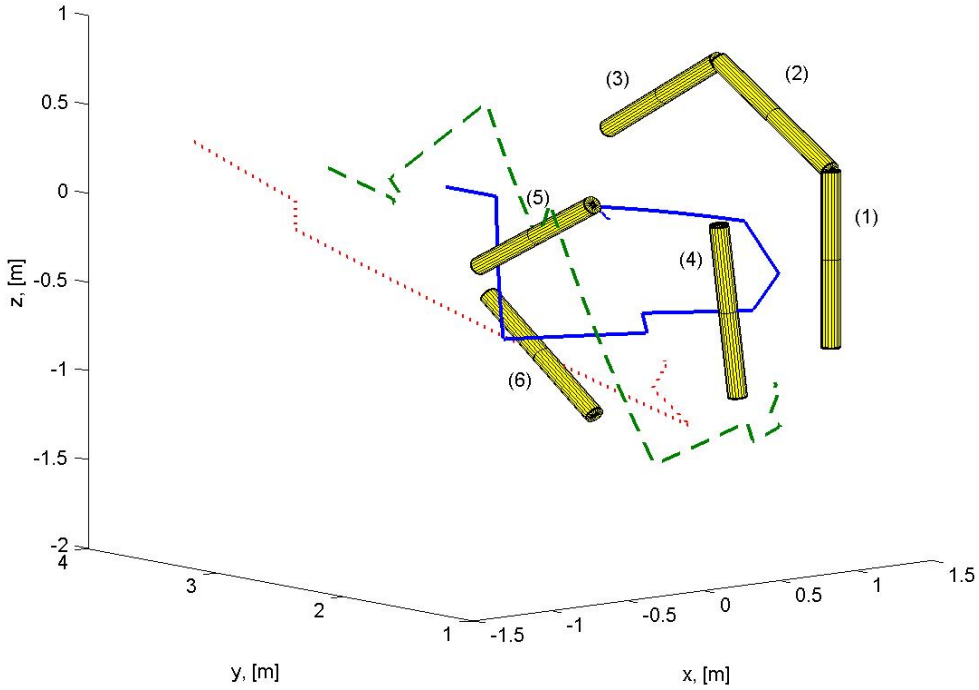

Fig. 7.6.d) Object configuration (t = 145 sec)

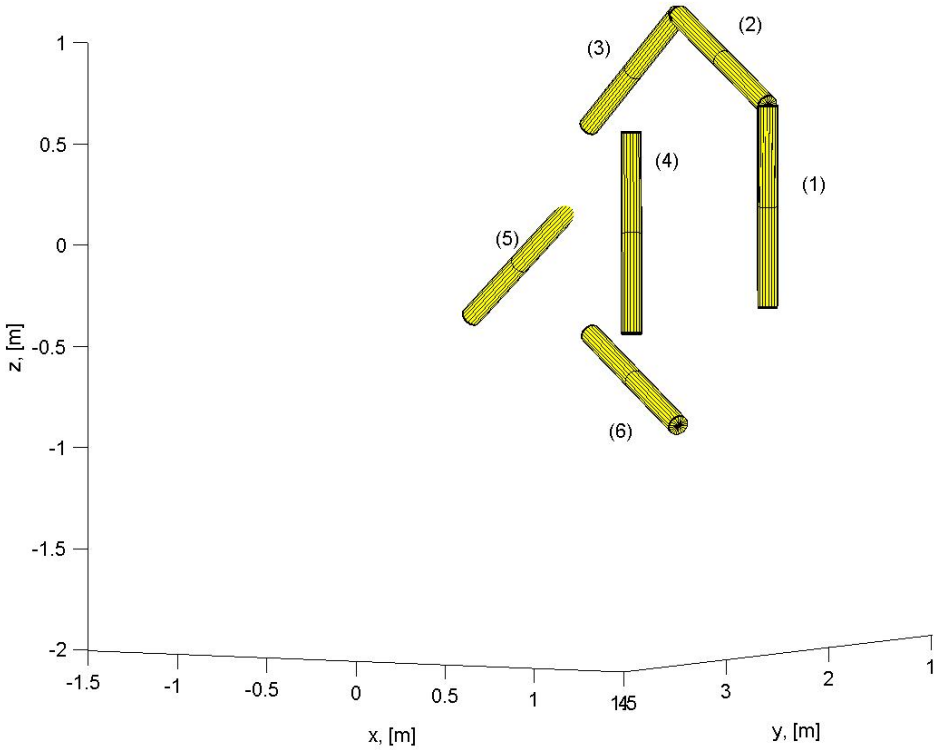

Fig. 7.6.e) Object configuration (t = 230 sec)

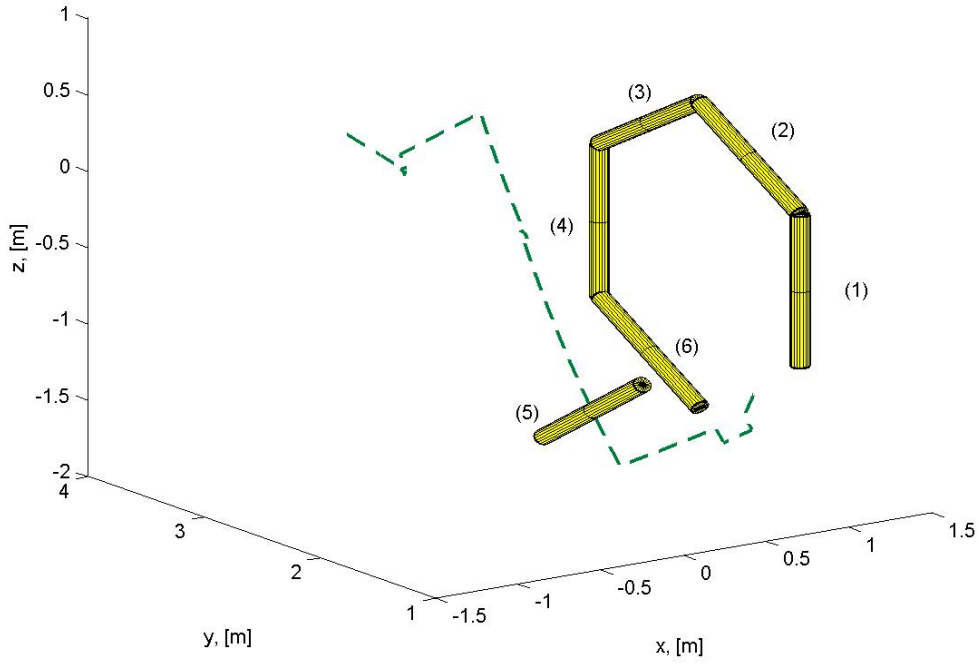

Fig. 7.6.f) Object configuration (t = 260 sec)

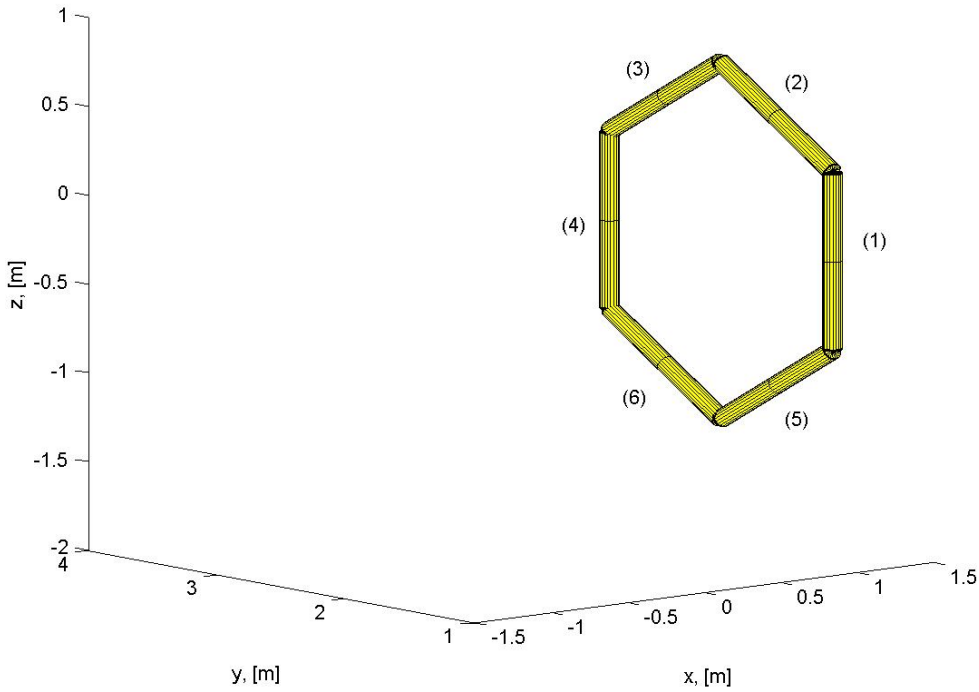

Fig. 7.6.g) Final configuration (t = 400 sec)

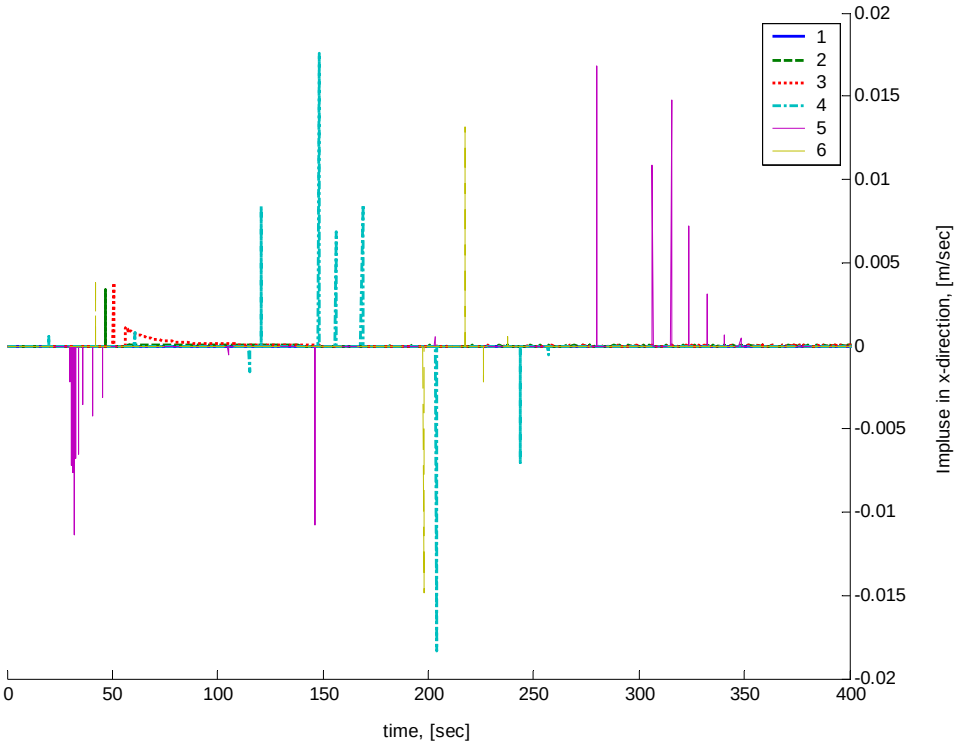

Fig. 7.7.a) Impulse in the *x*-direction

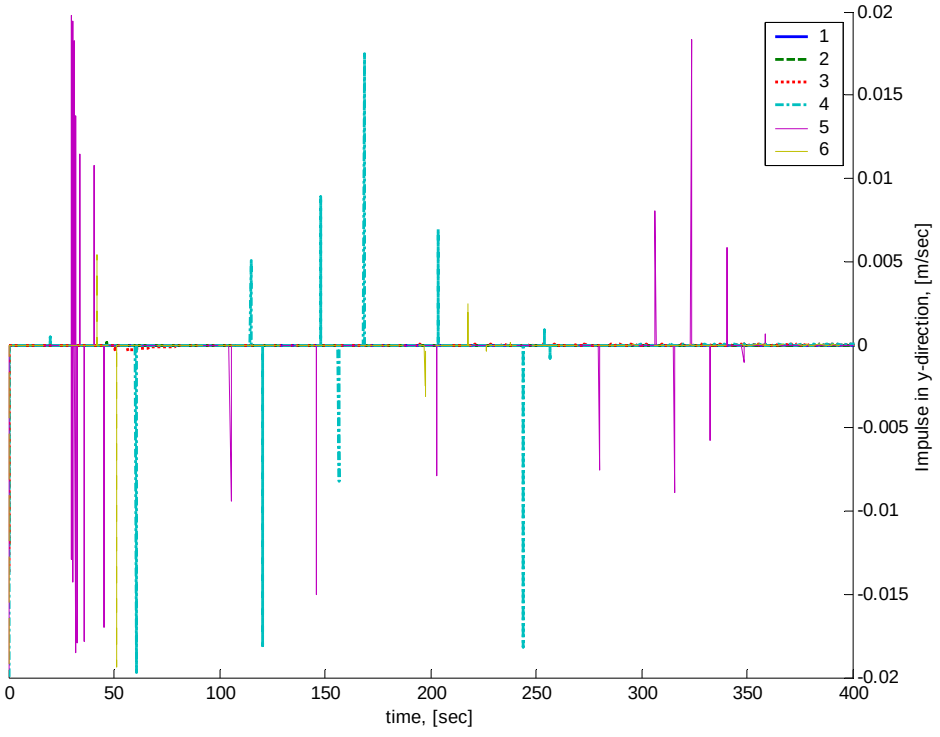

Fig. 7.7.b) Impulse in the *y*-direction

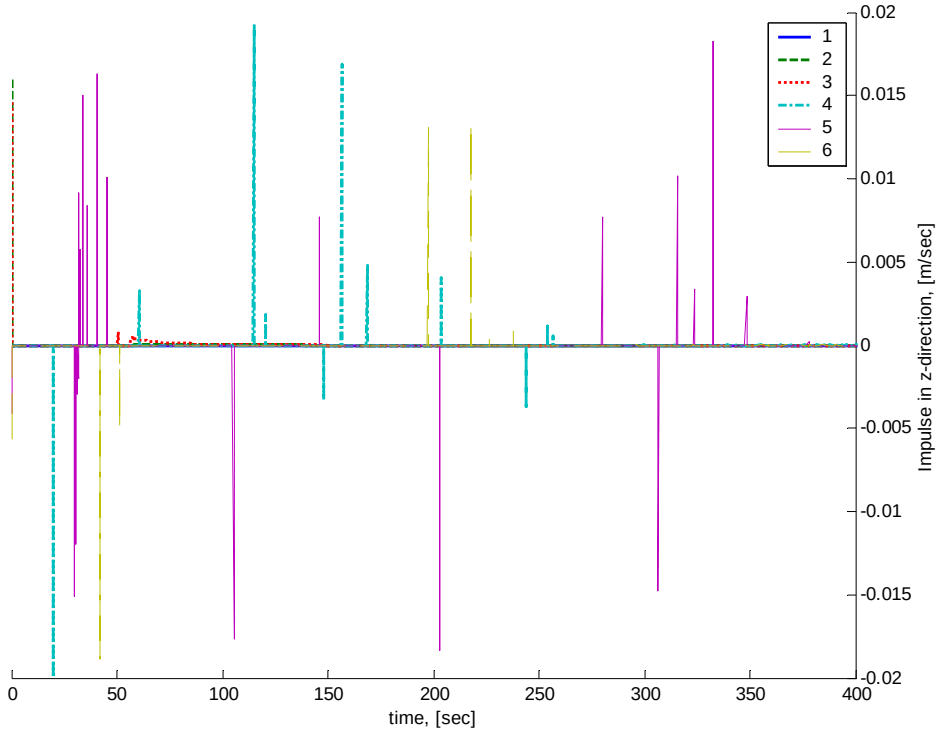

Fig. 7.7.c) Impulse in the *z*-direction

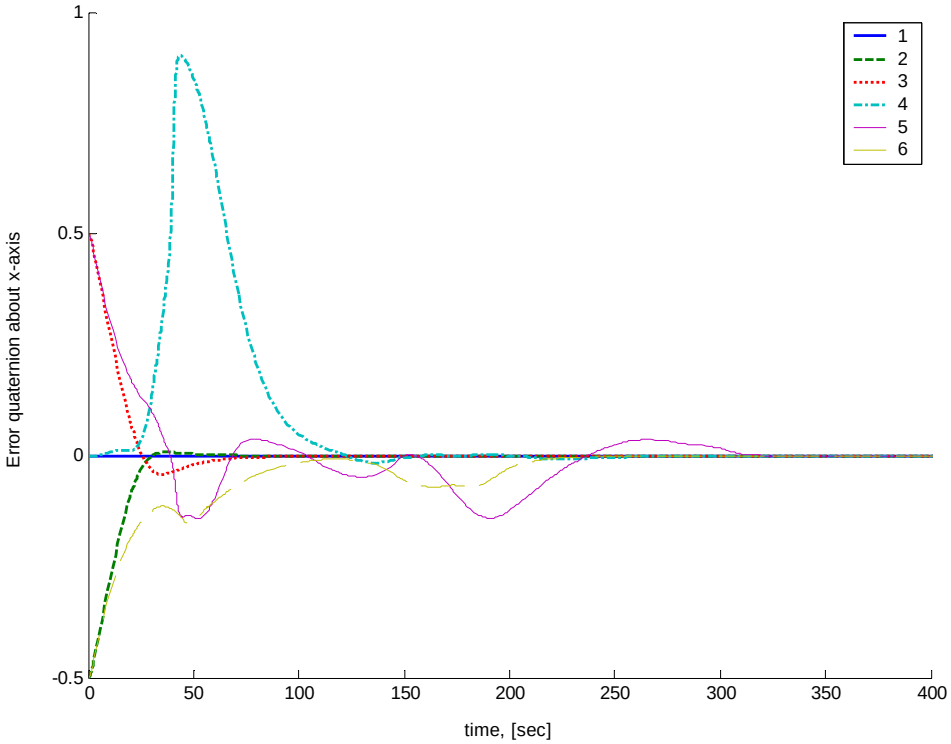

Fig. 7.8.a) Error quaternions about the *x*-axis

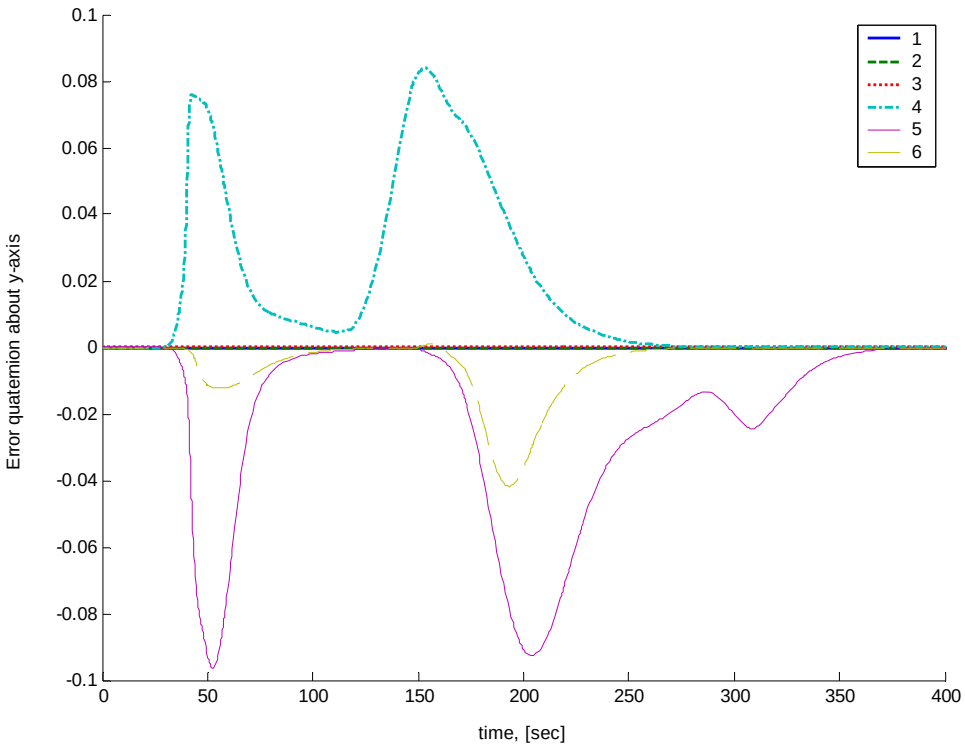

Fig. 7.8.b) Error quaternions about the *y*-axis

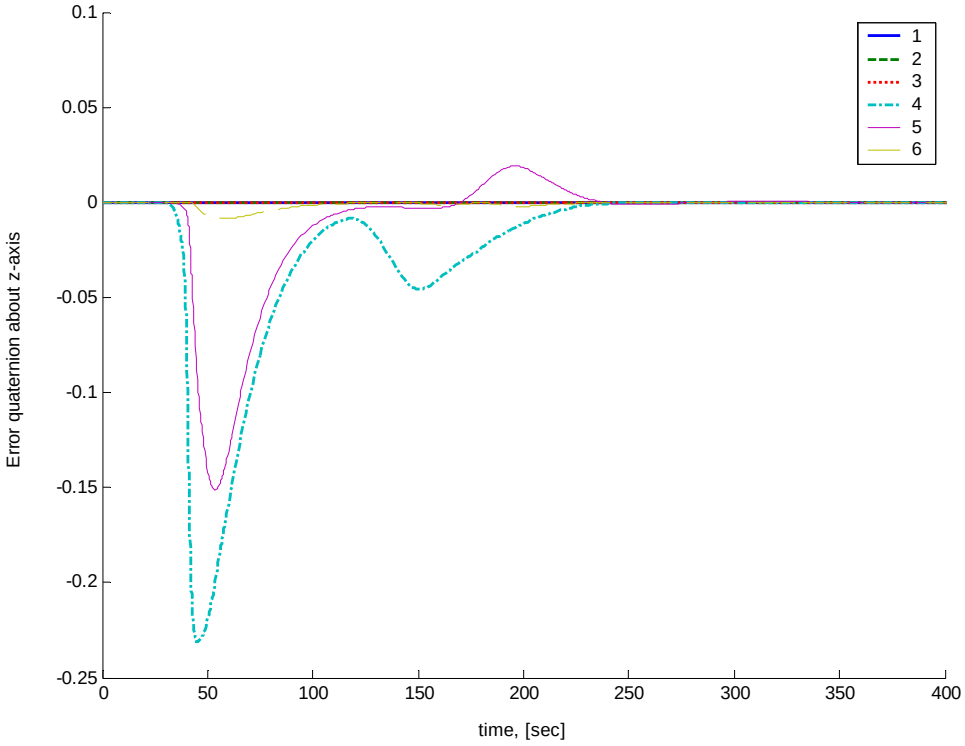

Fig. 7.8.c) Error quaternions about the *z*-axis

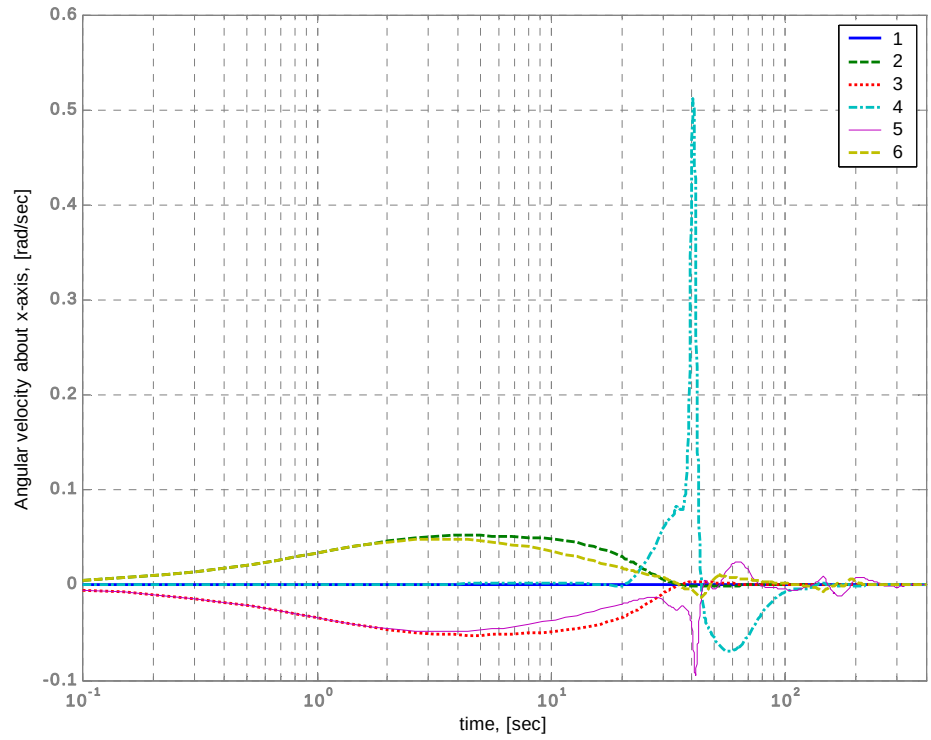

Fig. 7.8.d) Angular velocity about the *x*-axis

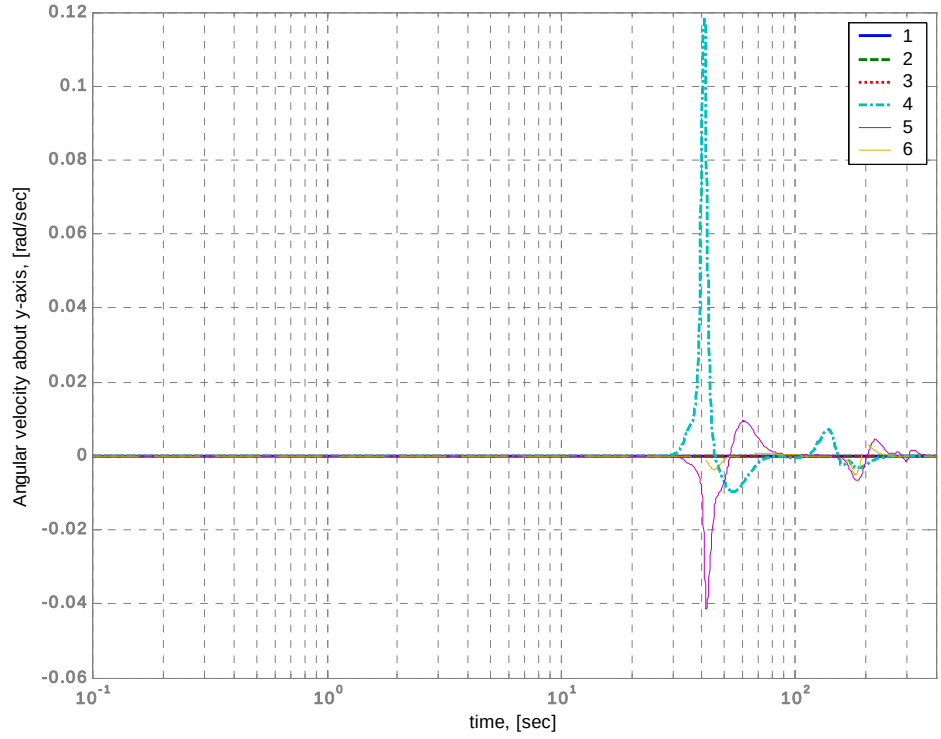

Fig. 7.8.e) Angular velocity about the *y*-axis

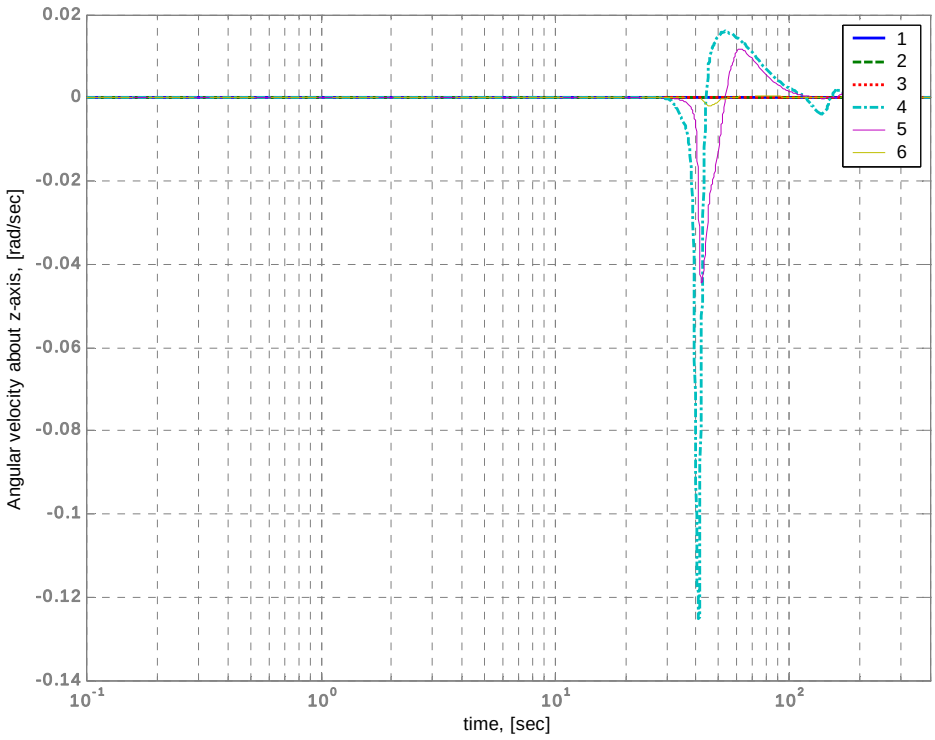

Fig. 7.8.f) Angular velocity about the *z*-axis

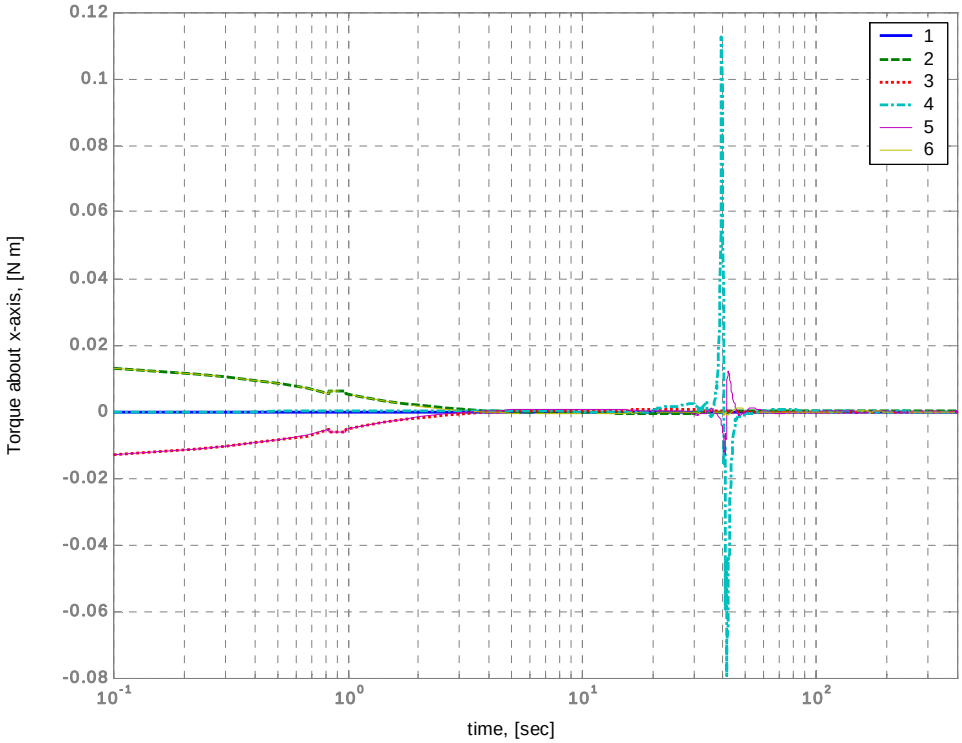

Fig. 7.9.a) Control torque about the *x*-axis

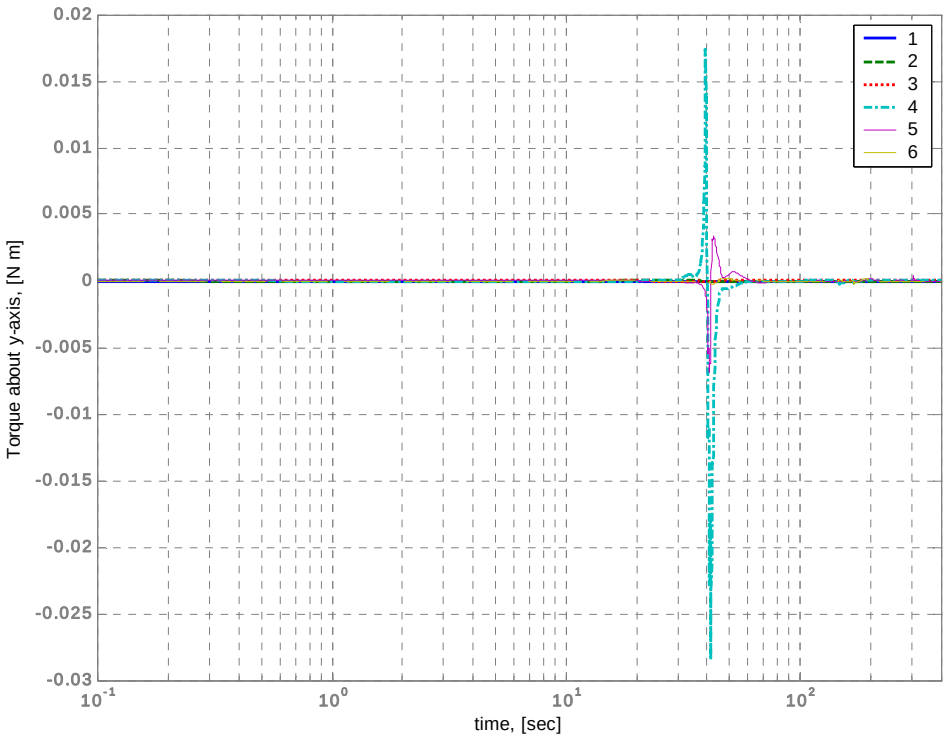

Fig. 7.9.b) Control torque about the *y*-axis

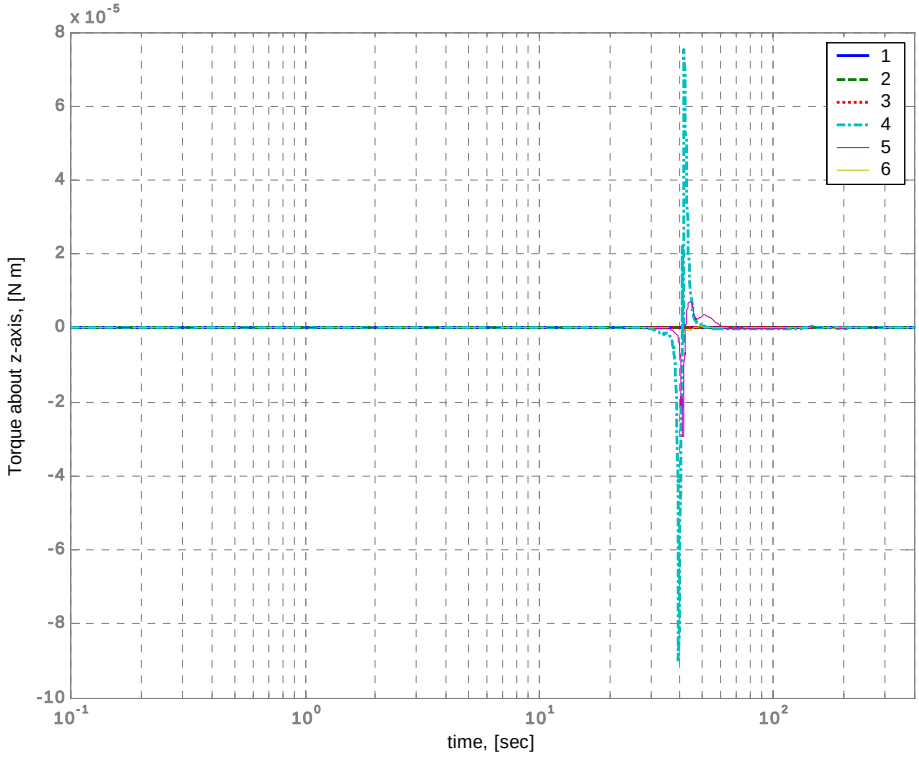

Fig. 7.9.c) Control torque about the *z*-axis

As the objects are disengaged, they are repelled away due to their mutual repulsive potentials, while later each object starts to move toward its new configuration. Using exactly the same parameters as in the first phase, the objects are able to reach their new goals and are assembled together in a line without collisions in 200 sec, Fig. 7.10. The middle objects such as (1) and (4) require larger impulses and consequently cost since they experience a more complicated potential field topology compared with those on the two ends as shown in Fig. 7.11 and in Table 7.2. Frequent rotational manoeuvres are also required either for object reorientations or for collision avoidance as shown in Fig. 7.12 as rotational parameters, error quaternions and angular velocities, and in Fig. 7.13 as the required continuous control torques.

element no.	Δv [m/sec]	element no.	Δv [m/sec]	element no.	Δv [m/sec]
1	0.26279	2	0.070863	3	0.060064
4	0.2029	5	0.062735	6	0.060405

Table 7.2 Second phase translation cost

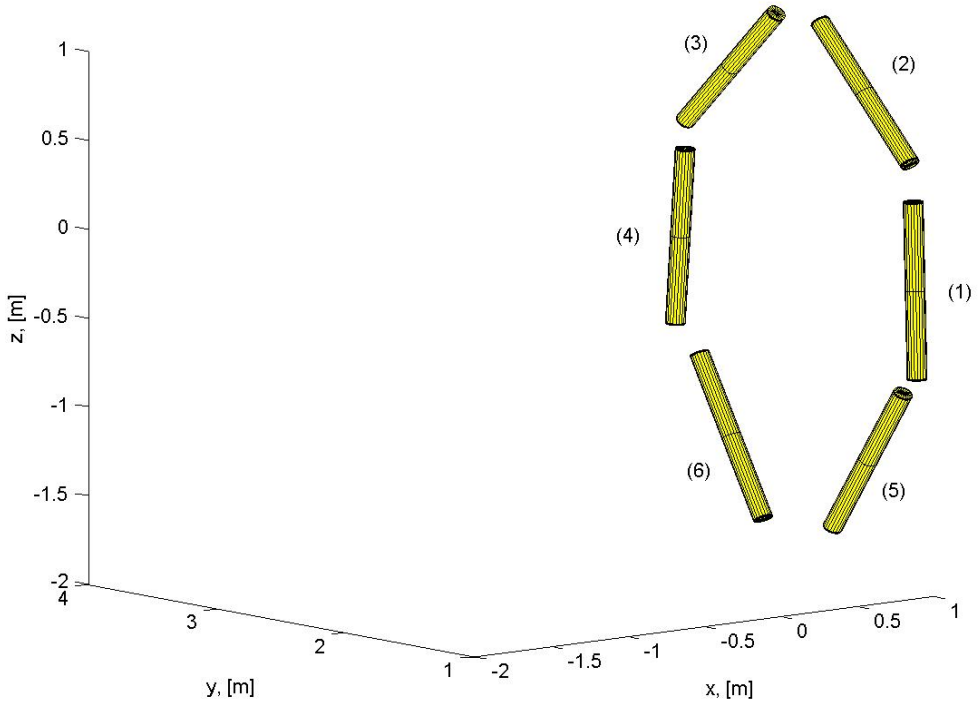

Fig. 7.10.a) Object configuration (t = 15 sec)

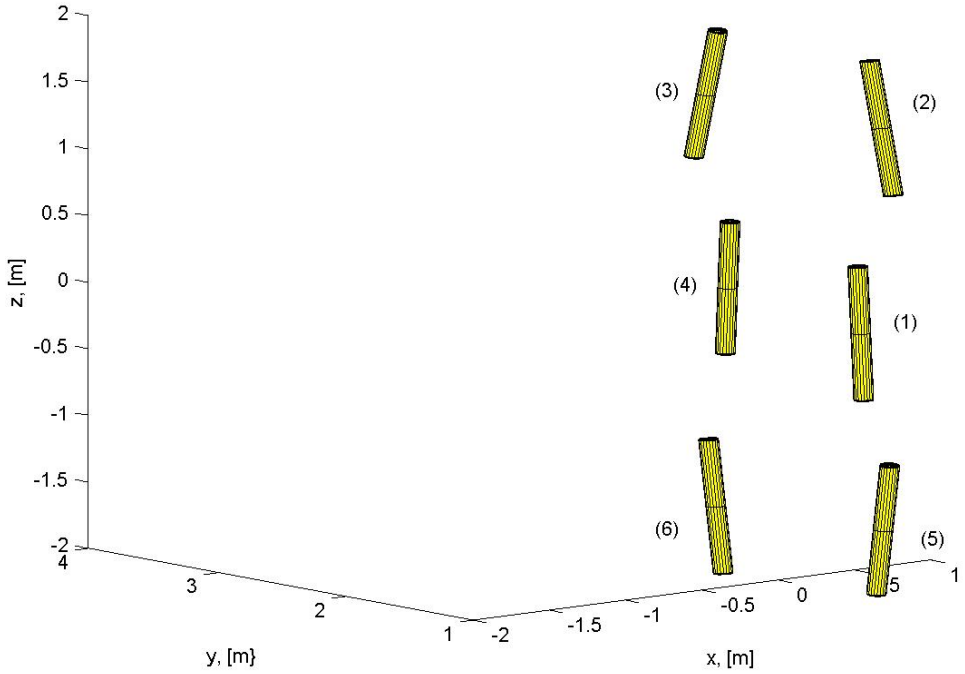

Fig. 7.10.b) Object configuration (t = 42 sec)

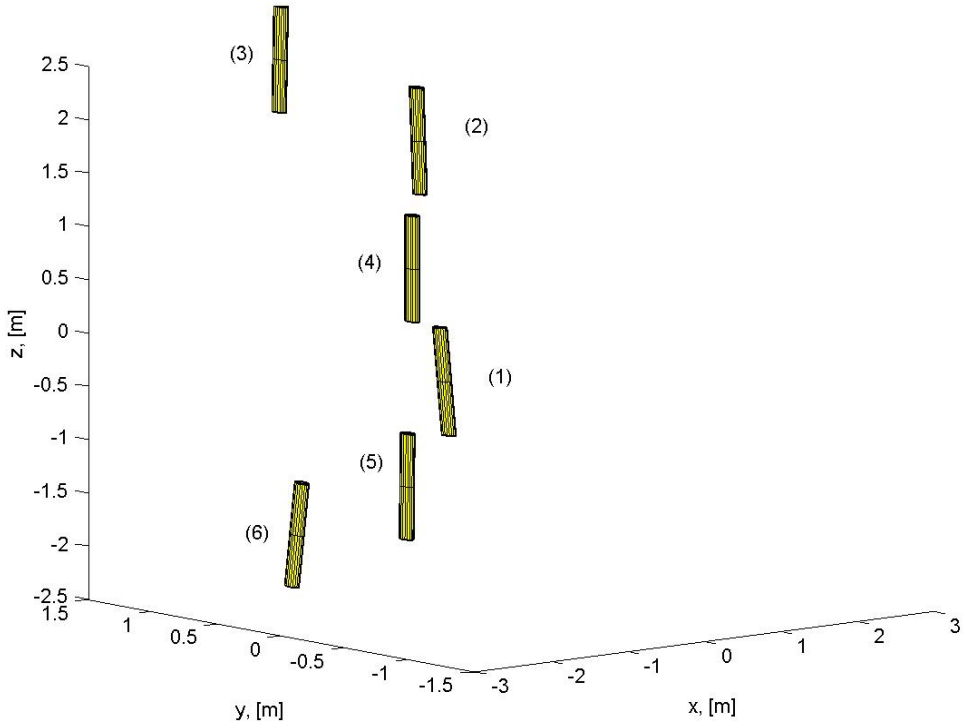

Fig. 7.10.c) Object configuration (t = 77 sec)

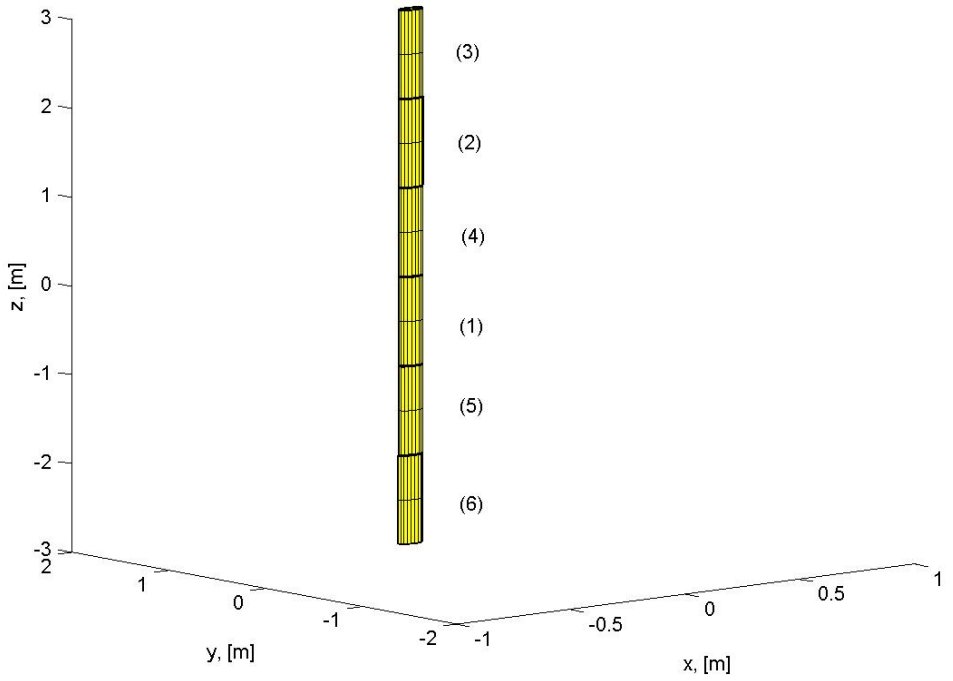

Fig. 7.10.d) Object configuration (t = 200 sec)

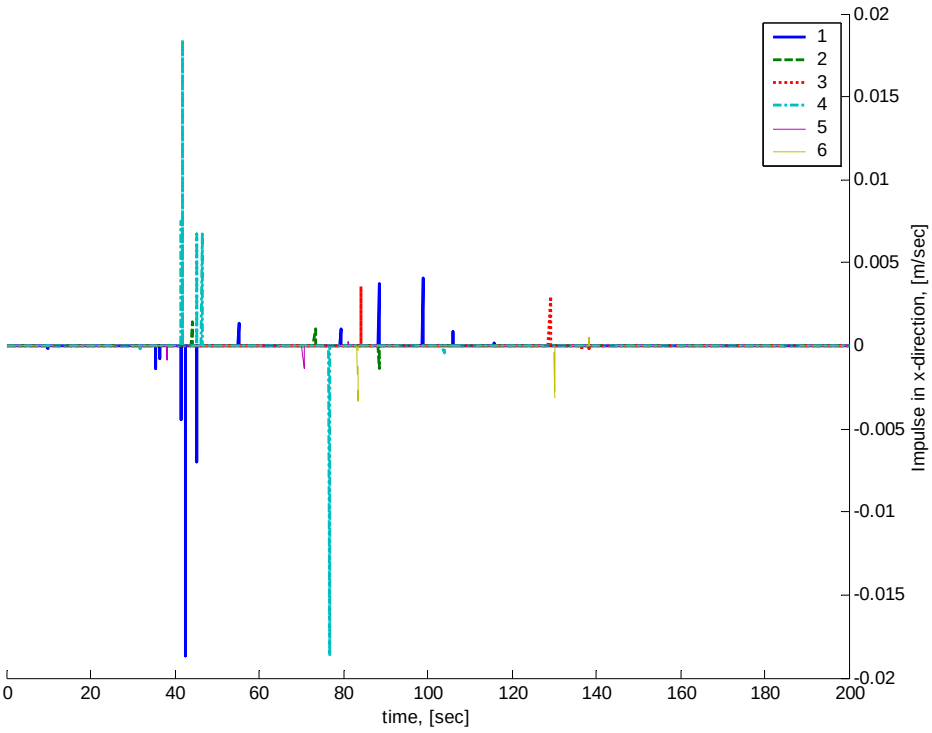

Fig. 7.11.a) Impulse in the *x*-direction

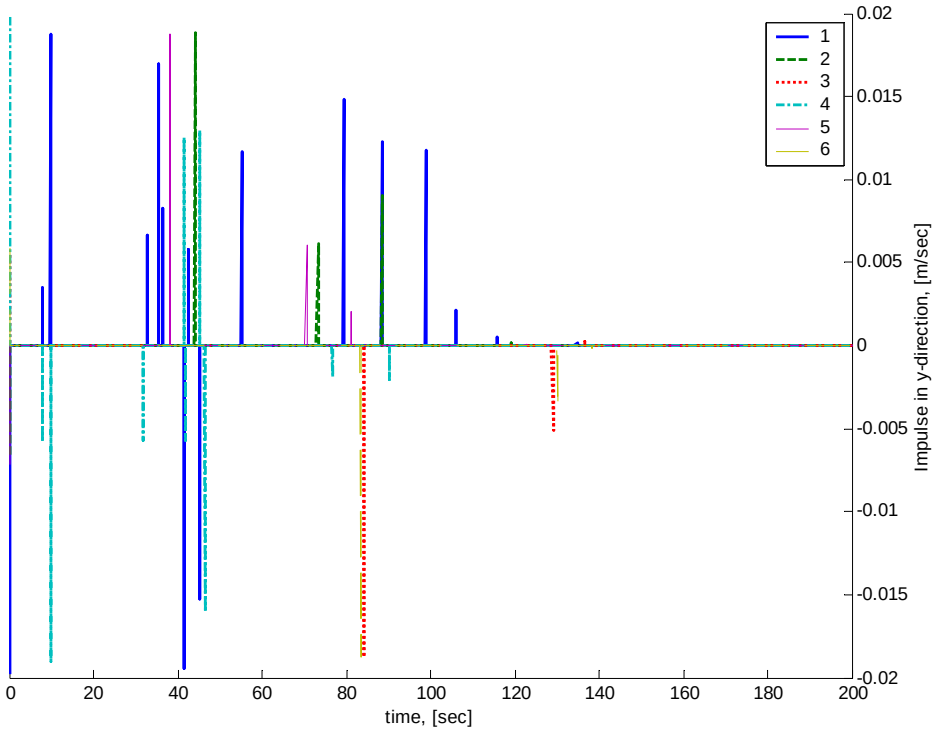

Fig. 7.11.b) Impulse in the *y*-direction

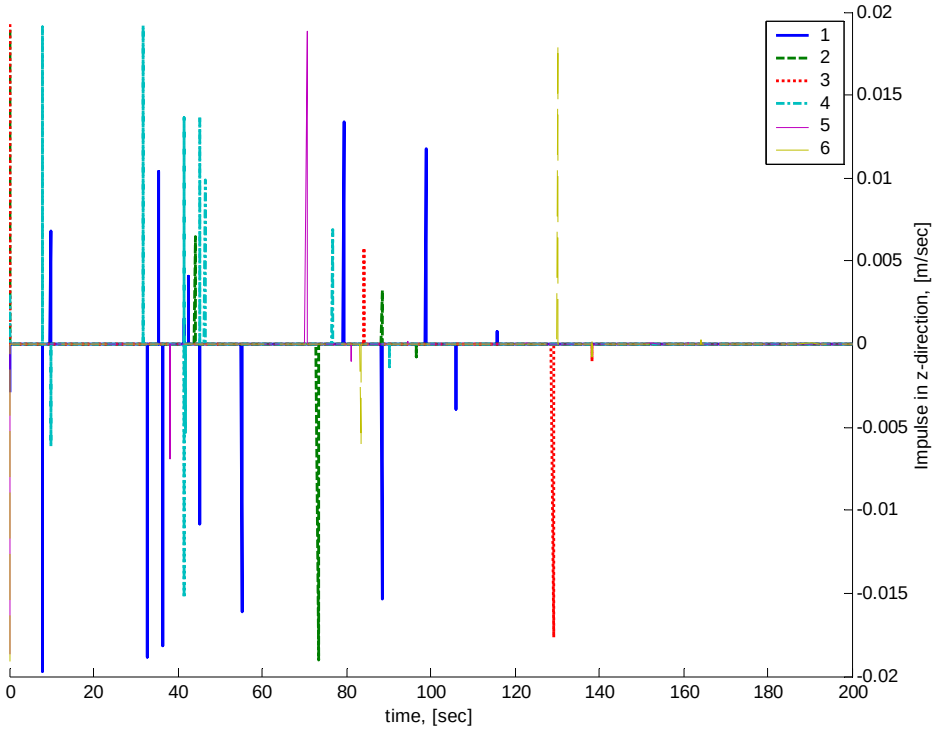

Fig. 7.11.c) Impulse in the *z*-direction

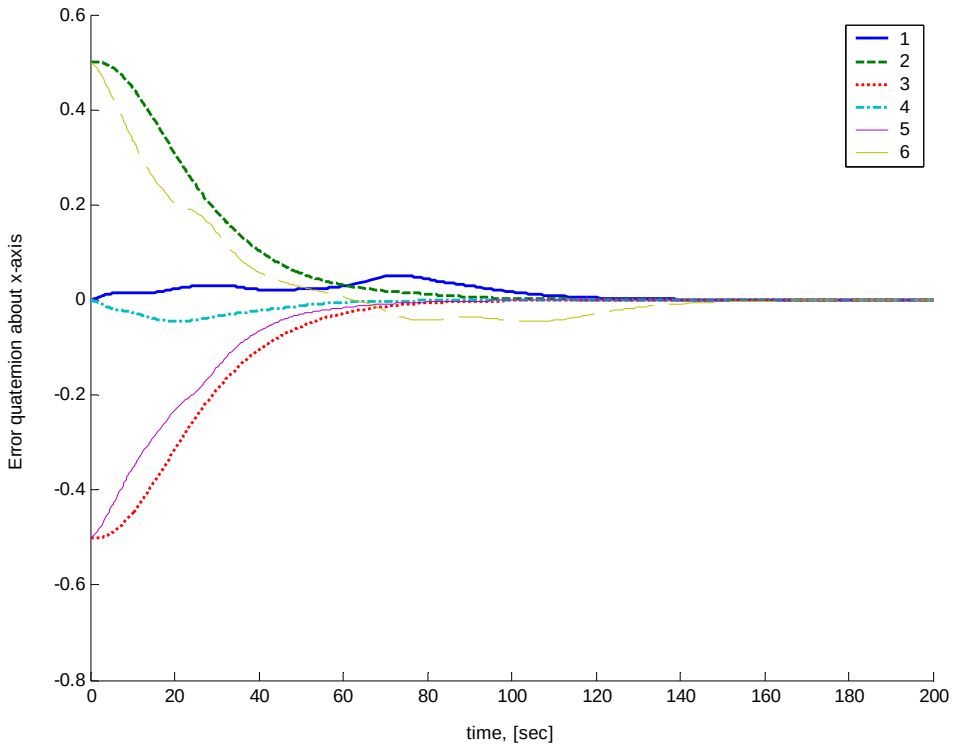

Fig. 7.12.a) Error quaternion about the *x*-axis

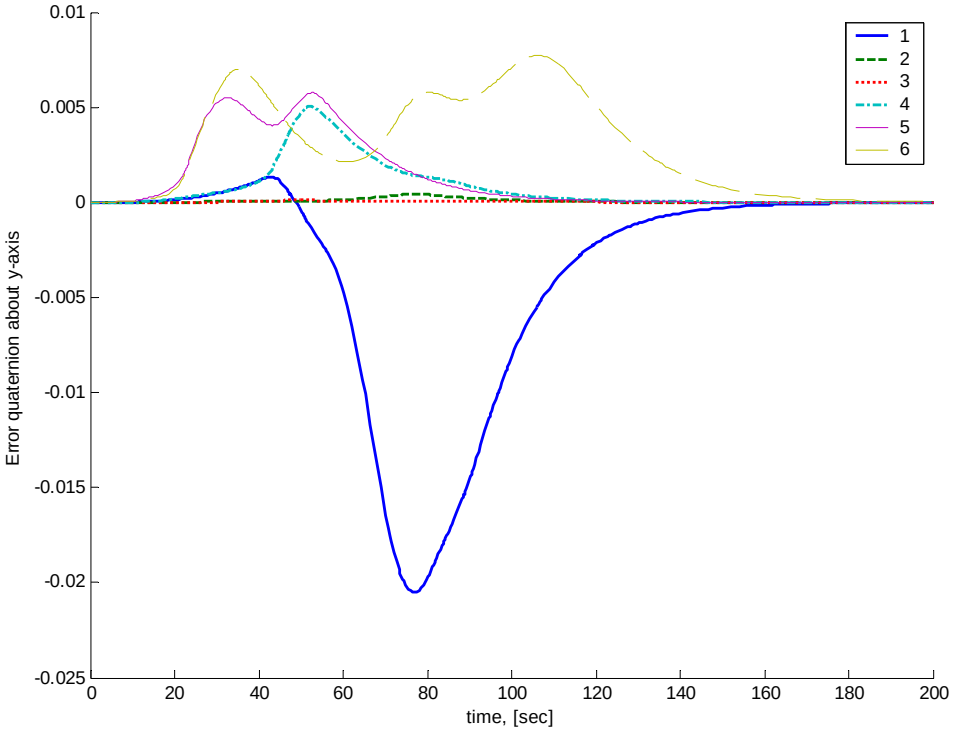

Fig. 7.12.b) Error quaternion about the *y*-axis

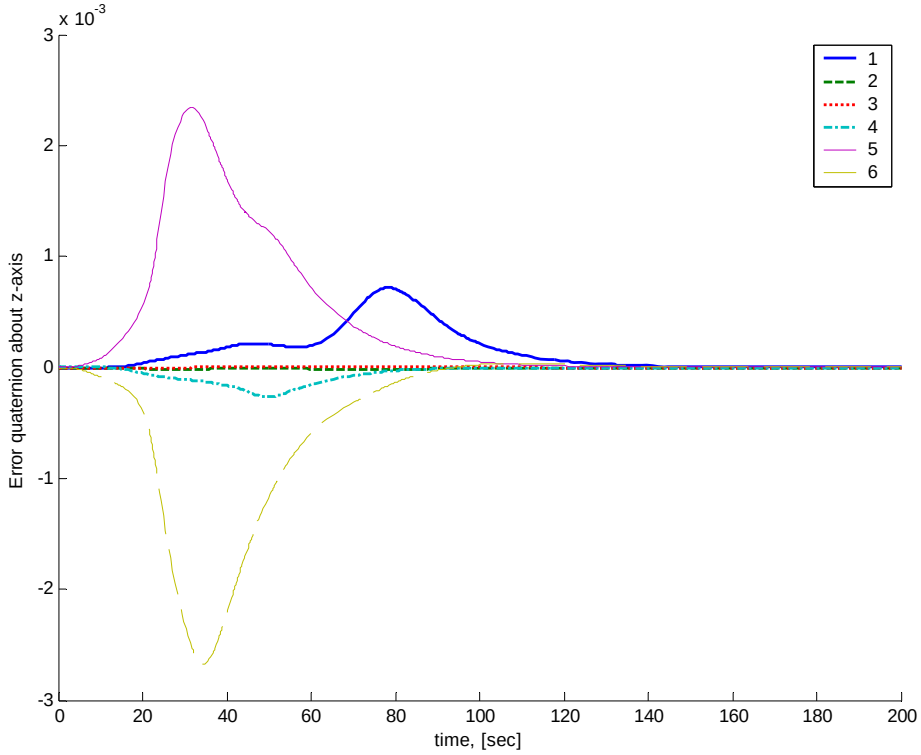

Fig. 7.12.c) Error quaternion about the *z*-axis

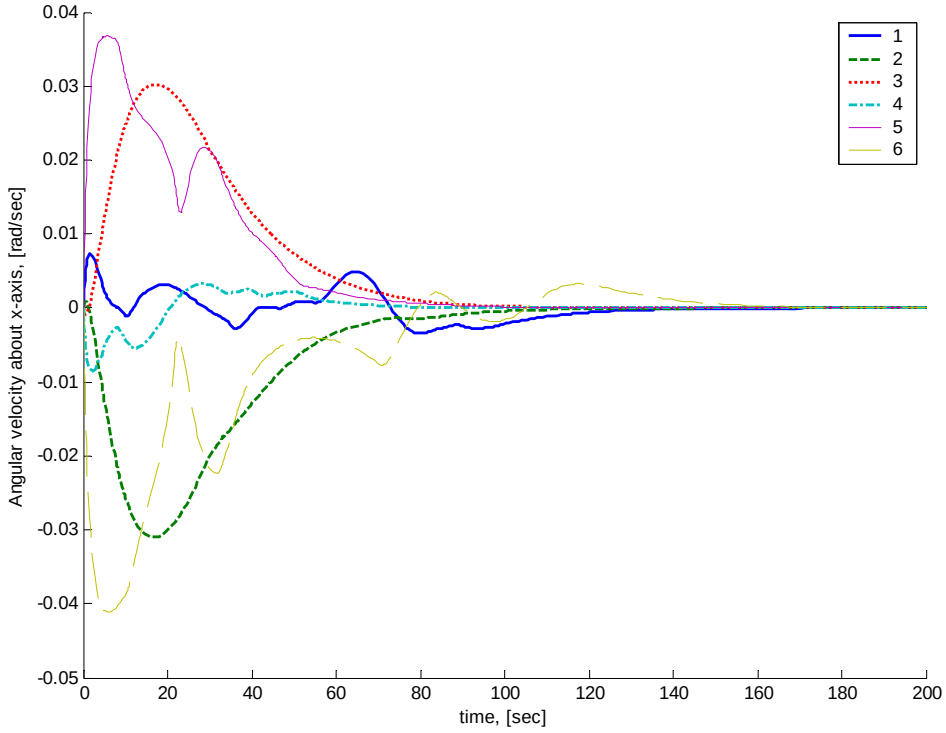

Fig. 7.12.d) Angular velocity about the *x*-axis

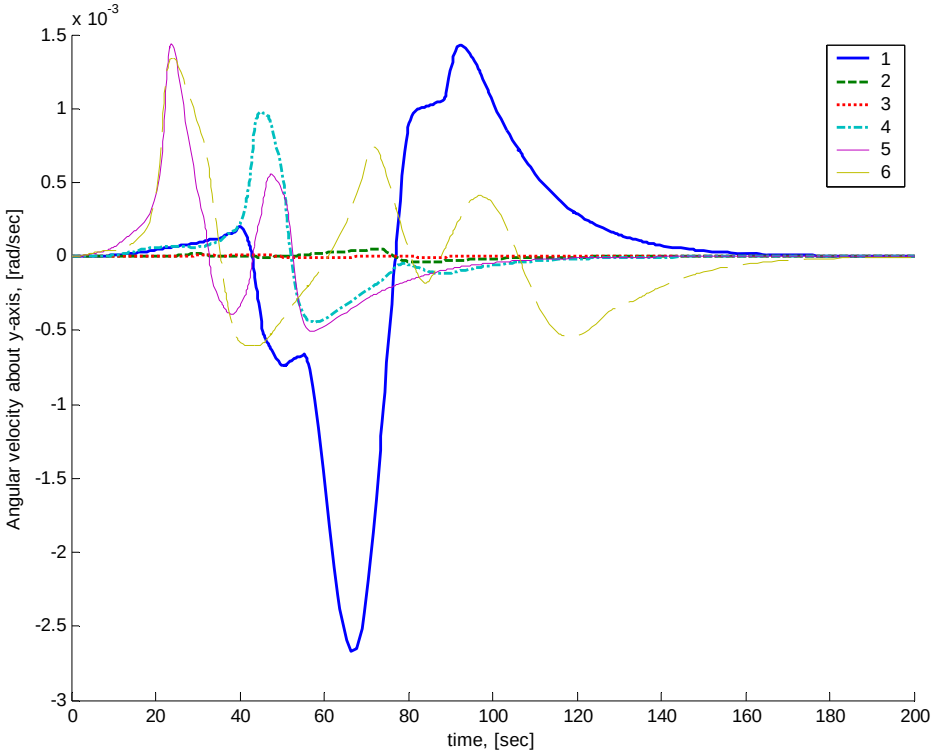

Fig. 7.12.e) Angular velocity about the *y*-axis

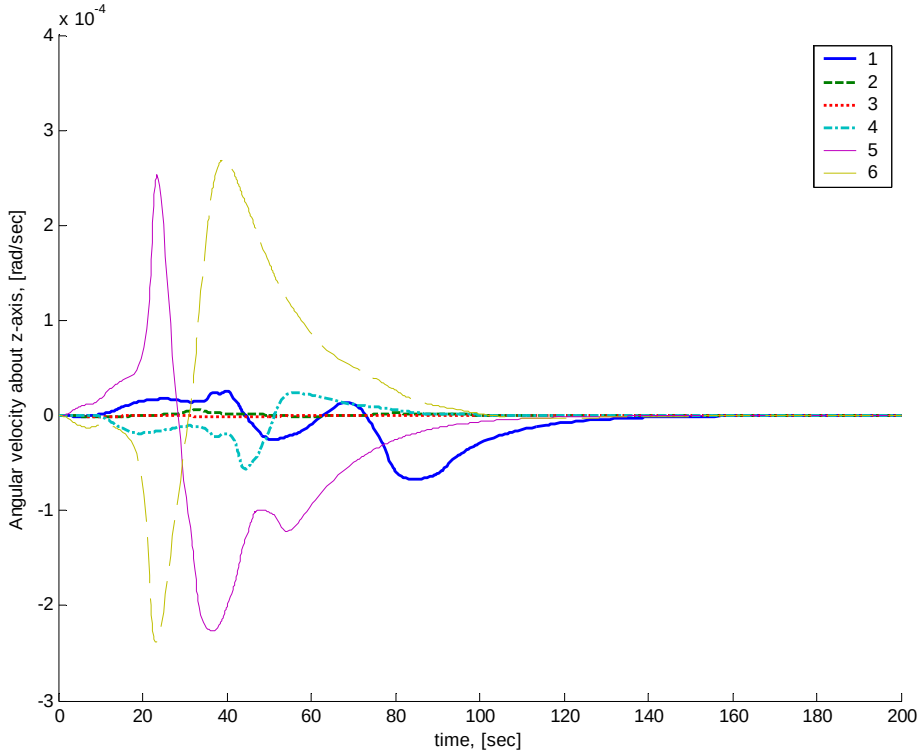

Fig. 7.12.f) Angular velocity about the *z*-axis

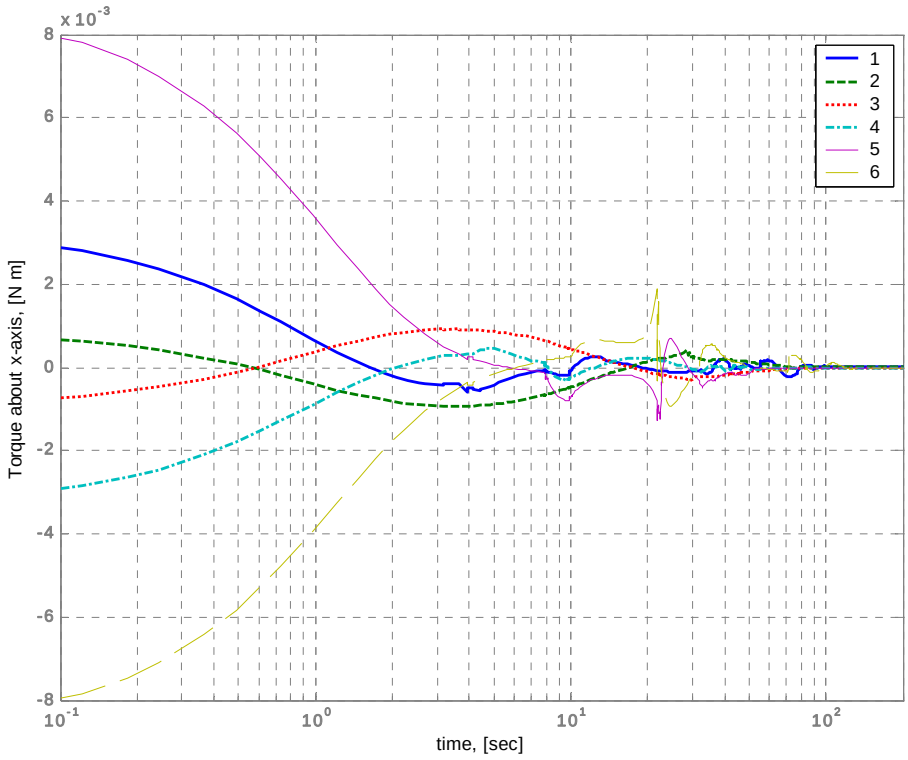

Fig. 7.13.a) Control torque about the *x*-axis

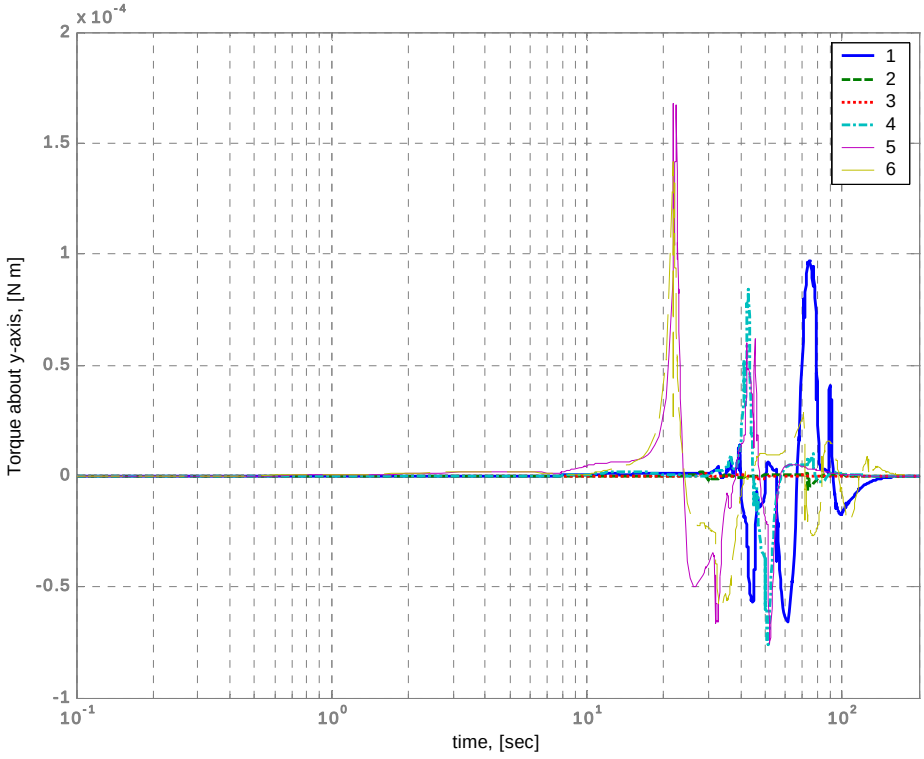

Fig. 7.13.b) Control torque about the *y*-axis

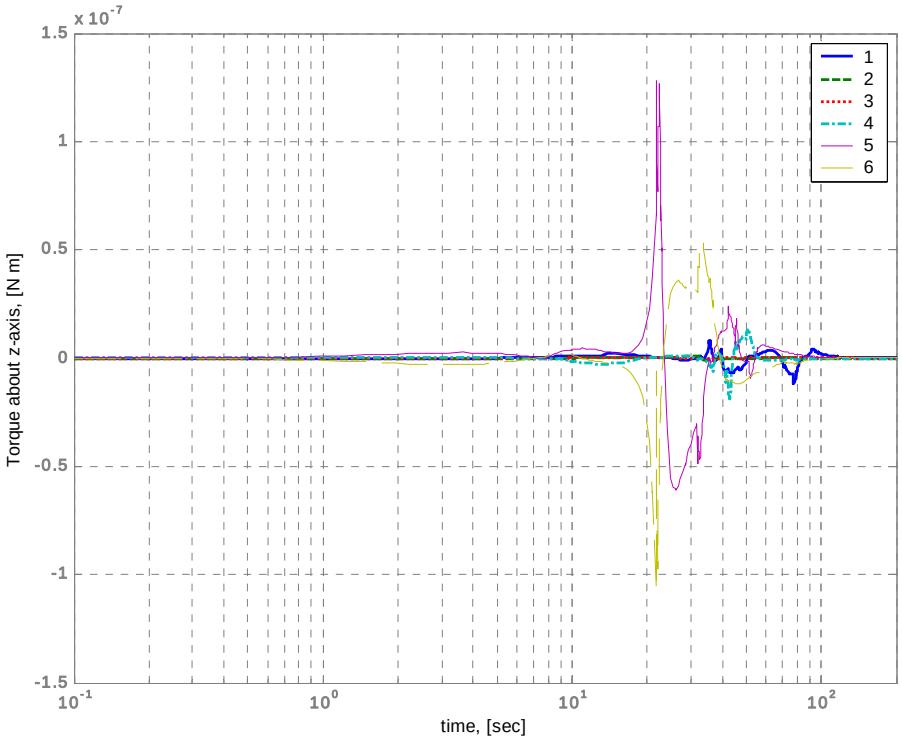

Fig. 7.13.c) Control torque about the *z*-axis

7.4 Conclusions

The potential field method proved its ability to perform successful motion planning for a free-flying robot used at the ISS. Merging impulsive motion and natural orbital motion of the free-flyer was carried out considering a pure impulse by limiting the maximum change in the object velocity. Coupling between translational and rotational motion facilitates free-flyer motion in the case of nearby obstacles through decreasing its global potential using both rotation and translation to avoid collision whilst maintaining a continuous approach to the goal.

Reconfiguration of a hexagonal structure through performing in/out of plane translation and rotation to avoid collision was performed. Complicated manoeuvres were required as a result of the close separation of the manoeuvring objects. As a result of these close manoeuvres, the constrained control impulse may not be enough to render the rate of change of the potential field to be negative, since other objects with a repulsive potential are nearby. Consequently, more impulses are required and a quasi-continuous control force is produced for some period of time during the manoeuvre.

8. CONCLUSIONS

8.1 Review

Many challenges are faced when conducting orbital manoeuvres which lead to successful on-orbit assembly of large structures. Different structural element shapes and sizes are in simultaneous translation and rotation to reach their goals whilst mutual collisions must be avoided, **chapter 1**. An attractive potentials is formed as two separate functions, the first for translation whereas the second for rotation. Consequently, no coupling exists between the two types of motion. The new attractive potential function proposed in this thesis merges translation and rotation in one function, consequently manoeuvring objects have some degree of freedom to enable them to choose which motion is more effective to decrease the overall potential field.

The translational part of the attractive potential function is defined in several forms to be used with different control strategies. These forms vary from the original parabolic function used in this thesis for the impulsive control strategy to a new combination of the parabolic and the conic functions used with the continuous control strategy, and a new usage of the hyperbolic function in the attractive potential.

The parabolic function is characterized by its provable stability defined through *Lyapunov*'s theorem. The required control impulses are therefore defined as the gradient of the parabolic function when the time derivative of the potential becomes non-negative. A better controller performance is achieved through anticipating the divergence of the motion by allowing the controller to be active when the time derivative of the potential becomes higher than some negative value rather than zero, as required for *Lyapunov*'s theorem. Parabolic functions are also applicable in the case of a continuous control strategy through defining the control force as a function of the attractive potential. This limits the attractive potential to being defined by position and orientation parameters only as defining it with velocity and angular velocity parameters leads to unbounded control forces.

A combination of parabolic and conical functions is used in the thesis in the case of the continuous control strategy. The new definition of the attractive potential

overcomes the drawbacks of the parabolic attractive potential when velocity and angular velocity parameters are introduced. A major advantage of this combination is to have a constant velocity over the workspace when no obstacles are nearby, hence no control force is needed. Stability is also guaranteed at the goal point where the parabolic function is used in some neighbourhood of the goal.

Another new definition of the attractive potential is discussed in this thesis through the hyperbolic function. It has the key advantages of both the parabolic and conic functions. The required control forces generated are similar to that of two impulse motion with an acceleration phase, coast phase, and braking phase.

The rotational part of the attractive potential is defined as a parabolic function based on the error quaternion parameters along with the object angular velocities. Continuous control torques are produced to ensure global convergence of the rotational motion. The use of error quaternions assists the required manoeuvre to reach the goal orientation since they can determine the shortest path to the goal, **chapter 2**.

Since several manoeuvring objects are in simultaneous motion to assemble the structure, repulsive potentials are introduced to prevent collisions between objects. The repulsive potential surrounds each object with a high potential zone to deflect any colliding object. A second role of the repulsive potential is to allow smooth contact with other objects to assemble the final structure.

Several repulsive potentials are used with potential field method; however superquadric functions have many advantages for structural assembly. The superquadric model is constructed with respect to the body frame of reference, and hence using quaternions it is possible to transform the superquadric shape to a global frame of reference. Since real structural element shapes and sizes are different, superquadrics are good choice due to their ability to represent several solid geometries in parametric form. A second advantage of the superquadric function is their close corresponding to the obstacle shape, consequently more free space is available for manoeuvring object motion.

The accuracy of the repulsive potential field calculation depends on the correct estimation of the separation distance between the superquadric shapes. More accurate methods are discussed through modifying the original pseudo-distance

method by adding the centre-to-centre distance to the calculation which enhances the distance estimation. A second new method is defined to calculate the centre-to-edge distance for motion planning problem using the radial Euclidian distance taking into consideration obstacle orientation through quaternion parameters. A third new method is defined by considering both obstacle and manoeuvring object sizes and shapes. This method calculates the edge-to-edge separation distance between two superquadric surfaces, and leads to the exact separation distance for some configurations. Superquadric repulsive potentials can be modified to be more representative of the workspace. Steep gradients in the potential provide more free space for the manoeuvring objects to move and allow motion in narrow passages, **chapter 3**.

The repulsive potential amplitude is also adjusted to avoid the 'goal non-reachable obstacle nearby problem' in which the goal point shifts due to the obstacle potential field. A suitable Gaussian function is used to diminish the repulsive potential amplitude as the manoeuvring object approaches its goal configuration, **chapter 4**.

The overall potential function is a superposition of the attractive and the repulsive potentials. The control laws generated, translation and rotation, are proven to guarantee global stability and convergence of the overall system. The mutual dependency of translation, rotation, and repulsive motion enhances the controller performance. The manoeuvring objects have the ability of mixing translation and rotation to avoid collisions whilst approaching their goal configuration, **chapter 5**.

Orbital mechanics effects manoeuvring object motion either by bringing it toward the goal point, or drifting away depending on the initial configuration. In the impulsive control strategy, the manoeuvring object velocity is determined from the linearised *Clohessy-Wiltshire* equations when the thrusters are off. In the continuous control strategy, the manoeuvring object acceleration is a linear superposition of the thruster acceleration and the natural orbital acceleration.

The criterion selected for controlling the switching on\off of the thrusters depends on the rate of change of the overall potential function. To guarantee stability, the controller should be switched on once the rate of change of the overall potential becomes non-negative. However, anticipation of this divergence gives better results as the total control cost and assembly time can be decreased. Early controller

intervention is required, especially, in a dense workspace. However early controller intervention results in increasing the total manoeuvre cost as it reduces the use of the natural orbital motion in bring manoeuvring objects to their goals. Increasing the maximum impulse decreases the assembly time and effects the total translation cost. The maximum impulse should then be chosen to optimize the trade-off between assembly duration and total manoeuvre cost, **chapter 6**.

Orbital reconfiguration is another successful challenge solved by the potential field method using superquadric repulsive potentials. A free-flyer was able to perform successful manoeuvres near a large space facility such as the ISS. Representing the ISS structure with a superquadric model gives the free-flyer space to move very close to the ISS surface while avoiding collision with it.

Structural elements (or small spacecrafts) were able to reconfigure to overcome failure or accomplish a new mission phases. Disengaging, reconfiguration, and reassembly are conducted without drifting from the initial positions by virtue of defining one potential function which represents all phases, **chapter 7**.

Finally, the proposed potential field method proves its ability to handle a range of orbital motion planning problems used in structural assembly, reconfiguration, and satellite constellations.

8.2 Future Work

- **Generalising superquadric model for complex shapes**

Real objects are not composed of one part, so it is required to study how superquadric functions could be used to model these parts together rather than decomposing to multiple primitive objects. It is required to define a set of superquadric functions that starts with the solid object model, and then converts smoothly to a spherical symmetric object.

- **Time dependent superquadric potential parameters**

Develop superquadric potentials with time dependent parameters resulting in configurable shapes of the repulsive potential that depends on the workspace

configuration to guarantee local minimum free fields and generate smooth trajectories.

- **Terrestrial and marine applications**

Since the hyperbolic model defines the required dynamic control parameters, velocity and acceleration, it is possible to be generalised for terrestrial and marine applications by defining sliding friction and drag forces. The mutual dependency of the dissipative forces and the object control accelerations should be defined through the control laws.

- **Object elasticity**

Large object deflections effect connection joint coordinates, consequently controllers should compensate these deflections to ensure perfect docking process especially in LEO.

REFERENCES

Antonelli, G., Chiaverini, S., Finotello, R., & Schiavon, R. (2001). Real-time path planning and obstacle avoidance for RAIS: an autonomous underwater vehicle. IEEE Journal of Oceanic Engineering, 26 (2), 216-227.

Avanzini, G., De Matteis, G., & Tarantini, V. (2005a). Control of an orbiting formation of satellites using the virtual structure approach. AAS/AIAA Astrodynamics Specialists Conference, Roma, Italy, Paper AAS 05-276.

Avanzini, G., De Matteis, G., & Tarantini, V. (2005b). Structural analogy for control of satellite formations. AAS/AIAA Astrodynamics Specialists Conference, Roma, Italy, Paper AAS 05-275.

Badawy, A., & McInnes, C.R. (2006a, August). Separation distance for robot motion control using superquadric obstacle potentials. International Control Conference, Glasgow, Scotland, paper no. 25.

Badawy, A., & McInnes, C.R. (2006b, October). Autonomous structure assembly using potential field functions. 57th International Astronautical Congress, Valencia, Spain, IAC-06-C1.P.3.04.

Badawy, A., & McInnes, C.R. (2006c, submitted Nov). On-orbit assembly using potential fields. Accepted for publication in The Journal of Guidance, Control, and Dynamics.

Badawy, A., & McInnes, C.R. (2007a, May). Free flyer manoeuvring round a space station. The Twelfth International Conference on Aerospace Science and Aviation Technology, ASAT-12, Cairo, Egypt, paper no. 36.

Badawy, A., & McInnes, C.R. (2007b, July). Robot motion planning using hyperboloid potential functions. World Congress on Engineering, London, paper ICME 15.

Badawy, A., & McInnes, C.R. (2007c, September). Generalized potential function approach for on-orbit assembly. 58th International Astronautical Congress, Hyderabad, India, IAC-07-C1.2.07.

Bajcsy, R., & Solina, F. (1987). Three dimensional object representation revisited. In the proceedings of The First International Computer Vision Conference, London, 231-241.

Bardinet, E., Cohen, L.D., & Ayache, N. (1995). A parametric deformable model to fit unstructured 3D data. Institute National de Recherche en Informatique et en Automatique, paper no 2617.

Barfoot, T.D., & Clark, C.M. (2004). Motion planning for formations of mobile robots. Robotics and Autonomous Systems, 46, 65-78.

Barr, A. (1981). Superquadrics and angle-preserving transformations. IEEE Computer Graphics and Applications, 1, 11-23.

Barr, A. (1984). Global and local deformations of solid primitives. Computer Graphics, 18 (3), 21-30.

Barraquand, J., Langlois, B., & Latombe, J-C. (1991). Numerical potential field technique for robot path planning. IEEE 5th International Conference on Advanced Robotics, 2, 1012-1017.

Branicky, M., & Newman, W. (1990, May). Rapid computation of configuration obstacles. Proceedings of the IEEE International Conference on Robotics and Automation, Cincinnati, 304-310.

Brock, O. (1999). Generating Robot Motion: The integration of planning and execution. PhD Dissertation, Stanford University.

Brooks, R.A., & Lozano-Pérez, T. (1982). A subdivision algorithm in configuration space for find path with rotation. Massachusetts Institute of Technology, A.I Memo no. 684.

Casasco, M., & Radice, G. (2003, August 3-7). Autonomous slew manoeuvring and attitude control using the potential function method. AAS/AIAA Astrodynamics Conference, Big Sky, AAS 03-612.

Cepolina, F., & Michelini, R.C. (2004). Robots in medicine: A survey of in-body nursing aids introductory overview and concept design hints. In Proc. of the 35th International Symposium on Robotics, Paris, France.

Chevalier, L., Jaillet, F., & Baskurt, A. (2003). Segmentation and superquadric modeling of 3D objects. Journal of WSCG, 11 (1), Plzen, Czech Republic.

Chiou, R., Kaufman, A.E., Liang, Z., Hong, L., & Achniotou, M. (1999). An interactive fly-path planning using potential fields and cell decomposition for virtual endoscopy. IEEE Transactions on Nuclear Science, 46 (4), 1045-1049.

Chuang, J. (1998). Potential based modelling of three dimensional workspace for obstacle avoidance. IEEE Transaction on Robotics and Automation, 14 (5), 778-785.

Chuang, J., & Ahuja, N. (1998). An analytically tractable potential field model of free space and its application in obstacle avoidance. IEEE Transaction on Systems, Man, and Cybernetics-part B: Cybernetics, 28 (5), 729-736.

Cohen, C., Diu, B., & Laloë, F. (1977). Quantum mechanics, volume 2. John Wiley and Sons, New York, 957-958.

Connolly, C.I., Burns, J.B., & Weiss, R. (1990). Path planning using *Laplace*'s equation., In Proc. IEEE International Conf. Robotics Automation, Cincinnati, OH.

Csáki, F. (1972). Modern control theories: nonlinear optimal and adaptive system. Akadémiai Kiadó Budapest, Chapter 5.

Fehse, W. (2005). Automated rendezvous and docking of spacecraft. Automatica, 41, 1295-1297.

Dattasharma, A., & Keerthi, S. (1995). An augmented Voronoi roadmap for 3D translational motion planning for a convex polyhedron moving amidst convex polyhedral obstacles. Theoretical Computer Science, 140, 205-230.

Gavin, A., Johnston, Y., & McInnes, C.R. (1997). Autonomous control of a ring of satellites. AAS/AIAA Space flight Mechanics Meeting, Alabama, paper AAS 97-104.

Ge, S.S., & Cui, Y.J. (2000). New potential functions for mobile robot path planning. IEEE Transaction on Robotics and Automation, 16 (5), 615-620.

Ge, S.S., & Cui, Y.J. (2002). Dynamic motion planning for mobile robots using potential field method. Autonomous Robots, 13, 207-222.

Goldberg, K. (1994). Completeness in robot motion planning. In Workshop on the Algorithmic Foundations of Robotics, San Francisco, California.

Graham, J.F. (1995). Space exploration from talisman of the past to gateway for the future. Chapter 5, from http://www.space.edu/projects/book/index.html

Harden, T. (1997). The implementation of artificial potential field based obstacle avoidance for a redundant manipulator. M. Sc thesis, The University of Texas at Austin.

Hayati, S., Volpe, R., Backes, P., Balaram, J., & Welch, R. (1996). Micromover research for exploration of Mars. Proceedings of the AIAA forum on Advanced developments in space robotics.

Henrich, D. (1997). Fast motion planning by parallel processing–a review. Journal of Intelligent and Robotic Systems, 20(1), 45-69.

Hwang, Y.K., & Ahuja, N. (1992). Gross motion planning – a survey. ACM Computing Surveys, 24 (3), 219-291.

Izzo, D., & Pettazzi, L. (2005, September). Equilibrium shaping: distributed motion planning for satellite swarm. 8th International Symposium on Artificial Intelligence, Robotics and Automation in Space, Munich, Germany.

Izzo, D., & Pettazi, L. (2007). Autonomous and distributed motion planning for satellite swarm. Journal of Guidance, Control, and Dynamics, 30 (2), 449-459.

Izzo, D., Pettazzi, L., & Ayre, M. (2005). Mission concept for autonomous on orbit assembly of a large reflector in space. 56th International Astronautical Congress, Japan, IAC-05-D1.4.03.

Jaklic, A., Leonardis, A., & Solina, F. (2000). Segmentation and recovery of superquadrics. Computational Imaging and Vision, 20, Kluwer, Dordrecth, Chapter 2.

Jan, Y.W., & Chiou, J.C. (2003). Minimum-time spacecraft manoeuvre using sliding-mode control. Acta Astronautica, 54, 69-75.

Katsoulas, D., & Jaklič, A. (2003). Fast recovery of piled deformable objects using superquadrics. Lecture notes in Computer graphics, Springer Berlin, 174-181.

Kavraki, L.E., & Latombe, J.-C. (1988). Probabilistic roadmaps for robot path planning. In Practical Motion Planning in Robotics: Current Approaches and Future Directions, John Wiley & Sons Ltd., 33-53.

Khatib, O. (1986). Real-time obstacle avoidance for manipulators and mobile robots. The International Journal of Robotics Research, 5 (1), 90-98.

Khosla, P., & Volpe, R. (1988). Superquadric artificial potentials for obstacle avoidance and approach. IEEE Conference on Robotics and Automation, Philadelphia, 3, 1778 -1784.

Kim, J., & Khosla, P. (1992). Real-time obstacle avoidance using harmonic potential functions. IEEE Transaction on Robotics and Automation, 8 (3),338-349.

Koren, Y., & Borenstein, J. (1991, April). Potential field methods and their inherent limitations for mobile robot navigation. Proceedings of the IEEE Conference on Robotics and Automation, Sacramento, California, 1398-1404.

Krivic, J., & Solina, F. (1993). Part-level object recognition using superquadrics. Computer Vision and Image Understanding, 95, 105-126.

Lagnemma, K., & Dubowsky, S. (2004). Mobile robots in rough terrain. Springer Tracts in Advanced Robotics, 12, Chapter 1.

Latombe, J-C. (1991). Robot motion planning. Kluwer Academic Publishers, Chapter 7.

Lee, L, (2004). Decentralized motion planning within an artificial potential framework (APF) for cooperative payload transport by multi-robot collectives. M.Sc, State University of New York at Buffalo.

Leonardis, A., Jaklič, A., & Solina, F. (1997). Superquadrics for segmenting and modelling range data. IEEE Transaction on Pattern Analysis and Machine Intelligence, 19 (11), 1289-1295.

Lumelsky, V.J., & Stepanov, A.A. (1987). Path-planning strategies for a point mobile automaton moving amidst unknown obstacles of arbitrary shape. Algorithmica, New York, 2 (4), 403–430.

Masoud, A.A., & Bayoumi, M. (1993, May). Robot navigation using the vector potential approach. IEEE International Conference on Robotics & Automation, Atlanta, Georgia, 805-811.

Masoud, S.A., & Masoud, A.A. (2000). Constrained motion control using vector potential fields. IEEE Transaction on Systems, Man, and Cybernetics-part A: Systems and Humans, 30 (3),251-272.

Masoud, S.A., & Masoud, A.A. (2002). Motion planning in the presence of directional and regional avoidance constraints using nonlinear, anisotropic, harmonic potential fields: a physical metaphor. IEEE Transaction on Systems, Man, and Cybernetics-part A: Systems and Humans, 32 (6), 705-723.

McFetridge, L., & Ibrahim, Y. (1998). New technique of mobile robot navigation using a hybrid adaptive fuzzy-potential field approach. Computers and Engineering, 35, 471-474.

McInnes, C.R. (1993). Autonomous proximity manoeuvring using artificial potential functions. ESA Journal, 17, 159-169.

McInnes, C.R. (1994). Large angle slew manoeuvres with autonomous Sun vector avoidance. Journal of Guidance, Control and Dynamics, 17 (4), 875-877.

McInnes, C.R. (1995). Potential function methods for autonomous spacecraft Guidance and Control. AAS/AIAA Astrodynamics Specialist Conference, Halifax, NS, Canada, AAS 95-447.

McInnes, C.R. (1996). Non-linear control for large angle attitude slew manoeuvres. Proceedings Third International Conference on Space Guidance, Navigation and Control Systems, ESTEC, Noordwijk, The Netherlands, ESA SP-381.

McQuade, F. (1997). Autonomous control for on-orbit assembly using artificial potential functions. Ph. D Dissertation, University of Glasgow.

McQuade, F., & McInnes, C.R. (1998). Co-operative control for on-orbit assembly of large space structures using potential field methods. University of Glasgow Departmental Report 9819.

McQuade, F., Ward, R., Ortix, F., & McInnes, C.R. (2003, Febreuary). The autonomous configuration of satellite formations using generic potential functions. 3rd International Workshop on Satellite Constellations and Formation Flying, Pisa, Italy.

Mukundan, R., & Ramakrishnan, K.R. (1995). A quaternion solution to the pose determination problem for rendezvous and docking simulations. Mathematics and Computers in Simulation, 39, 143-153.

Murata, S., Kurokawa, H., Yoshida, E., Tomita, K., & Kokaji, S. (1998). A 3-D self-reconfigurable structure. Proc. IEEE Int. Conf. on Robotics and Automation, 432–439.

Neuhaus, P., & Kazerooni, H. (2001, December). Industrial-strength human-assisted walking robots. IEEE Robotics and Automation Magazine, 18-25.

Nilsson, N.J. (1969, May). A mobile automaton: an application of artificial intelligence techniques. Proceedings of the 1st International Joint Conference on Artificial Intelligence, Washington, D.C., 509–520.

Palacín, J., Salse, J.A., Valgañón, I., & Clua, X. (2004, October). Building a mobile robot for a floor-cleaning operation in domestic environments. IEEE Transactions on Instrumentation and Measurement, 53 (5), 1418-1424.

Paul, R.P. (1981). Robot manipulators: mathematics, programming, and control. The MIT press.

Pires, N., Loureiro, A., Godinho, T., Ferreira, P., Fernando, B., & Morgado, J. (2003, June). Welding robots. IEEE Robotics and Automation Magazine, 45-55.

Prussing, J.E., & Conway, B.A. (1993). Orbital mechanics. Oxford University Press.

Quaternion representation of aeroplane attitude characteristics. (2002). Engineering sciences data unit, report no. 98024, Retrieved May 2007 from http://www.esdu.com

Radice, G., & McInnes, C.R. (1999, December). Constrained on-board attitude control using gas jet thrusters. The Aeronautical Journal, 549-556.

Rimon, E., & Kodischek, D.E. (1992). Exact robot navigation using artificial potential functions. IEEE Transactions on Robotics and Automation, 8 (5), 501-518.

Roger, A.B. (2003). Free-flyer path planning in the proximity to large space structures. Ph. D Dissertation, University of Glasgow.

Roger, A.B., & McInnes, C.R. (2000). Safety constrained free-flyer path planning at the International Space Station. Journal of Guidance, Control, and Dynamics, 23 (6), pp. 971-979.

Roy, A.E. (2005). Orbital motion. Institute of Physics Publishing Bristol and Philadelphia. Fourth edition, chapter 4.

Salcudean, S.E., Zhu, W.H., Abolmaesumi, P., Bachmann, S., & Lawrence, P.D. (1999, October). A robot system for medical ultrasound. ISRR'99, Snowbird, Utah, 152-159.

Sastry, S. (1999). Nonlinear systems: analysis, stability, and control. Springer-Verlag, New York, chapter 5.

Schaub, H., & Alfriend, K.T. (2001). Impulsive feedback control to establish specific mean orbit elements of spacecraft formations. Journal of Guidance, Navigation and Control, 24 (4), 739–745.

Schenker, P., and others (2000). Reconfigurable robots for all terrain exploration. SPIE. Symposium on sensor fusion and decentralized control in robotic systems III.

Sharir, M. (1997). Algorithmic motion planning. In Handbook of Discrete and Computational Geometry, 733- 754.

Shen, W.M., Krivokon, M., Chiu, H., Everist, J., Rubenstein, M., & Venkatesh, J. (2006). Multimode locomotion via SuperBot reconfigurable robots. Autonomous Robot, 20, 165-177.

Shimoda, S., Kuroda, Y., & Iamnemma, K. (2005). Potential field navigation of high speed unmanned ground vehicles on uneven terrain. Proceedings of IEEE International conference on Robotics and Automation, Barcelona, Spain.

Solina, F. & Bajcsy, R. (1990). Recovery of parametric models from range images: the case for superquadrics with global deformations. IEEE transaction on pattern analysis and machine intelligence, 12 (2), 131-147.

Solina, F., Leonardis, A., & Macer, A. (1994, May). A direct part-level segmentation of range images using volumetric models. IEEE International Conference on Robotics and Automation, 3, 2254-2259.

Ta, K-Y., & Baltes, J. (2006). Fuzzy potential energy for a map approach to robot navigation. Robotics and Autonomous Systems, 54, 574–589

Tzafestas, S.G, Tzamtzi, M.P., & Rigatos, G.G. (2002). Robust motion planning and control of mobile robots for collision avoidance in terrains with moving objects. Mathematics and Computers in Simulation, 59, 279-292.

Ünsal, C., & Khosla, P. (2000). Solutions for 3-D self-reconfiguration in a modular robotic system: implementation and motion planning. Proceedings of SPIE, Sensor Fusion and Decentralized Control in Robotic Systems III, SPIE, 4196, 388-401.

Van den Berg, J.P., & Overmars, M.H. (2005). Roadmap based motion planning in dynamic environments. IEEE Transactions on Robotics, 21 (5), 885-897.

Volpe, R. (1990). Real and artificial forces in the control of manipulators: theory and experiments. Ph. D Dissertation, Carnegie Mellon University.

Volpe, R., & Khosla, P. (1990). Manipulator control with superquadric artificial potential functions: theory and experiments. IEEE Transaction on Systems, Man, and Cybernetics, 20 (6), 1423-1436.

Wein, R., Berg, J., & Halperin, D. (2007). The visibility–Voronoi complex and its applications. Computational Geometry, 36, 66–87.

Wiesbin, C., et al. (1999). Autonomous Rover Technology for Mars Sample Return. International Symposium on Artificial Intelligence, Robotics, and Automation in Space.

Wie, B. (1998). Space vehicle dynamics and control. AIAA Education series.

Wisniewski, R. & Kulczycki, P. (2005). Slew manoeuvre control for spacecraft equipped with star camera and reaction wheels. Control Engineering Practice, 13, 349-356.

Yuan, X. (2002, July). An interactive approach of assembly planning. IEEE Transactions on Systems, Man, and Cybernetics-Part A: Systems and Humans, 32 (4), 522-526.

Zhang, Y. (2003a). Experimental comparison of superquadric fitting objective functions. Pattern Recognition Letters, 24, 2185-2193.

Zhang, Y. (2003b). Superquadric representation of scenes from multi-view range data. Ph.D. thesis, University of Tennessee.

APPENDIX A: QUATERNION ALGEBRA

A.1 Introduction

Quaternion parameters are widely used for orientation determination especially in space sciences. They have advantages over other methods that make quaternions more suitable for orbital motion planning problems. The quaternion vector is defined in this thesis by **q** and is composed of 4 parameters as (Quaternion, 2002):

$$\mathbf{q} = q_1\boldsymbol{i} + q_2\boldsymbol{j} + q_3\boldsymbol{k} + q_4 \tag{A.1}$$

where the quaternion parameters q_1, q_2, q_3, q_4 are real numbers and $\boldsymbol{i}$, $\boldsymbol{j}$, $\boldsymbol{k}$ are defined as:

$$\boldsymbol{ii} = -1, \qquad \boldsymbol{ij} = -\boldsymbol{ji} = \boldsymbol{k} \tag{A.2.a}$$

$$\boldsymbol{jj} = -1, \qquad \boldsymbol{j\,k} = -\boldsymbol{kj} = \boldsymbol{i} \tag{A.2.b}$$

$$\boldsymbol{kk} = -1, \qquad \boldsymbol{ki} = -\boldsymbol{ik} = \boldsymbol{j} \tag{A.2.c}$$

These parameters are called hyper-complex numbers that should not be confused with the unit vectors of the Cartesian coordinate system. The conjugate of the quaternion vector is defined as:

$$\mathbf{q}^* = -q_1\boldsymbol{i} - q_2\boldsymbol{j} - q_3\boldsymbol{k} + q_4 \tag{A.3}$$

A quaternion vector of unit length can be used to define a coordinate transformation matrix. Assume a hyper-complex quantity **Q** as:

$$\mathbf{Q} = X\boldsymbol{i} + Y\boldsymbol{j} + Z\boldsymbol{k} \tag{A.4}$$

Then the operation

$$\mathbf{Q}' = \mathbf{q}^* Q \mathbf{q} \tag{A.5}$$

$$\mathbf{Q}' = \left(-q_1\boldsymbol{i} - q_2\boldsymbol{j} - q_3\boldsymbol{k} + q_4\right)\left(X\boldsymbol{i} + Y\boldsymbol{j} + Z\boldsymbol{k}\right)\left(q_1\boldsymbol{i} + q_2\boldsymbol{j} + q_3\boldsymbol{k} + q_4\right) \tag{A.6}$$

so that:

$$\begin{bmatrix} X' \\ Y' \\ Z' \end{bmatrix} = \begin{bmatrix} \mathbf{i} & \mathbf{j} & \mathbf{k} \end{bmatrix} \begin{bmatrix} q_1^2 - q_2^2 - q_3^2 + q_4^2 & 2(q_1 q_2 + q_3 q_4) & 2(q_1 q_3 - q_2 q_4) \\ 2(q_1 q_2 - q_3 q_4) & -q_1^2 + q_2^2 - q_3^2 + q_4^2 & 2(q_2 q_3 + q_1 q_4) \\ 2(q_1 q_3 + q_2 q_4) & 2(q_2 q_3 - q_1 q_4) & -q_1^2 - q_2^2 + q_3^2 + q_4^2 \end{bmatrix} \begin{bmatrix} X \\ Y \\ Z \end{bmatrix} \tag{A.7}$$

By replacing all parameters in Eq. (A.7) with the corresponding quaternion parameters, it is possible to develop the general transformation matrix which can be written as (Paul, 1981):

$$\mathbf{T} = \begin{bmatrix} q_1^2 - q_2^2 - q_3^2 + q_4^2 & 2(q_1 q_2 + q_3 q_4) & 2(q_1 q_3 - q_2 q_4) & x_s \\ 2(q_1 q_2 - q_3 q_4) & -q_1^2 + q_2^2 - q_3^2 + q_4^2 & 2(q_2 q_3 + q_1 q_4) & y_s \\ 2(q_1 q_3 + q_2 q_4) & 2(q_2 q_3 - q_1 q_4) & -q_1^2 - q_2^2 + q_3^2 + q_4^2 & z_s \\ 0 & 0 & 0 & 1 \end{bmatrix} \tag{A.8}$$

The previous transformation is used to determine the relative orientation between two objects. The transformation calculation is considered as a crucial parameter in obstacle potential field estimation in the case of superquadric obstacle representation.

A.2 Quaternion Parameter Determination

A rotation matrix **R** is used to describe the orientation of a body frame with respect to an inertial frame of reference. The matrix **R** is a 3x3 orthonormal matrix which consists of three orthogonal unit vectors which are the basis of the body frame of reference with respect to the inertial frame, meaning that

$$\mathbf{R}^{\mathrm{T}}\,\mathbf{R} = \boldsymbol{I} \tag{A.9.a}$$

and

$$\mathbf{R}^{\mathrm{T}} = \mathbf{R}^{-1} \tag{A.9.b}$$

The elementary rotation matrixes are defined as (Wie, 1998):

$$\mathbf{R}_1(\theta_1)=\begin{bmatrix}1 & 0 & 0\\ 0 & cos(\theta_1) & sin(\theta_1)\\ 0 & -sin(\theta_1) & cos(\theta_1)\end{bmatrix} \tag{A.10.a}$$

$$\mathbf{R}_2(\theta_2)=\begin{bmatrix}cos(\theta_2) & 0 & -sin(\theta_2)\\ 0 & 1 & 0\\ sin(\theta_2) & 0 & cos(\theta_2)\end{bmatrix} \tag{A.10.b}$$

$$\mathbf{R}_3(\theta_3)=\begin{bmatrix}cos(\theta_3) & sin(\theta_3) & 0\\ -sin(\theta_3) & cos(\theta_3) & 0\\ 0 & 0 & 1\end{bmatrix} \tag{A.10.c}$$

The rotation between multiple frames can be written as

$$\mathbf{R_{1\to 3}} = \mathbf{R_{1\to 2}}\mathbf{R_{2\to 3}} \tag{A.11}$$

where $R_{i\to j}$ means the rotation matrix of frame *j* with respect to frame *i*. The rotation matrix has three interpretations:

1. It determines the relative orientation between two frames.
2. It represents the coordinate transformation between the coordinates of a body expressed in two frames having the same origin.
3. It represents a vector rotation in the same frame.

Quaternion parameters are then determined for orientation determination through the following steps:

1. Choose a certain rotation sequence, $\mathbf{R}=\mathbf{R}_3(\theta_3)\to\mathbf{R}_2(\theta_2)\to\mathbf{R}_1(\theta_1)$, for Euler angles as:

$$\mathbf{R}=\frac{1}{cos(\theta_2)}\begin{bmatrix}cos(\theta_2) & sin(\theta_1)sin(\theta_2) & cos(\theta_1)sin(\theta_2)\\ 0 & cos(\theta_1)cos(\theta_2) & -sin(\theta_1)cos(\theta_2)\\ 0 & sin(\theta_1) & cos(\theta_1)\end{bmatrix} \tag{A.12}$$

2. Calculate the eigenaxis, **e**, as:

$$\mathbf{e} = \begin{bmatrix} e_1 \\ e_2 \\ e_3 \end{bmatrix} = \frac{1}{2\,sin(\theta)} \begin{bmatrix} R_{23} - R_{32} \\ R_{31} - R_{13} \\ R_{12} - R_{21} \end{bmatrix} \tag{A.13}$$

where θ is the angle of the eigenaxis.

3. Determine the angle θ from the relation:

$$e_1^2 + e_2^2 + e_3^2 = 1 \tag{A.14}$$

4. Quaternion parameters are then determined as:

$$\mathbf{q} = \begin{bmatrix} q_1 \\ q_2 \\ q_3 \\ q_4 \end{bmatrix} = \begin{bmatrix} e_1\,sin(\theta/2) \\ e_2\,sin(\theta/2) \\ e_3\,sin(\theta/2) \\ cos(\theta/2) \end{bmatrix} \tag{A.15}$$

Finally, the kinematic differential equation relating the quaternion parameters and object angular velocity is defined as:

$$\begin{bmatrix} \dot{q}_1 \\ \dot{q}_2 \\ \dot{q}_3 \\ \dot{q}_4 \end{bmatrix} = \frac{1}{2} \begin{bmatrix} q_4 & -q_3 & q_2 & q_1 \\ q_3 & q_4 & -q_1 & q_2 \\ -q_2 & q_1 & q_4 & q_3 \\ -q_1 & -q_2 & -q_3 & q_4 \end{bmatrix} \begin{bmatrix} \omega_1 \\ \omega_2 \\ \omega_3 \\ 0 \end{bmatrix} \tag{A.16}$$